Mathematical approaches to modelling healing of full thickness circular skin wounds

Lucie Bowden

Worcester College

University of Oxford

A thesis submitted for the degree of

Doctor of Philosophy

October 2015

Acknowledgements

First and foremost I would like to thank Professors Helen Byrne, Derek Moulton and Philip Maini. I have been extremely fortunate to have supervisors with such vast knowledge and experience. This work would not have been possible without their invaluable suggestions, guidance and support; it has been a pleasure working with you.

Besides my principle supervisors I would like to thank our experimental collaborators Dr. Paul Liu and Dr. Xiao Tian Wang for sharing their experimental data, for stimulating and insightful discussions, and for their generous hospitality during my visit to Brown University.

I express my gratitude to Professors Alain Goriely and Jonathan Sherratt for agreeing to be my examiners, for their feedback and for an enjoyable discussion.

I gratefully acknowledge the Engineering and Physical Sciences Research Council for funding through the Systems Biology Doctoral Training Centre. I will take this opportunity to thank all the academic and administrative staff at the DTC for their organisation and delivery of the programme and for their support throughout my DPhil.

I would like to thank Worcester College for being my home for many years and OUWAFC for being my friends.

To my family and friends, thank you for all your love and encouragement, I would not be here without you. Lastly I would like to thank Zipora, for being there for me throughout. Not only for her endless support and motivation giving me the strength and confidence in the final stages, but for her patience and commitment to proof-reading my thesis. Your constant love, kindness and generosity is greatly appreciated.

Abstract

Wound healing is a complex process, in which a sequence of interrelated events at both the cell and tissue levels interact and contribute to the reduction in wound size. For diabetic patients, many of these processes are compromised, so that wound healing slows down and in some cases halts. In this thesis we develop a series of increasingly detailed mathematical models to describe and investigate healing of full thickness skin wounds.

We begin by developing a time-dependent ordinary differential equation model. This phenomenological model focusses on the main processes contributing to closure of a full thickness wound: proliferation in the epidermis and growth and contraction in the dermis. Model simulations suggest that the relative contributions of growth and contraction to healing of the dermis are altered in diabetic wounds.

We investigate further the balance between growth and contraction by developing a more detailed, spatially-resolved model using continuum mechanics. Due to the initial large retraction of the wound edge upon injury, we adopt a non-linear elastic framework. Morphoelasticity theory is applied, with the total deformation of the material decomposed into an addition of mass and an elastic response. We use the model to investigate how interactions between growth and stress influence dermal wound healing. The model reveals that contraction alone generates unrealistically high tension in the dermal tissue and, hence, volumetric growth must contribute to healing. We show that, in the simplified case of homogeneous growth, the tissue must grow anisotropically in order to reduce the size of the wound and we postulate mechanosensitive growth laws consistent with this result. After closure the surrounding tissue remodels, returning

to its residually stressed state. We identify the steady state growth profile associated with this remodelled state. The model is used to predict the outcome of rewounding experiments as a method of quantifying the amount of stress in the tissue and the application of pressure treatments to control tissue synthesis.

The thesis concludes with an extension to the spatially-resolved mechanical model to account for the effects of the biochemical environment. Partial differential equations describing the dynamics of fibroblasts and a regulating growth factor are coupled to equations for the tissue mechanics, described in the morphoelastic framework. By accounting for biomechanical and biochemical stimuli the model allows us to formulate mechanistic laws for growth and contraction. We explore how disruption of mechanical and chemical feedback can lead to abnormal wound healing and use the model to identify specific treatments for normalising healing in these cases.

Contents

Chapter 1

Introduction

1.1 Motivation

Wound healing is a complex process, which is not fully understood. In diabetic wounds, intrinsic pathobiological abnormalities and extrinsic factors contribute to an even more complex wound environment. Hallmarks of diabetes, such as higher risk of macrovascular diseases, neuropathy and hyperglycaemia, can result in delayed healing [American Diabetes Association, 2006] and, in extreme cases, lower limb amputations [Adler et al., 1999]. In the UK, wound care costs the National Health Service £1 billion a year [Falanga, 2005]. The clinical demand for treatments that can enhance wound healing, for example, in diabetic patients, is stimulating a vast amount of biomedical research.

Advances in wound management will come from a greater understanding of the mechanisms controlling wound healing. Collecting data is expensive and testing a hypothesis can be very time consuming. Although much experimental research has been carried out, progress is often slow: the involvement of theoretical approaches and mathematical modelling represents an alternative strategy for accelerating progress. Modelling can be used to test a biological hypothesis before it undergoes experimental

testing. Models can also be used to improve the design of experiments by highlighting areas where more measurements are needed to test a theory.

Model predictions require experimental verification. If predictions derived from the models agree with experimental data then the model provides a possible explanation for the biological behaviour. Equally, experimental data are needed to design models: the more information we have about a process, the more accurately it can be described during model development. As it is difficult to conduct *in vivo* investigations in a non-invasive manner, realistic mathematical models that are based on known cell behaviours provide a useful framework for studying wound healing. As well as mathematical models, reproducible animal models that recapitulate aspects of impaired wound healing have an important role to play [Martínez-Santamaría et al., 2013].

The theoretical work presented in this thesis was motivated by a collaboration with an experimental group from the Alpert Medical School of Brown University. Dr. Paul Liu and his group have developed a mouse model to study diabetic wound healing. Data from their laboratory consist of time courses of averaged wound areas from non-diabetic and diabetic mice. In Chapter 2 we will discuss these experimental data as they are integral to the development of our first model of wound healing.

Fundamental difficulties in linking modelling and experimental efforts in wound healing relate to over-parameterisation of the mathematical models and the technical difficulty associated with obtaining suitable experimental data for model validation. In this thesis we present a series of increasingly detailed mathematical models for the healing of a full thickness wound. We focus on minimising complexity whilst retaining the dominant features involved in the healing of full thickness circular wounds. The models are used to investigate healing mechanisms and the causes and effects of healing abnormalities.

In the current chapter we introduce the research problem. The biology of wound

healing is described in Section 1.2 together with recent experimental advances in understanding wound healing mechanisms and pathologies. Following this, in Section 1.3 the relevant mathematical literature is reviewed. The use of morphoelasticity as our main modelling framework is motivated in Section 1.4. Finally, in Section 1.5 we summarise our thesis aims and outline the contents of the remaining chapters.

1.2 The biology of wound healing

The skin forms a barrier between the body and the external environment, offering protection and regulation. Human skin is primarily divided into three layers (see Figure 1.1). The outermost epidermal layer is made from densely packed epithelial cells. The dermis is a thicker layer of collagenous elastic tissue, in which the main cell type is the fibroblast. Beneath the dermis lies a fatty layer called the sub-dermis, providing the body with insulation.

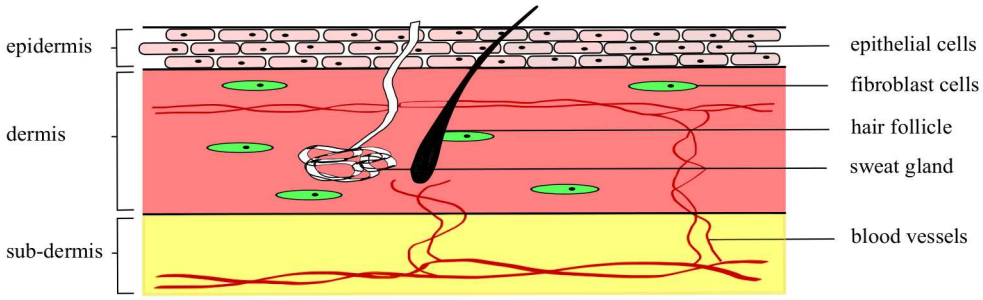

Figure 1.1: Schematic of the skin. A cross-section through the three main layers of the skin. The epidermis contains layers of tightly packed epithelial cells. The dermis consists of fibroblasts, blood vessels, sweat glands and hair follicles, surrounded by elastic tissue made primarily of collagen. The sub-dermis is a fatty tissue with a network of blood vessels.

Surface (or superficial) wounds disrupt the epidermis and are a result of a graze on thin-skinned areas of the body, such as knees and elbows. More problematic are full thickness wounds that also damage the dermis. Arising from a surgical procedure or traumatic accident, full thickness wounds undergo a more complex healing cascade

as they require the repair and regeneration of the dermal and epidermal layers. The dermis never fully closes as granulation tissue is formed in the wound space and, over time, is remodelled into scar tissue. Scar tissue can be distinguished from healthy dermal tissue by its aligned collagen fibres and inferior mechanical properties. All dermal wounds result in some degree of scarring with the exception of foetal wounds [Larson et al., 2010] and wounds in certain animals, for example, geckos and salamanders [Godwin and Rosenthal, 2014, Peacock et al., 2015].

1.2.1 Normal wound healing

Normal healing of full thickness wounds in mammalian adults involves the co-ordination of a series of interrelated biochemical and biomechanical processes. It proceeds in four distinct phases (see Figure 1.2), starting with haemostasis, followed by inflammation, proliferation and, finally, remodelling. In practice, however, these processes overlap.

Immediately after wounding, the intrinsic tension in the surrounding tissue causes the skin to recoil [Kiehart, 1999]. Haemostasis is an instantaneous response to wounding. Damaged capillaries allow blood flow into the wound, causing platelets to aggregate and form a temporary seal or clot in the opening. The clot is made primarily from fibrin and is a source of the growth factors that are needed during the subsequent healing phases [Wahl et al., 1989]. The growth factors in the wound space initiate the inflammatory phase, which lasts for up to a week [Jeffcoate et al., 2004], during which inflammatory cells, for example leukocytes, neutrophils and macrophages, migrate into the wound. The inflammatory cells produce chemicals that stimulate the proliferative phase, which entails angiogenesis, epithelialisation and fibroplasia. Angiogenesis is the process by which new blood vessels sprout from existing damaged vessels to increase local blood supply and involves the directed movement of endothelial cells, via chemotaxis, up spatial gradients of growth factors that include vascular endothelial growth factor (VEGF). Proliferation in the epidermal layer of the skin

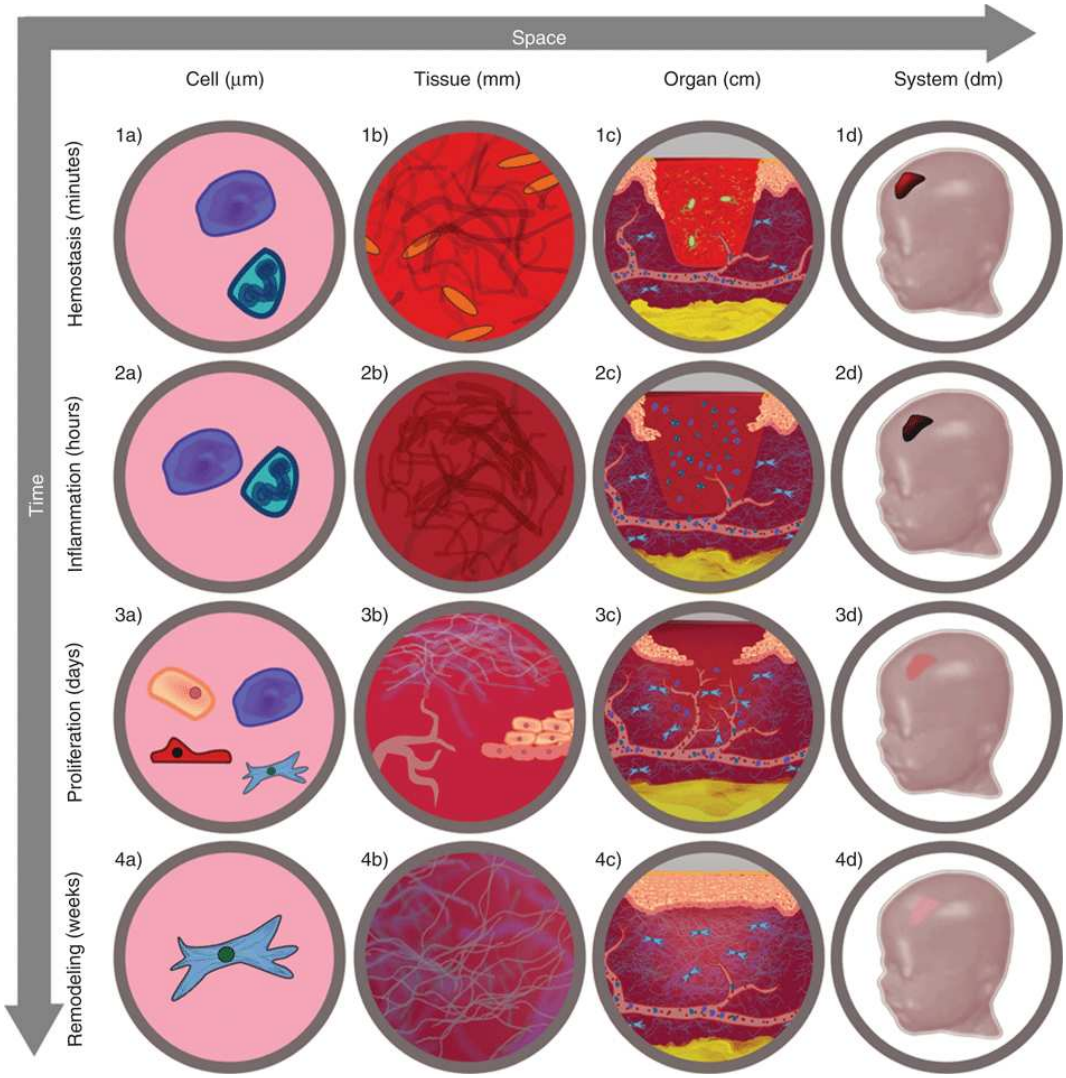

Figure 1.2: Spatio-temporal spectrum of wound healing. Wound healing processes span from minutes to months and from cell to system level. Haemostasis takes place within the first few minutes, inflammation within hours, proliferation days and remodelling weeks. Spatially the length scales vary from the cell (μm), tissue (mm), organ (cm) to the system level (dm). Figure reproduced from Tepole and Kuhl [2013].

is termed epithelialisation and proceeds more quickly than dermal proliferation. A combination of proliferation and migration of epithelial cells contributes to the regeneration of the epidermis. In the dermis, the proliferative phase is described as fibroplasia. During fibroplasia, fibroblasts resident in the surrounding dermal tissue are stimulated to proliferate, synthesise and contract the tissue by a family of fibroblast growth factors (FGF) produced during the inflammatory phase [Clark, 1988]. Fibroblasts that remain in the dermal tissue contribute to tissue regeneration while those that migrate into the wound space initiate the deposition of new extracellular matrix (ECM) by producing collagen. Contraction begins approximately 2 to 5 days post wounding. Contraction is the process by which the wound shrinks and is thought to occur by a combination of contractile fibroblasts in the wound space [Monaco and Lawrence, 2003] and migrating fibroblasts arranged around the wound edge. After closure, cellular activity decreases and the collagen matrix and surrounding dermal tissue is remodelled over a period of several months.

1.2.2 Diabetes associated impaired healing

Diabetes is a common, life-long health condition. Worldwide there are 285 million adults with diabetes, with this number estimated to increase by 54% by 2030 [Shaw et al., 2010]. Diabetes can be categorised into type I ($\sim 10\%$) and type II ($\sim 90\%$). The former results from an inability to produce insulin, whereas the latter is an inability to efficiently use the body's insulin. In both cases, the conversion of glucose into glycogen is inhibited, leading to high blood glucose levels, or hyperglycaemia. Symptoms of hyperglycaemia, such as higher risk of macrovascular disease and neuropathy, are associated with both types of diabetes [American Diabetes Association, 2006].

More than 100 physiological factors contribute to wound healing deficiencies in diabetic individuals [Brem and Tomic-Canic, 2007]. As mentioned above, normal

wound healing requires the coordinated integration of complex biological and molecular events. In a diabetic wound these events may be disrupted by a combination of intrinsic and extrinsic factors, resulting in delayed healing. Intrinsic factors include the patient's health condition and age, whereas extrinsic factors are associated with external stimuli, such as temperature, pressure and infection.

Often in type I diabetes, macrovascular disease limits blood supply to the foot, causing problems in diabetic foot ulcers. Microcirculatory deficiencies, which are an early occurrence in diabetes, cause reduction in capillary size and thickening of the basement membrane, a thin layer of fibres separating the epidermis from the dermis. This can result in altered migration of leukocytes, contributing to infection [Falanga, 2005]. A common intrinsic factor associated with diabetics is neuropathy, a collection of disorders affecting the nervous system. The associated loss of protective sensation is a major risk factor for increased rates of unnoticed trauma to the wound.

Infection is a major cause of morbidity and hospitalisation and in many cases leads to impaired healing and even amputation. Obesity is often a characteristic of type II diabetes. As a consequence of being overweight, patients experience high loading on their feet, increasing the chance of developing foot ulcers. Mechanical stress and compressive forces have been shown to favour overgrowth of bacteria [Ctercteko et al., 1981], leading to infection of foot wounds. Hyperglycaemia, hypoxia and metabolic effects can cause decreased function of macrophages and neutrophils, and thereby increased risk of infection [Jeffcoate et al., 2004].

High glucose levels have been known to induce resistance of fibroblasts to growth factors, slowing down or inhibiting proliferation [Hehenberger et al., 1998]. Decreased cell and growth factor response, diminished peripheral blood flow and decreased local angiogenesis can result in slower re-epithelialisation rates. Less is known about other factors which may compromise the mechanical properties of the skin. Insufficient contraction may delay healing, increasing the risk of infection, whilst excessive con-

traction often compromises the quality of repair and may cause substantial scarring [Hinz, 2006].

1.2.3 The mechanism of wound contraction

Wound contraction is the process by which the wound margins move inwards, resulting in a reduction in wound size. Full thickness wounds in adult humans heal partially by wound contraction (approximately 20% [Catty, 1965]). In rodents, contraction of the wound edges is the main healing mechanism contributing to approximately 80% of the reduction in wound size [McGrath and Simon, 1983]. The mechanisms driving wound contraction are not fully understood. Early theories supposed that the central granulation tissue shrinks due to loss of material, water or shortening of collagen fibres [Loeb, 1920], although evidence of this is still lacking. Under this theory, attachments between the shrinking granulation tissue and the surrounding intact dermis cause the wound edges to be pulled inwards. A series of experiments have challenged the assumptions that the reduction in volume of granulation tissue is a result of dehydration of collagen fibres and concluded that cells were responsible for generating a contractile force on the granulation tissue [Abercrombie et al., 1956, Grillo et al., 1958]. Furthermore, *in vitro* experiments have shown that fibroblast cells can contract a collagen lattice and hence reduce its size [Bell et al., 1979], supporting the theory of cell-mediated contraction.

Watts et al. [1958] challenged the shrinking granulation hypothesis as the primary mechanism for wound contraction. Experiments on guinea pigs showed that excising only the central granulation tissue during healing did not affect contraction of the wound. However, excising the dermal tissue at the wound edge caused the wound to retract. This work led to the 'picture-frame' hypothesis, whereby fibroblast cells arranged around the wound edge pull the dermal tissue inwards as they migrate towards the wound centre. Further, the authors showed that movement of the dermal

edges is not caused by pushing from peripheral tissue. They therefore concluded that the contraction force is localised to a thin strip around the wound edge.

Much research has been done experimentally [Carlson and Longaker, 2004, Dallon and Ehrlich, 2008] on the contraction and reorganisation of fibroblast populated collagen lattices [Bell et al., 1979]. Mathematical models of the organisation of collagen fibrils by fibroblasts [Dallon et al., 1999, Dallon, 2000, McDougall et al., 2006] have also been developed to investigate causes and possible preventions of scar formation. These *in vitro* and *in silico* studies have increased our understanding of the role of granulation tissue and its components in the remodelling and mechanical organisation of subsequent scar tissue. Recently, *in vivo* investigations into cell types and their function within granulation tissue have contributed to our understanding of remodelling and scar related pathologies [Hinz et al., 2001, Hinz, 2007].

The work discussed above [Watts et al., 1958], and other similar studies [Gross et al., 1995], show that the central granulation has little or no role in the active 'pulling' of the dermal edges inwards. Although the mechanism of contraction has been localised to the wound edge, Gross et al. [1995] showed that disruption normal to the wound edge does not alter the rate of wound closure, hence wound contraction does not proceed by a 'purse-string' mechanism as observed in embryos [Martin and Lewis, 1992]. These findings suggest that the dominant source of contraction is the fibroblast cells, located at the wound edge. Contraction of the wound contents may not directly cause inward movement of the dermal edges, but it has been shown to be important in the later stages of scar remodelling [Nedelec et al., 2000]. A schematic summarising the differences between the two mechanisms of wound contraction is presented in Figure 1.3.

As we will discuss in Section 1.3, most mathematical models of dermal wound healing consider the formation and remodelling of the granulation tissue into scar tissue. In this thesis we are interested in the timescale over which the wound closes

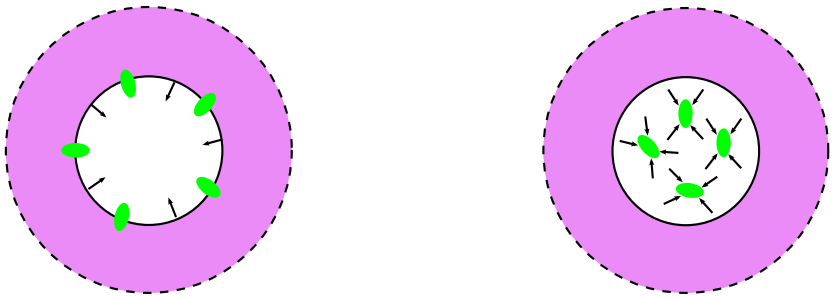

(a) Contraction (b) Remodelling

Figure 1.3: Differences between wound contraction and remodelling. An annular region of dermal tissue surrounding a circular wound. a) The 'picture-frame' hypothesis for wound contraction: fibroblast cells arrange themselves at the wound edge and pull the healthy dermal tissue inwards as they migrate towards the wound centre. b) Remodelling of granulation tissue: fibroblast cells migrating through the granulation tissue lay down and align collagen fibrils. Static myofibroblasts exert contractile forces on the surrounding tissue increasing compaction and rigidity.

and therefore do not consider this process. The granulation tissue may offer stability to the wound but its interaction with the moving dermal edge and influence on the rate of dermal healing is not clear. For these reasons it is omitted from our modelling.

1.2.4 The role of the mechano-chemical environment in wound healing

The adaptation of skin to changes in body shape and size has been observed in many physiological circumstances. For example, the skin must expand to cover the body during growth, pregnancy and obesity. Since healing requires the expansion of skin to cover a defect, many of the processes that contribute to wound healing may be influenced by mechanical forces. Therefore the application of forces provides a potential method of controlling the speed and quality of wound closure. Cells involved in wound healing, such as epithelial cells and fibroblasts, have been shown to respond to a variety of mechanical stimuli such as compression, stretch and shear [Hinz et al., 2001, Lumpkin and Caterina, 2007]. The cells convert the mechanical stimuli into biological or chemical signals, via a process known as mechano-transduction.

Successful wound healing requires a careful balance of chemical signals and mechanical stimuli. Recent experimental and theoretical work in wound healing has focussed on TGFβ, fibroblasts (and their differentiated forms), the mechanical environment and their interactions.

Fibroblasts are the main cell type involved in dermal wound healing. They are activated by chemical signals in response to injury. The main growth factors involved in fibroblast activity are platelet derived growth factor (PDGF) and transforming growth factor (TGFβ) [Pierce et al., 1989, Cordeiro et al., 2000]. The chemically driven migration and proliferation of fibroblasts results in high fibroblast density close to the wound and lower ones far from the wound.

The fibroblast phenotype determines its role in collagen synthesis and wound contraction. A combination of chemical and mechanical factors stimulates changes in fibroblast activity (see Figure 1.4). Firstly, quiescent fibroblasts develop a migratory phenotype and generate small traction forces on the tissue. This change is regulated by cytokines released locally by inflammatory cells. The migratory fibroblasts differentiate into myofibroblasts in response to increased mechanical stress levels [Gabbiani, 2003, Hinz, 2007]. This phenotype change can be detected by an increase in α-smooth muscle actin (α-SMA). Expression of α-SMA is controlled by TGFβ [Desmoulière et al., 1993], ECM proteins and the mechanical environment [Hinz, 2007]. Myofibroblasts are the main cell type present in the wound space and are responsible for remodelling of the granulation tissue into scar tissue, which occurs over a period of several months to years [Gabbiani, 2003, Hinz, 2007]. It is the remodelling stage of healing that can result in pathologies such as fibrosis (excessive fibroplasia and ECM production). Release of tension from the tissue induces cell death [Hinz et al., 2001]. If tension is relieved too early, a wound may fail to contract and the scar tissue fail to mature. Conversely, too much tension can result in increased scar formation [Meyer and McGrouther, 1991].

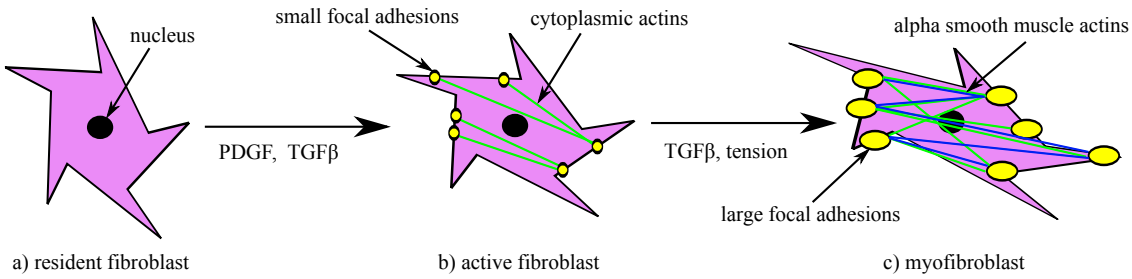

Figure 1.4: Phenotypic changes in fibroblast cells. Upon injury, inflammatory cells release growth factors, such as PDGF and TGFβ, stimulating resident fibroblasts to migrate towards the wound, synthesise material and exert small traction forces on the tissue. In response to TGFβ and mechanical tension, active fibroblasts differentiate into contractile myofibroblasts, identified by an increased expression of α-SMA.

1.2.5 Current treatments

Management of wounds remains a challenging issue. The development of effective treatments will minimise pain and inconvenience for patients, especially those who experience abnormal healing. Improved treatments could also have a substantial economic impact on healthcare systems with limited budgets.

A traditional approach to treating wounds is through debridement, the removal of dead tissue from the wound area. Methods include surgical removal, the use of enzymes, maggots or dressings [Singh et al., 2013]. One of the major problems with compromised wound healing is an imbalance in the levels of key growth factors and cytokines. Consequently, correcting this imbalance has been a major goal of many treatments. For example, hypoxia, a shortage of oxygen, appears not only to inhibit wound healing by blocking fibroblast proliferation, collagen production, and capillary angiogenesis but also to increase the risk of infection, in some cases causing the development of chronic wounds. In such cases, treatment via hyperbaric oxygen therapy (HBOT) has been shown to aid healing [Thackham et al., 2008]. Other treatments that are under development include stem cell therapy, gene therapy and the grafting of bioengineered skin [Bello et al., 2001]. In areas of the world where these treatments are not available, inexpensive alternatives must be provided. Traditional

treatment methods, such as the application of dressings and pressure bandages, need to be re-assessed.

The vast amount of money spent on wound care and the repeated trauma experienced by patients highlight the need for better treatments which will improve the quality of life of patients. As well as the development of new treatments, the aim, for many clinicians, is to identify optimal protocols for the application of existing and/or new treatments. By combining biological knowledge with the ability to test treatments and protocols theoretically, mathematical modelling represents a powerful tool for improving wound care development.

1.3 Review of current mathematical models of wound healing

Mathematical modelling in biological and medical applications, such as wound healing, can provide mechanistic insight into the relative importance of processes that are believed to contribute to healing, and has the potential to generate experimentally testable predictions. Wound healing has been studied in a mathematical and computational context for over 30 years (see Tepole and Kuhl [2013] for a recent review). Models of wound healing have been developed using approaches that include: agent-based models (ABM), ordinary differential equation models (ODE), partial differential equation models (PDE) and hybrid models. A selection of mathematical models are summarised in Table 1.1 with the most relevant being discussed in the following sections.

Agent-based models are computational models that simulate discrete events, such as interactions between individual cells, and are popular amongst biologists due to their intuitive approach [Walker et al., 2004, Sun et al., 2009]. Simulation results are visual, easy to interpret and relate to experiments such as scratch assays. Rules

Table 1.1: Summary of methods used for mathematical models of wound healing. Models are categorised into their modelling approach. Table adapted from Arciero and Swigon [2013].

Model	Examples	Phenomenon modelled	Tissue type
ABM	Walker et al. [2004]	migration and proliferation	epithelium
	Mi et al. [2007]	inflammation	diabetic wound
	Sun et al. [2009]	migration and proliferation	epidermis
ODE	McGrath and Simon [1983]	wound area	dermis
	Cukjati et al. [2000]	wound area	dermis
	Waugh and Sherratt [2006, 2007]	macrophage dynamics	diabetic wound
	Murphy et al. [2011]	contraction	dermis
	Segal et al. [2012]	collagen production	dermis
	Bianchi et al. [2015]	lymphangeogenesis	diabetic wound
PDE	Sherratt and Murray [1990, 1992]	migration and proliferation	epidermis
(reaction-diffusion)	Wearing and Sherratt [2000]	keratinocyte growth factor signalling	epidermis
	Menon et al. [2012]	keratinocyte-fibroblast interaction	epidermis and dermis
PDE	Tranquillo and Murray [1992]	contraction	dermis
(mechano-chemical)	Tracqui et al. [1995]	contraction	dermis
	Olsen et al. [1995]	contraction	dermis
	Olsen et al. [1999]	collagen alignment	dermis
	Xue et al. [2009]	inflammation	diabetic wound
	Flegg et al. [2010]	angiogenesis and HBOT	chronic wound
	Vermolen and Javierre [2012]	wound closure	epidermis and dermis
	Yang et al. [2013]	wound contraction	dermis
	Wu and Ben Amar [2015]	circumferential buckling	epidermis
Hybrid	Dallon et al. [1999], Dallon [2000]	collagen alignment	dermal scar
	McDougall et al. [2006]	collagen alignment	dermal scar
	Cumming et al. [2010]	collagen alignment	dermal scar

are based on cell behaviour and interactions. As each rule is derived individually, this approach can readily incorporate more species and/or interactions. However, the amount of data needed to determine cell and molecular level rules for an ABM on the tissue level is vast. Furthermore, the number of cells involved in wound healing is typically large enough to justify a continuum approach.

Ordinary differential equation models describe the time evolution of wound healing but focus on spatially-averaged variables. Many models focus on the dynamics of wound area and, as such, can be readily translated to a clinical setting where wounds are often characterised according to the percentage of wound area remaining [McGrath and Simon, 1983]. Other ODE models account for interactions between cells and chemicals [Waugh and Sherratt, 2006]. Spatial effects are neglected by either assuming a well mixed system, or by introducing compartments to represent different tissues. ODE models represent a simple framework within which to integrate different physical processes.

Partial differential equation models of wound healing can be divided into two types: reaction-diffusion equations (RDE) and mechano-chemical models. RDEs are formulated by considering interactions between the different components involved in healing, with dependent variables representing the spatio-temporal evolution of cell and chemical concentrations [Sherratt and Murray, 1990, 1992]. RDEs are particularly suitable for studying epidermal healing, since the epidermis is made primarily of cells whose behaviour is controlled mainly by growth factors.

Mechano-chemical models of wound healing are essentially formulated as RDEs. Unlike RDE models, mechano-chemical models can be used to determine tissue displacement, stress and strain and, as such, represent a natural framework within which to account for the influence of contraction and mechano-transduction on wound healing [Tranquillo and Murray, 1992]. In order to describe these mechanical features of the healing tissue an additional phenomenological equation is required, combining a

constitutive law for the mechanical properties of the tissue, and the influence of the cells on the tissue.

A more recent approach to modelling wound healing concerns hybrid models [Dallon, 2000, McDougall et al., 2006, Cumming et al., 2010]. A hybrid framework can integrate both discrete and continuous variables. Since wound healing spans several spatial scales (e.g. chemical, cell and tissue), it is natural to consider a hybrid approach that accounts for cells as discrete entities and chemical species and ECM as continua. This framework is used to model scarring and ECM remodelling in which fibroblasts rearrange fibre directions within a collagen network.

In the remainder of this section we review the mathematical literature that has contributed to our understanding of wound healing. Models that are particularly relevant to the present work are described in more detail.

1.3.1 Models of epidermal healing

During epidermal healing, wound closure is thought to involve two processes: cell division at the wound edge, and cell migration into the wound. These processes are regulated by growth factors produced by cells in the wound and surrounding tissue. For example, epidermal growth factor (EGF) is produced by macrophages in the wound space. Models for epidermal healing investigate the influence of these regulatory chemicals on mitotic and migratory cell rates.

Sherratt and Murray's model for epidermal wound healing [Sherratt and Murray, 1990] was among the earliest of its type. It consists of two RDEs representing mass conservation of cells and a mitosis-regulating chemical. Model solutions show how cell density profiles evolve during healing of a radially symmetric wound. They compared the impact on healing of growth factors that promote and inhibit mitosis. Model solutions yielded rates of wound closure that were in good agreement with experimental data.

Many extensions and variations of Sherratt and Murray's model have been developed. For example, in Sherratt and Murray [1992] the authors showed how, for wounds of the same initial area, the initial shape of the wound affects its rate of closure. These results could be used to guide the shape of surgical wounds, to ensure that they heal as quickly as possible.

Although it is clear from a combination of theoretical and experimental results that epidermal growth factors contribute largely to the regulation of cell mitosis, more recent work has focussed on the effects of keratinocyte growth factor (KGF) [Wearing and Sherratt, 2000]. Although KGF affects the growth of keratinocytes in the epidermis and, therefore, plays a major role in epidermal healing, it is produced in the dermis. Interaction between these two skin layers has not been studied in great detail but models that consider both the epidermis and dermis could help to increase our understanding of full thickness wound healing (see Chapter 2).

Wu and Ben Amar [2015] used an alternative, morphoelastic approach to study re-epithelialisation of a circular wound, modelling the epidermal tissue as neo-Hookean. This theoretical framework, which we discuss in Section 1.4, allows for the study of growth in a non-linear elastic material. The authors assume homogeneous volumetric growth in an annular region surrounding a circular wound. They show that certain choices of initial wound size and tissue stiffness can destabilise the assumed circular geometry.

1.3.2 Models of dermal healing

Dermal wound healing is much less well documented and understood, both experimentally and mathematically, than epidermal healing. Most mathematical models for dermal healing consider the final three wound healing phases: inflammation, proliferation and remodelling. The models account for a small number of the interactions involved, choices being based on the available data and the questions being addressed.

Early models of dermal wound healing focussed on contraction. Tranquillo and Murray [1992] specialised a general model for tissue biomechanics [Murray et al., 1988] to describe the mechanical contraction of a wound during healing. Fibroblast and ECM densities were formulated as RDEs subject to passive advection, with the fibroblasts also subject to random migration and logistic growth. The cell-ECM composite is viewed as an isotropic solid, with linear viscoelastic properties. The additional mechanical equation, from which the tissue displacement, stress and strain are calculated, combines terms for the elastic stress, viscous stress and tractional stress exerted by the fibroblasts. Initially, fibroblasts occupy the surrounding dermal tissue, so that traction forces cause a retraction of the wound boundary. As fibroblasts reach a uniform distribution throughout the wound space and surrounding dermis the wound boundary contracts back to its original position. This model showed that without any biochemical stimuli wound contraction would not occur. By introducing a chemical mediator Tranquillo and Murray [1992] showed that wound contraction could be achieved in three different ways: chemically driven cell traction, proliferation or migration. However, the assumption of linear viscoelasticity meant that the degree of wound contraction observed in the model simulations was far less than that observed experimentally [McGrath and Simon, 1983].

Olsen et al. [1995] discriminated between the roles of fibroblasts and myofibroblasts in dermal healing. Fibroblasts are assumed to be motile, synthesise ECM and exert small traction forces, whereas myofibroblasts are assumed to be static and enhance the traction forces exerted on the ECM. The expression of cell phenotype and behaviour is regulated by a growth factor diffusing outwards from the wound centre. Moreover, in contrast to Tranquillo and Murray [1992], ECM turnover is considered. A steady state analysis shows that the displacement is identically zero. However, in practice, the healed wound is permanently contracted. The authors show that the tissue can achieve a permanently contracted steady state if collagen kinetics are neglected, i.e.

production and degradation of ECM are ignored. While this may be an appropriate assumption for later stages of wound healing, at early times ECM production is much greater than degradation.

In subsequent work, Olsen and co-workers view the ECM as an anisotropic material [Olsen et al., 1999] and consider two types of fibre alignment: flux-induced alignment, caused by traction forces exerted by migrating fibroblasts on the ECM; and stress-induced alignment, caused by mechanical forces associated with wound contraction. Only by combining these processes did their model agree with experimental data. Alignment of collagen fibres is considered to be an important aspect of wound healing, with the extent of anisotropy determining the mechanical integrity of new tissue.

McDougall et al. [2006] adopted a hybrid approach, spanning two length scales: fibroblasts at the cell-scale were modelled as discrete entities while ECM and growth factors were modelled as continua at the tissue-scale. The effects on collagen alignment of growth factors such as TGFβ, which has been shown to influence scarring [Shah et al., 1992, Gabbiani, 2003], were investigated. Their results suggested that decreasing the sensitivity of fibroblast orientation to growth factor gradients could be a possible direction for anti-scarring treatments. A more random fibroblast orientation would result in a lower degree of collagen alignment.

Cumming et al. [2010] developed a two-dimensional hybrid model of dermal healing that accounts for cells, chemicals and fibres acting across three different length scales. As in McDougall et al. [2006], they investigated the effects of TGFβ on healing and subsequent scarring. They found that reducing the number of TGFβ receptors on macrophages and fibroblasts resulted in a smaller degree of alignment of collagen fibres, interpreted as reduced scarring. This is because fibroblasts synthesise collagen fibres in the direction of migration. Therefore, consistent with the results of McDougall et al. [2006], less directed fibroblast migration results in more randomised

collagen orientation.

More recently, Segal et al. [2012] focussed on the contribution that collagen accumulation makes to the healing of a wound. Although most models of dermal healing comprise a system of PDEs, Segal et al.'s model involves a system of time-dependent ODEs and tracks changes in the levels of pathogens, inflammatory cells, collagen and fibroblasts. In addition, fibroblasts are assumed to progress through phases of proliferation, migration and activation. During the activation phase, fibroblasts produce collagen. The model was validated against collagen accumulation experiments and then used to investigate therapies, such as increased oxygen concentration and fibroblast proliferation. Although complexity was reduced by adopting an ODE framework, the model contains 36 parameters that need to be determined experimentally. Additionally the model neglects the contribution of contraction to wound closure.

Murphy et al. [2011] also developed an ODE model of dermal wound closure, that accounts for wound contraction. Morphoelasticity is used to describe growth in the tissue and the mechanical properties and stresses involved. Spatial variations are neglected and the domain is compartmentalised into the wound space and undamaged tissue. The model accounts for fibroblasts, ECM and strain inside and outside the wound and myofibroblasts and TGFβ inside the wound. The rate at which fibroblasts switch to myofibroblasts is assumed to be controlled by TGFβ and mechanical stress. The model reproduces behaviour comparable to experimental data from normal healing [McGrath and Simon, 1983] and is used to investigate the effects of the duration of the inflammatory response (varied TGFβ decay rate) and the rate of myofibroblast apoptosis on wound contraction. A longer inflammatory response or reduced rate of apoptosis results in a higher number of myofibroblasts and, therefore, greater contraction of the wound.

1.3.3 Models of epidermal and dermal healing

Vermolen and Javierre [2012] have developed a mechano-chemical model of wound healing that accounts for the epidermis and dermis. Their model comprises a system of 8 parabolic PDEs and is solved using a finite element method so that healing in complex geometries can be simulated. Their model includes equations for dermal wound contraction based on work by Tranquillo and Murray [1992], a vascular network of angiogenesis [Gaffney et al., 2002], and epidermal wound closure as an extension of the original model for epidermal healing by Sherratt and Murray [1990]. The key dependent variable linking epidermal and dermal healing is the oxygen concentration, a nutrient vital for healthy healing that is supplied to both layers by the evolving vascular network. Although the model is based on extensions to models developed by other authors, it provides a more complete description of healing by considering several overlapping processes in both the epidermis and dermis. It is also important to note that the model contains 28 parameters, and that these were estimated from a range of different experimental and theoretical papers.

1.3.4 Models of diabetic wound healing

As well as modelling normal healing, several models focus on healing pathologies, the most prevalent being the diabetic wound. Many of the models discussed above consider growth factor control as a method of treatment. Flegg et al. [2010] model the response of chronic wounds to treatment via HBOT, aiming to identify optimal protocols for its delivery.

Diabetic wounds are often characterised by a prolonged inflammation phase. This has been modelled using an ODE framework [Waugh and Sherratt, 2006] by considering macrophages and TGFβ species. The authors distinguish between inflammatory and repair macrophages and assume that the proportion of inflammatory macrophages is greater in a diabetic than a normal wound. Simulations show that both populations

decrease to almost zero in a normal wound, but persist in the diabetic wound. The initial proportion of inflammatory to repair macrophages is the key parameter in the persistence of inflammation.

The effects of the inflammatory response have also been studied in a PDE framework that considers fibroblasts, macrophages, capillaries, wound nutrients and the tissue mechanics [Xue et al., 2009]. The ECM is modelled as a viscoelastic material with a stress-strain relationship similar to Tranquillo and Murray [1992]. Additionally Xue et al. [2009] assume that the wound pressure is proportional the the ECM density. By introducing pressure, the model could be used to investigate the effects of applying external pressures to the healing wound, although the authors leave this to future work.

1.4 Large deformations and morphoelasticity

With growth being fundamental to the normal development of biological tissues, the interplay between growth and mechanics is of great importance. To develop and expand clinical treatments and preventions, a primary objective is to understand how growth processes are disrupted in pathology. In general, growth is a complex process regulated by the biochemical and biomechanical environment. Depending on the function and location of the tissue, growth can occur through different mechanisms. For example, hard tissues, such as bone, nails, horns, antlers and seashells, undergo surface growth, which can be described by accretion or removal of material on a tissue surface. Since hard tissues undergo small deformations, they are usually modelled using the theory of linear elasticity [Cowin and Firoozbakhsh, 1981, Hart, 1990]. In soft tissues, growth is typically distributed throughout the material and is termed volumetric growth.

Soft tissues are more easily deformable than hard tissues. As a result, finite defor-

mation and elasticity theories are often needed to accurately describe their behaviour [Humphrey, 2003]. The components of biological soft tissues ensure that mechanical integrity, strength and flexibility are maintained [Fung, 1990]. Biological tissues are geometrically and structurally complex. Constitutive assumptions are developed in order to describe this complexity [Mooney, 1940, Rivlin, 1948a]. Fibres and cells within a tissue are typically oriented anisotropically to facilitate functionality [Fung, 1990].

The mechanics of soft tissues are often best represented by hyperelastic materials whose response to stress is characterised by a strain-energy function. Selecting appropriate strain-energy functions for hyperelastic materials is an important area of research that requires experimental observations [Fung, 1993]. Assuming a hyperelastic material in the framework of finite elasticity, growth can be modelled by decomposing the deformation gradient into a growth tensor and an elastic tensor. This decomposition is appropriate when the growth timescale is considered to be slow in comparison to the elastic timescale. The growth tensor describes the local addition of mass, and the elastic tensor describes the elastic reorganisation, ensuring compatibility of the material. This separability hypothesis was first proposed by Skalak et al. [1982] and then formulated for differential growth by Rodriguez et al. [1994].

Continuum mechanics and non-linear elasticity not only offer a natural framework for studying growth but they also provide information about the stresses experienced by the material. The feedback between stress and growth is important in elastic tissues. The growth of some soft tissues has been shown to be regulated by stress. For example hypertrophy of the arterial wall under high loading [Fung, 1990] or the growth of solid tumours [Ambrosi and Mollica, 2004]. Differential growth often results in residual stress in the material. Residual stress can be defined as the stress that remains in a tissue after external loads have been removed. The existence of residual

stress suggests that the body is incompatible in a stress-free grown state and this can be demonstrated experimentally by performing cuts in a tissue and observing its deformation. Using this technique, evidence of residual stress in tissues such as blood vessels [Vaishnav and Vossoughi, 1987, Liu and Fung, 1988], the heart [Omens and Fung, 1990], the trachea [Han and Fung, 1991] and the brain [Xu et al., 2009] has been found.

Morphoelasticity provides a mathematically tractable approach to study the consequences of growth and remodelling. It has been applied to a number of biological tissues, including arteries [Taber and Eggers, 1996, Rachev et al., 1998, Taber, 1998, 2001, Goriely and Vandiver, 2010], the heart [Lin and Taber, 1995], the trachea [Moulton and Goriely, 2011], plant stems [Goriely et al., 2010], tumours [Ambrosi and Mollica, 2004, Ciarletta et al., 2011] and the skin [Ciarletta and Ben Amar, 2012, Wu and Ben Amar, 2015]. With few exceptions [Xu et al., 2009], most models restrict attention to symmetrical geometries, providing a biologically reasonable simplification and allowing for further analysis, such as the stability of the system [Goriely and Vandiver, 2010, Moulton and Goriely, 2011, Wu and Ben Amar, 2015].

Despite its wide applicability, few mathematical models of wound healing incorporate non-linear elasticity. Yang et al. [2013] developed a biomechanical model of wound healing that focussed on the formation and remodelling of scar tissue, which has non-linear elastic properties. Wu and Ben Amar [2015] used the decomposition of the deformation tensor to study the closure of a circular epidermal wound. Contraction of the non-linear elastic tissue was assumed to be generated by circumferential resorption analogous to a model of embryonic wound healing [Taber, 2009].

Morphoelasticity offers a simple framework for understanding the responses of the dermal tissue to growth processes and applied forces such as wound contraction. Further information about morphoelasticity is included in Chapter 3 where we develop the governing equations and present an example problem before using it to derive a

model of dermal wound healing in Chapter 4.

1.5 Summary

In this chapter we have reviewed the biological and mathematical literature relevant to wound healing. With the gold standard of wound care research aimed at scarless healing, contraction of the granulation tissue and scar remodelling is a major theme in models of dermal healing. However, the effects of wound contraction on the dermal tissue surrounding the wound could also have a major influence on tissue growth and the rate of wound closure. In this thesis we take an alternative approach and study the tissue surrounding the wound. Motivated by our experimental collaboration and the demand for better treatments for diabetic wounds, we consider the main processes regulating the rate of wound closure and aim to identify factors that can disrupt normal healing.

An optimal mathematical model for wound healing, as stated by Cukjati et al. [2000], should satisfy the following criteria:

“

- It should have a minimum number of parameters.
- Variables described in the model should be measurable so that collection of experimental data is possible.
- It should give a good fit to the experimental data.
- It should be capable of predicting the wound healing process with reasonable accuracy.
- It should have a biophysical basis.
- It should improve the general understanding of wound healing. ”

These criteria underpin the research presented in this thesis.

1.5.1 Problems addressed in this thesis

Although there is a vast literature dedicated to modelling wound healing, there are still many open problems. In this thesis we address the following:

1. **Development of simple models of wound healing easily comparable with data:** Many current mathematical models have a large number of parameters and are, hence, difficult to validate against available data. We aim to develop a model consistent with the available data to enable for model validation and comparisons between the data and model solutions. Within our established experimental collaboration, the models should also generate predictions that can subsequently be tested experimentally.

2. **Differences in normal and diabetic healing:** A main aim of this work is to identify processes which may be compromised in diabetic healing and other healing abnormalities. The differences between diabetic and normal healing are vast. Consequently, it is difficult to find a generic treatment. Many biochemical differences have been discovered but information about mechanical differences is lacking. By formulating a mechanical model for wound healing we aim to learn more about mechanical disruptions associated with diabetes.

3. **The influence of the biomechanical environment on dermal wound healing:** Biological soft tissues typically undergo volumetric growth. As a result, residual stresses can be present within the tissue. This is observed when the dermal edges retract after injury. Stresses within the tissue can regulate growth or tissue remodelling. During repair the dermal tissue is subject to growth and contraction. By improving understanding of the effects that stress has on growth and the rate of wound closure, we can suggest mechanically motivated experiments and test possible treatments.

4. **Integration of the biochemical and biomechanical environment:** Wound closure proceeds by a combination of synthesis of new tissue and wound contraction. These processes are regulated by fibroblasts. The behaviour of fibroblasts is determined by chemical and mechanical stimuli. By developing a mechanistic model of dermal wound healing accounting for the biomechanical and biochemical environment we can investigate how the combination of these stimuli influence dermal healing.

The objective of this work is to develop simple mathematical models of wound healing that will help us to better understand the growth and contraction processes and how pathologies can arise from a disruption or dysregulation of the biochemical and/or biomechanical environment.

1.5.2 Thesis structure

In this chapter we have provided an overview of the biology of wound healing, reviewed some of the mathematical approaches and models in this area and introduced a modelling framework which will be used in later chapters. The remainder of this thesis is organised as follows:

In Chapter 2 we present a simple, phenomenological model that couples epidermal and dermal healing of a full thickness circular wound. Motivated by the level of the available data we develop a spatially-averaged model formulated as a system of time-dependent ODEs with an aim to keep the number of parameters to a minimum. The model focusses on what we consider to be the main processes contributing to closure of a full thickness wound: proliferation in the epidermis and growth and contraction in the dermis. The governing equations are derived by coupling mass balances for the epidermal and dermal tissues to a phenomenological momentum balance for the dermis in which friction, elastic recoil and contraction forces are assumed to be in equilibrium. The time-dependent variables of the model are directly related to the

experimental observables. This model is used to determine differences between normal and diabetic healing and the application of a theoretical treatment is tested.

Driven by the conclusions and limitations of this first model we turn to a more detailed spatially-resolved framework. Although most models of wound contraction assume linear elasticity, the initial large retraction of the wound edge upon injury [McGrath and Simon, 1983] suggests that a small strain approximation may not be appropriate and, hence, we adopt a non-linear elastic framework. In Chapter 3 the theory of morphoelasticity is introduced and the equations of motion are derived. We demonstrate the use of this framework by presenting an example of growth in an elastic cylinder.

In Chapter 4, the epidermis is neglected and the dermal tissue is viewed as a hyperelastic cylinder that surrounds the wound and is subject to symmetric deformations. We adopt a morphoelastic framework so that the total deformation of the tissue can be decomposed into an addition of mass and an elastic response. This approach allows us to investigate how interactions between growth and stress influence dermal wound healing. Contraction of the wound is governed by a phenomenological law by which radial tension is imposed at the wound edge and growth is formulated such that tension induces addition of material.

In Chapter 5 we compare the two modelling approaches. In order to compare results and conclusions with the previous time-dependent ODE model, we simplify the morphoelastic model by neglecting body forces and assuming growth is constant and localised in a region close to the wound margin. The underlying mechanisms and results of the two modelling approaches can then be directly contrasted.

Missing in these models however is a mechanistic description for growth and contraction. Although the full spatially-resolved morphoelastic model considers tissue mechanics, it lacks biochemical stimuli for growth with contraction driven phenomenologically. Hence, in Chapter 6, the biochemical environment is introduced by cou-

pling the growth and mechanics of the dermal tissue, represented in the morphoelastic framework, to partial differential equations describing the dynamics of fibroblasts, the main cell type responsible for dermal healing and TGFβ, a regulating growth factor. We perform numerical simulations of this model to understand how disruption of mechanical and chemical feedback can lead to abnormal (either excessive or insufficient) wound healing.

Finally, in Chapter 7 we discuss our results and identify possible directions for further investigation.

1.5.3 Publications

Some of the work presented in this thesis has been published in international peer reviewed journals:

Chapter 2: LG Bowden, PK Maini, DE Moulton, JB Tang, XT Wang, PY Liu, HM Byrne. An ordinary differential equation model for full thickness wounds and the effects of diabetes. *J. Theor. Biol.,* (361):87–100, 2014.

JB Tang, XT Wang and PY Liu designed and performed the experiments. LG Bowden did the modelling and wrote the manuscript under the supervision of HM Byrne, DE Moulton and PK Maini.

Chapter 4: LG Bowden, HM Byrne, PK Maini, DE Moulton. A morphoelastic model for dermal wound closure. *Biomech. Model. Mechanobiol.,* 10.1007/s10237-015-0716-7, 2015.

LG Bowden did the work and wrote the manuscript under the supervision of HM Byrne, DE Moulton and PK Maini.

Chapter 2

An ordinary differential equation model for epidermal and dermal wound healing

2.1 Introduction

Existing models of wound healing have tended to focus on either epidermal or dermal healing. Full thickness wounds injure the epidermis and the dermis, and therefore require both layers to heal simultaneously. In healthy skin these layers interact both chemically and mechanically. Reaction-diffusion models have been proposed to study the influence of biochemical interactions between the two layers and shown to generate spatial patterns [Cruywagen and Murray, 1992]. In terms of wound healing, however, this coupling is sparsely documented. There are also few mathematical models; these are discussed briefly below.

Mathematical models involving growth factor control of epidermal wound healing have focussed on epidermal growth factor (EGF), which is produced in the epidermis. However, the activity of keratinocyte growth factor (KGF), which is produced by

fibroblast cells, is restricted to epidermal cells and has been shown to be a stronger mitogen than EGF [Marchese et al., 1990]. Considering KGF as a mediator of epidermal-dermal interactions, Wearing and Sherratt [2000] developed a biochemical model via a system of PDEs, representing mass conservation of KGF, cell receptors and epithelial cell density. They used their model to identify an optimal concentration of KGF for the rate of re-epithelialisation and found that a concentration as high as that found in the wound following injury can cause a decrease in the rate of healing. A simplified submodel (by neglecting the cell density equation) was studied to predict the effects of KGF concentration and epidermal-dermal interactions on the signalling range of KGF. Although increasing both KGF concentration and the rate of interactions between receptors and the growth factor individually result in a larger signalling range, the interaction rate had a much larger impact.

Menon et al. [2012] extended this work to include dermal healing. Although they considered healing of the epidermis and the dermis, they focussed on biochemical stimuli and ignored dermal contraction. They accounted for several growth factors thought to be involved in crosstalk between fibroblasts and keratinocytes, such as platelet-derived growth factor (PDGF) which is produced by the degrading clot, and TGFβ, whose production is regulated by fibroblasts. Simulation results were obtained for different cases, including normal healing, prolonged inflammation, hypoxic conditions and application of treatments. The model predicted that prolonged inflammation can cause excessive collagen production, which may result in hypotrophic scarring.

As discussed in Chapter 1, Vermolen and Javierre [2012] couple epidermal and dermal healing through the supply of oxygen to the epidermis from a vascular network in the dermis. Although the coupling is biochemical, they also account for dermal contraction and develop a biomechanical model formulated as a system of PDEs. Their main results relate to epidermal wound closure. Model simulations show that,

in the early stages of healing, cells in the epidermis migrate towards the wound, whereas at later stages, cells proliferate perpendicular to the surface of the skin. These observations are in agreement with experiments with the model revealing that qualitative changes in the oxygen profiles provide a possible explanation for this behaviour. At early times, simulations show an oxygen gradient parallel to the skin surface with no significant change in the perpendicular direction. However, for later times, the gradient of the oxygen concentration becomes significant in the direction perpendicular to the surface of the skin, stimulating cell movement and proliferation upwards.

The models described above (and in Chapter 1) have increased our understanding of the individual processes involved in wound healing. However, given that these processes overlap and interact in both time and space, models that consider them in combination may provide a more realistic description of wound healing. As well as the need to consider how the different processes in healing interact, we note that it is difficult to validate detailed mathematical models given the quality of data currently available. Therefore, in this chapter we develop a simple model, formulated as a system of time-dependent ODEs, in terms of variables that can be easily measured, namely wound areas. At a gross level, wound closure occurs due to proliferation and contraction, so these form the primary components of our model. By focussing on the net effect of these processes, rather than on the underlying mechanistic details, we develop an idealised model, containing a small number of parameters that can be used to test hypotheses about how diabetes modifies proliferation and contraction. We describe below the experiments and data that motivated this theoretical study.

2.1.1 The experimental data

In order to characterise differences in wound healing between non-diabetic and diabetic mice, our collaborators conducted a series of experiments on non-diabetic mice

and mice in which type II diabetes was induced by deleting the leptin receptor gene [Coleman, 1978]. Two full thickness wounds of radius 4 mm were inflicted on the backs of the mice, bilateral to the spine, using surgical scissors. Three non-diabetic and three diabetic mice were euthanised each day post wounding; thus six wounds were harvested for each time point. This continued until wound closure, defined by closure of the epidermal gap (day 21 in the non-diabetic group and day 33 in the diabetic group). Histological samples were taken in order to measure the epidermal and dermal gaps.

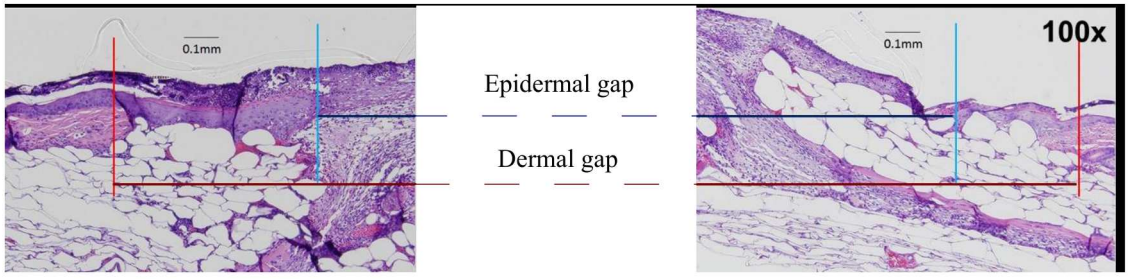

Figure 2.1: Histological slides. An example of the histological samples obtained from a mouse wound. The invading fronts of the epidermis and dermis are identified from staining, and the epidermal and dermal gaps are measured. Image provided by our collaborators.

From the histological data (see Figure 2.1), invading fronts in both the epidermis (due to epithelial cells growing over granulation tissue) and the dermis (due to contraction and new dermal tissue) were visible. Time courses obtained by averaging the epidermal and dermal wound areas associated with the non-diabetic and diabetic groups are presented in Figure 2.2. The data in Figure 2.2 support the view that wound healing occurs over different timescales. For both the epidermal and dermal curves we observe a rapid increase in wound area immediately after wounding.[1] After this initial recoil, the epidermal wound area gradually decreases until closure. As a

[1]In fact, in the non-diabetic case the wound initially contracts followed by a recoil. We do not know what causes this behaviour, so for the purpose of this work we begin the modelling after this contraction and before the recoil phase, given by the first data point in Figure 2.2(a).

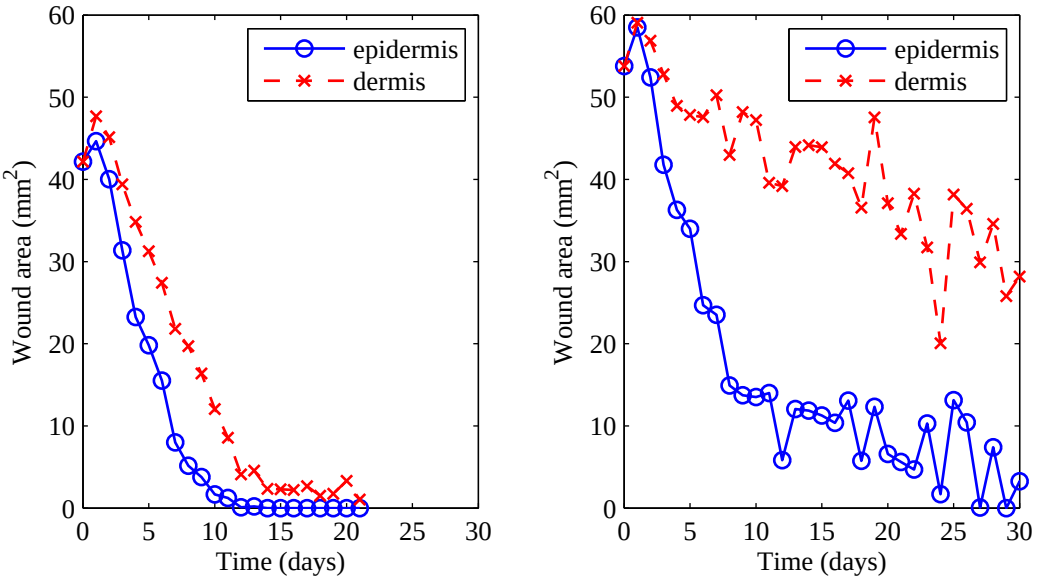

(a) Non-diabetic (b) Diabetic

Figure 2.2: Wound areas from experimental data. Average wound areas for the epidermis and the dermis in both non-diabetic and diabetic mice were recorded over a time period of 21 and 33 days. The sample size for each day is six wounds, two on each of the three mice. The initial wound radius was designed to be 4 mm and the wounds remained approximately circular throughout the experiments. Figures produced from data provided by our collaborators.

consequence of granulation tissue synthesis in the dermal gap (defined by the dermal wound space), the dermal wound never fully closes. By comparing the data in Figures 2.2(a) and (b) we see that the diabetic epidermis closes 9 days later than the non-diabetic epidermis, with the diabetic dermis healing even more slowly than the non-diabetic dermis. These differences indicate that a larger dermal gap remains when the diabetic wound closes, a feature which could result in a more prominent scar. We observe that, for both non-diabetic and diabetic mice, the epidermis advances more rapidly into the wound space than the dermis, forming an overhang of the epidermal layer, which grows on top of the granulation tissue synthesised in the wound space. While it is evident from the data presented in Figure 2.2 that healing in diabetic wounds is delayed, it is not clear which processes are responsible for the compromised healing.

2.1.2 Outline

In Figure 2.3 we present a schematic diagram which clarifies how the surface areas of the wound space, the healing epidermis and dermis, are defined and inter-related. In this diagram, the granulation tissue that is covered by new epidermis is the region of re-epithelialisation. The granulation tissue in the epidermal gap is not measured in the data presented and is therefore not discussed in this work.

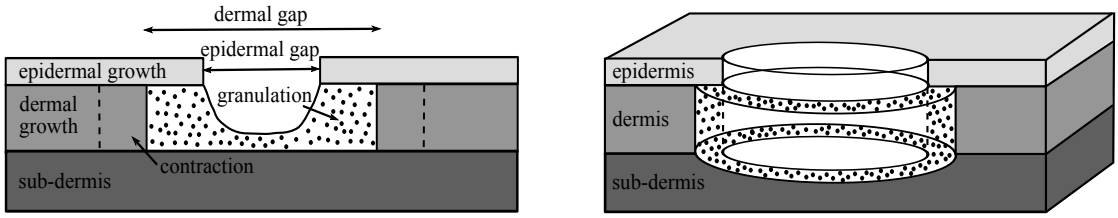

(a) Definition of terms (b) Radially symmetric interpretation

Figure 2.3: Schematic representation of the wound space. The data given in Figure 2.2 show the epidermal layer healing more quickly than the dermal layer, growing over the granulation tissue (given by the dotted area) and, hence, protruding into the wound space. The schematic diagram shows the arrangement of the epidermal and dermal tissues during healing, in preparation for introducing the mathematical model and its dependent variables in the next section.

In this chapter, rather than developing a detailed model, we model in a simplified manner the main processes that contribute to the closure of a full thickness wound: proliferation and migration of epithelial cells in the epidermis; tissue growth in the dermis; and contraction of the dermal tissue. Our experimental data detail how the wound areas of the epidermis and the dermis change over time. Therefore, in Section 2.2, we develop a model that comprises time-dependent ODEs, with the epidermal and dermal wound areas as the dependent variables, and that can be compared with the given data. In Section 2.3 we use asymptotic techniques to show how our model can be analysed on different, well-defined timescales and how the processes that drive healing change from one timescale to the next. In Section 2.4 we perform a focussed parameter sensitivity analysis on our model, concentrating on those parameters that are thought to be compromised in diabetic healing. By fitting the model to

the experimental data from non-diabetic and diabetic wounds, we are able to estimate the system parameters and identify those which differ markedly between non-diabetic and diabetic wounds. Finally, in Section 2.5 we summarise our results and explain how they could be used to suggest strategies for improving wound healing for diabetic patients.

2.2 Model development

Since the data presented in Figure 2.2 are spatially-averaged, we formulate our model as a system of time-dependent ODEs, relating the changes in wound areas of the epidermis and the dermis to the dominant processes driving wound closure. The governing ODEs represent: conservation of mass of new epidermal tissue; conservation of mass of new dermal tissue; and a phenomenological force balance for the dermis. When developing our model we note that the experimental wounds were formed by excising a circular region of tissue of radius 4 mm, with the depth of epidermal and dermal tissues approximately 0.1 mm. For simplicity, and since the wound radii were much greater than their depth, we view the wounds as two-dimensional, and focus on how the area of the epidermis and dermis change during healing by supposing that the wounds are radially symmetric, an assumption that is consistent with the histology (see Figure 2.4). We will consider the time duration of healing to be from initial injury until closure of the epidermis. During this time period we do not account for remodelling of the dermis post closure or the synthesis of granulation tissue in the wound space.

The schematic diagram presented in Figure 2.5 illustrates the wound geometry that we consider and introduces the system variables. Due to retraction (recoil), immediately following wounding, the wound increases in area from its initial value of A_0 to A_R, both constant values determined from the data. The areas of the epidermal

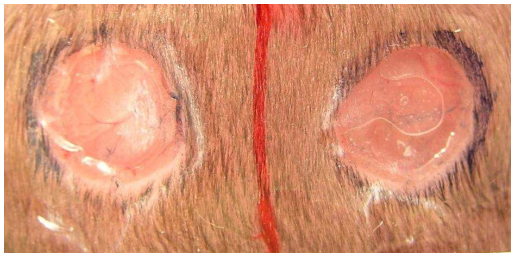

Figure 2.4: Photograph of the wounds. Two circular wounds were inflicted on each mouse, one on each flank. The wounds were photographed with the dressing on, after the day 0 measurement. We observe that the wounds remain approximately circular. Image provided by our collaborators.

and dermal wounds at time t are denoted $A_e(t)$ and $A_d(t)$, respectively. In the dermis, where we consider the combined effects of growth and contraction, it is convenient to introduce an additional variable $A_s(t) \in (A_d, A_R)$ to characterise the dermal wound. We suppose that the area of the dermal wound healed by new tissue is $A_R - A_s$ and deduce that the amount of contraction experienced by the dermal tissue will be proportional to $A_s - A_d$. We remark that both $A_e(t)$ and $A_d(t)$ can be directly related to the epidermal and dermal data presented in Figure 2.2, whereas $A_s(t)$ is not discernible from the data.

2.2.1 Mass balance for new epidermal tissue

Following Clark [1988], we suppose that the epidermis heals by a combination of cell migration and proliferation. Early work on cell proliferation in mouse epidermis revealed that mitotic activity was abnormally high in an annulus of width 1 mm surrounding the wound [Bullough and Laurence, 1960]. More recently, Usui et al. [2008] showed that, in humans, epithelial cell migration occurs at the wound margin, and that proliferation is upregulated in an area surrounding the wound, which can be up to 1 cm from the wound edge. Such behaviour was found in both non-diabetic and diabetic wounds. Upregulation of mitosis at this distance from the wound has also been observed in rat corneal epithelial wounds of varying sizes [Sandvig et al.,

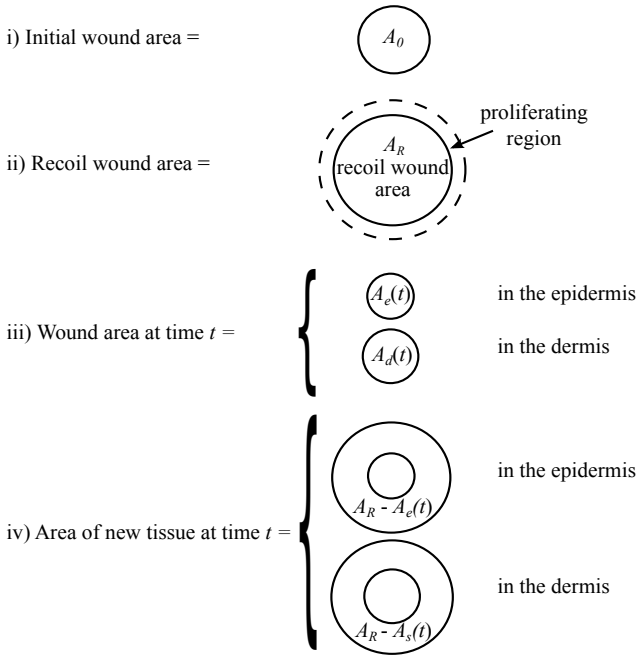

Figure 2.5: Definition of wound areas and system variables. A radially symmetric interpretation of the wound areas. (i) The initial wound area of the epidermal and dermal layers is given by A_0. (ii) Following wounding the tissues in both layers retract to an area $A_R > A_0$. Proliferation in both the epidermis and dermis is assumed to be localised to a small annular region surrounding the recoiled wound. (iii) The areas of the epidermal and dermal wounds are given by the time dependent variables $A_e(t)$ and $A_d(t)$, respectively, and typically $0 \leq A_e(t) \leq A_d(t)$. (iv) As the epidermal tissue proliferates, the area of new epidermal tissue is given by $A_R - A_e(t)$. Similarly, the area of new dermal tissue is given by $A_R - A_s(t)$, where the time dependent variable $A_s(t)$ is the area of the relaxed dermal wound. The dermal wound is also subject to contractile forces, with the amount of contraction at time t assumed to be proportional to the area difference $A_s - A_d$.

2009]. Following Usui et al. [2008], we localise proliferation to the new epidermal tissue and a small annulus surrounding the initial wound margin.[2] Cells from the wound margin are assumed to migrate towards the wound centre to assist in closing the wound. We assume further that the net effect of these processes can be described by a modified logistic growth law, in which the growth rate contains contributions from proliferation in the newly synthesised tissue and an additional area surrounding

[2]We note that, qualitatively, our results are robust to this choice. In Appendix A.5 we compare our results for the chosen form of epidermal growth rate with that which is proportional to the wound circumference.

the initial wound margin. By applying the principle of mass balance to the new epidermal tissue, $A_R - A_e(t)$, we deduce that:

$$\frac{\mathrm{d}}{\mathrm{d}t}(A_R - A_e(t)) = r^*(A_R - A_e(t))\left(1 - \frac{A_R - A_e(t)}{A^*}\right), \tag{2.1}$$

where A^* is its carrying capacity and the growth rate r^* has the form:

$$r^* = r\left(1 + \frac{\nu A_R}{A_R - A_e(t)}\right). \tag{2.2}$$

In Equation (2.2), the parameter r represents the assumed constant rate at which new epidermal tissue grows, while the area-dependent term represents additional growth from the annulus surrounding the initial wound margin, the parameter ν indicating the proportion of the area, A_R, which contributes to this effect. Epithelial cells are known preferentially to migrate over a smooth, moist surface, such as the new dermal tissue, rather than granulation tissue [Krawczyk, 1971, Martin, 1997]. A possible reason for this is that the granulation tissue is filled with fibrin and cellular debris, which the epithelial cells need to remove before advancing [Krawczyk, 1971]. We account for this by assuming that, in Equation (2.1), the carrying capacity A^* depends on the dermal wound area. The maximum value for the carrying capacity of new epidermal tissue is A_R, corresponding to the dermis being fully healed ($A_d = 0$). As the dermal wound area, $A_d(t)$, decreases, the new dermal tissue offers a platform for preferential growth and migration of epidermal tissue, and the carrying capacity will increase. We therefore assume that the carrying capacity takes the following form:

$$A^* = A_R - \gamma A_d(t), \tag{2.3}$$

where the parameter $\gamma \in [0, 1)$ measures the degree to which the carrying capacity depends on the dermal wound area. We remark that if $\gamma = 0$, then the epidermis

heals independently of the dermis, with a carrying capacity of A_R.

Substituting Equations (2.2) and (2.3) into (2.1), we obtain the following ODE for $A_R - A_e(t)$, the area of new epidermal tissue at time t:

$$\frac{\mathrm{d}}{\mathrm{d}t}(A_R - A_e(t)) = r(A_R - A_e(t) + \nu A_R)\left(1 - \frac{A_R - A_e(t)}{A_R - \gamma A_d(t)}\right). \tag{2.4}$$

2.2.2 Mass balance for new dermal tissue

In the dermis we assume that contraction and growth drive healing. Both processes are regulated by fibroblasts which accumulate close to the wound edge and in the wound space following injury. When modelling proliferation in the dermis, we consider two mechanisms. Firstly, there is a basal proliferation from the healthy skin, which is localised close to the wound. Secondly, the growth rate of the new and surrounding tissue is enhanced by the amount of stretch it experiences. Such mechanosensitive behaviour is known to occur during dermal wound healing [Chiquet, 1999, Pietramaggiori, 2007]. As for epidermal tissue, we assume that the growth of new dermal tissue follows a modified logistic growth law. By applying the principle of mass balance to the new dermal tissue, $A_R - A_s(t)$, we deduce that:

$$\frac{\mathrm{d}}{\mathrm{d}t}(A_R - A_s(t)) = k^*(A_R - A_s(t))\left(1 - \frac{A_R - A_s(t)}{A_R}\right), \tag{2.5}$$

where k^* is the growth rate of the dermal tissue and A_R is the carrying capacity. As with the epidermal growth rate, we write:

$$k^* = k\left(1 + \frac{\nu A_R}{A_R - A_s(t)}\right), \tag{2.6}$$

where the first term represents the growth rate of the new dermal tissue and the second term the contribution to growth from the annulus surrounding the initial wound margin. For simplicity we assume that the areas of the annuli surrounding

the wound that contribute to epidermal and dermal tissue are identical (ν is the same in Equation (2.2) and (2.6)). We decompose the growth rate k into basal and mechanosensitive contributions. In order to quantify the mechanosensitive contribution, we introduce the normalised area of additional tissue due to contraction, $\Psi \in [0, 1)$:

$$\begin{aligned}\Psi &= \frac{\text{area of stretched tissue} - \text{area of relaxed tissue}}{\text{area of stretched tissue}} \\ &= \frac{(A_R - A_d(t) + \nu A_R) - (A_R - A_s(t) + \nu A_R)}{A_R - A_d(t) + \nu A_R} \\ &= \frac{A_s(t) - A_d(t)}{A_R - A_d(t) + \nu A_R},\end{aligned} \tag{2.7}$$

so that $\Psi \in [0, 1)$ provides a measure of the stretch experienced by the dermal tissue ($\Psi = 0$ if $A_s = A_d$). We assume that k is a linearly increasing function of Ψ so that

$$k = k_0 + k_1 \left(\frac{A_s(t) - A_d(t)}{A_R - A_d(t) + \nu A_R} \right), \tag{2.8}$$

where k_0 represents the assumed constant basal growth rate, and the constant of proportionality k_1 represents how mechanosensitive the dermal tissue is.

Substituting Equations (2.6) and (2.8) into (2.5) we obtain the following ODE for $A_R - A_s(t)$, the area of new dermal tissue at time t:

$$\begin{aligned}\frac{\mathrm{d}}{\mathrm{d}t}(A_R - A_s(t)) = &\left(k_0 + k_1 \left(\frac{A_s(t) - A_d(t)}{A_R - A_d(t) + \nu A_R} \right) \right) \\ &\times (A_R - A_s(t) + \nu A_R) \left(1 - \frac{A_R - A_s(t)}{A_R} \right).\end{aligned} \tag{2.9}$$

2.2.3 Force balance for the dermis

In order to close the model, it remains to determine the evolution of $A_d(t)$. In this section we propose a phenomenological force balance to specify $A_d(t)$. The schematic in Figure 2.6 shows the forces we assume to be acting on the dermal tissue. Since the

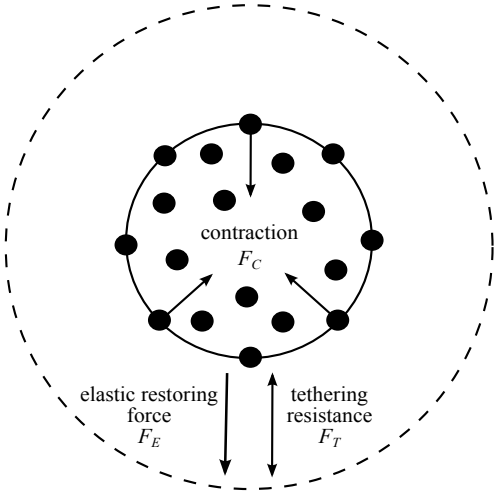

Figure 2.6: Forces acting on the dermis. The inner circle represents the dermal wound area, $A_d(t)$, and the outer dashed circle the relaxed dermal wound area, $A_s(t)$. The elastic response (F_E) pulls the wound open to its relaxed state. Fibroblasts, represented by black circles, arrange on the wound edge and infiltrate the granulation tissue. The fibroblasts contract (F_C) the surrounding tissue in order to decrease the dermal wound area. Friction (F_T) due to tethering to the subdermal layer acts to resist motion of the dermis.

timescale of interest is on the order of days, which is much longer than that associated with inertial effects, we neglect inertial terms and assume that the forces due to the elastic response, contraction and tethering are in equilibrium so that

$$0 = F_E + F_C + F_T, \tag{2.10}$$

where F_E denotes the elastic restoring force, F_C the contractile force and F_T the tethering resistance. We note that, under the assumption of radial symmetry, all forces will act in the radial direction.

When the skin is injured, residual tension causes it to spring open to a relaxed state [Kiehart, 1999]. Given that elastic fibres are distributed throughout the surrounding tissue, we assume that the elastic restoring force, which causes the recoil of the wound, is proportional to the annular area of stretched tissue surrounding the wound,

$A_s(t) - A_d(t)$. We write the radial component of the elastic restoring force as

$$F_E = E(A_s(t) - A_d(t)), \tag{2.11}$$

where E is the elastic restoring force per unit area.

In normal, healthy tissue contraction typically begins 2 to 5 days post wounding, by which time fibroblasts have migrated towards the wound edge with some infiltrating the wound space in response to chemical growth factors released during the inflammatory phase [Stadelmann et al., 1998]. When defining the contractile force we account for this delay by introducing the continuous switch function

$$\mathcal{H}(t - t_c) = \frac{1}{2}\left[\tanh\left(\frac{t - t_c}{\theta}\right) + 1\right], \tag{2.12}$$

where t_c is the time delay in days and θ is the gradient of the switch. Various contraction mechanisms are thought to contribute to the reduction in wound size [Watts et al., 1958, Ehrlich, 1988, Kolodney and Wysolmerski, 1992, Nedelec et al., 2000]. Here we consider a combination of these mechanisms. Fibroblasts within the wound space apply a contractile force causing the granulation tissue to shrink [Ehrlich, 1988, Kolodney and Wysolmerski, 1992]. Due to attachments between the granulation tissue and the healthy dermal tissue, this pulls the wound edge inwards, decreasing the area of the dermal wound. Further, fibroblasts arranged around the wound edge migrate into the wound pulling the surrounding tissue inwards. Since the fibroblasts migrate into the wound and can occupy the dermal wound space, we assume that the contractile force is proportional to the area of the dermal wound.[3]

[3]We note that an additional term proportional to the wound circumference could be considered to separate the two contracting mechanisms, however in order to maintain simplicity we consider only one term.

We can now write the form of the radial component of the contractile force as

$$F_C = c\mathcal{H}(t - t_c)A_d, \tag{2.13}$$

where c is the contractile force per unit area.

Attachments between the dermal and subdermal layers resist the motion of the dermis and we assume that this tethering force is proportional to the velocity of the dermis, $\mathrm{d}A_d/\mathrm{d}t$. Thus, when the wound area is increasing due to the elastic response, $\mathrm{d}A_d/\mathrm{d}t > 0$ and the tethering force resists this motion. Similarly, when the wound area is decreasing due to contraction, $\mathrm{d}A_d/\mathrm{d}t < 0$ and the tethering force resists the contractile force. Guided by these observations we assume, for simplicity, that the tethering force can be written as

$$F_T = \mu\frac{\mathrm{d}A_d}{\mathrm{d}t}, \tag{2.14}$$

where μ is the tethering coefficient.

Combining the above assumptions, we obtain the following ODE relating the dermal wound area, $A_d(t)$, to the relaxed dermal wound area, $A_s(t)$:

$$0 = E(A_s - A_d) - c\mathcal{H}(t - t_c)A_d - \mu\frac{\mathrm{d}A_d}{\mathrm{d}t}. \tag{2.15}$$

2.2.4 Initial conditions

Following excision at $t = 0$ of tissue of area A_0, the wound retracts instantaneously, exposing a larger region $A_R > A_0$. These observations, together with our assumption that the epidermis is not under tension during healing, lead us to prescribe the following initial conditions for the dependent variables:

$$A_e(0) = A_R, \quad A_s(0) = A_R, \quad A_d(0) = A_0. \tag{2.16}$$

The conditions in Equation (2.16) close our phenomenological model of wound healing.

Equations (2.4), (2.9) and (2.15) constitute three coupled ODEs for the time evolution of the wound areas A_e, A_s and A_d. Before presenting model solutions, it is convenient to restate the governing equations, suitably rearranged to clarify their interactions:

$$\frac{\mathrm{d}A_e}{\mathrm{d}t} = -r(A_R(1+\nu) - A_e)\left(\frac{A_e - \gamma A_d}{A_R - \gamma A_d}\right), \tag{2.17a}$$

$$\frac{\mathrm{d}A_s}{\mathrm{d}t} = -\left(k_0 + k_1\left(\frac{A_s - A_d}{A_R(1+\nu) - A_d}\right)\right)(A_R(1+\nu) - A_s)\frac{A_s}{A_R}, \tag{2.17b}$$

$$\mu\frac{\mathrm{d}A_d}{\mathrm{d}t} = E(A_s - A_d) - c\mathcal{H}(t - t_c)A_d, \tag{2.17c}$$

where $\mathcal{H}(t - t_c)$ is defined in Equation (2.12) and the initial conditions satisfy Equation (2.16).

2.2.5 The non-dimensionalised equations

In practice, when constructing numerical and approximate analytical solutions we use a dimensionless version of Equations (2.17). It is convenient to non-dimensionalise the governing equations by introducing the following scalings for the dependent and independent variables:

$$A_e^* = \frac{A_e}{A_R}, \quad A_s^* = \frac{A_s}{A_R}, \quad A_d^* = \frac{A_d}{A_R}, \quad t^* = \frac{t}{T},$$

where T is an appropriately chosen timescale. Dimensionless parameters are defined as follows:

$$\lambda = rT, \quad \beta_0 = k_0 T, \quad \beta_1 = k_1 T, \quad \alpha = \frac{c}{E}, \quad \epsilon = \frac{\mu}{ET}, \quad t_c^* = \frac{t_c}{T}, \quad \theta^* = \frac{\theta}{T}.$$

where the new parameters ϵ and α, respectively, represent the strength of the frictional and contractile forces relative to the elastic force.

By omitting the asterisks we arrive at the following non-dimensionalised system

$$\frac{\mathrm{d}A_e}{\mathrm{d}t} = -\lambda(1+\nu-A_e)\left(\frac{A_e-\gamma A_d}{1-\gamma A_d}\right), \tag{2.18a}$$

$$\frac{\mathrm{d}A_s}{\mathrm{d}t} = -\left(\beta_0+\beta_1\left(\frac{A_s-A_d}{1+\nu-A_d}\right)\right)(1+\nu-A_s)A_s, \tag{2.18b}$$

$$\epsilon\frac{\mathrm{d}A_d}{\mathrm{d}t} = A_s - A_d - \alpha\mathcal{H}(t-t_c)A_d, \tag{2.18c}$$

with initial conditions

$$A_e(0)=1, \quad A_s(0)=1, \quad A_d(0)=\frac{A_0}{A_R}\equiv K_d. \tag{2.18d}$$

The dimensionless parameters λ, β_0, β_1, ϵ, α, t_c, θ and K_d are non-negative constants whose physical interpretations are stated in Table 2.1.

2.3 Model behaviour

We anticipate that Equations (2.18) should reproduce the natural progression of healing, with an initial rapid recoil phase, followed by a period of cell proliferation and tissue growth, with contraction contributing at later stages. The recoil phase occurs within hours of healing. This rapid recoil suggests a large elastic restoring force relative to the resistant force associated with tethering of the dermis to the underlying layers. We therefore expect that ϵ will be small in comparison to the other model parameters. Since we are concerned with the time until wound closure, our timescale of interest is on the order of days. With $0 < \epsilon \ll 1$, we can apply the method of matched asymptotic analysis to Equations (2.18) to verify that the model reproduces the different phases of healing on the appropriate timescales.

The natural timescales of interest are: wound recoil, which occurs for $t = \mathcal{O}(\epsilon)$; before contraction is switched on when $t < t_c$; and, when contraction is activated for $t \geq t_c$. In order for Equations (2.18) to be analytically tractable we approximate the continuous switch function in Equation (2.12) by the Heaviside step function

$$H(t - t_c) = \begin{cases} 0 & \text{for } t < t_c \\ \\ 1 & \text{for } t \geq t_c \end{cases}, \tag{2.19}$$

so that contraction is either on or off. We note that, in the limit as $\theta \to 0$, then $\mathcal{H}(t - t_c) \to H(t - t_c)$ and the numerical solution of Equations (2.18) tends to the asymptotic solution. Exploiting the fact that ϵ is very small, we find asymptotic expansions of the model solutions, $A_e(t), A_s(t)$ and $A_d(t)$.

2.3.1 Approximate solutions

We consider Equations (2.18) and replace the continuous contraction switch, $\mathcal{H}(t-t_c)$, with the Heaviside function, $H(t-t_c)$ in Equation (2.19), in order to clearly separate the system dynamics for $t < t_c$ and $t \geq t_c$, and for analytical tractability. The system we analyse is therefore,

$$\frac{\mathrm{d}A_e}{\mathrm{d}t} = -\lambda(1 + \nu - A_e)\left(\frac{A_e - \gamma A_d}{1 - \gamma A_d}\right), \tag{2.20a}$$

$$\frac{\mathrm{d}A_s}{\mathrm{d}t} = -\left(\beta_0 + \beta_1\left(\frac{A_s - A_d}{1 + \nu - A_d}\right)\right)(1 + \nu - A_s)A_s, \tag{2.20b}$$

$$\epsilon\frac{\mathrm{d}A_d}{\mathrm{d}t} = A_s - A_d - \alpha H(t - t_c)A_d, \tag{2.20c}$$

where the initial conditions satisfy Equation (2.18d).

Since ϵ is small this system gives rise to a boundary layer for $t = \mathcal{O}(\epsilon)$ in which $\mathrm{d}A_d/\mathrm{d}t$ is large and, hence, the solution $A_d(t)$ is rapidly evolving. We first seek the solution on this fast timescale, which we call the inner solution (inside the boundary

layer).

2.3.1.1 Inner solution: $t = \mathcal{O}(\epsilon)$

We rescale time such that $t = \epsilon\tau$ and introduce dependent variables $\bar{A}_e(\epsilon, \tau) = A_e(t)$, $\bar{A}_s(\epsilon, \tau) = A_s(t)$ and $\bar{A}_d(\epsilon, \tau) = A_d(t)$. Since for small times ($t = \epsilon\tau \ll t_c$) $H(t - t_c) = 0$, Equations (2.20) transform on the fast timescale to give

$$\frac{\mathrm{d}\bar{A}_e}{\mathrm{d}\tau} = -\epsilon\lambda(1 + \nu - \bar{A}_e)\left(\frac{\bar{A}_e - \gamma\bar{A}_d}{1 - \gamma\bar{A}_d}\right), \tag{2.21a}$$

$$\frac{\mathrm{d}\bar{A}_s}{\mathrm{d}\tau} = -\epsilon\left(\beta_0 + \beta_1\left(\frac{\bar{A}_s - \bar{A}_d}{1 + \nu - \bar{A}_d}\right)\right)(1 + \nu - \bar{A}_s)\bar{A}_s, \tag{2.21b}$$

$$\frac{\mathrm{d}\bar{A}_d}{\mathrm{d}\tau} = \bar{A}_s - \bar{A}_d, \tag{2.21c}$$

where the initial conditions satisfy Equation (2.18d). We consider a power series expansion in ϵ of the dependent variables of the form

$$\bar{A}_e(\epsilon, \tau) = \bar{A}_{e_0}(\tau) + \epsilon\bar{A}_{e_1}(\tau) + \mathcal{O}(\epsilon^2), \tag{2.22}$$

with $\bar{A}_s(\epsilon, \tau)$ and $\bar{A}_d(\epsilon, \tau)$ formulated in the same manner. Substituting the power series expansions into Equations (2.21) and equating the coefficients of different powers of ϵ it is possible to obtain the following asymptotic expansions,

$$\bar{A}_e(\epsilon, \tau) = 1 - \epsilon\nu\lambda\tau + \mathcal{O}(\epsilon^2), \tag{2.23a}$$

$$\bar{A}_s(\epsilon, \tau) = 1 - \epsilon\left[\nu\beta_0\tau - \nu\beta_1 \log\left((1 - K_d)e^{-\tau} + \nu\right)\right] + \mathcal{O}(\epsilon^2), \tag{2.23b}$$

$$\begin{aligned}\bar{A}_d(\epsilon, \tau) = 1 &- (1 - K_d)e^{-\tau} - \epsilon\left[\nu\beta_0\left(\tau + e^{-\tau} - 1\right) - \beta_1(1 - K_d)e^{-\tau}\tau\right. \\ &-\beta_1\left((1 - K_d)e^{-\tau} + \nu\right)\log\left((1 - K_d)e^{-\tau} + \nu\right) \\ &\left.+\beta_1 e^{-\tau}(1 - K_d + \nu)\log(1 - K_d + \nu)\right] + \mathcal{O}(\epsilon^2).\end{aligned} \tag{2.23c}$$

On this timescale, we deduce that, at leading order, $\bar{A}_d$ increases exponentially, representing the recoil of the wound, while $\bar{A}_s$ and $\bar{A}_e$ remain constant. The expansions in Equations (2.23) break down at $\mathcal{O}(\epsilon)$ for $\tau = \mathcal{O}(\epsilon^{-1})$, implying that for $t = \mathcal{O}(1)$ the solutions depend upon additional processes, i.e. there will be a different dominant balance. The dominant process here is retraction of the dermis.

2.3.1.2 Outer solution: $t < t_c$

As $\tau \to \infty$ the inner solution breaks down and we revert to the original time variable, t. On this timescale we introduce dependent variables $\hat{A}_e(\epsilon, t) = A_e(t)$, $\hat{A}_s(\epsilon, t) = A_s(t)$ and $\hat{A}_d(\epsilon, t) = A_d(t)$ and solve Equations (2.20) with $H(t - t_c) = 0$ since $t < t_c$. For the initial conditions we consider the limit as $\tau \to \infty$ of the solutions in the boundary layer before the expansion breaks down, i.e. to $\mathcal{O}(1)$, giving

$$\hat{A}_e(\epsilon, 0) = \lim_{\tau \to \infty} \bar{A}_e(\epsilon, \tau) = 1, \tag{2.24a}$$

$$\hat{A}_s(\epsilon, 0) = \lim_{\tau \to \infty} \bar{A}_s(\epsilon, \tau) = 1, \tag{2.24b}$$

$$\hat{A}_d(\epsilon, 0) = \lim_{\tau \to \infty} \bar{A}_d(\epsilon, \tau) = 1. \tag{2.24c}$$

For our approximations we will take $\gamma = 0$ in order to obtain an analytical solution for $\hat{A}_e$. This assumption implies that the epidermis does not preferentially grow on the dermis rather than the granulation tissue and, hence, the epidermal and dermal equations decouple. We consider power series expansions of the form

$$\hat{A}_e(\epsilon, t) = \hat{A}_{e_0}(t) + \epsilon \hat{A}_{e_1}(t) + \mathcal{O}(\epsilon^2), \tag{2.25}$$

with $\hat{A}_s(\epsilon, t)$ and $\hat{A}_d(\epsilon, t)$ formulated in the same manner. Substituting the power

series expansions into Equations (2.20) and equating powers of ϵ we obtain,

$$\hat{A}_e(\epsilon,t) \approx \frac{1+\nu}{1+\nu e^{\lambda(1+\nu)t}}, \tag{2.26a}$$

$$\hat{A}_s(\epsilon,t) = \frac{1+\nu}{1+\nu e^{\beta_0(1+\nu)t}} + \epsilon\hat{A}_{s_1} + \mathcal{O}(\epsilon^2), \tag{2.26b}$$

$$\hat{A}_d(\epsilon,t) = \frac{1+\nu}{1+\nu e^{\beta_0(1+\nu)t}} + \epsilon\hat{A}_{d_1} + \mathcal{O}(\epsilon^2), \tag{2.26c}$$

where,

$$\hat{A}_{s_1}(t) = \frac{\beta_1\nu(1+\nu)^2 e^{\beta_0(1+\nu)t}}{(1+\nu e^{\beta_0(1+\nu)t})^2} \log\left(\frac{(1+\nu)e^{\beta_0(1+\nu)t}}{1+\nu e^{\beta_0(1+\nu)t}}\right), \tag{2.27a}$$

$$\hat{A}_{d_1}(t) = \frac{\nu(1+\nu)^2 e^{\beta_0(1+\nu)t}}{(1+\nu e^{\beta_0(1+\nu)t})^2} \left(\beta_0 + \beta_1 \log\left(\frac{(1+\nu)e^{\beta_0(1+\nu)t}}{1+\nu e^{\beta_0(1+\nu)t}}\right)\right). \tag{2.27b}$$

At leading order, on this timescale, $\hat{A}_e$ and $\hat{A}_s$ decrease logistically, representing a proliferative phase in both the epidermis and the dermis. The rates are proportional to $1+\nu$, which represents the area of the active region surrounding the wound. Here we see only basal growth in the dermis since contraction is not yet active, and $\hat{A}_{d_0} = \hat{A}_{s_0}$. However, to $\mathcal{O}(\epsilon)$, $\hat{A}_d$ and $\hat{A}_s$ differ. The appearance of β_1 in the expressions for $\hat{A}_{s_1}$ and $\hat{A}_{d_1}$ leads us to speculate that, for $t > t_c$, mechanosensitive growth will contribute. The dominant process here is basal growth.

2.3.1.3 Transition layer: $t \approx t_c$

As $t \to t_c$ contraction becomes active. We note that for $t \approx t_c$, the change in H will affect the solution $A_d(t)$. We write power series expansions for $A_s(t) = \breve{A}_s(\epsilon,t)$ and $A_d(t) = \breve{A}_d(\epsilon,t)$ of the form

$$\breve{A}_s(\epsilon,t) = \breve{A}_{s_0}(t) + \epsilon\breve{A}_{s_1}(t) + \mathcal{O}(\epsilon^2), \tag{2.28a}$$

$$\breve{A}_d(\epsilon,t) = \breve{A}_{d_0}(t) + \epsilon\breve{A}_{d_1}(t) + \mathcal{O}(\epsilon^2). \tag{2.28b}$$

Substituting the power series expansions into Equation (2.20c) with $H(t-t_c)=1$ and equating powers of ϵ we obtain,

$$\breve{A}_e(\epsilon,t) = \hat{A}_e(\epsilon,t), \tag{2.29a}$$

$$\breve{A}_s(\epsilon,t) = \hat{A}_s(\epsilon,t), \tag{2.29b}$$

$$\breve{A}_d(\epsilon,t) = \frac{\hat{A}_{s_0}}{1+\alpha} + \epsilon\left(\frac{\hat{A}_{s_1} - \frac{1}{1+\alpha}\frac{\mathrm{d}\hat{A}_{s_0}}{\mathrm{d}t}}{1+\alpha}\right) + \mathcal{O}(\epsilon^2), \tag{2.29c}$$

where

$$\hat{A}_{s_0}(t) = \frac{1+\nu}{1+\nu e^{\beta_0(1+\nu)t}}, \tag{2.30}$$

and $\hat{A}_{s_1}(t)$ is given by Equation (2.27a). As contraction becomes active, the solutions $\breve{A}_e$ and $\breve{A}_s$ remain the same as those for $t<t_c$, whereas there is a jump in $\breve{A}_d$ across $t=t_c$. We now observe a contribution to reduction in dermal wound size due to contraction. Now that contraction is active we expect that the difference $\breve{A}_s - \breve{A}_d$ will stimulate mechanosensitive proliferation.

2.3.1.4 Outer solution: $t > t_c$

Contraction is now activated as $t>t_c$. We note that this will affect the solutions A_s and A_d but since we have taken $\gamma=0$ in order to obtain analytical solutions, there will be no change in A_e. We write power series expansions in ϵ for $A_s(t)=\tilde{A}_s(\epsilon,t)$ and $A_d(t)=\tilde{A}_d(\epsilon,t)$ given by

$$\tilde{A}_s(\epsilon,t) = \tilde{A}_{s_0}(t) + \epsilon\tilde{A}_{s_1}(t) + \mathcal{O}(\epsilon^2), \tag{2.31a}$$

$$\tilde{A}_d(\epsilon,t) = \tilde{A}_{d_0}(t) + \epsilon\tilde{A}_{d_1}(t) + \mathcal{O}(\epsilon^2), \tag{2.31b}$$

and take initial conditions which satisfy the previous solutions for $t = t_c$,

$$\tilde{A}_s(\epsilon, 0) = \breve{A}_s(\epsilon, t_c), \tag{2.32a}$$

$$\tilde{A}_d(\epsilon, 0) = \breve{A}_d(\epsilon, t_c). \tag{2.32b}$$

Substituting the power series expansions into Equations (2.20b) and (2.20c) and equating powers of ϵ we obtain,

$$\frac{\mathrm{d}\tilde{A}_{s_0}}{\mathrm{d}t} = -\left(\beta_0 + \alpha\beta_1\left(\frac{\tilde{A}_{d_0}}{1+\nu-\tilde{A}_{d_0}}\right)\right)(1+\nu-\tilde{A}_{s_0})\tilde{A}_{s_0}, \tag{2.33a}$$

$$\tilde{A}_{d_0} = \frac{\tilde{A}_{s_0}}{1+\alpha}. \tag{2.33b}$$

We observe that the equation for $\tilde{A}_{s_0}$ now depends on β_1, indicating that, to $\mathcal{O}(1)$, mechanosensitive proliferation is contributing to the reduction in dermal wound area.

2.3.2 Analytical results

In Figure 2.7 we compare the approximate solutions obtained from the asymptotic analysis with numerical solutions (see Section 2.4) of the full model. On the appropriate timescale, the leading order asymptotic solutions are a good approximation to the numerical solution of the full model. As expected, on timescales outside those for which the asymptotic solutions are valid the agreement between the two solutions decreases. We deduce that the leading order asymptotic solutions account for the dominant processes occurring on the associated timescale.

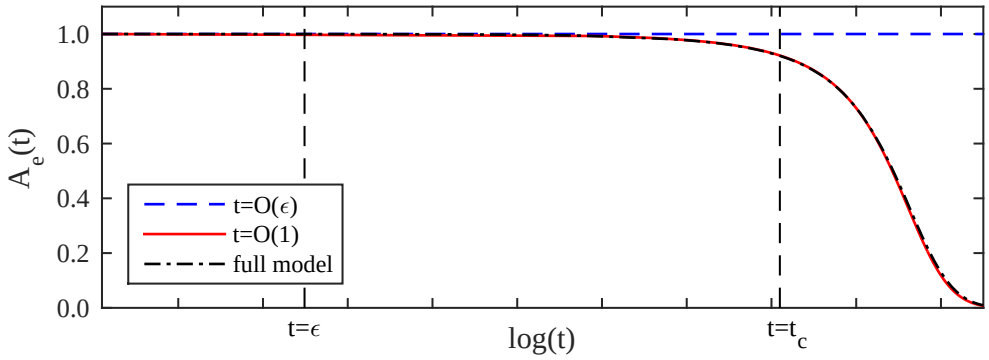

(a) Approximate solutions for A_e.

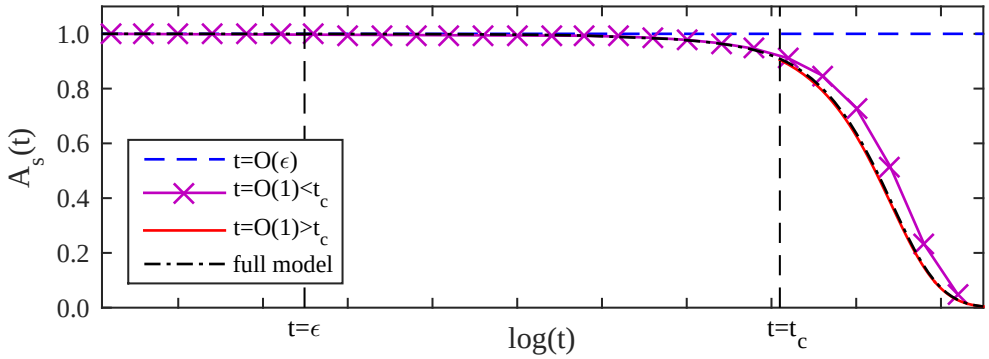

(b) Approximate solutions for A_s.

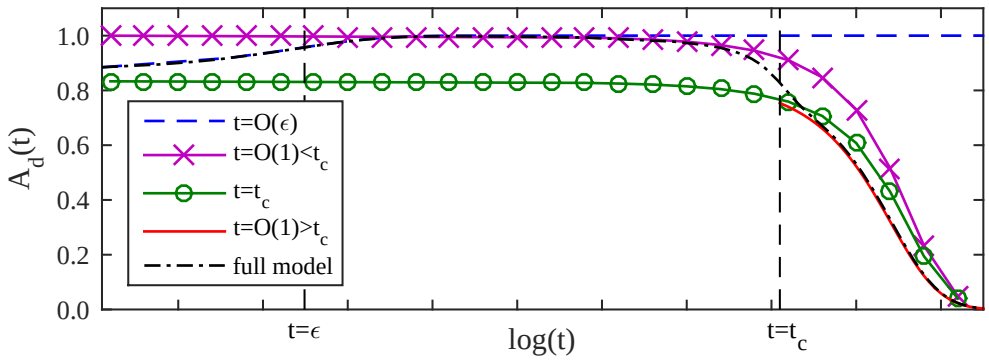

(c) Approximate solutions for A_d.

Figure 2.7: Comparison of approximate solutions with numerical solutions of the full model. Leading order, approximate solutions for a) $A_e(t)$, b) $A_s(t)$ and c) $A_d(t)$ on each timescale are shown to be in good agreement, in the appropriate regions, with numerical solutions to the full model given by Equations (2.18). Parameter values: $\theta = 1, t_c = 3$, $\epsilon = 0.01$, $\lambda = 0.55274$, $\beta_0 = 0.2950$, $\beta_1 = 0.0124$, $\alpha = 0.2144$, $\gamma = 0.0027$, $\nu = 0.0904$.

Our asymptotic analysis reveals that the physical mechanisms that dominate healing change over time in the following way:

1. Exponential recoil of the dermal wound area for $t = \mathcal{O}(\epsilon)$ given by the leading order term in Equation (2.23c).

2. Proliferation in the epidermis and basal proliferation in the dermis for $t = \mathcal{O}(1)$ and $t < t_c$ detected by the appearance of λ and β_0 in the leading order terms of Equations (2.26).

3. Contraction and mechanosensitive proliferation in the dermis for $t = \mathcal{O}(1)$ and $t > t_c$ detected by the appearance of α and β_1 in the leading order terms of Equations (2.33).

In the next section we solve Equations (2.18) numerically in order to establish whether the model is in good qualitative agreement with wound healing data. By fitting the model to non-dimensionalised experimental data we aim also to identify those processes which differ markedly between non-diabetic and diabetic healing (in mice).

2.4 Numerical Results

In this section we solve Equations (2.18) numerically using the stiff differential equation solver `ode15s` in MATLAB. We also use a least squares fitting method to determine the best fits to the data presented in Figure 2.2. By comparing the parameters associated with the best fits for the non-diabetic and diabetic cases we go on to suggest a theoretical treatment that may enhance healing of diabetic wounds.

2.4.1 Least squares analysis

We use the method of least squares (see Appendix A.3) to fit Equations (2.18) to the non-dimensionalised data and, in this way, obtain estimates for the model parameters $\{\lambda, \beta_0, \beta_1, \alpha, \gamma, \nu\}$. The data in Figure 2.2 are non-dimensionalised by scaling the area by the maximum wound area (A_R) and time by an appropriate timescale (T) which is taken to be 1 day (see Appendix A.1 for details). The dimensionless parameters $t_c = 3$, $\theta = 1$ and $\epsilon = 0.01$ are fixed, these values being justified by a numerical parameter sensitivity analysis (for details see Appendix A.4).

The best fits of the model to the non-diabetic and diabetic data are presented in Figure 2.8 and reveal that the model fit to the non-diabetic data (mean squared error, MSE = 0.0017) is slightly better than the fit to the diabetic data (MSE = 0.0067). This is likely due to the greater amount of noise in the diabetic data.

The parameter values associated with the best fit curves are stated in Table 2.1. By comparing the non-diabetic and diabetic parameter sets, we see that the epidermal (λ) and dermal (β_0 and β_1) growth rates are lower in the diabetic wounds than in the control wounds by 20%, 75% and 80%, respectively. Contraction (α) is also compromised in diabetic healing but the decrease (25%) is less prominent than the reduction in the dermal growth rate parameters. Regarding the influence of the dermis on epidermal healing, we observe that the estimate of γ for diabetic wounds is much greater than that for non-diabetic wounds, indicating that the diabetic epidermis is more sensitive to new dermal tissue than the non-diabetic one. Equivalently, the diabetic epidermis has a reduced affinity for the granulation tissue synthesised in the wound space than the non-diabetic epidermis.

We note further that, in comparison to the other growth parameters, mechanosensitive growth (β_1) is small. By setting $\beta_1 = 0$ in Equations (2.18), we investigate how well the data can be described when mechanosensitive growth is neglected. The MSE associated with the best fit curves in Figure 2.8 are compared with those obtained

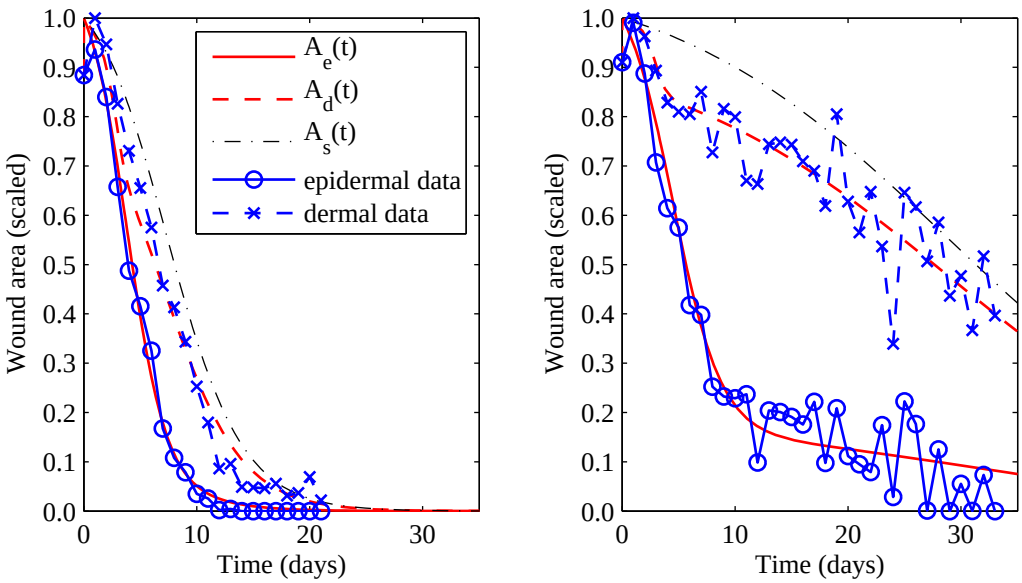

(a) Non-diabetic (b) Diabetic

Figure 2.8: Wound areas for the best fits of the model to data. The numerical solutions of Equations (2.18) are fit to the data given in Figure 2.2 by optimising the parameter set $\Phi^* = \{\lambda, \beta_0, \beta_1, \alpha, \gamma, \nu\}$ using a least squares analysis. The parameters $\theta = 1, t_c = 3$ and $\epsilon = 0.01$ are fixed. (a) Best fit to the non-diabetic data with parameters $\lambda = 0.5274$, $\beta_0 = 0.2950$, $\beta_1 = 0.0592$, $\alpha = 0.2144$, $\gamma = 0.0027$, $\nu = 0.0904$. (b) Best fit to the diabetic data with parameters $\lambda = 0.4258$, $\beta_0 = 0.0715$, $\beta_1 = 0.0026$, $\alpha = 0.1593$, $\gamma = 0.1868$, $\nu = 0.1000$.

Table 2.1: Dimensionless parameters associated with the best fits of the model to data. The dimensionless parameter values associated with the best fits to non-diabetic and diabetic data.

parameter	physical interpretation	non-diabetic	diabetic
λ	epidermal growth rate	0.5274	0.4258
β_0	basal dermal growth rate	0.2950	0.0715
β_1	mechanosensitive dermal growth rate	0.0124	0.0026
α	contraction with respect to elastic response	0.2144	0.1593
γ	epidermal dependence on dermis	0.0027	0.1868
ν	proportion of proliferative region	0.0904	0.1000

with no mechanosensitive growth. The results are presented in Table 2.2 and indicate that the best fit curves with $\beta_1 = 0$ yield the same MSE as those for which $\beta_1 > 0$.

In order to investigate whether mechanosensitive growth is small or whether the data (or model) cannot distinguish between the two types of dermal growth, we

Table 2.2: Comparison of mean square error between the different combinations of dermal growth. Table summarising how the MSE between the experimental data and the mathematical model depends on the processes that regulate dermal growth. (i) β_0 and β_1 optimised, (ii) $\beta_1 = 0$ and β_0 optimised and (iii) $\beta_0 = 0$ and β_1 optimised. In each case the parameters λ, α, γ and ν are also estimated as part of the fitting process.

	MSE	
type of growth	non-diabetic	diabetic
(i) basal and mechanosensitive ($\beta_0, \beta_1 > 0$)	0.0017	0.0067
(ii) basal only ($\beta_1 = 0 < \beta_0$)	0.0017	0.0067
(iii) mechanosensitive only ($\beta_0 = 0 < \beta_1$)	0.0084	0.0082

perform model simulations in which the basal growth rate of the dermis is negligible ($\beta_0 = 0$). The associated MSEs presented in Table 2.2 suggest that the model with only mechanosensitive growth ($\beta_0 = 0 < \beta_1$) describes the data less well than that with only basal growth ($\beta_1 = 0 < \beta_0$). These results suggest that the effect of mechanosensitive growth is negligible. This is because the MSE for basal growth only ($\beta_1 = 0 < \beta_0$) is the same as that with $\beta_0, \beta_1 > 0$.

When $\beta_1 = 0$, β_0 is the parameter which changes most significantly between the best fits to the non-diabetic and diabetic data. Guided by this observation we estimate the value of β_0 (with $\beta_1 = 0$) that gives the best fit to the diabetic data whilst holding the parameters λ, α, γ and ν fixed at the values obtained from the best fit to the non-diabetic data (see Table 2.1). This fit is presented in Figure 2.9 and yields an MSE = 0.0170. Although the MSE associated with this fit is greater than that when all parameters are free, the resulting solution for the dermal healing curve is qualitatively similar to that in Figure 2.8(b) and the higher MSE is likely to be a result of qualitative differences in the epidermal curves. This suggests that the dominant effect driving the delay in diabetic healing may be due to a lower rate of basal growth in the dermis.

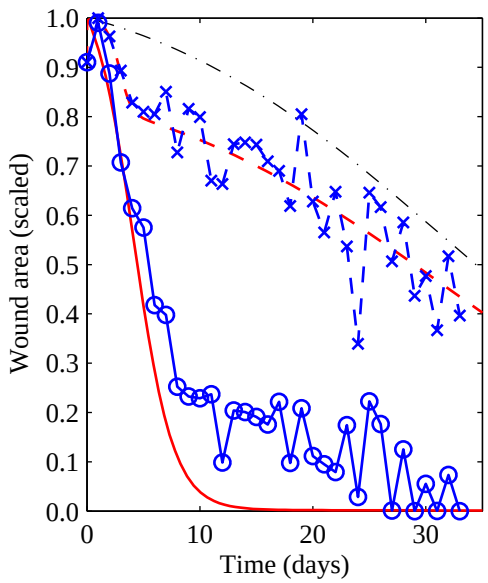

Figure 2.9: The best fit to the diabetic data with lower basal dermal growth only. The parameter set $\Phi = \{\lambda, \alpha, \gamma, \nu\}$ is fixed according to the best fit to the non-diabetic data, given in Table 2.1, $\beta_1 = 0$, $\theta = 1, t_c = 3$ and $\epsilon = 0.01$ are fixed. Only β_0 is optimised in the least squares approximation yielding $\beta_0 = 0.0645$.

2.4.2 Processes contributing to wound closure

The main factor that delays healing in diabetic wounds is closure of the dermis. From the data in Figure 2.2, healing is tracked by movement of the dermal and epidermal edges. Movement of the dermal edge is due to synthesis and contraction. However, it is not possible to uniquely decompose these processes from the data. Plots of the time evolution of A_s and A_d give an indication of the relative contributions of growth and contraction to dermal healing. Figure 2.10 shows how the contributions of dermal growth, contraction and re-epithelialisation to total healing can be calculated from the model simulations. Figure 2.11 shows how the relative contributions of these processes to healing change, over time, for the best fits in Figure 2.8.

Figure 2.11 can be used to estimate the net contribution of each process at wound closure (day 14 in the non-diabetic wounds and day 33 in the diabetic wounds as determined by the data). Our results suggest that re-epithelialisation contributes more to healing in the diabetic wound than the non-diabetic wound (approximately 30% in

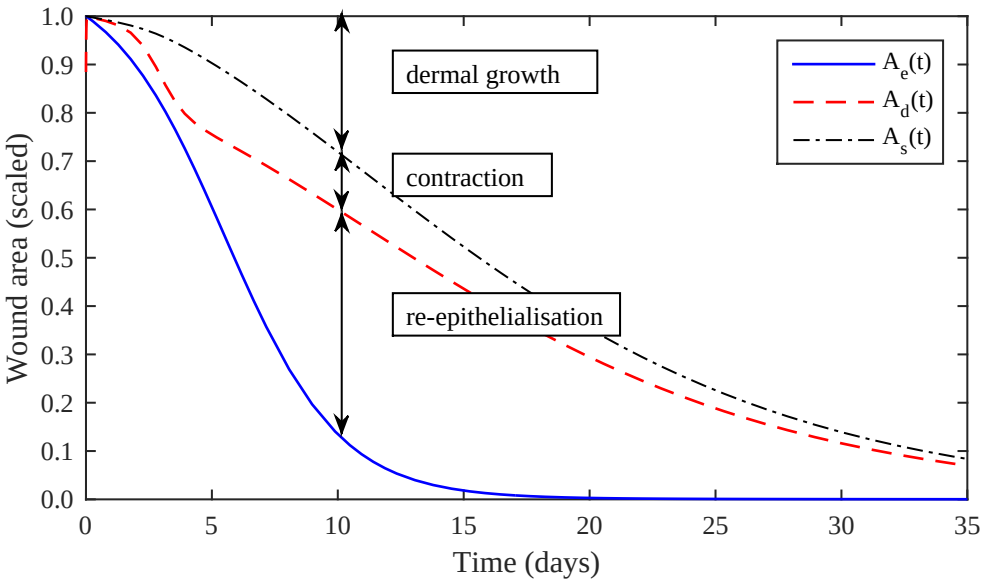

Figure 2.10: Definition of the different processes contributing to healing as functions of the model variables. The numerical solutions of Equations (2.18) can be used to calculate the contribution of re-epithelialisation, contraction and dermal growth to healing. The area healed by re-epithelialisation (epidermis covering granulation tissue) is given by $A_d(t) - A_e(t)$. The area healed by contraction is given by $A_s(t) - A_d(t)$ and by dermal growth is $1 - A_s(t)$.

comparison to 10%). The large amount of granulation tissue in the dermal gap could cause severe scarring and, therefore, it would be beneficial for the dermis to close more quickly, with greater contributions from contraction and tissue synthesis. Figure 2.11 also suggests the relative contributions from contraction and dermal growth differ markedly between non-diabetic and diabetic healing, with more contraction in the diabetic wounds. In Section 2.4 we found that the contraction parameter (α) was lower in the diabetic wounds (see Table 2.1) and, hence, that the diabetic tissue is less contractile than the non-diabetic tissue. However, the reduction in dermal growth in the diabetic wounds is more marked than the reduction in contraction (see Table 2.1), so that a greater proportion of the diabetic wounds is healed by contraction than in the non-diabetic wounds (10% in comparison to 2%). Further, the proportion of the diabetic wounds healed by dermal growth is only 60% whereas it is almost 90% in the non-diabetic wounds.

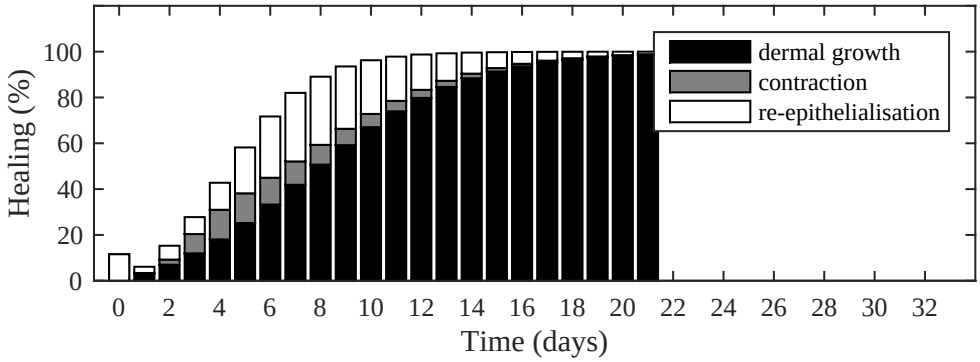

(a) Non-diabetic

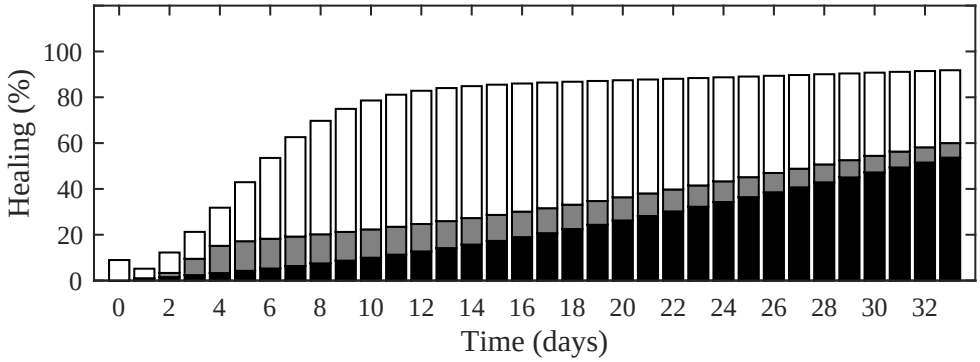

(b) Diabetic

Figure 2.11: Contributions from re-epithelialisation, dermal growth and dermal contraction predicted by best fits of the model to data. The numerical solutions of Equations (2.18) are fit to the data given in Figure 2.2 and the contributions to healing according to Figure 2.10 are plotted for each day until closure.

Combining the above results, we conclude that increasing basal growth in the dermis is likely to have a significant effect on increasing the overall rate of healing of diabetic wounds. In the next section we test this hypothesis by performing a parameter sensitivity analysis in which the parameter for basal growth in the dermis, β_0, is varied.

2.4.3 Treatment intervention

In this section we use our mathematical model to investigate the efficacy of a (theoretical) treatment in which the basal growth rate in the dermis (i.e. the parameter β_0)

is increased. Non-diabetic wounds typically close by day 14 (Figure 2.8(a)), by which time $A_d = 0.05$. All parameters are fixed according to the best fit of the model to the diabetic data (see Table 2.1). By increasing only β_0 we show how the time taken until $A_d = 0.05$ changes when our theoretical treatment is applied. The parameter β_0 is fixed at its elevated value for $t > 0$ and results are presented in Figure 2.12.

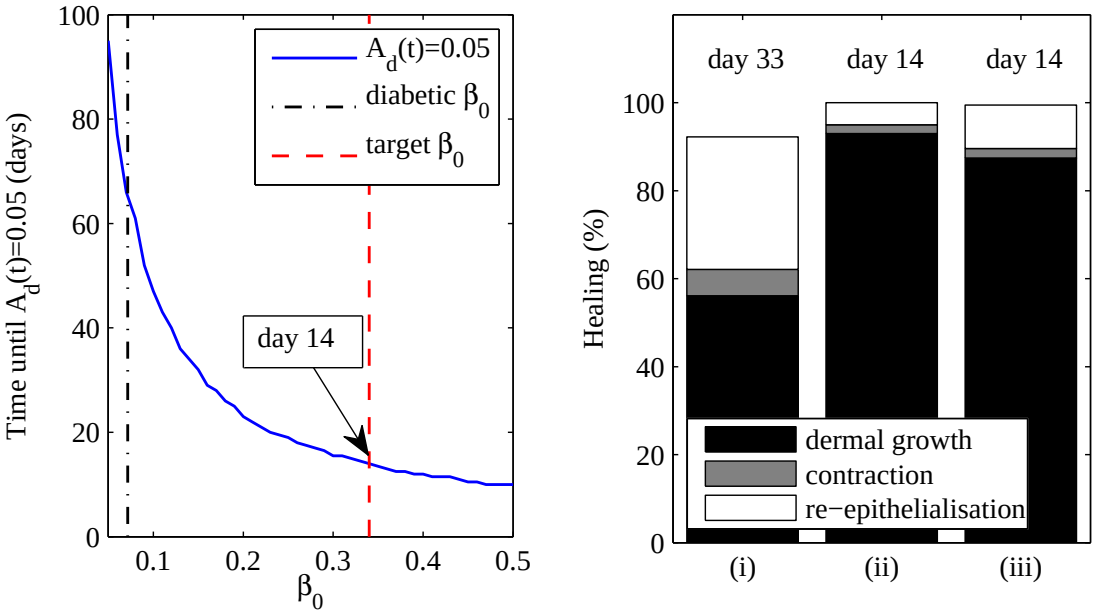

(a) Time to closure as a function of β_0

(b) Contributions to healing

Figure 2.12: Increasing β_0 as a treatment strategy. a) Parameter sensitivity analysis showing how, for the diabetic tissue, the time at which the dermal curve reaches $A_d(t) = 0.05$ decreases as β_0 increases. The value of β_0 as estimated by the best fit of Equations (2.18) to the diabetic data in Figure 2.2 is 0.0715 (dash-dotted black) and the target treatment value is $\beta_0 = 0.34$ (dashed red). By increasing β_0 to 0.34 the diabetic dermis will reach $A_d = 0.05$ by day 14, mimicking closure of the non-diabetic wounds. All other parameters are fixed at the diabetic values in Table 2.1. b) Comparison of the contributions to healing for (i) the diabetic case ($\beta_0 = 0.0715$) (ii) the diabetic case with β_0 increased to the target value ($\beta_0 = 0.34$) and (iii) the non-diabetic case ($\beta_0 = 0.2950$).

From Figure 2.8(a) we deduce that closure of non-diabetic wounds is achieved by day 14. By increasing β_0, as shown in Figure 2.12(a), from the estimated diabetic value of $\beta_0 = 0.0715$ to an enhanced value of $\beta_0 = 0.34$, the model predicts that the diabetic wounds will also close by day 14, normalising healing time. Figure 2.12(a)

suggests that for increased values of β_0 the time taken to heal plateaus at a minimum value of about 10 days. Similar behaviour is seen in simulations of treatment to non-diabetic wounds (results not shown). Figure 2.12(b) shows how increasing β_0 from 0.0715 to 0.34 alters the contributions of contraction and growth to dermal healing in the diabetic wound, making healing more closely resemble what is seen in non-diabetic tissue.

Fitting the model to the data suggested that the contribution from mechanosensitive proliferation in the dermis was much less than that from basal proliferation. We compared the contribution to healing of contraction and dermal growth and found that healing due to dermal growth is much lower for diabetic wounds than for non-diabetic ones. This results in a higher proportion of the wound being healed by contraction for the diabetic case. We investigated a treatment for increased basal growth and showed that it is theoretically possible to mimic normal healing by increasing just one of the parameters in our model (representing basal dermal growth). Combining the above results, we suggest that increased dermal growth is the most effective target for treatment in order to speed up the rate of healing in diabetic wounds and normalise the proportion of healing due to contraction and dermal growth.

2.5 Conclusion

Existing mathematical models of wound healing typically focus on epithelialisation for epidermal healing, tissue growth in dermal healing or wound contraction. In practice, wound healing involves a combination of these processes. The work in this chapter represents a simple attempt to couple epithelialisation in the epidermis and contraction and tissue growth in the dermis. We have developed a new mathematical model which describes how the epidermal and dermal areas of a wound change over time, in response to these key processes. By developing the model in tandem with

experimental data, we were able to compare its dynamics directly with the data.

By fitting the model to the data we identified parameters which may differ markedly between non-diabetic and diabetic healing in mice. Our results suggest that, in both cases, the effects of mechano-transduction on tissue synthesis are negligible. Moreover, the dermal growth rate and contractile force were lower in the diabetic wounds, a prediction which is consistent with the literature [Xu et al., 2013]. However, the reduction in the dermal growth rate in diabetic wounds (75% lower) is more prominent than the reduction in contraction (25% lower), so that the contribution of contraction to healing is greater in diabetic wounds compared to non-diabetic wounds (10% rather than 2%). This implies that, although both contraction and tissue growth are compromised in diabetic healing, it is likely to be more beneficial to increase the basal growth rate of new tissue in the dermis than to stimulate increased contraction in order to normalise healing. These model predictions also highlight the need for additional, more detailed experiments that can distinguish between contraction and dermal growth during wound healing.

Our results suggest that the longer time taken for the diabetic wounds to close is mainly due to a reduced rate of basal growth in the dermis. When β_0 was increased 5-fold the model predicted healing of the diabetic wound more closely resembled non-diabetic healing. There are many possible treatments that could yield an increase in parameter β_0. For example, supplemental arginine and vitamin C, have been shown to accelerate wound healing by improving activation and stimulation of collagen synthesis [Ringsdorf and Cheraskin, 1982, Barbul et al., 1990]. Well-established treatments, such as the application of occlusive dressings, can increase the rate of dermal epithelialisation by providing a moist wound environment [Alvarez et al., 1983]. The treatments mentioned here are inexpensive and therefore readily available for treating diabetic wounds.

Through asymptotic analysis we showed that the model successfully reproduces

the phases of healing in the sequence described in the literature. The asymptotic analysis also reveals which biophysical processes are dominant during each healing phase, information which could be used to guide the development of more effective treatments for normalising aberrant wound healing.

In our model the epidermal growth rate is assumed to be proportional to the combined area of newly synthesised epidermal tissue and an annulus surrounding the initial wound. We compared these results with others for which the epidermal growth rate was proportional to the circumference of the epidermal wound, an assumption which is consistent with Bullough and Laurence [1960]. We found that the numerical solutions of the epidermal healing curve were qualitatively similar (see Figure A.2 in Appendix A.5) although our choice of growth rate gave a better fit to the data. Further, assuming the growth rate is proportional to the wound circumference, the parameters obtained by fitting to the data did not change our results regarding differences in the healing of non-diabetic and diabetic wounds.

Although the proposed model is simple, it is formulated at a level which is consistent with the data available. Having determined that the most interesting behaviour and healing abnormalities lie in the dermal layer of the skin, we focus on dermal healing for the remainder of the thesis. It is clear that a careful balance between growth and contraction is required for healing to proceed normally.

One of the main limitations of the current model is that is does not account for spatial variation. This variation could be important in the growth of the tissue due to spatially heterogeneous fibroblast density and stress profiles of the healing tissue. For the remaining chapters we turn to a spatially-resolved framework in which we can investigate, in more detail, the mechanical processes occurring during dermal healing.

In the next chapter we introduce a general formulation for volumetric growth in a non-linear elastic material. This formulation is then used in Chapters 4 - 6 to develop a mechanical model of dermal wound healing.

Chapter 3

General formulation of elastic growth

3.1 Introduction

Continuum mechanics and non-linear elasticity provide a natural framework for studying growth in elastic tissues. Soft biological tissues typically undergo volumetric growth which often induces residual stress in the body. Further, biological tissues such as the heart [Fung, 1990] and the skin [Kessler et al., 2001] have been shown to experience stress induced growth. Understanding the feedback between stress and growth in a healing tissue could provide valuable insight into biomechanical wound pathologies.

The theory of morphoelasticity assumes that the timescale of growth is much slower than that of elasticity. Therefore the total deformation of an elastic body can be viewed as a combination of two separable processes; the addition of mass and an elastic response [Rodriguez et al., 1994]. Since growth takes place locally, incompatibilities in the material may arise. Integrity is restored through elastic reorganisation.

In this chapter the theory of morphoelasticity is outlined and the equations re-

quired to solve such problems are derived and applied through a simple example of a growing cylinder.

3.2 The geometric deformation tensor

Consider a continuous stress-free, elastic body $\mathcal{B}$, initially occupying the region $\mathcal{R}_0 \subset \mathbb{R}^3$. Then $\mathcal{R}_0$ denotes the reference configuration of the body and is defined by the position vector $\mathbf{X}$. Suppose, at time t, the body is deformed to a new configuration $\mathcal{R}_t$, referred to as the current configuration with position vector $\mathbf{x} = \chi(\mathbf{X}, t)$. The map from the reference to the current configuration can be described by a geometric deformation tensor [Spencer, 1980],

$$\mathcal{F} = \frac{\mathrm{d}\mathbf{x}}{\mathrm{d}\mathbf{X}}. \tag{3.1}$$

At any given time we expect the deformation $\mathcal{F}$ to be a continuous, one-to-one map. Therefore the current position $\mathbf{x}$ of the body can be cast in terms of the independent variable $\mathbf{X}$ and the deformation $\mathcal{F}$ or, alternatively, the original position $\mathbf{X}$ of the body can be cast in terms of the independent variable $\mathbf{x}$ and the deformation $\mathcal{F}^{-1}$.

3.2.1 Decomposition of the deformation tensor

The deformation of an elastic body can be viewed as a combination of two processes [Rodriguez et al., 1994]. Firstly, the addition or removal of material in the stress-free state contributes to a change in mass of the body. The growth tensor describes local addition of material and can thus introduce incompatibility. Secondly, to accommodate for this, the body may undergo an elastic deformation. The total deformation can be decomposed as

$$\mathcal{F} = \mathcal{A} \cdot \mathcal{G}, \tag{3.2}$$

where $\mathcal{A}$ is the elastic deformation tensor and $\mathcal{G}$ is the growth tensor. This composition of mappings is represented schematically in Figure 3.1.

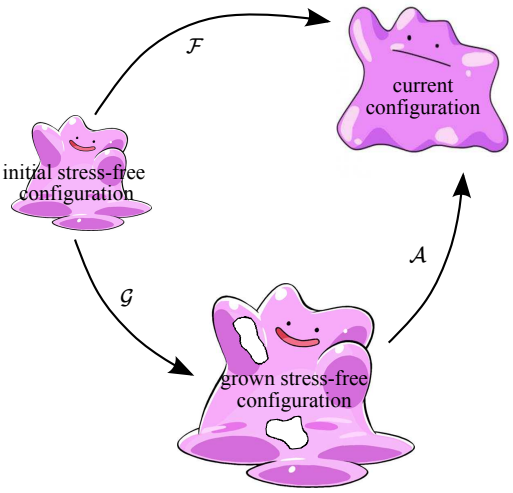

Figure 3.1: The deformation of an elastic body. The deformation tensor $\mathcal{F}$ can be decomposed into a growth tensor $\mathcal{G}$, describing the local addition of material, and an elastic tensor $\mathcal{A}$, describing the elastic response of the body.

The decomposition of the deformation tensor is the fundamental assumption of morphoelasticity. Growth is slow and hence a quasi-static process is assumed. For any change in mass that occurs, the system is assumed to be in mechanical equilibrium. We assume that, at any time t, the deformation $\mathcal{F}$ is well-defined and proceed in deriving the equations of motion.

3.3 Conservation of momentum

Let an elastic body $\mathcal{B}$ with density ρ at point $\mathbf{x}$ be subject to body forces $\mathbf{b}$ and a surface traction $\mathbf{t}_n$. By the balance of linear momentum

$$\int_{\mathcal{B}} \rho(\mathbf{x},t)\mathbf{b}(\mathbf{x},t)\ \mathrm{d}v + \int_{\partial\mathcal{B}} \mathbf{t}_n\ \mathrm{d}s = \int_{\mathcal{B}} \rho(\mathbf{x},t)\ddot{\mathbf{x}}(\mathbf{X},t)\ \mathrm{d}v, \tag{3.3}$$

where a dot represents a derivative with respect to time. The traction force is given by $\mathbf{t}_n = \mathbf{T}\cdot\mathbf{n}$, where $\mathbf{n}$ is the unit normal and $\mathbf{T}$ is the symmetric, Cauchy stress

tensor. The Cauchy stress tensor defines the stress in the deformed configuration. Substituting for $\mathbf{t}_n$ in Equation (3.3) and applying the divergence theorem, we have

$$\nabla \cdot \mathbf{T} + \rho \mathbf{b} = \rho \ddot{\mathbf{x}}, \tag{3.4}$$

where the divergence of the Cauchy stress tensor is taken with respect to the current position $\mathbf{x}$.

If the body is in mechanical equilibrium, and in the absence of body forces, Equation (3.4) reduces to

$$\nabla \cdot \mathbf{T} = \mathbf{0}. \tag{3.5}$$

Equation (3.5) is solved subject to suitable boundary conditions which can take various forms. Most commonly either the normal components of the stress (dead-loading) or the deformation (rigid-loading) are fixed on the boundary, $\partial\mathcal{B}$.

3.4 Constitutive stress-strain relationship

Assuming that the body is hyperelastic, the response of the material to stress is characterised by a strain-energy function, $W = W(\mathcal{A})$. If the material is assumed to be incompressible then the Cauchy stress, $\mathbf{T}$, is related to the elastic deformation tensor, $\mathcal{A}$, by [Eringen, 1962]

$$\mathbf{T} = \mathcal{A} \cdot \frac{\partial W}{\partial \mathcal{A}} - p\mathbb{I}, \tag{3.6}$$

where the hydrostatic pressure p ensures incompressibility and $\mathbb{I}$ is the identity tensor.

3.4.1 Strain-energy function

Identifying suitable strain-energy functions for hyperelastic materials is an important area of research and requires experimental observations [Fung, 1993]. Strain-energy functions are cast in terms of the components of the elastic strain tensor, α_1, α_2 and α_3. Various strain-energy functions have been proposed for modelling the mechanical behaviour of such tissues, and these can be categorised into two main families; power law and limited chain extensibility models. Attention will be restricted to power law strain-energy functions[1] of which a general form is given by [Knowles, 1977]

$$W = \frac{\mu}{2c}\left[\left(1 + \frac{c}{n}(I_1 - 3)\right)^n - 1\right], \tag{3.7}$$

where $I_1 = \alpha_1^2 + \alpha_2^2 + \alpha_3^2$ is the first invariant of the Cauchy-Green elastic tensor $(\mathcal{A} \cdot \mathcal{A}^T)$, $\mu > 0$ is the shear elastic modulus and c and n are positive material constants. For soft tissues, the constant c typically lies between 3 and 20 [Goriely et al., 2006]. For $n = 1$, we have the neo-Hookean strain-energy function

$$W = \frac{\mu}{2}(I_1 - 3). \tag{3.8}$$

The neo-Hookean model is the natural generalisation of Hooke's law for large deformations [Rivlin, 1948a]. Equation (3.8) has been used to describe the mechanical behaviour of many different biological tissues including the trachea [Moulton and Goriely, 2011], elastin [Watton et al., 2009], cardiac tissue [Cherubini et al., 2008], plant stems [Goriely et al., 2010] and the skin [Wu and Ben Amar, 2015].

Many soft tissues exhibit a hardening at large strain known as strain stiffening.

[1]For any finite deformation of an ideal rubber-like material, it is assumed that the components of the elastic strain tensor can take values from $0 < \alpha_i < \infty$. However, real rubber-like materials can not be compressed or extended indefinitely and hence constitutive models have been developed to characterise this limiting extensibility [Gent, 1996, Horgan and Saccomandi, 2002]. We do not consider these models in this thesis. Instead we will consider model observables such as the stress in order to characterise the behaviour of the tissue at large strain. For example, for sufficiently large stress, the tissue would be expected to tear (see Chapter 4).

This can be modelled by Equation (3.7) for $n > 1$. If $n \to \infty$ in Equation (3.7) then we arrive at the Fung strain-energy function [Fung, 1967]

$$W = \frac{\mu}{2c}\left[\exp(c(I_1 - 3)) - 1\right]. \tag{3.9}$$

The Fung model approaches the neo-Hookean model in the limit $c \to 0$.

Some biological tissues are better represented by anisotropic strain-energy functions, which consider different forms of strain-energy function or parameter values in different fibre directions of the tissue [Holzapfel et al., 1996, Holzapfel, 2001, Rezakhaniha et al., 2011]. However, for simplicity, we restrict to isotropic materials in this thesis.

3.5 Evolution of growth

The growth of an elastic body is described by a continuous time-dependent process, where, for each time increment, the volume of the tissue is updated according to the growth tensor $\mathcal{G}$. The growth of the body can therefore be prescribed by a differential equation of the form

$$\frac{\mathrm{d}\mathcal{G}}{\mathrm{d}t} = g(\mathbf{T}, \mathcal{F}, \mathcal{G}, \beta; \mathbf{X}, t), \tag{3.10}$$

where the function g may depend on the stress, the deformation, the growth or other factors β such as chemical or nutrient concentration. $\mathbf{T}$, $\mathcal{G}$ and β may also depend on position and time. Typically $\mathcal{G} = \mathbb{I}$ at $t = 0$, corresponding to no growth initially.

In the next section we will demonstrate how the equations of motion may be solved by considering a simple example of a growing cylinder.

3.6 A growing elastic cylinder

In this section we consider a growing cylinder. We introduce cylindrical coordinates, (R, Θ, Z), so that the cylinder occupies the domain

$$A \leq R \leq B, \quad 0 \leq \Theta \leq 2\pi, \quad 0 \leq Z \leq L.$$

The cylinder is subject to an axisymmetric deformation, (r, θ, z), given by

$$r = r(R, t), \quad \theta = \Theta, \quad z = \lambda(t)Z,$$

represented schematically in Figure 3.2.

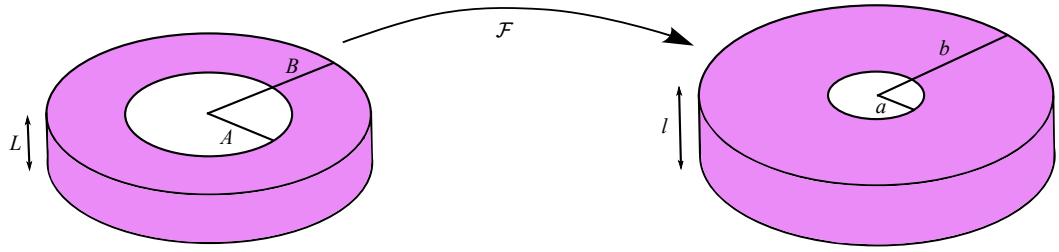

Figure 3.2: Relationship between the reference and current configurations. In the reference configuration the cylinder occupies the domain $A \leq R \leq B$, $0 \leq \Theta \leq 2\pi$ and $0 \leq Z \leq L$. After the deformation $\mathcal{F}$, the cylinder is mapped to the current configuration, occupying the region $a \leq r \leq b$, $0 \leq \theta \leq 2\pi$ and $0 \leq z \leq l$, at time t.

3.6.1 Deformation

In the axisymmetric cylindrical coordinate system, the deformation gradient tensor is given by [Rivlin, 1948b]

$$\mathcal{F} = \operatorname{diag}\left(\frac{\partial r}{\partial R}, \frac{r}{R}, \lambda\right). \tag{3.11}$$

Decomposing the deformation gradient tensor such that $\mathcal{F} = \mathcal{A} \cdot \mathcal{G}$, the tensors $\mathcal{A}$ and $\mathcal{G}$ are defined as follows,

$$\mathcal{A} = \text{diag}(\alpha_r, \alpha_\theta, \alpha_z) \quad \text{and} \quad \mathcal{G} = \text{diag}(\gamma_r, \gamma_\theta, \gamma_z), \tag{3.12}$$

where α_r, α_θ and α_z are the principle stretches in the radial, circumferential and axial directions, respectively. The components of the growth tensor, γ_r, γ_θ and γ_z, represent radial, circumferential and axial growth (or resorption) respectively. Note that each γ_i can be a function of position R, such that $\gamma_i > 1$ (< 1) signifies a local increase (decrease) in mass in the i direction. If the material is incompressible then $\det(\mathcal{A}) = 1$ and $\det(\mathcal{F}) = \det(\mathcal{G})$ describes the change in volume due to growth only.

Setting $\mathcal{F} = \mathcal{A} \cdot \mathcal{G}$ gives

$$\frac{\partial r}{\partial R} = \alpha_r \gamma_r, \tag{3.13a}$$

$$\frac{r}{R} = \alpha_\theta \gamma_\theta, \tag{3.13b}$$

$$\lambda = \alpha_z \gamma_z. \tag{3.13c}$$

Setting $\alpha = \alpha_\theta$ and assuming incompressibility together with Equation (3.13c), it is straightforward to show that the components of the elastic strain tensor can be expressed in terms of the strain variables α and λ,

$$\mathcal{A} = \text{diag}\left(\frac{\gamma_z}{\alpha\lambda}, \alpha, \frac{\lambda}{\gamma_z}\right), \quad \text{where} \quad \alpha = \frac{r}{\gamma_\theta R}. \tag{3.14}$$

By eliminating α in Equations (3.13a) and (3.13b) we obtain a differential equation for the map $r(R, t)$

$$\frac{\partial r}{\partial R} = \gamma_r \gamma_\theta \gamma_z \frac{R}{\lambda r}, \tag{3.15}$$

which can be integrated to give

$$r^2(R,t) = a^2(t) + 2\int_A^R \frac{\gamma_r(\tilde{R},t)\gamma_\theta(\tilde{R},t)\gamma_z(\tilde{R},t)\tilde{R}}{\lambda(t)}\,\mathrm{d}\tilde{R}. \tag{3.16}$$

For given growth functions $\gamma_i(R,t)$ where $i = r,\theta,z$, the deformation is fully determined, at time t, once $a(t)$ and $\lambda(t)$ are known. These two time-dependent unknowns are resolved by imposing appropriate boundary conditions (see Section 3.6.4).

3.6.2 Cauchy stress

The Cauchy stress tensor $\mathbf{T} = \mathrm{diag}(T_{rr}, T_{\theta\theta}, T_{zz})$ has radial, circumferential and axial components. For plane stress, the only non-trivial component of Equation (3.5) is

$$\frac{\partial T_{rr}}{\partial r} + \frac{1}{r}(T_{rr} - T_{\theta\theta}) = 0. \tag{3.17}$$

Given a strain-energy function $W = W(\alpha_r, \alpha_\theta, \alpha_z)$, and referring to Equation (3.6), the stress-strain relationship for a hyperelastic material can be written in component form as

$$T_{rr} = \alpha_r W_1 - p, \tag{3.18a}$$

$$T_{\theta\theta} = \alpha_\theta W_2 - p, \tag{3.18b}$$

$$T_{zz} = \alpha_z W_3 - p, \tag{3.18c}$$

where W_i (for $i = 1,2,3$) are the partial derivatives of W with respect to its i^{th} argument. Given that the elastic strain tensor can be written in terms of α and λ (see Equation (3.14)), it is convenient to define the auxiliary strain-energy function

$$\hat{W}(\alpha,\lambda) = W\left(\frac{\gamma_z}{\alpha\lambda}, \alpha, \frac{\lambda}{\gamma_z}\right). \tag{3.19}$$

Substituting Equations (3.18a), (3.18b) and (3.19) into (3.17) yields a partial differential equation for the radial component of the Cauchy stress tensor

$$\frac{\partial T_{rr}}{\partial r} = \frac{\alpha \hat{W}_\alpha}{r}. \tag{3.20}$$

By eliminating p in Equations (3.18), it is possible to show that the circumferential and axial components of the stress satisfy

$$T_{\theta\theta} = T_{rr} + \alpha \hat{W}_\alpha \quad \text{and} \quad T_{zz} = T_{rr} + \lambda \hat{W}_\lambda. \tag{3.21}$$

3.6.3 Governing equations

We note that there is a one-to-one map between the reference and current configuration. Our convention is generally to view all spatially-dependent variables as functions of the independent variable R and time t. So, for example, we write $T_{rr}(r,t)$ as $T_{rr}(R,t) = T_{rr}(r(R,t),t)$. Using Equation (3.15) the differential equation for the radial stress in Equation (3.20) can be re-written in terms of the independent variable R. Given suitable growth laws, the deformation and stress are determined, at time t, by the following quasi-static equations

$$r^2 = a^2 + 2\int_A^R \frac{\gamma_r \gamma_\theta \gamma_z \tilde{R}}{\lambda}\, \mathrm{d}\tilde{R}, \tag{3.22a}$$

$$\frac{\partial T_{rr}}{\partial R} = \frac{\gamma_r \gamma_\theta \gamma_z R}{\lambda r^2} \alpha \hat{W}_\alpha, \tag{3.22b}$$

$$T_{\theta\theta} = T_{rr} + \alpha \hat{W}_\alpha, \tag{3.22c}$$

$$T_{zz} = T_{rr} + \lambda \hat{W}_\lambda, \tag{3.22d}$$

where

$$\hat{W}(\alpha,\lambda) = W\left(\frac{\gamma_z}{\alpha\lambda}, \alpha, \frac{\lambda}{\gamma_z}\right) \quad \text{and} \quad \alpha = \frac{r}{\gamma_\theta R}. \tag{3.23}$$

The mechanical description is completed by prescribing appropriate boundary conditions.

3.6.4 Boundary conditions

In an open cylinder, there are three free surfaces: the inside, the outside, and the top (without loss of generality, the bottom surface may be assumed to be fixed in space). On each surface we can impose the deformation or the normal component of the stress[2], resulting in three boundary conditions to solve Equation (3.22b) and determine the unknowns a and λ that appear in Equations (3.22). The possible boundary conditions are therefore to specify:

1. On the inner surface: the deformation, a, or the radial stress, $T_{rr}|_{R=A}$.
2. On the outer surface: the deformation, b, or the radial stress, $T_{rr}|_{R=B}$.
3. On the top: the deformation, λ, or the axial load N_z.

The axial load applied to the cylinder is obtained by integrating the axial stress over the annulus

$$N_z = 2\pi \int_a^b T_{zz} r \, \mathrm{d}r. \tag{3.24}$$

For a growing cylinder, unconstrained in the axial direction, $N_z = 0$.

For illustrative purposes, here we choose to close our model by imposing stress-free boundary conditions and no axial deformations so that

$$T_{rr}|_{R=A} = 0, \quad T_{rr}|_{R=B} = 0 \quad \text{and} \quad \lambda = 1. \tag{3.25}$$

[2]We note that, due to incompressibility, the deformation can not be imposed on all three surfaces. If the deformation is imposed on two of the surfaces, then the third is determined by Equation (3.22a).

3.6.5 Constant growth

For simplicity, we neglect axial and circumferential growth and consider constant growth in the radial direction. With $\mathcal{G} = \text{diag}(\gamma, 1, 1)$, Equations (3.22) can be solved subject to Equations (3.25) to obtain

$$r = \sqrt{a^2 + \gamma(R^2 - A^2)}, \tag{3.26a}$$

$$T_{rr} = \frac{\mu}{2\gamma}\left[\gamma^2 \log\left(\frac{R^2}{A^2}\right) - \log\left(\frac{r^2}{a^2}\right) + (\gamma A^2 - a^2)\left(\frac{1}{r^2} - \frac{1}{a^2}\right)\right], \tag{3.26b}$$

$$T_{\theta\theta} = T_{rr} + \mu\left(\frac{r^2}{R^2} - \frac{R^2}{r^2}\right), \tag{3.26c}$$

where the inner radius of the cylinder, $r = a$, is chosen so that $T_{rr}|_{R=B} = 0$. In Figure 3.3 the radial and circumferential components of the stress tensor are plotted as functions of R, following a single time-independent growth step. In Figure 3.3(a) we take $\gamma_r = 1.2$: this is the case for radial growth, which creates circumferential compression on the inner boundary and tension on the outer boundary. In Figure 3.3(a) we take $\gamma_r = 0.8$: this is the case for radial resorption, resulting in circumferential tension at the inner boundary and compression at the outer boundary. In both cases, the radial stress is subject to stress-free boundary conditions, with radial growth causing compression in the bulk of the material and resorption causing tension.

3.7 Other forms of growth

The example in the previous section employs a simple form for the growth tensor. By assuming constant growth the deformation can be integrated and analytical solutions found. However, the use of this simplification is restricted in biological tissues. In many tissues, growth is influenced by the location of the material, implying that the growth tensor is a function of position. Further, growth may vary in response to local stresses and strains. The form of the biomechanical growth law in Equation (3.10) is

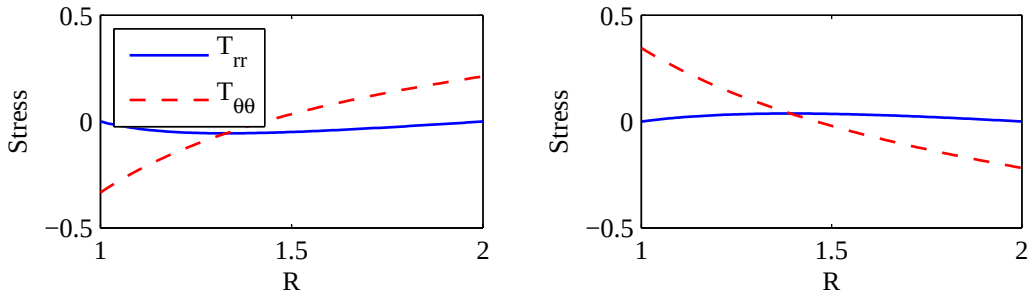

(a) Constant isotropic growth (b) Constant isotropic resorption

Figure 3.3: Radial and circumferential stresses for constant radial growth. The radial (solid blue) and circumferential (dashed red) components of the stress tensor, given by Equations (3.26b) and (3.26c), are plotted as functions of the reference variable R. The cylinder, with $A = 1$, $B = 2$ and $\mu = 1$, is subject to constant radial (a) growth with $\gamma = 1.2$ and (b) resorption with $\gamma = 0.8$. The radial stress is zero on the boundaries with the bulk of the material in compression due to growth and tension due to resorption. Growth causes circumferential compression on the inner edge and tension on the outer edge whereas resorption causes circumferential tension on the inner edge and compression on the outer edge.

an unresolved issue but nevertheless implies that $\mathcal{G}$ can take non-trivial forms that depend on physical variables such as the stress.

3.8 Conclusion

In this chapter we have introduced a theoretical framework for modelling growth in an elastic tissue. In the next chapter we use this theory to develop a morphoelastic model of dermal wound healing that accounts for contraction and mechanically induced growth.

Chapter 4

A morphoelastic model of dermal wound healing

4.1 Introduction

In the previous chapter we introduced the theories of continuum mechanics and non-linear elasticity. Morphoelasticity provides a framework which can be used to understand the laws driving growth and contraction in biological tissues. It can be used to determine the stress experienced by the tissue while also providing a mechanistic approach for describing and determining the forces exerted on the tissue. As we perceive stress-induced growth to be key in dermal wound healing and this could not be adequately modelled using the spatially-averaged framework developed in Chapter 2, in this chapter we use the theory of morphoelasticity to develop a new model of dermal wound healing. By proposing a spatially-resolved framework we benefit from the possibilities of incorporating anisotropic and heterogeneous growth.

If mechanical effects are included in models of wound contraction this is typically via linear elasticity (see Section 1.3 for a review). Several factors highlight the importance of the mechanical environment in healing and the value of a non-linear elastic

modelling framework. When a circular wound is formed in mice, following injury the skin retracts causing the wound to increase to 120% of its initial area [McGrath and Simon, 1983]. The retraction suggests that residual tension is released when the skin is cut, while the large degree of retraction points to a non-linear regime. It is also known that growth can be stimulated by local changes in mechanical stress [Fung, 1990, Hinz et al., 2001, Ambrosi and Mollica, 2004, Lumpkin and Caterina, 2007]. Such stress is generated in healing tissue by wound contraction, largely driven by fibroblast activity at the wound edge. While models of wound contraction typically focus on the interior of the wound, e.g. the formation and remodelling of the central granulation tissue into scar tissue [Cumming et al., 2010, Yang et al., 2013], the 'pulling' of the fibroblasts on the surrounding dermal tissue directly impacts the stress and growth in the tissue, which is crucial for the final size of the defect and the potential for scarring.

The model developed in Chapter 2 suggested that diabetes mainly affected dermal healing, in particular growth in the dermal tissue surrounding the wound. Guided by these conclusions, and for simplicity, here we focus attention on dermal healing. We do not explicitly model re-epithelialisation, incorporating only the effects of the epidermis on the dermis. Recall our schematic of the skin from Figure 1.1, which we have adapted here in Figure 4.1 to represent, in simple terms, the tissues involved in the healing of a full thickness wound. While the skin is comprised of three layers, only the dermis is considered in this chapter. The dermal layer is an elastic tissue subject to both growth and contraction which can be modelled in the proposed framework. By postulating mechanosensitive growth laws, we aim to understand how the mechanical environment in the dermal tissue surrounding the wound impacts healing. We use the model to gain mechanistic insights, to investigate the feedback between growth and contraction in dermal closure, and to predict behaviours that can be tested experimentally.

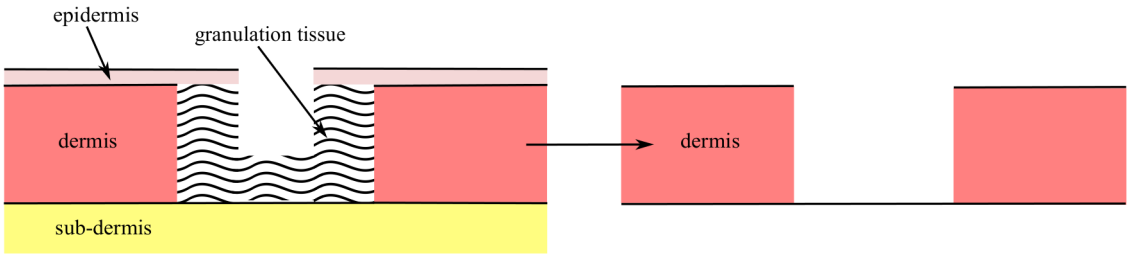

Figure 4.1: Model simplification. The schematic shows the epidermal, dermal and subdermal layers. Our focus is on wounding that damages the epidermal and dermal layers. Granulation tissue forms in the wound space as the dermal edge advances inwards due to a combination of growth and contraction. The epidermis grows atop the newly formed granulation tissue. We will consider only the dermal layer of the skin in our model.

In the next section the model is developed by considering the wound geometry, the tissue mechanics (balance of linear and angular momentum) and by prescribing constitutive laws relating stress to strain, and for growth. The full model is stated in Section 4.3. In Sections 4.4 and 4.5 we present typical results of wound healing simulations. We show that the model can exhibit normal healing behaviour and demonstrate the effect of key parameters on healing. In Section 4.6 we consider the possibility of the tissue remodelling to a steady state after closure. In Section 4.7 the model is used to predict the outcome of hypothetical rewounding experiments as a method of determining the stress in the tissue and the effects of applying pressure to control wound closure. Finally, in Section 4.8, we summarise and discuss the work in this chapter.

4.2 Model development

In this next section we discuss the geometry of the dermal tissue and the mechanical equations developed in Chapter 3 are defined for the current problem in Section 4.2.2. By considering the recoil of a wound upon injury, we calculate the stress-free state and the residual stress in the unwounded tissue in Section 4.2.3. An appropriate domain

size and realistic range for the tissue stiffness are determined by simulating the mechanical equations in Sections 4.2.4 and 4.2.5, respectively. The presence of volumetric growth is demonstrated by considering contraction of the wound (in Section 4.2.6) and the form of mechanosensitive growth law is motivated by a simple analysis of homogeneous growth (in Section 4.2.7). The growth laws are given in Section 4.2.8 with body forces and boundary conditions discussed in Sections 4.2.9 and 4.2.10, respectively.

4.2.1 Geometry

In Figure 4.2 we present experimental data from our collaborators showing how the thickness of the dermis changes over time. The data are averaged over six tissue samples from healing wounds in non-diabetic and diabetic mice. Initially, we observe an increase in thickness at the wound edge (solid curves) of approximately 40%. We interpret this as accumulation of the skin as the wound edge recoils. Between days 1 and 4 the thickness of the wound edge continues to increase. This could be caused by either a build up of granulation tissue or growth in the dermal tissue. Following this, between days 4 and 10, the dermis thins, likely due to contraction causing the dermis to be pulled in, towards the wound centre. After this phase the dermal thickness increases, probably due to a reduction in contractile activity and continued growth of the tissue. The trend is qualitatively similar for both the non-diabetic and diabetic data. We observe that away from the wound edge (dashed curves) the dermal thickness is different to that at the wound edge suggesting a non-uniform thickness and deformation.

Given the evidence for temporal fluctuations in dermal thickness, we allow for deformations in the axial direction. The thickness of the dermal tissue may be affected by a combination of attachment to the epidermis restricting axial movement, growth and mechanical forces such as contraction.

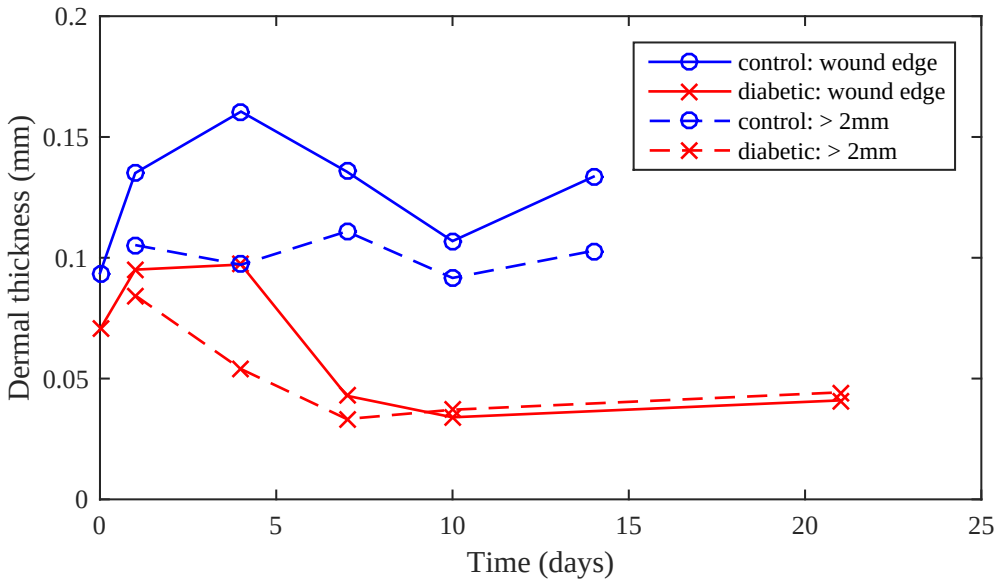

Figure 4.2: Thickness of dermis in non-diabetic and diabetic mice. Time course of averaged data for the thickness of the dermal layer collected at the wound edge from day 0 (solid) and greater than 2 mm from the wound edge into the healthy dermal tissue from day 1 (dashed). Data are averaged over six wounds for each time point. Although the data are noisy we observe an increase in thickness at the wound edge, consistent for both non-diabetic (blue) and diabetic (red) tissue samples. At greater than 2 mm from the wound edge, the thickness of the non-diabetic dermis remains approximately constant whereas the diabetic dermis thins over the first week and then stays approximately constant.

In this chapter the dermal tissue is viewed as a cylindrical hyperelastic body surrounding the wound such that the outer radius is far from the wound edge and the effects of dermal tissue external to the cylinder can be approximated by imposing a boundary condition at the outer edge. Mechanical testing has shown that the skin is almost incompressible [North and Gibson, 1978] and, hence, we assume the dermal cylinder is an incompressible material. Attention is restricted to symmetric deformations, such that the radial and axial coordinates R_0 and Z_0 in the stress-free reference configuration are deformed, at time t, to r and z in the current configuration, respectively. The geometrical region associated with the reference configuration is

$$A_0 \leq R_0 \leq B_0, \quad 0 \leq \Theta \leq 2\pi, \quad 0 \leq Z_0 \leq L_0,$$

where A_0, B_0 and L_0 denote the wound radius, the outer radius of the modelling domain and the initial thickness of the tissue in the stress-free configuration, respectively. This region is deformed in the current configuration to

$$a \leq r \leq b, \quad 0 \leq \theta \leq 2\pi, \quad 0 \leq z \leq l,$$

by the maps

$$r = r(R_0, t), \quad \theta = \Theta, \quad z = \lambda(t) Z_0,$$

where λ is the axial stretch.

The geometry is pictured schematically in Figure 4.3. In order to account for residual tension in the skin, we identify four configurations. The pre-wounded tissue is denoted by state S_1 – this tissue is in a state of residual tension, which for a finite cylinder can be assumed to arise from a pressure T_{res} applied by the external skin. If excised, the residual tension is relieved and the tissue relaxes to a stress-free configuration, denoted S_0. We assume a wound of radius A is formed in the tissue at time $t = 0$, at which point the stress on the inner surface is relieved and the wound fully recoils to a radius a_R by time t_R – we refer to this configuration as state S_2. Contractile activity of the fibroblasts then creates a pressure f_c at the inner edge, so that at times $t > t_R$ the wound radius is a; this current state is referred to as S_3. The duration of wound recoil is on the order of hours and growth begins after approximately a day [Ghosh et al., 2007], thus there is assumed to be no growth between states S_0, S_1 and S_2.

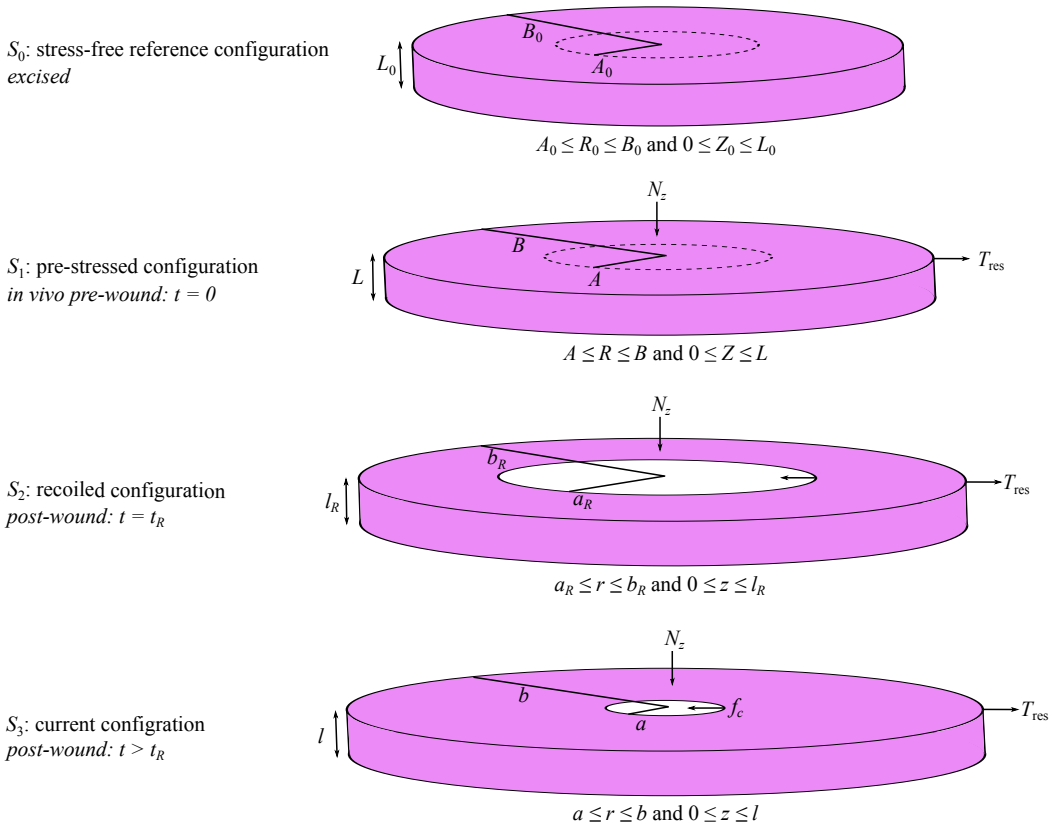

Figure 4.3: Schematic representation of the model geometry. Distance from the wound centre in the stress-free configuration can be described by the independent variable R_0, where $A_0 \le R_0 \le B_0$. The cylinder represents the dermal tissue and, under some deformation $\mathcal{F}$, the reference configuration of the tissue is mapped to the current configuration. Distance from the wound centre in the current configuration can be described by the dependent variable $r = r(R_0, t)$, where $a \le r \le b$, at time t. *In vivo* the tissue is residually stressed with external radial pressure T_{res} MPa and axial load N_z N. After wounding, tension is released on the wound edge causing the wound to recoil, resulting in the recoiled configuration, where $a_R \le r \le b_R$. As the wound heals it is subject to contraction modelled as a radial pressure, f_c MPa, on the wound edge. Far from the wound the tissue remains residually stressed.

4.2.2 Mechanical description

Following the theory of morphoelasticity outlined in Chapter 3 we write the symmetrical deformation of an incompressible cylinder as

$$\frac{\partial r}{\partial R_0} = \frac{\gamma_r \gamma_\theta \gamma_z R_0}{\lambda r}, \tag{4.1}$$

where γ_r, γ_θ and γ_z are the radial, circumferential and axial components of the growth tensor.

The system mechanics are described by the balance of linear momentum

$$\rho\ddot{\mathbf{x}} - \nabla \cdot \mathbf{T} - \rho\mathbf{b} = \mathbf{0}, \tag{4.2}$$

where the Cauchy stress tensor $\mathbf{T}$ is symmetric and diagonal with radial, circumferential and axial components denoted T_{rr}, $T_{\theta\theta}$ and T_{zz}, respectively.

The stress-strain constitutive relationship for an incompressible and hyperelastic material [Eringen, 1962] with strain-energy function $W = W(\alpha_r, \alpha_\theta, \alpha_z)$ in component form is

$$T_{rr} = \alpha_r W_r - p, \quad T_{\theta\theta} = \alpha_\theta W_\theta - p, \quad T_{zz} = \alpha_z W_z - p, \tag{4.3}$$

where $W_i = \partial W/\partial\alpha_i$ (for $i = r, \theta, z$) and α_r, α_θ and α_z are the radial, circumferential and axial components of the elastic strain tensor.

The mechanical description is completed by prescribing appropriate boundary conditions. In this chapter we typically specify the radial stress $T_{rr}|_{r=a,b}$ and the axial load, $N_z = \int T_{zz}\, \mathrm{d}A$, with integration over the top of the annulus.

We model the dermis as a neo-Hookean material [Rivlin, 1948a] with strain-energy function

$$W(\alpha_r, \alpha_\theta, \alpha_z) = \frac{\mu}{2}\left(\alpha_r^2 + \alpha_\theta^2 + \alpha_z^2 - 3\right). \tag{4.4}$$

We will consider the effects of our choice of strain-energy function on the healing dermis in Section 4.4.2.

4.2.3 A residually stressed state

An assumption of morphoelasticity is that $\mathcal{F}$ describes a deformation from a stress-free reference configuration. Since the skin is naturally residually stressed *in vivo*, we

require a map from the observed residually stressed configuration, S_1, to the unknown stress-free configuration, S_0. In this section we determine S_0 and estimate the value of T_{res} by considering the initial recoil upon wounding. The experimental data are given as a time series of averaged wound areas with measured quantities including the initial wound radius A, the recoiled wound radius a_R, and the tissue thickness L. Given these measurements, the reference geometry and the residual stress can be calculated in the following way.

Let $\mathcal{F}_1$ and $\mathcal{F}_2$ denote, respectively, the deformations from the stress-free configuration (S_0) to the residually stressed (S_1) and recoiled (S_2) configurations. If a material point in S_0, S_1 and S_2 is given by $\mathbf{X_0}$, $\mathbf{X}$ and $\mathbf{x_R}$, respectively, then $\mathcal{F}_1 = \frac{\partial \mathbf{X}}{\partial \mathbf{X_0}}$ and $\mathcal{F}_2 = \frac{\partial \mathbf{x_R}}{\partial \mathbf{X_0}}$. The recoil phase occurs within hours, a much shorter time-frame than that for tissue growth [Ghosh et al., 2007]. Therefore, it is reasonable to assume that no growth occurs during recoil. Hence for the deformations $\mathcal{F}_1$ and $\mathcal{F}_2$ we take $\mathcal{G} = \mathbb{I}$.

Assuming no body forces and that the tissue is in mechanical equilibrium, the balance of linear momentum supplies

$$\nabla \cdot \mathbf{T} = \mathbf{0}. \tag{4.5}$$

For plane stress, the only non-trivial component of Equation (4.5) is

$$\frac{\partial T_{rr}}{\partial r} + \frac{1}{r}(T_{rr} - T_{\theta\theta}) = 0. \tag{4.6}$$

In S_1, the residual tension is assumed to be due to pressure at the external boundary, so that $T_{rr}|_{R_0=B_0} = T_{\text{res}}$. Upon injury the wound edge is relieved of tension, causing it to retract to a size bigger than that of the initial wound. Therefore, in the recoiled configuration S_2, we have $T_{rr}|_{R_0=A_0} = 0$. Far from the wound we expect the healthy dermis to remain residually stressed so that $T_{rr}|_{R_0=B_0} = T_{\text{res}}$ in S_2.

The deformation $\mathcal{F}_1$ is found by solving Equation (4.1) with $\mathcal{G} = \mathbb{I}$ (no growth has

occurred yet) and R being the current variable, yielding

$$R = \frac{R_0}{\sqrt{\lambda_1}}, \tag{4.7}$$

where λ_1, the axial stretch associated with the deformation $\mathcal{F}_1$, is determined by imposing $R|_{R_0=B_0} = B$ in Equation (4.7), resulting in

$$R = \frac{B}{B_0} R_0. \tag{4.8}$$

The components of the elastic tensor are

$$\alpha_r = \alpha_\theta = \frac{B}{B_0} \quad \text{and} \quad \alpha_z = \frac{B_0^2}{B^2}. \tag{4.9}$$

Since $\alpha_r = \alpha_\theta$, Equations (4.3) and (4.4) give $T_{rr} = T_{\theta\theta}$. Imposing $T_{rr}|_{R_0=B_0} = T_{\text{res}}$ in Equation (4.6) we deduce that $T_{rr} \equiv T_{\text{res}}$ is constant. From Equation (4.3), the axial stress is also constant and can be determined from the boundary condition

$$N_z = 2\pi \int_0^B T_{zz} R \, \mathrm{d}R = \pi T_{zz} B^2. \tag{4.10}$$

Assuming no axial load in S_1 ($N_z = 0$) it follows that $T_{zz} = 0$ in Equation (4.10). Therefore, the residually stressed configuration is one of constant planar isotropic stress with $\mathbf{T}^* = \text{diag}(T_{\text{res}}, T_{\text{res}}, 0)$. For a neo-Hookean material with $N_z = 0$, Equations (4.3), (4.4) and (4.9) imply

$$T_{\text{res}} + \mu \left(\frac{B_0^4}{B^4} - \frac{B^2}{B_0^2} \right) = 0. \tag{4.11}$$

For the deformation $\mathcal{F}_2$, Equation (4.1) with $\mathcal{G} = \mathbb{I}$ and $r|_{R_0=A_0} = a_R$ gives

$$r^2 = \frac{R_0^2 - A_0^2}{\lambda_2} + a_R^2, \tag{4.12}$$

where λ_2 is the axial stretch associated with the deformation $\mathcal{F}_2$. The radial stress is determined by substituting Equations (4.3) and (4.4) into Equation (4.6) and integrating subject to $T_{rr}|_{r=a_R} = 0$ to obtain

$$T_{rr} = \frac{\mu}{2\lambda_2}\left[\log\left(\frac{\lambda_2(r^2 - a_R^2) + A_0^2}{A_0^2}\right) - \log\left(\frac{r^2}{a_R^2}\right) + \left(\frac{A_0^2}{\lambda_2} - a_R^2\right)\left(\frac{1}{r^2} - \frac{1}{a_R^2}\right)\right]. \quad (4.13)$$

Imposing $T_{rr}|_{r=b_R} = T_{\text{res}}$, Equations (4.11) and (4.13) can then be equated to eliminate T_{res}, giving

$$\frac{1}{2\lambda}\left[\log\left(\frac{B^2}{A^2}\right) + (A_0^2 - \lambda_2 a_R^2)\left(\frac{1}{B_0^2 - A_0^2 + \lambda_2 a_R^2} - \frac{1}{\lambda_2 a_R^2}\right) - \log\left(\frac{B_0^2 - A_0^2 + \lambda_2 a_R^2}{\lambda_2 a_R^2}\right)\right] + \left(\frac{B_0^4}{B^4} - \frac{B^2}{B_0^2}\right) = 0 \quad (4.14)$$

where λ_2 is found by assuming no axial load, that is,

$$2\pi \int_{a_R}^{b_R} T_{zz} r \, \mathrm{d}r = 0. \quad (4.15)$$

Given measurements of the initial (A) and recoiled (a_R) wound radii, respectively, the thickness of the tissue *in vivo* (L), the tissue stiffness (μ), and the outer radius (B), Equations (4.14) and (4.15) can be solved simultaneously for B_0 and λ_2. The stress-free reference geometry, $\{A_0, B_0, L_0\}$, is then fully determined and the residual stress, T_{res}, is given by Equation (4.11).

4.2.4 Domain size

From Equation (4.11), we note that the residual stress depends on the outer radius B. However, we expect this to saturate with large B, thus we seek a domain size sufficiently large such that T_{res} in Equation (4.11) is not affected by small changes in the location of the outer radius. Before continuing, we note that there exists a wide range of parameter values and wound sizes in the literature. This is partly due

to measurements being taken from different species. Since most data available are for wound healing in mice we choose our reference variables and parameter values accordingly. Following the experiments of McGrath and Simon [1983] (in which circular wounds in mice retract to a radius approximately 110% of the initial cut), we take an initial wound radius $A = 4$ mm that recoils to $a_R = 4.4$ mm. For these values we compute T_{res} in Equation (4.11) while varying B – the result is plotted in Figure 4.4 for three different choices of μ[1]. We observe that T_{res} asymptotes as B increases; thus, for a wound of initial radius $A = 4$ mm, we assign the outer radius of the domain to $B = 20$ mm.

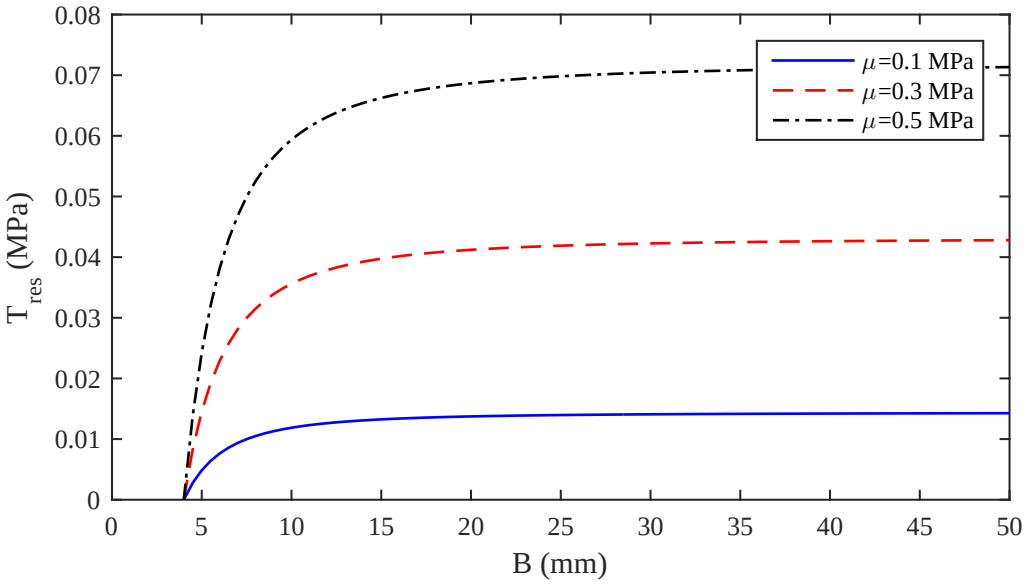

Figure 4.4: Residual stress as a function of the outer radius. The residual stress is calculated from Equation (4.11) for a wound with $A = 4$ mm, $a_R = 4.4$ mm and $L = 0.1$ mm for increasing B. The shear elastic modulus is $\mu = 0.1$ (solid blue), $\mu = 0.3$ (dashed red) and $\mu = 0.5$ MPa (dash-dotted black). The calculated residual stress increases as the shear elastic modulus increases. For sufficiently large modelling domain T_{res} plateaus.

Note that we have assumed that the wound and surrounding tissue are planar. Therefore, although a radius of 20 mm may be wider than the flank of the mouse,

[1]In fact, when scaling the stress tensor by the shear elastic modulus, the curves in Figure 4.4 are identical.

it is less than the dimensions of the full skin of the mouse, if the skin were to be planar. As mice have low levels of resting stress [Aarabi et al., 2007], it is likely that the residual stress in human skin is greater than that shown in Figure 4.4.

4.2.5 Shear elastic modulus

Measured values for the shear elastic modulus μ for dermal tissue may vary by a factor of 3000 depending on the model and experimental apparatus used [Diridollou et al., 2000]. A large range of residual stress in the skin has also been reported, between 0.005 and 0.1 MPa [Diridollou et al., 2000, Aarabi et al., 2007, Jacquet et al., 2008, Flynn et al., 2011]. As the stress has linear dependence on μ, we can use the residual stress calculation to estimate a physiological range for μ.

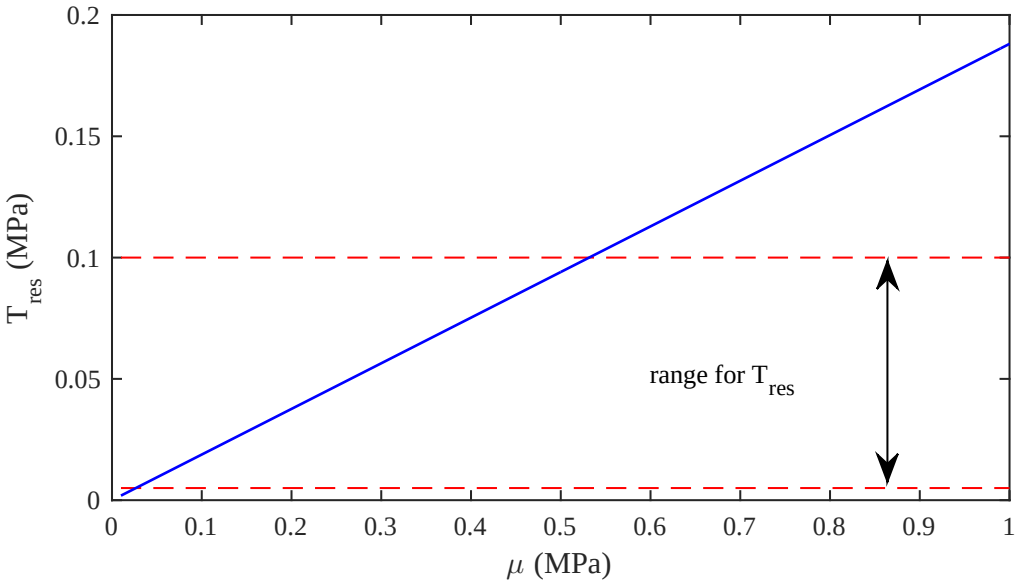

Figure 4.5: Residual stress as a function of the shear elastic modulus. The residual stress is calculated according to Equation (4.11) for a wound with $A = 4$ mm, $a_R = 4.4$ mm and $L = 0.1$ mm for varying μ. For biologically realistic values of the residual stress as stated in the literature, the shear elastic modulus must lie in the range $0.02 < \mu < 0.52$ MPa.

In Figure 4.5 we plot T_{res} against μ. For $0.02 < \mu < 0.52$ MPa, the residual stress lies within the previously reported range $0.005 < T_{\text{res}} < 0.1$ MPa. Although

the biological literature estimates that the shear stress can take values between 0.006 and 20 MPa, our model suggests that $\mu > 0.52$ MPa yields unphysiological values of the residual stress.

4.2.6 Contraction alone

The calculations of Section 4.2.3 have established the stress-free state and the residual tension. We now turn to the healing of the wound. One of our modelling aims is to explore the impact of mechanosensitive growth during dermal healing. This requires the definition of an evolution law for the growth tensor $\mathcal{G}$. As a starting point we assume that no growth occurs and that wound closure is driven by contraction only. We use the mechanical framework to quantify the degree of stress that would be generated in the tissue in this scenario.

Wound contraction in adult dermal wounds is driven by fibroblasts that localise on the wound edge and pull the tissue inwards [Ehrlich, 1988, Ehrlich and Rajaratnam, 1990]. The data presented in Figure 2.2 indicate that, after wound closure (defined by closure of the epidermis), the non-diabetic dermal radius is reduced to approximately 0.6 mm. If there is no growth, we can simply impose a deformation from the post-wound state S_2 to an equilibrium configuration in which the wound radius has decreased by the appropriate amount. From Equations (4.3), (4.4) and (4.6) we deduce that the radial stress at the inner boundary required to deform the wound radius from its original size to its final contracted size a_c, is given by

$$T_{rr}|_{R_0=A_0} = T_{\text{res}} - \frac{\mu}{2\lambda}\left[\log\left(\frac{B_0^2}{A_0^2}\right) - \log\left(\frac{B_0^2 - A_0^2 + \lambda a_c^2}{\lambda a_c^2}\right) + \left(A_0^2 - \lambda a_c^2\right)\left(\frac{1}{B_0^2 - A_0^2 + \lambda a_c^2} - \frac{1}{\lambda a_c^2}\right)\right], \tag{4.16}$$

where λ is determined by solving Equation (4.15) and the reference variables and residual stress are as calculated in Section 4.2.3.

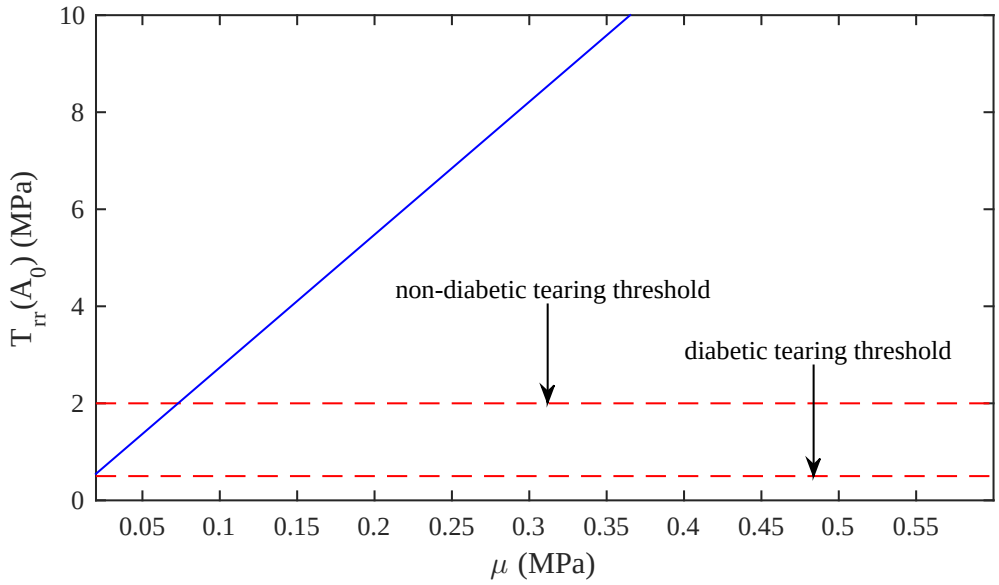

Figure 4.6: Radial stress on the inner boundary required for dermal closure with no growth. Equation (4.16) is solved for varied values of μ and N_z with reference variables: $A = 4$ mm, $a_R = 4.4$ mm, $B = 20$ mm, $L = 0.1$ mm and final wound radius $a_c = 0.6$ mm. For a wide range of parameter values, the radial stress calculated is higher than the dermal tissue can physically withstand.

Mechanical testing reveals that, on average, mouse skin fails to withstand stresses higher than 2 MPa [Bermudez et al., 2011] and samples of dermis from diabetic mice tear at stresses as low as 0.5 MPa. In Figure 4.6 we plot the stress at the inner edge as a function of μ. We find that, for a wide range of μ, the radial stress on the wound edge is higher than 2 MPa. Further, for all realistic values of μ, determined in Section 4.2.5, the radial stress exceeds 0.5 MPa. This suggests that if healing occurs by contraction alone then stresses higher than the tissue can withstand will be generated. Thus for a wound to reduce by the degree observed experimentally, volumetric growth must contribute to closure, relieving the high tension generated by contraction.

We further note that the circumferential stress at the wound edge can be computed from Equations (4.3), (4.4) and (4.16) revealing a highly compressive circumferential stress. This can be observed for the planar case ($\lambda = 1$) in Figure 4.7 where we plot

the radial and circumferential stresses as functions of position for contraction only. As well as a high radial tension and circumferential compression at the wound edge we observe a rapid change in both stresses as functions of the reference configuration. However, if the stresses were plotted as functions of the current configuration, this gradient would be less pronounced.

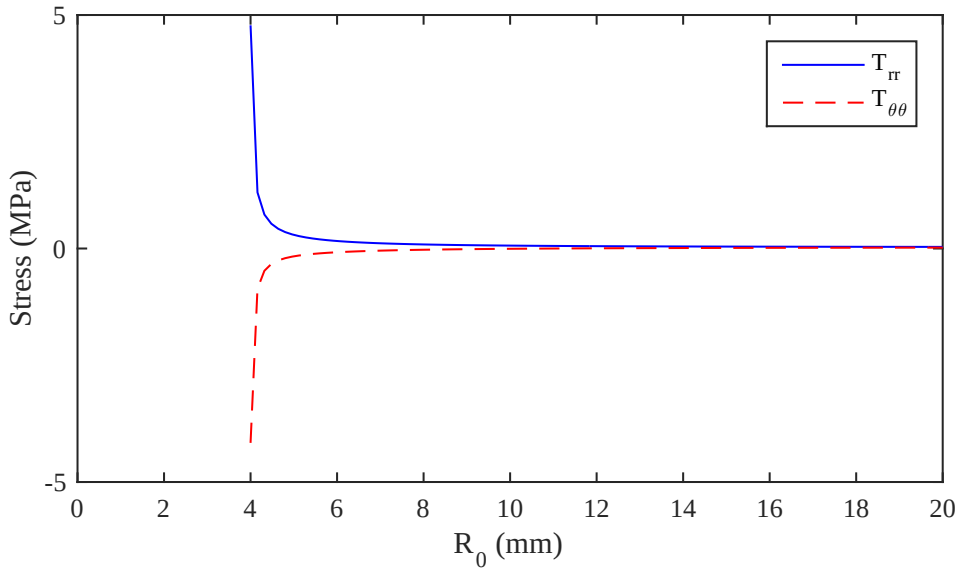

Figure 4.7: Radial and circumferential stress for dermal closure with no growth. Equations (4.3), (4.4) and (4.6) are solved with $T_{rr}|_{R_0=B_0} = T_{\text{res}}$. Parameter values and reference variables: $\mu = 0.2$ MPa, $\lambda = 1$, $A = 4$ mm, $a_R = 4.4$ mm, $B = 20$ mm, $L = 0.1$ mm and $a_c = 0.6$ mm. The radial (solid blue) and circumferential (dashed red) stresses are plotted as functions of position.

4.2.7 Anisotropic homogeneous growth

Growth of the tissue is described by a continuous time-dependent process. In order to gain intuition for a sensible growth law it is instructive to analyse the effect of pure growth in a simple setting. We neglect all body forces and boundary loads, and consider the effect of time-independent anisotropic but homogeneous planar growth on an annulus of tissue. That is, we take γ_r and γ_θ as constants (with $\gamma_z = 1$ and $\lambda = 1$), and consider the deformation and stress due to growth alone in the $(\gamma_r, \gamma_\theta)$ plane. We

seek to gain a qualitative understanding of the impact of radial and circumferential growth on the geometry of the tissue by looking for biologically realistic constraints on the growth of the cylinder.

Under these simplifications the deformation and stress satisfy

$$\frac{\partial r}{\partial R_0} = \gamma_r \gamma_\theta \frac{R_0}{r}, \tag{4.17a}$$

$$\frac{\partial T_{rr}}{\partial R_0} = \frac{\mu \gamma_r \gamma_\theta R_0}{r^2} \left(\frac{r^2}{\gamma_\theta^2 R_0^2} - \frac{\gamma_\theta^2 R_0^2}{r^2} \right). \tag{4.17b}$$

Solving Equations (4.17) subject to stress-free boundary conditions, we obtain an implicit equation for the current wound radius a in terms of γ_r, γ_θ and the reference variables:

$$\begin{aligned} 0 =& \frac{\gamma_r}{2\gamma_\theta} \log\left(\frac{B_0^2}{A_0^2}\right) - \frac{\gamma_\theta}{2\gamma_r} \log\left(\frac{\gamma_r\gamma_\theta(B_0^2 - A_0^2) + a^2}{a^2}\right) \\ &+ \frac{\gamma_\theta}{2\gamma_r}\left(a^2 - \gamma_r\gamma_\theta A_0^2\right)\left(\frac{1}{a^2} - \frac{1}{\gamma_r\gamma_\theta(B_0^2 - A_0^2) + a^2}\right). \end{aligned} \tag{4.18}$$

Similarly, we can obtain an implicit equation for the outer radius of the cylinder, b, by using Equation (4.17a) to substitute for a in Equation (4.18),

$$\begin{aligned} 0 =& \frac{\gamma_r}{2\gamma_\theta} \log\left(\frac{B_0^2}{A_0^2}\right) - \frac{\gamma_\theta}{2\gamma_r} \log\left(\frac{b^2}{b^2 - \gamma_r\gamma_\theta(B_0^2 - A_0^2)}\right) \\ &+ \frac{\gamma_\theta}{2\gamma_r}\left(b^2 - \gamma_r\gamma_\theta B_0^2\right)\left(\frac{1}{b^2 - \gamma_r\gamma_\theta(B_0^2 - A_0^2)} - \frac{1}{b^2}\right). \end{aligned} \tag{4.19}$$

Equations (4.18) and (4.19) allow us to explore the effect of differential radial (γ_r) and circumferential (γ_θ) growth on the cylinder.

4.2.7.1 Regions of parameter space

We solve Equations (4.18) and (4.19) numerically[2] to find the curves in $(\gamma_r, \gamma_\theta)$ space on which $a = A_0$ and $b = B_0$, respectively. In Figure 4.8 we show how the $(\gamma_r, \gamma_\theta)$ parameter space can be decomposed into distinct regions, each associated with a different grown configuration. We anticipate, for normal healing, that growth in the dermis will cause the inner radius, a, to decrease and fill the wound space. At the same time, the outer radius, b, should not change markedly so that material is not compressed or stretched far from the wound. This behaviour, with $a < A_0$ and $b \approx B_0$, corresponds to those parts of regions 5 or 6 in Figure 4.8 that are close to the curve $b = B_0$.

We observe that close to the curve $b = B_0$, as γ_r increases, γ_θ decreases, indicating that growth must be anisotropic. This is consistent with the modelling assumptions of Wu and Ben Amar [2015]: they constrain $\gamma_\theta < 1$ in order to obtain wound closure. If growth were isotropic, i.e. $\gamma_r = \gamma_\theta$, the configuration of the cylinder would lie in region 4 (along the black dotted line) and growth would cause the wound to expand. Hence isotropic growth is counterproductive for wound healing. We may also interpret growth which yields $a = A_0$ (or $a > A_0$) as corresponding to the stalled healing we might associate with untreated diabetic ulcers. We do not investigate this case in our work as the diabetic wounds from the experimental data presented in Chapter 2 do heal, although more slowly than the non-diabetic wounds.

We represent, schematically, the current configurations for each region in Figure 4.9. Although regions 1 and 6 are qualitatively the same, in region 1 material

[2]The implicit equations are solved numerically using a root-finding algorithm and an arc-length continuation method. Details of these methods are given in Appendix B.1.1 and B.1.2. In order to check that our numerical solutions are correct we perform asymptotic analysis on Equations (4.18) and (4.19). This analysis further allows us to determine how the radial and circumferential growth laws should be inter-related at extreme values of γ_r and γ_θ. We seek the limits of the curves $a = A_0$ and $b = B_0$ as $\gamma_r \to 0$ and $\gamma_r \to \infty$. By finding these limits we determine the points to which we would expect our growth functions to tend for large times. Results of the asymptotic analysis are given in Appendix B.2.

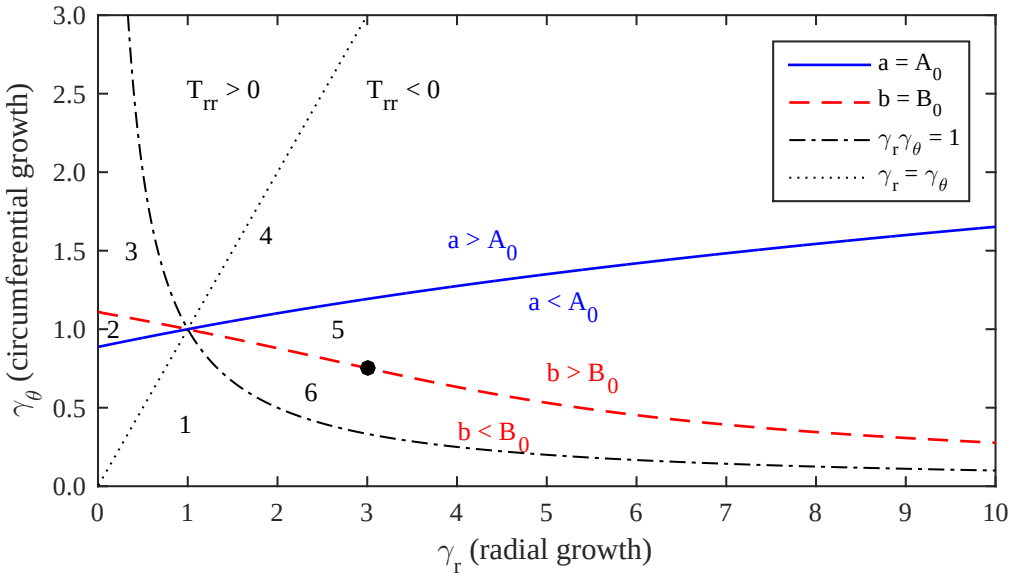

Figure 4.8: Analysis of compatible growth laws. Equations (4.18) and (4.19) are solved numerically to find the curves in $(\gamma_r, \gamma_\theta)$ space such that $a = A_0$ (solid blue) and $b = B_0$ (dashed red). The dashed black line represents no growth, i.e. $\gamma_r\gamma_\theta = 1$ and the black dotted line represents isotropic growth, i.e. $\gamma_r = \gamma_\theta$. Regions 1 to 6 represent different grown configurations of the dermal cylinder. For $\gamma_r > \gamma_\theta$ growth causes radial compression, whereas for $\gamma_\theta > \gamma_r$, growth causes radial tension. Reference variables are $A_0 = 4$ mm and $B_0 = 5$ mm corresponding to a proliferative band of width 1 mm surrounding the wound.

is removed whereas in region 6 it is synthesised. A similar difference distinguishes regions 3 and 4.

We observe that addition of material creates a compressive stress, $T_{rr} < 0$, (see Figure 4.10) and hence conclude that growth serves to counteract the excessive tension created by contraction. On the other hand, both growth and contraction create a compressive circumferential stress near the wound edge. A highly compressive circumferential stress can result in circumferential buckling (see Wu and Ben Amar [2015] for example), which could mark the onset of scarring. The effect of contraction and growth is counteracted by the fact that the circumferential stress is tensile in the recoiled wound.

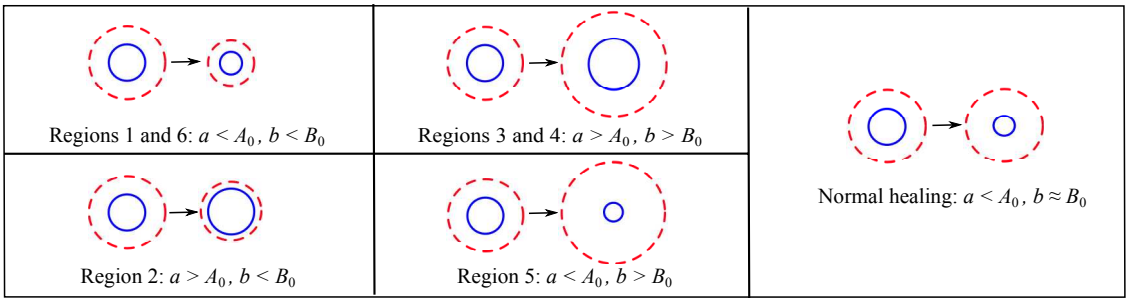

Figure 4.9: Grown configurations of the dermal cylinder. The reference configuration is compared with the current configuration after the deformation described by Equation (4.17a) with a satisfying (4.18), b satisfying (4.19), $A = 4$ mm and $B = 5$ mm. The inner radius ($A_0 \to a$) is shown in solid blue and the outer radius ($B_0 \to b$) in dashed red.

4.2.7.2 On geometry

The above analysis highlights the interplay between geometry and mechanics in the wound healing process. In essence, filling a wound in a circular geometry involves a packing problem. In a circular geometry, in order to extend inward radially the tissue must also vary in the orthogonal direction, undergoing circumferential resorption and/or being put in circumferential compression. In a one-dimensional Cartesian geometry – a 'slash wound' – no such geometrical issues exist. The tissue can grow in one Cartesian direction with no change in deformation or stress induced in the orthogonal directions. Such issues, clearly visible at the tissue level, must be resolved through coordinated activities at the cell level. From a tissue-scale modelling viewpoint, such processes are manifest in feedback between mechanical stress and growth. For this, we next turn to heterogeneous growth laws.

4.2.8 Mechanosensitive growth laws

In general, our growth laws comprise an evolution equation for the growth tensor of the form discussed in Chapter 3. In the current chapter, we are interested in mechanically stimulated growth and postulate the form $\dot{\mathcal{G}} = \mathbf{K}(\mathbf{T} - \mathbf{T}^*)\mathcal{G}$, with $\mathbf{K}$ a diagonal tensor so that stress in a given direction induces growth only in that

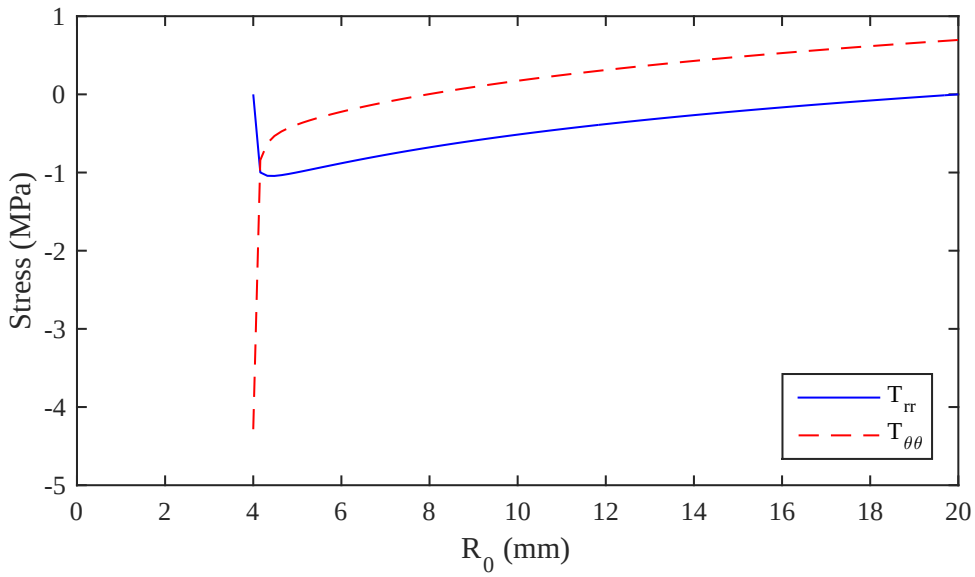

Figure 4.10: Radial and circumferential stress for homogeneous planar growth. Equations (4.17) are solved with stress-free boundary conditions and the radial (solid blue) and circumferential (dashed red) stresses are plotted as functions of position. We take $\mu = 0.2$ MPa and $\lambda = 1$ with reference variables: $A = 4$ mm, $a_R = 4.4$ mm and $B = 20$ mm. The growth components are $\gamma_r = 3$ and $\gamma_\theta = 0.75$ marked by $\bullet$ in Figure 4.8.

direction. In component form this is expressed as

$$\frac{\partial \gamma_r}{\partial t} = k(T_{rr} - T_{\text{res}})\gamma_r, \tag{4.20a}$$

$$\frac{\partial \gamma_\theta}{\partial t} = m(T_{\theta\theta} - T_{\text{res}})\gamma_\theta, \tag{4.20b}$$

$$\frac{\partial \gamma_z}{\partial t} = nT_{zz}\gamma_z. \tag{4.20c}$$

In Equations (4.20) k, m and n are growth rate parameters and T_{res} is the resting residual stress. We note that contraction leads to high radial tension ensuring that $T_{rr} > 0$ and close to the wound edge $T_{\theta\theta} < 0$. This observation suggests that γ_r and γ_θ will naturally evolve towards the 'wound filling' location of the phase space in Figure 4.8 if k, m, and n are non-negative. Initially, no growth occurs so that $\mathcal{G}|_{t=0} = \mathbb{I}$. Equations (4.20), with $k, m, n > 0$, imply that stress higher than the residual stress $\mathbf{T}^*$ stimulates growth, whereas stress lower than the residual stress causes

resorption. This has been observed in wound healing where fibroblast proliferation and collagen synthesis is enhanced in the presence of tension [Kessler et al., 2001] and release of tension can induce fibroblast cell death [Grinnell et al., 1999, Chipev and Simon, 2002]. Similar assumptions and growth laws have been used in other biological applications such as embryonic wound closure [Taber, 2009] and remodelling of arteries [Alford et al., 2008].

4.2.9 Timescales and recoil dynamics

As the dermis moves this causes friction against the underlying subdermis. Assuming that there is a frictional body force resisting radial motion of the dermis, Equation (4.2) can be written as

$$\rho\ddot{\mathbf{x}} - \nabla \cdot \mathbf{T} + q\dot{\mathbf{x}} = \mathbf{0}, \tag{4.21}$$

where q the coefficient of friction. If the wound opens, $\dot{\mathbf{x}} > 0$ and the drag term acts towards the wound centre whereas if the wound closes $\dot{\mathbf{x}} < 0$ and drag acts away from the wound centre.

We now use dimensional arguments to justify whether the time-dependent terms in Equation (4.21) are relevant during healing. Let χ denote a characteristic length and t_e, t_d and t_g the elastic, drag and growth timescales, respectively. From Equations (4.3) and (4.4), we deduce that the Cauchy stress tensor scales with the shear elastic modulus, μ. The elastic timescale can be determined by balancing the first two terms in Equation (4.21), giving $t_e = (\rho\chi^2/\mu)^{1/2}$.

The healing of the wound occurs on the growth timescale, which is on the order of days [Ghosh et al., 2007]. Typical values for the tissue density, 10^{-6} kg mm^{-3}, shear elastic modulus, 0.2 MPa (see Section 4.2.5), and characteristic length, 4 mm, reveal that $t_e \approx \mathcal{O}(10^{-4})$ seconds. Unsurprisingly, $t_e \ll t_g$ and it is appropriate to neglect

inertial terms in Equation (4.21).

Balancing the second and third terms in Equation (4.21) gives a drag timescale of $t_d = q\chi^2/\mu$. The drag timescale sets the time of wound recoil, which is on the order of hours. This gives $q \approx \mathcal{O}(10^{-3})$ MPa days mm^{-2}. In Chapter 2 we found that the friction coefficient was at least an order of magnitude smaller than the other model parameters. Therefore the friction term has negligible effect on the system unless $\dot{\mathbf{x}}$ is large. From wound healing experiments we anticipate that $\dot{\mathbf{x}}$ will be large initially, as the wound recoils. Once the recoil is complete, the tissue velocity is much slower, and the drag plays a negligible role, i.e the tissue is essentially in mechanical equilibrium during the growth and contraction phase. The model behaviour with respect to friction is investigated more thoroughly in Section 4.4.3. We further note that, in practice, the dermal tissue is tethered to the underlying layers and although this may have some effect on the movement of the dermis these interactions have not been well studied. We therefore restrict the body force to a drag term only: based on our experience in Chapter 2, we expect this will produce the desired behaviour.

4.2.10 Boundary conditions

The 'pulling' of the dermal edges is assumed to be caused by fibroblasts arranged close to the wound edge. We therefore impose radial tension at $R_0 = A_0$ according to a contraction function. Far from the wound the tissue is assumed to be residually stressed. This translates to the following boundary conditions

$$T_{rr}(A_0, t) = f_c \quad \text{and} \quad T_{rr}(B_0, t) = T_{\text{res}}, \tag{4.22}$$

where f_c is a contraction function acting on the wound edge and T_{res} is the uniform planar residual stress of the unwounded dermis calculated in Section 4.2.3.

In Chapter 6 we will couple contraction to a mechanistic description of fibroblast

activity. For now we approximate the contractile force that the fibroblasts exert by a phenomenological function. In particular we assume that the total radial stress exerted by the fibroblasts at the wound edge is proportional to its circumference. We have chosen this law since we would expect the number of fibroblasts to be restricted by space. We further assume that the stress exerted switches on at a given time ($t = t_c > 0$) post wounding, since it takes time for the fibroblasts to migrate to the wound edge. For simplicity we represent the contractile activity of the fibroblasts as

$$f_c(t) = fa(t)\mathcal{H}(t; t_c, t_m), \tag{4.23}$$

where f is the contraction coefficient, a is the wound radius and $\mathcal{H}$ is a linear switch function, parametrised by t_c and t_m. For simplicity (to minimise the number of model parameters) and to capture the time at which contraction begins and when it reaches a maximum, we use a piecewise linear switch function of the form

$$\mathcal{H}(t; t_c, t_m) = \begin{cases} 0 & \text{for } t < t_c \\ \frac{t-t_c}{t_m-t_c} & \text{for } t_c < t < t_m \\ 1 & \text{for } t > t_m. \end{cases} \tag{4.24}$$

The switch function approximates the time taken for fibroblasts to migrate to the wound edge and begin contracting the tissue. Contraction begins approximately 2 days post wounding and attains its maximal value approximately $5 - 14$ days after injury [Monaco and Lawrence, 2003]. In Equation (4.24), t_c is the time at which fibroblasts start to localise around the margin and t_m is the time at which the fibroblasts exert their maximum contractile effect. We use the linear form of the switch function as opposed to the Heaviside approximation in Chapter 2 since we have biological ranges from the literature for the two parameters in Equation (4.24).

The axial deformation, $\lambda(t)$, is determined by imposing

$$N_z(t) = \frac{2\pi}{\lambda(t)} \int_{A_0}^{B_0} \gamma_r \gamma_\theta \gamma_z T_{zz} R_0 \, \mathrm{d}R_0, \tag{4.25}$$

where N_z is the load applied to the top of the dermal cylinder. In Equation (4.25) we model the resistance of the epidermal layer to axial deformation of the dermis by defining the axial load in the following way

$$N_z = \eta(1 - \lambda), \tag{4.26}$$

where η is a constant of proportionality, describing the dependence of the dermal thickness on the axial load. Thickening of the dermis causes a negative load, pushing the dermis back down and, similarly, thinning causes a positive load, pulling the dermis back up.

4.3 The full model

For numerical purposes it is appropriate to compute the dependent variables in terms of the reference configuration. For completeness, we now restate the full model in

terms of the reference variable, R_0,

$$\frac{\partial r}{\partial R_0} = \gamma_r \gamma_\theta \gamma_z \frac{R_0}{\lambda r}, \tag{4.27a}$$

$$\frac{\partial T_{rr}}{\partial R_0} = \frac{\gamma_r \gamma_\theta \gamma_z R_0}{\lambda r} \left[\frac{\alpha \hat{W}_\alpha}{r} + q \frac{\partial r}{\partial t} \right], \tag{4.27b}$$

$$T_{\theta\theta} = T_{rr} + \alpha \hat{W}_\alpha, \tag{4.27c}$$

$$T_{zz} = T_{rr} + \lambda \hat{W}_\lambda, \tag{4.27d}$$

$$\frac{\partial \gamma_r}{\partial t} = \begin{cases} 0 & \text{for } t \leq t_R \\ k(T_{rr} - T_{\text{res}})\gamma_r & \text{for } t > t_R \end{cases}, \tag{4.27e}$$

$$\frac{\partial \gamma_\theta}{\partial t} = \begin{cases} 0 & \text{for } t \leq t_R \\ m(T_{\theta\theta} - T_{\text{res}})\gamma_\theta & \text{for } t > t_R \end{cases}, \tag{4.27f}$$

$$\frac{\partial \gamma_z}{\partial t} = \begin{cases} 0 & \text{for } t \leq t_R \\ nT_{zz}\gamma_z & \text{for } t > t_R \end{cases}. \tag{4.27g}$$

In Equations (4.27) $t = t_R$ is the time at which the wound has fully recoiled. The recoil phase occurs on the order of hours, ending before growth and contraction begin ($t_R < t_c$). The boundary conditions determining the deformation (a and λ) and the radial stress are given by

$$T_{rr}(A_0, t) = fa(t)\mathcal{H}(t; , t_c, t_m), \tag{4.27h}$$

$$T_{rr}(B_0, t) = T_{\text{res}}, \tag{4.27i}$$

$$N_z(t) = \frac{2\pi}{\lambda(t)} \int_{A_0}^{B_0} \gamma_r \gamma_\theta \gamma_z T_{zz} R_0 \, \mathrm{d}R_0 \equiv \eta(1 - \lambda(t)). \tag{4.27j}$$

The initial conditions for the components of the growth tensor are given by

$$\gamma_r(R_0, 0) = 1, \quad \gamma_\theta(R_0, 0) = 1 \quad \text{and} \quad \gamma_z(R_0, 0) = 1. \tag{4.27k}$$

Note that, under the assumption of incompressibility, $\hat{W}$ is an auxiliary strain-energy function of only two variables. Unless specified otherwise, the tissue follows a neo-Hookean strain-energy function, given by

$$\hat{W}(\alpha, \lambda) = \frac{\mu}{2}\left(\frac{\gamma_z^2}{\alpha^2\lambda^2} + \alpha^2 + \frac{\lambda^2}{\gamma_z^2} - 3\right), \quad \text{where} \quad \alpha = \frac{r}{\gamma_\theta R_0}. \tag{4.27l}$$

Since γ_r, γ_θ and γ_z depend on R_0, Equations (4.27) are solved numerically in MATLAB. For each time increment, the growth in Equations (4.27e)-(4.27g) are updated via a forward Euler scheme [Press et al., 1994]. The radial deformation and radial stress in Equations (4.27a) and (4.27b) are then updated using the boundary value problem solver `bvp4c`, subject to the boundary conditions in Equations (4.27h)-(4.27j). Details of the numerical method are given in Appendix B.1.3.

4.4 Model behaviour

In this section we present typical model solutions, obtained using the parameter values stated in Table 4.1. The parameter values are either taken from the biological literature, estimated from model behaviour in the previous sections or chosen to give good qualitative agreement with the wound healing data.

The plot of the dermal wound radius, $a(t)$, presented in Figure 4.11, reveals three distinct phases. During the first phase, which lasts for approximately 2 days, the wound radius first retracts to 110% of the initial value due to residual tension in the surrounding tissue and then plateaus before growth and contraction are activated. During the second phase ($2 < t < 14$ days) the wound radius decreases rapidly due to contraction at the wound edge and proliferation of the surrounding tissue. At later times ($t > 14$ days), as the wound radius decreases, contraction slows down, since it is proportional to the current wound radius. As a result of the mechanosensitive properties of the tissue, growth also slows down and the wound radius begins to

Table 4.1: Parameters for the morphoelastic model. Table summarising the parameters that appear in the mathematical model in Equation (4.27) along with their physical interpretation, default values chosen for the model and supporting references where appropriate.

parameter	physical interpretation	units	physical range	reference	default
k	radial growth	$\text{MPa}^{-1}\ \text{days}^{-1}$	$k > 0$		0.2
m	circumferential growth	$\text{MPa}^{-1}\ \text{days}^{-1}$	$m > 0$		0.1
n	axial growth	$\text{MPa}^{-1}\ \text{days}^{-1}$	$n > 0$		0.1
f	contraction	N mm^{-3}	$0 < f < 1.325$	[Uhal et al., 1998, Wrobel et al., 2002]	0.2
t_c	contraction begins	days	$2 - 5$	[Monaco and Lawrence, 2003]	2
t_m	maximum contraction	days	$5 - 14$	[Monaco and Lawrence, 2003]	14
q	friction	MPa days mm^{-2}	$q = \mathcal{O}(10^{-3})$	estimated in Section 4.2.9	0.002
μ	shear elastic modulus	MPa	$0.02 < \mu < 0.52$	estimated in Section 4.2.5	0.2
N_z	axial load	N			
η	load coefficient	N			10
A	initial wound radius	mm	$A > 0$	[McGrath and Simon, 1983]	4
a_R	recoiled wound radius	mm	$a_R > A$	[McGrath and Simon, 1983]	4.4
B	domain size	mm	$B > a_R$	estimated in Section 4.2.4	20
L	tissue thickness	mm	$L > 0$	data in Figure 4.2	0.1

plateau. We note that the healing curve is qualitatively similar to the experimental data presented in Figure 2.2 and that of McGrath and Simon [1983].

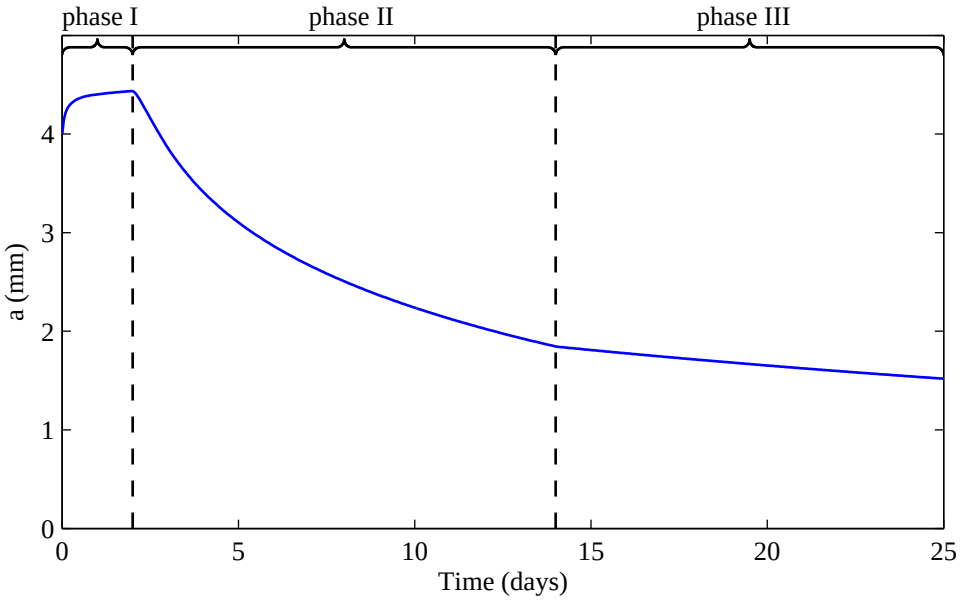

Figure 4.11: Typical model solution with healing phases. Equations (4.27) are solved numerically and the wound radius $a(t)$ is plotted as a function of time. Reference variables and parameters are specified using the default values in Table 4.1. The healing curve can be separated into three distinct phases representing the initial recoil, a proliferative and contracting phase and finally the rate of closure slows down as contraction and growth decrease.

In Figure 4.12 we plot the growth and stress components as functions of radius R_0 at days 5, 10 and 25. As expected, since growth is mechanosensitive, with the growth rates in Equations (4.20) depending linearly on the stress, the growth profiles are qualitatively similar to the stress. Radial growth increases over time as the radial stress increases due to contraction. The piecewise linear step function reaches a maximum at day 14 and we observe that the radial stress at day 25 is less than that on day 10. As expected, radial growth and stress are larger closer to the wound edge. The dermis is in compression in the circumferential and axial directions and, as a consequence, material is resorbed in these directions. With $\gamma_\theta < 1 < \gamma_r$, we are in a regime associated with normal healing as identified in Section 4.2.7, for which the wound radius decreases whilst the outer radius remains approximately constant. We

interpret the removal of tissue from the circumferential direction ($\gamma_\theta < 1$) as tissue remodelling – the actual change in volume is locally given by $\det(\mathcal{G}) - 1$, which is positive.

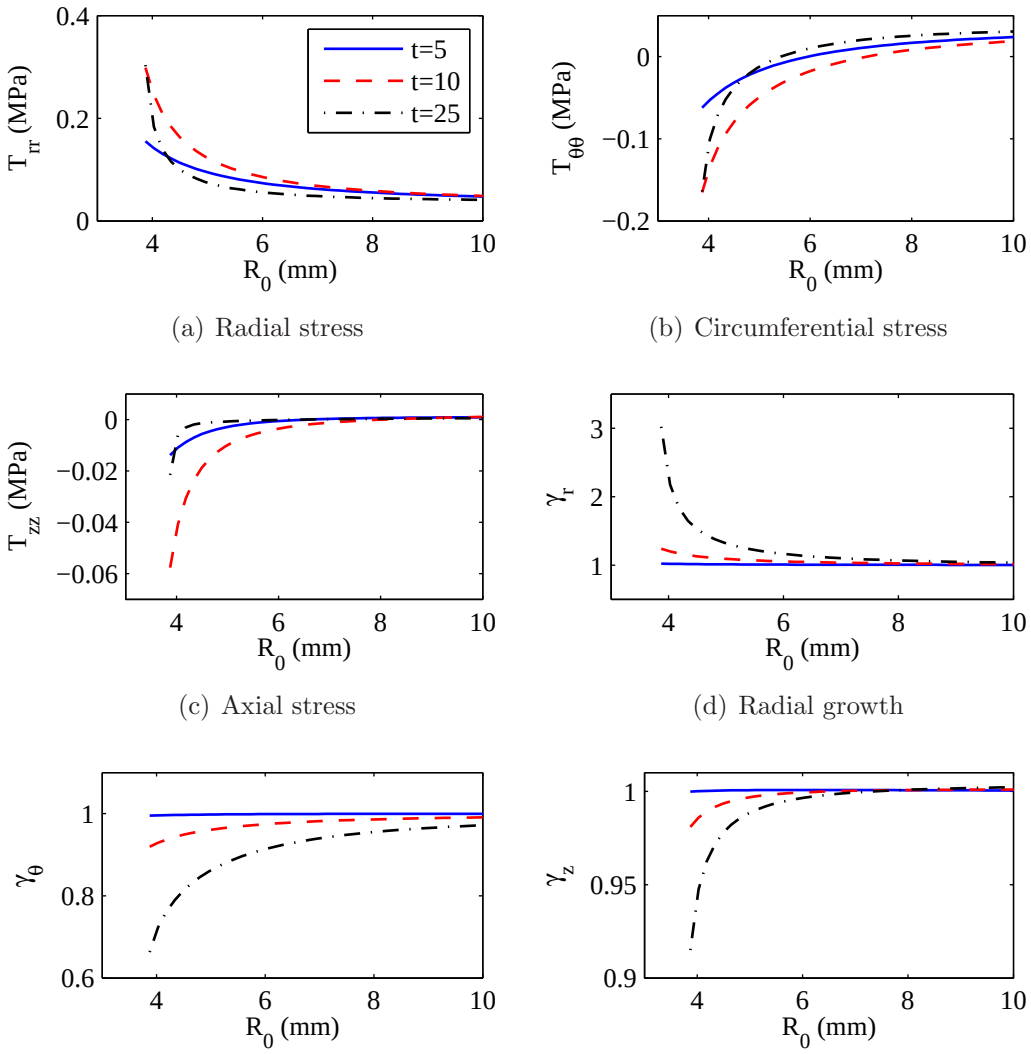

(a) Radial stress

(b) Circumferential stress

(c) Axial stress

(d) Radial growth

(e) Circumferential growth

(f) Axial growth

Figure 4.12: Typical model solution for the stress and growth. Equations (4.27) are solved numerically. (a) The radial stress T_{rr}, (b) the circumferential stress $T_{\theta\theta}$, (c) the axial stress T_{zz}, (d) the radial growth γ_r, (e) the circumferential growth γ_θ and (f) the axial growth γ_z are plotted as functions of position at 5 (solid blue), 10 (dashed red) and 25 (dash-dotted black) days. Reference variables and parameters are specified using the default values in Table 4.1. The radial stress is higher closer to the wound edge, resulting in higher radial growth there. The tissue is in compression circumferentially and axially, resulting in resorption of material in these directions.

4.4.1 Characterisation of healing phases

In this section we calculate certain quantities to characterise the different phases of healing depicted in Figure 4.11. These quantities are:

- The growth rate at a position x mm from the current wound edge

$$G_r(x,t) = \frac{1}{\bar{\gamma}_r(x,t)\bar{\gamma}_\theta(x,t)\bar{\gamma}_z(x,t)}\frac{\partial}{\partial t}(\bar{\gamma}_r(x,t)\bar{\gamma}_\theta(x,t)\bar{\gamma}_z(x,t)),$$

  where $\bar{\gamma}_i(r(R_0,t),t) = \gamma_i(R_0,t)$ for $i = r,\theta,z$.

- The average volumetric growth rate

$$\bar{G}(t) = \int_0^{L_0}\int_0^{2\pi}\int_{A_0}^{B_0}\frac{1}{\gamma_r\gamma_\theta\gamma_z}\frac{\partial}{\partial t}(\gamma_r\gamma_\theta\gamma_z)R_0 \, \mathrm{d}R_0\mathrm{d}\Theta\mathrm{d}Z_0.$$

- The growth rate of a material point starting at a position X mm from the initial wound edge

$$G_R(X,t) = \frac{1}{\gamma_r(X,t)\gamma_\theta(X,t)\gamma_z(X,t)}\frac{\partial}{\partial t}(\gamma_r(X,t)\gamma_\theta(X,t)\gamma_z(X,t)).$$

In Figure 4.13 we plot these growth measures for the simulation presented in Figure 4.11, at days 1, 8 and 20 representing phases I, II and III, respectively. There is no growth while the wound recoils (phase I). The growth rate is highest during phase II, a conclusion that is consistent across the three growth measures. We observe that the growth rate at a fixed material point decreases as that point moves away from the wound edge in the current configuration (see Figure 4.13(c)). The radial stress as a function of position, R_0, is plotted for each of the three phases in Figure 4.13(d). In phases II and III the tissue is in tension close to the wound edge. Away from the wound edge the stress in phase III is lower than that in phase II, since contraction is decreasing but growth continues due to the difference in current and resting stress.

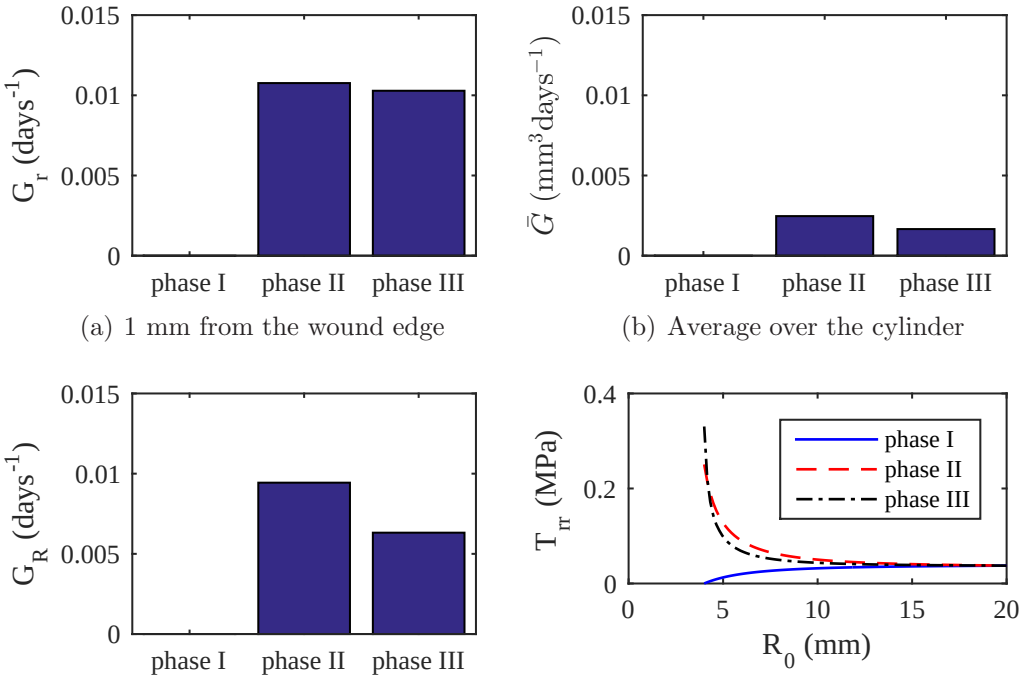

(a) 1 mm from the wound edge

(b) Average over the cylinder

(c) 4.8 mm from the wound centre

(d) Radial stress

Figure 4.13: Different growth rate measures and the radial stress for each healing phase. Equations (4.27) are solved numerically. Phase I, II and III are represented by days 1, 8 and 20, respectively. (a) The growth rate at a fixed distance from the wound edge (1 mm), (b) the average growth rate across the dermis and (c) the growth rate at a fixed material point starting at 0.8 mm from the initial wound edge, are compared for each of the three phases. (d) The radial stress as a function of R_0. Reference variables and parameters are specified using the default values in Table 4.1. We observe the same qualitative behaviour for each growth measure; no growth during the recoil phase, high growth during the contractile phase and lower growth when contraction decreases.

4.4.2 Choice of strain-energy function

The model in Equations (4.27) depends on the strain-energy function $W = W(\alpha_r, \alpha_\theta, \alpha_z)$, which we have assumed to be neo-Hookean. In this section we compare the model behaviour for neo-Hookean and Fung strain-energy functions and Hooke's law for linear elasticity.

- **Hooke's law** states that the stress tensor is linearly proportional to the strain

tensor such that

$$E(\alpha_r - 1) = T_{rr} - \frac{1}{2}(T_{\theta\theta} + T_{zz}),$$
$$E(\alpha_\theta - 1) = T_{\theta\theta} - \frac{1}{2}(T_{rr} + T_{zz}),$$
$$E(\alpha_z - 1) = T_{zz} - \frac{1}{2}(T_{rr} + T_{\theta\theta}),$$

where E is Young's modulus of elasticity and is related to the shear elastic modulus by $E = 3\mu$. This is the simplest law relating stress and strain [Slaughter, 2003]. Hooke's law is valid for small strain.

- A common choice for a hyperelastic material is the **neo-Hookean** strain-energy function

$$W(\alpha_r, \alpha_\theta, \alpha_z) = \frac{\mu}{2}(\alpha_r^2 + \alpha_\theta^2 + \alpha_z^2 - 3),$$

where μ is the shear modulus.

- The **Fung** strain-energy function exhibits strain-stiffening properties

$$W(\alpha_r, \alpha_\theta, \alpha_z) = \frac{\mu}{2c}\left[e^{c(\alpha_r^2+\alpha_\theta^2+\alpha_z^2-3)} - 1\right],$$

where μ is the shear modulus and, for soft tissues, c is typically $3 < c < 20$.

The calculation to determine the stress-free state from the recoil measurements in Section 4.2.3 assumed a neo-Hookean strain-energy. For comparison, we calculate the stress-free configuration for Hooke's law and a Fung elastic material (details are in Appendix B.3). We would expect that, since the Fung strain-energy encompasses strain-stiffening, the residual stress required to deform the wound radius from the initial to the recoiled measurement would be greater than when assuming a neo-Hookean model. For Hooke's law we would expect the residual stress to be lower than the non-linear approximations.

The calculated stress-free state and residual stress are presented in Table 4.2 for the different choices of strain-energy. As anticipated, the value of the residual stress required to cause the observed recoil is lower for the Hooke's law model. This discrepancy arises because the initial recoil of the wound constitutes a large deformation (approximately 10% increase in wound radius) and hence Hooke's law of linear elasticity gives different results from the neo-Hookean law.

Table 4.2: Stress-free state and residual stress for different strain-energy functions. Table summarising the calculated stress-free state and residual stress in the dermal tissue when assuming a Hookean, neo-Hookean or Fung material. The residually stressed state is $A = 4$ mm, $B = 20$ mm, $L = 0.1$ mm and the recoiled wound radius is $a_R = 4.4$ mm. The mechanical parameters are $E = 0.6$ MPa, $\mu = 0.2$ MPa and $c = 3$.

stress-free state	Hooke	neo-Hookean	Fung
A_0	3.8814	3.8728	3.8702
B_0	19.4069	19.3638	19.3510
L_0	0.1062	0.1067	0.1068
T_{res}	0.0351	0.0376	0.0399

Equations (4.27) are solved for neo-Hookean and Fung strain-energy functions given in Equations (4.29) and the results are presented in Figure 4.14. When incorporating a strain-stiffening term, for example the Fung strain-energy function, the healing curve and the growth profile change qualitatively and the radial stress is much higher at the wound edge. For simplicity we shall henceforth focus on the neo-Hookean model since it has fewer parameters than the Fung model whilst incorporating non-linear effects.

4.4.3 The effects of friction

In Section 4.2.9 we found that the timescale for recoil was given by $t_d = q\chi^2/\mu$ and estimated that if recoil occurs on a timescale of hours then $q \approx \mathcal{O}(10^{-3})$ MPa days mm^{-2}. By comparison of the different timescales in healing, we postulated that friction would have an effect on the recoil phase since $\partial r/\partial t \gg 1$, but for the remainder of healing

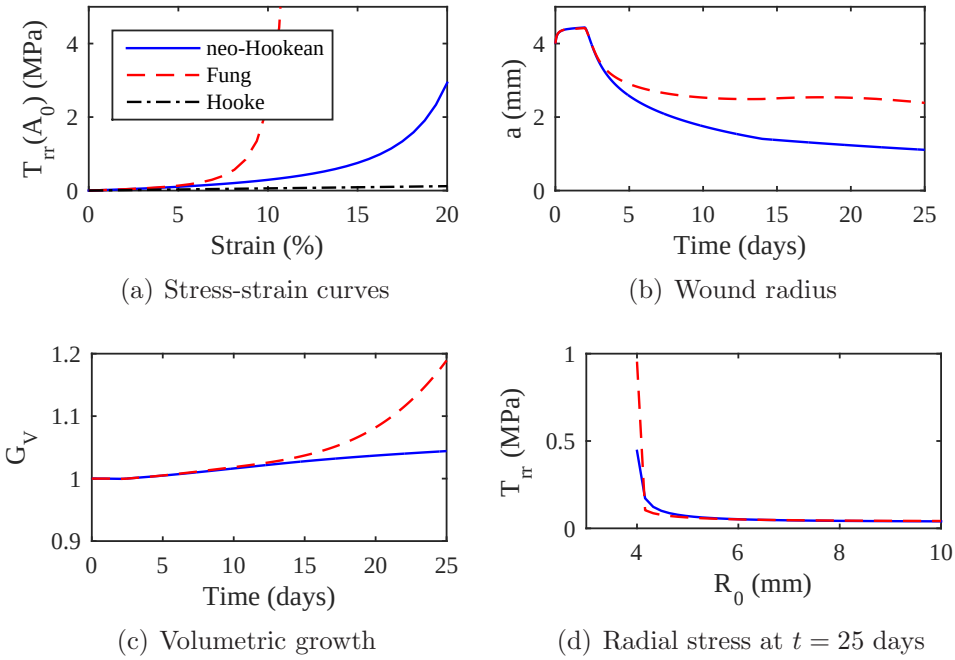

(a) Stress-strain curves (b) Wound radius

(c) Volumetric growth (d) Radial stress at $t = 25$ days

Figure 4.14: Comparison of the model behaviour for different strain-energy functions. (a) Stress-strain curves for neo-Hookean, Fung, and Hookean materials are plotted. Equations (4.27) are solved numerically for neo-Hookean and Fung strain-energy functions and (b) the wound radius and (c) the total volumetric growth are plotted as functions of time. (d) The radial stress at day 25 is plotted as a function of position. Reference variables are $A = 4$ mm and $B = 20$ mm. Parameter values are $k = 0.2$ days^{-1}, $m = 0.1$ days^{-1}, $n = 0.1$ days^{-1}, $f = 0.4$ N mm^{-3}, $t_c = 2$ days, $t_m = 14$ days, $E = 0.6$ MPa, $\mu = 0.2$ MPa, $c = 3$, $q = 0.002$ N days mm^{-2}, $N_z = 0$ N and $A_R = 4.4$ mm.

the drag term will be negligible. By simulating healing for different values of q, the effects of friction on healing are investigated in this section.

In Figure 4.15(a) we show how the time taken for the wound to fully recoil changes as we vary the friction coefficient q. We also show how changes in q affect the recoil phase of the healing process (see Figure 4.15(b)) and the post-recoil phases of the healing curve (see Figure 4.15(c)). For the simulations in Figure 4.15(b) contraction and growth are neglected and the effects of friction on the recoil of the wound only are considered. We observe that, for larger values of q, the recoil takes longer. In Figure 4.15(c) we assume that the wound recoils immediately and switch friction on for the remainder of the simulation. This allows us to study the effects of friction

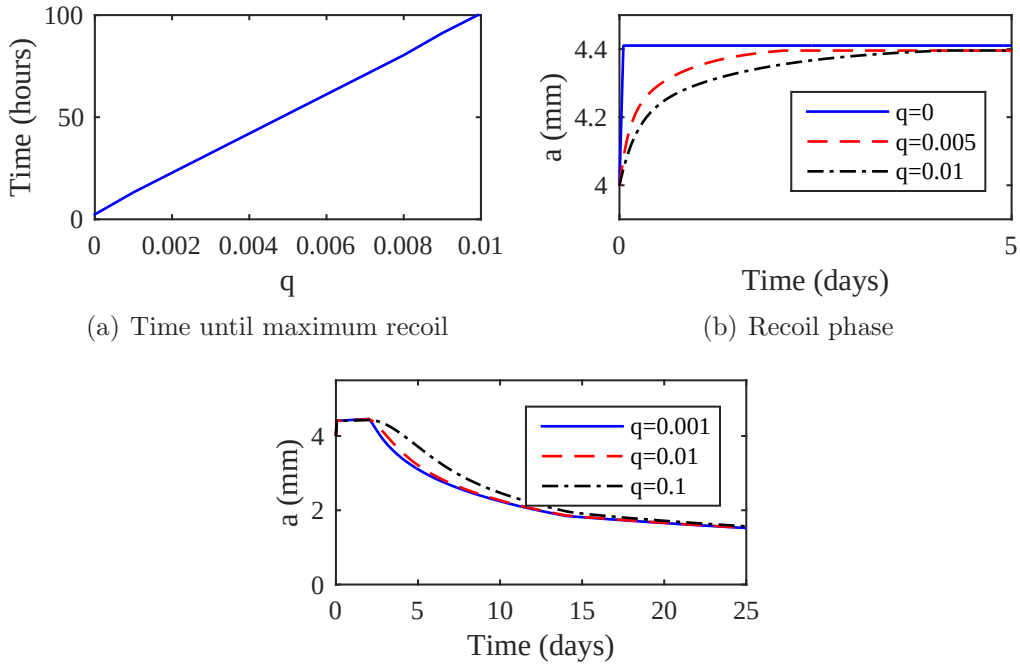

(a) Time until maximum recoil

(b) Recoil phase

(c) Post-recoil phase

Figure 4.15: Effect of varying the friction coefficient, q. Equations (4.27) are solved numerically. (a) The time taken for the wound to fully recoil as a function of q, (b) evolution of the wound radius, $a(t)$, during the recoil phase for $q = 0$ (solid blue), $q = 0.005$ (dashed red), and $q = 1$ (dash-dotted black) and (c) evolution of the wound radius, $a(t)$, post recoil, for $q = 0.001$ (solid blue), $q = 0.01$ (dashed red), and $q = 0.1$ (dash-dotted black). Reference variables and parameters are specified using the default values in Table 4.1. Friction affects the recoil phase of healing but has a negligible effect on healing at later times.

on healing, independent of the time taken for the wound to recoil. We observe that values of q which have a large effect on the recoil phase have negligible effect on the remainder of the healing curve (e.g. $q = 0.01$). To observe a significant change in the later stages of healing, q must vary by approximately two orders of magnitude. For larger values of q phase II of healing is slowed down. However by day 25, the wound radius curve for different values of q converge, with the wound radius beginning to plateau at approximately the same value. We have used different values of q in Figure 4.15(b) and (c) because much larger values of q were needed to observe a significant difference in the healing curve post recoil than in the recoil phase.

Based on the results in Figure 4.15(a) we fix $q = 0.002$ since, for the chosen parameter values, this ensures the recoil occurs within the first day. We conclude that the inclusion of a drag term in the balance of linear momentum equation gives the desired behaviour.

4.4.4 The effect of boundary conditions

There is uncertainty in the tissue behaviour far from the wound. In our model development we have assumed that far from the wound the tissue is in a residually stressed state and prescribed a boundary condition consistent with this physiological assumption. In the absence of suitable experimental data other boundary conditions should also be considered. In this section we consider three choices for the boundary conditions and analyse their effect on the system behaviour. The three choices are:

1. Fixed stress: impose a boundary condition for the radial stress at the outer edge and assign the axial load.

2. Fixed position: impose a boundary condition for the deformation at the outer edge and assign the axial load.

3. Mixed: impose a boundary condition for the radial stress and the deformation at the outer edge.

In each case, the boundary condition for the inner surface of the cylinder is determined by the contraction function. That is, the radial stress at the wound edge is given by Equation (4.27h).

4.4.4.1 Fixed stress

The healthy tissue far from the wound is in a pre-stressed state. Before wounding the dermis is residually stressed. Upon wounding a stress gradient is formed from the

stress-free inner boundary to the residually stressed outer boundary. From the boundary condition in Equation (4.27h), the stress on the outer boundary is maintained at a fixed value

$$T_{rr}(B_0, t) = T_{\text{res}}. \tag{4.30}$$

The mechanosensitive growth laws, notably Equation (4.27e), ensure that there is no radial growth far from the wound. However, by fixing the radial stress at the outer boundary the unfixed deformation allows for movement of the dermis far from the wound.

4.4.4.2 Fixed position

If we assume that far from the wound there is no movement of the skin, then instead of prescribing a fixed stress, we fix the position of the outer boundary. Accordingly we calculate the stress required for the initial recoil (see Section 4.2.3) and then fix the position of the outer boundary to that of the recoiled configuration

$$r(B_0, t) = b_R \quad \text{where} \quad b_R = \sqrt{\frac{B_0^2 - A_0^2}{\lambda_2} + a_R^2}. \tag{4.31}$$

Since the radial stress is not fixed, this may cause stress to accumulate at the outer boundary stimulating growth. In practice, we anticipate that, sufficiently far from the wound, the skin should not move and would remain in its pre-stressed state, hence both conditions should hold.

4.4.4.3 Mixed condition

Due to incompressibility, Equations (4.30) and (4.31) may be satisfied if λ is chosen such that $r(B_0, t) = b_R$. Solving Equation (4.27a) and imposing $b = b_R$ gives

$$\lambda(t) = \frac{2}{b_R^2 - a(t)^2} \int_{A_0}^{B_0} \gamma_r \gamma_\theta \gamma_z R_0 \, \mathrm{d}R_0. \tag{4.32}$$

Although imposing Equations (4.30) and (4.31) would enable for both a fixed position and fixed radial stress at the external boundary, the axial load can no longer be prescribed via Equation (4.27j), since λ is determined by Equation (4.32).

4.4.4.4 Conclusions

In Figure 4.16 we compare the effects of each of the boundary conditions on the time evolution of the wound radius, the dermal thickness, the total growth at the outer boundary and the radial stress at the outer boundary. The results suggest that the choice of boundary condition does not affect the healing curve. When a fixed stress is prescribed the trend in the axial deformation is counter to what we might expect. Although immediately after wounding the dermis thickens, the dermal thickness then decreases until approximately day 3. By contrast, the data in Figure 4.2 show an increase in the dermal thickness at the wound edge after the first few days. We argue that the accumulation of tissue at the wound edge observed in the data could be due to granulation tissue and not the surrounding healthy dermis. Both the fixed position and mixed boundary conditions ensure that the dermal thickness continues to increase over the first 3 days. At later times the mixed boundary condition causes the dermis to become thinner. This could be due to material resorption far from the wound, which we observe in Figure 4.16(c). For a fixed position at the external boundary, the dermis thickens for later times due to an increase in volume (see Figure 4.16(c)). Since deformations are symmetric, the axial deformation is uniform across the cylinder, representing an averaged change in the thickness of the dermis. Therefore, although the data in Figure 4.2 show a significant increase in dermal thickness at the wound edge, in fact, at a distance 2 mm from the wound, the thickness is approximately unchanged. In the absence of data on the axial deformation further from the wound edge, we cannot discriminate between the trends depicted in Figure 4.16(b).

We note that, since all three choices of boundary conditions give identical healing

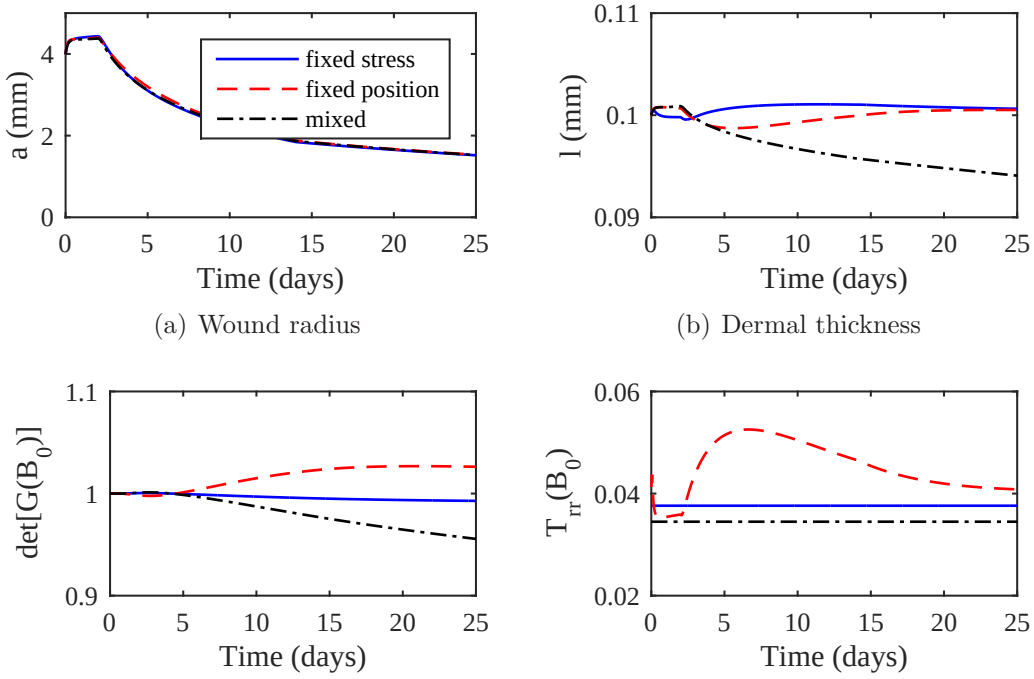

(a) Wound radius (b) Dermal thickness

(c) Growth at the outer boundary (d) Radial stress at the outer boundary

Figure 4.16: Model observables for different external boundary conditions. Equations (4.27) are solved numerically with different boundary conditions. (a) The wound radius, $a(t)$, (b) the dermal thickness, $l(t)$, (c) the growth at $R_0 = B_0$ and (d) the radial stress at $R_0 = B_0$ are plotted as functions of time. Reference variables and parameters are specified using the default values in Table 4.1.

curves, the experimental data are insufficient to predict what is happening far from the wound. The model has shown that the choice of boundary condition influences other model observables. In order to discriminate between these conditions we require more experimental data, such as measures of the stress far from the wound or a fixed distance from the wound and whether these remain constant in time.

Although none of the given boundary conditions perform as we would expect for all model solutions, we choose the fixed stress boundary condition since, given the model observables, model behaviour under these conditions is closest to what we might expect whilst still allowing us to prescribe an axial load to model the behaviour of the epidermis or pressure treatments. In the remainder of this chapter we fix the radial stress on the outer boundary using Equation (4.27i).

4.5 Numerical parameter sensitivity analysis

Ultimately, we are interested in the time to closure and the quality and mechanical properties of the healed tissue. In Figure 4.17 we show how the wound radius at day 25 changes as we vary the default model parameters by ±10%, one parameter at a time. We observe that increasing the radial growth sensitivity k causes the wound radius to decrease. Increasing the rate of circumferential resorption (since the circumferential stress is negative) accelerates wound closure in a manner similar to that seen by increasing the contraction coefficient. Interestingly, circumferential resorption has previously been used as a contractile mechanism in a model of epidermal wound closure [Wu and Ben Amar, 2015] and embryonic wound closure [Taber, 2009]. The effect of axial growth on the wound radius is negligible and, as expected, increasing tissue stiffness has a detrimental effect on wound closure: a stiffer tissue will deform less when subject to a given force.

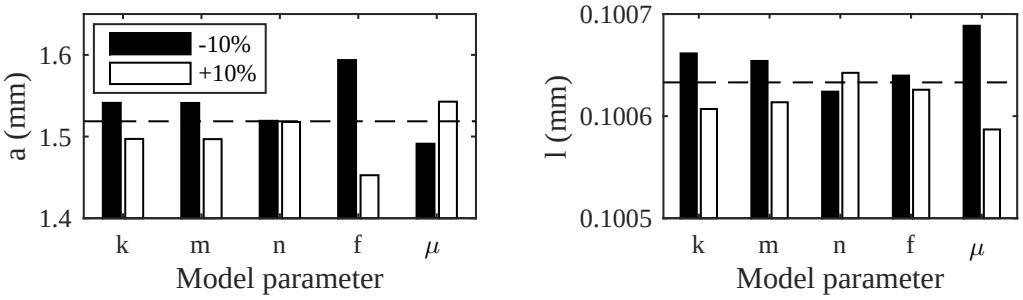

(a) Final wound radius (b) Final dermal thickness

Figure 4.17: Effect of model parameters on the final wound radius and dermal thickness. Equations (4.27) are solved numerically. Each model parameter is varied by ±10% of its default value. (a) The wound radius and (b) the dermal thickness, at day 25 are recorded. The dashed lines indicate the wound radius/dermal thickness when all parameters are fixed at their default values. All reference variables and parameters are specified using the default values in Table 4.1. Increasing the radial and circumferential growth parameters, k and m, and the contraction coefficient, f, decreases the wound radius and increases the dermal thickness at day 25. Increasing the axial growth parameter, n, has negligible effect on both the wound radius and dermal thickness at day 25. Increasing the tissue stiffness, μ, decreases the wound radius and increases the dermal thickness at day 25.

We also tested the sensitivity of the axial deformation to parameter variation and found that this is negligible for all system parameters (see Figure 4.17(b)): the fluctuations in the dermal thickness at day 25 are less than 1% of the total thickness.

4.5.1 Addition or removal of material

We hypothesised that growth of the dermal tissue is mechanosensitive and linearly proportional to the stress, with constants of proportionality k, m and n in the radial, circumferential and axial directions, respectively. From our discussion of contraction in Section 4.2.6 we concluded that growth acts to reduce the radial tension caused by contraction. For the growth laws in Equations (4.20) the constants k, m and n are non-negative. We note that, if $\det(\mathcal{G}) > 1$, then there is a net gain of material (and a net loss if $\det(\mathcal{G}) < 1$).

In order to determine whether different growth laws give rise to a net gain or loss of material we introduce the following function which computes the total volume of the cylinder:

$$M(t) = 2\pi L \int_{A_0}^{B_0} \gamma_r(R_0, t)\gamma_\theta(R_0, t)\gamma_z(R_0, t)R_0 \, \mathrm{d}R_0, \tag{4.33}$$

and note that a positive (negative) gradient for $M(t)$ at time t corresponds to the addition (removal) of material.

Numerical simulations show that for certain choices of the growth parameters the system loses material. Further, as illustrated in Figure 4.18, different parameter choices may produce similar healing curves but different profiles for $M(t)$. Figure 4.18(b) shows the mass function in Equation (4.33), which is monotonically increasing for $k = 0.4$, $m = 0.1$, but monotonically decreasing for $k = 0.1$, $m = 0.2$. Although the healing curves are indistinguishable (see Figure 4.18(a)), in one regime there is a net gain of material and in the other a net loss. As a result of loss of

material, the outer boundary of the dermal cylinder shrinks, effectively pulling in tissue from the surrounding areas (results not shown). In Figure 4.18(c) we observe that, for healing to proceed in this manner, the tissue far from the wound edge is in greater tension than when there is addition of mass. For example, at day 25, where $R_0 \approx 5$ mm the radial stress for a net loss of material is approximately double that for a net gain of material.

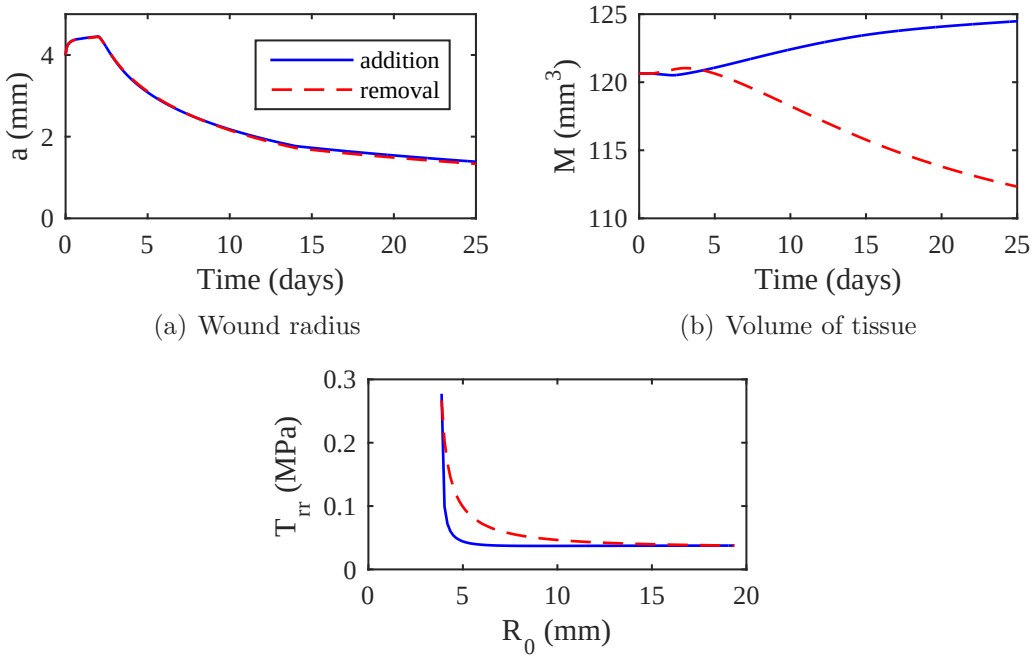

(a) Wound radius

(b) Volume of tissue

(c) Radial stress at day 25

Figure 4.18: Effect of a net gain and loss of material on model observables. Equations (4.27) are solved numerically. (a) The wound radius and (b) the volume of tissue, given in Equation (4.33), are plotted as functions of time. (c) The radial stress, T_{rr}, at day 25 is plotted as a function of position. For a net gain of material (solid blue) the growth parameters are $k = 0.4$, $m = 0.1$, $n = 0$ and for a net loss of material (dashed red) the growth parameters are $k = 0.1$, $m = 0.3$, $n = 0$. All other reference variables and parameters are specified using the default values in Table 4.1.

In view of the above we must be careful when choosing growth parameters to ensure that we obtain realistic behaviour and not a net loss in material which may be biologically unrealistic. By evaluating the mass function in Equation (4.33) we can reject model simulations which may not be biologically realistic. In order for the

wound to heal with a net gain in material, we require a higher radial than circumferential ($k > m$) growth rate. Such anisotropy in the growth rates requires cells to sense the radial direction. Given that fibroblasts migrate radially in response to chemical growth factor gradients [Pierce et al., 1989, Chung et al., 2001] such directional bias for growth is feasible.

4.6 Remodelling after closure

We anticipate that after the wound has closed, the dermal tissue remodels to its natural state of residual stress. Due to granulation tissue and scar formation in the wound space, the dermis is prevented from closing completely. Therefore eventually the dermal edge stalls. The mechanism by which the dermal edge halts is not known but could involve a combination of contraction ceasing (due to inactivation of fibroblasts), the radial stress reaching a threshold value or the granulation tissue in the wound space acting as a physical barrier, preventing further inward movement of the dermis. The questions we consider are whether the halted tissue will reach an equilibrium state, returning to the base residual stress and, if so, how long the remodelling will take.

We simulate the remodelling period of the dermal tissue by halting the wound edge at some point $t = T$. We choose $T = 25$ days as a representative time by which the granulation tissue fills the wound space but note that the stimulus that halts movement of the dermal edge could easily be modified to account for other effects.

We solve Equations (4.27) for $0 \leq t \leq T$. For $t > T$ we switch the boundary conditions from the fixed load specified in Equations (4.27h)-(4.27j) to a fixed displacement so that

$$r(A_0, t) = a(T), \quad r(B_0, t) = b(T), \quad \lambda(t) = \lambda(T). \tag{4.34}$$

This fixes the deformation, preventing the wound from closing further. Due to in-

compressibility and a fixed deformation, there can be no net change in material so that $\frac{\partial}{\partial t}(\det(\mathcal{G})) = 0$. We therefore have the following system for $t > T$ (= 25 days):

$$\frac{\partial \gamma_r}{\partial t} = k(T_{rr} - T_{\text{res}})\gamma_r, \tag{4.35a}$$

$$\frac{\partial \gamma_\theta}{\partial t} = m(T_{\theta\theta} - T_{\text{res}})\gamma_\theta, \tag{4.35b}$$

$$\frac{\partial \gamma_z}{\partial t} = nT_{zz}\gamma_z, \tag{4.35c}$$

$$T_{\theta\theta} = T_{rr} + \alpha\hat{W}_\alpha, \tag{4.35d}$$

$$T_{zz} = T_{rr} + \lambda\hat{W}_\lambda, \tag{4.35e}$$

$$\frac{\partial}{\partial t}(\gamma_r\gamma_\theta\gamma_z) = 0. \tag{4.35f}$$

Combining Equations (4.35a)-(4.35c) and (4.35f) yields a relationship for the stress in terms of the growth and the strain

$$T_{rr} = \frac{(k+m)T_{\text{res}} - (m\alpha\hat{W}_\alpha + n\lambda\hat{W}_\lambda)}{k+m+n}, \tag{4.36}$$

where $\hat{W}$ is defined in Equation (4.27l). The components of the growth tensor and the circumferential and axial stress satisfy Equations (4.35a)-(4.35e) and the radial stress is updated according to Equation (4.36).

In Figures 4.19(a)-(c) we plot the components of the stress tensor at days 25, 50 and 100. At day 25, we observe a large radial tension at the wound edge, with circumferential and axial compression of similar magnitude. Over the remodelling period these profiles relax to a steady state, with the stress returning to the residually stressed state ($T_{rr} = T_{\theta\theta} = T_{\text{res}}$ and $T_{zz} = 0$). In Figures 4.19(d) and (e) the components of the stress and growth tensors are plotted as functions of position at day 200, after the system has reached steady state. Figure 4.19(f) shows how the spatial average of the components of the growth tensor evolve over time. We find that growth has slowed down by day 50 and that by day 100 the remodelling phase

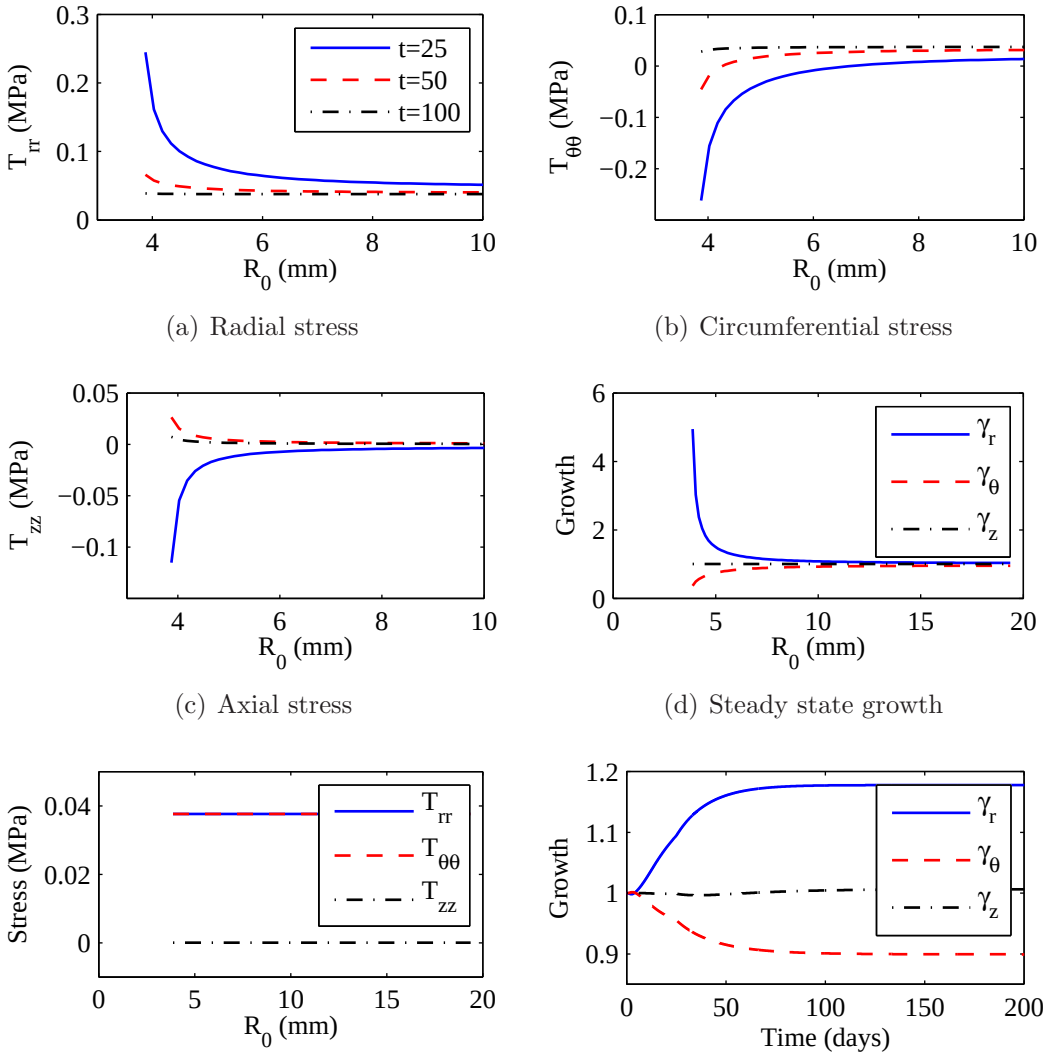

(a) Radial stress (b) Circumferential stress

(c) Axial stress (d) Steady state growth

(e) Steady state stress (f) Average growth

Figure 4.19: Remodelling of the dermal tissue. Equations (4.27) are solved numerically for $0 < t < 25$. At $t = 25$ the position of the wound edge is fixed by switching the boundary condition from a fixed load (Equations (4.27h)-(4.27j)) to a fixed displacement specified by Equation (4.34). (a) The radial stress T_{rr}, (b) the circumferential stress $T_{\theta\theta}$ and (c) the axial stress T_{zz} are plotted as functions of position at $t = 25$, 50 and 100 days. (d) The radial, circumferential and axial growth and (e) stress are plotted as functions of position at 200 days. (f) The average radial, circumferential and axial growth are plotted as functions of time. Reference variables and parameters are specified using the default values in Table 4.1. The growth reaches a steady state by approximately day 100 and the stress returns to the isotropic planar stress $\mathbf{T}^*$.

is essentially complete.

4.6.1 Sensitivity of remodelling time to model parameters

We now simulate the remodelling scenario for healing while varying the growth rate and tissue stiffness parameters. The results are given as a bar graph of the time taken for the tissue to reach a steady state in Figure 4.20. Steady state is defined as[3]

$$\frac{\partial \gamma_r}{\partial t} = \frac{\partial \gamma_\theta}{\partial t} = \frac{\partial \gamma_z}{\partial t} = 0. \tag{4.37}$$

In order to make a reliable comparison, the model parameters are not changed for the first 25 days of healing. After day 25, when the tissue begins to remodel, each model parameter is varied by $\pm 10\%$ of its default value. We observe that the tissue stiffness (μ) has the greatest effect on the remodelling time, such that as μ is increased by 10%, the time taken for the tissue to reach steady state is reduced by approximately 10 days. For the remaining model parameters tested, the remodelling time is between 120 and 150 days. Comparing the sensitivity of the remodelling time to the model parameters with that of the final wound radius we observe some significant differences. In Figure 4.17(a) the radial and circumferential growth parameters had a similar effect on the final wound radius, however in Figure 4.20 circumferential growth has a much greater effect than radial growth. This may be due to the degree of radial versus circumferential stress the tissue needs to recover. We observe in Figures 4.19(a) and (b) that at day 25 the radial and circumferential stresses at the wound edge are 0.2451 and -0.2621 MPa, respectively. With a positive resting stress ($T_{\text{res}} = 0.0376$ MPa) the growth rates in Equations (4.20) imply that the circumferential growth rate dominates the radial growth rate. Surprisingly, varying the axial growth rate, which had negligible effect on the healing curve, has a significant effect on the remodelling

[3]Numerically we define steady state to be such that each $\frac{\partial \gamma_i}{\partial t}$ is below a positive threshold value close to zero. For the simulations in Figure 4.20 the threshold was taken to be 10^{-5}.

time. We postulate that this is due to the fixed axial deformation and therefore axial growth has a much greater effect on the system[4].

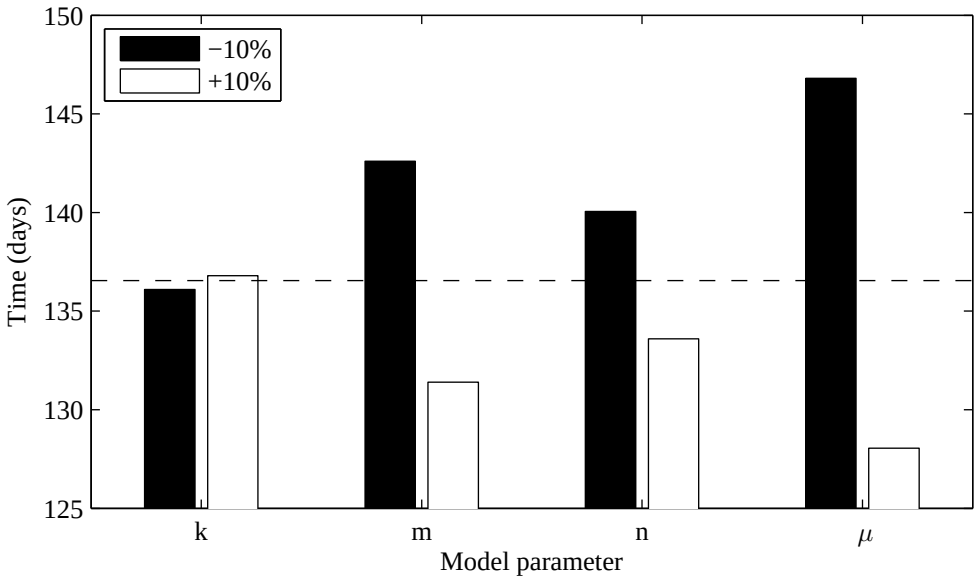

Figure 4.20: Effect of model parameters on remodelling time. Equations (4.27) are solved numerically for $0 < t < 25$. At $t = 25$ the position of the wound edge is fixed by switching the boundary condition from a fixed load (Equations (4.27h)-(4.27j)) to a fixed displacement specified by Equation (4.34). During the remodelling phase, each model parameter is varied by $\pm 10\%$ of its default value and the time taken to reach steady state is recorded. The dashed line indicates the remodelling time when all parameters are fixed at their default values. Reference variables and parameters are specified using the default values in Table 4.1.

4.6.2 Steady state solution

Figure 4.19 shows that, for the parameter values in Table 4.1, the stress reaches a steady state for which $\mathbf{T} = \mathbf{T}^*$. The growth laws in Equations (4.20) ensure that this is the only steady state solution. A natural question is whether the growth profile (for example, that shown in Figure 4.19(d)) needed to reach this state is unique. At

[4]To test this we ran simulations where the axial deformation was not fixed according to $\lambda(t) = \lambda(T)$ but instead satisfied the spring condition in Equation (4.27j). Results are shown in Figure B.2 in Appendix B.5. In this case, the sensitivity of the remodelling time to the axial growth parameter was significantly lower than that presented in Figure 4.20.

steady state we have

$$\frac{\partial r}{\partial R_0} = \frac{\gamma_\theta \gamma_r \gamma_z R_0}{\lambda r}, \tag{4.38a}$$

$$T_{\theta\theta} = T_{rr} + \alpha \hat{W}_\alpha, \tag{4.38b}$$

$$T_{zz} = T_{rr} + \lambda \hat{W}_\lambda. \tag{4.38c}$$

For a fixed deformation with $\mathbf{T} = \mathbf{T}^*$, solving Equations (4.38) for the components of the growth tensor gives

$$\gamma_\theta = \sqrt{\frac{\lambda}{\gamma_z}} \frac{r}{R_0}, \tag{4.39a}$$

$$\gamma_r = \sqrt{\frac{\lambda}{\gamma_z}} \frac{\partial r}{\partial R_0}, \tag{4.39b}$$

$$\left(\frac{\gamma_z}{\lambda}\right)^3 - \frac{T_{\text{res}}}{\mu}\left(\frac{\gamma_z}{\lambda}\right)^2 - 1 = 0. \tag{4.39c}$$

Since $\lambda, \mu > 0$, Equation (4.39c) has only one real root for $T_{\text{res}} > -\left(\frac{27}{4}\right)^{\frac{1}{3}} \mu$ given by

$$\gamma_z = \left(\frac{C}{6\mu} + \frac{2T_{\text{res}}^2}{3\mu C} + \frac{T_{\text{res}}}{3\mu}\right)\lambda, \tag{4.40}$$

$$\text{where} \quad C = \left[12\mu^2 \sqrt{\frac{12T_{\text{res}}^3 + 81\mu^3}{\mu}} + 8T_{\text{res}}^3 + 108\mu^3\right]^{\frac{1}{3}},$$

and three distinct real roots for $T_{\text{res}} < -\left(\frac{27}{4}\right)^{\frac{1}{3}} \mu$. That is, if the residual stress is negative (i.e. the skin is in compression before wounding) and large enough, there are three possible choices for γ_z at steady state. Therefore, the roots of Equation (4.39c) depend on the residual stress where there is always one positive root. For $T_{\text{res}} < -\left(\frac{27}{4}\right)^{\frac{1}{3}} \mu$ there is a fold bifurcation with two extra roots, however these are both negative. The qualitative behaviour of this bifurcation does not change for different values of μ and λ.

Since the growth profiles of γ_r and γ_θ depend on γ_z and we require $\gamma_z > 0$ in Equations (4.39) for physiologically real solutions we conclude that the steady state profiles of the growth components in Figure 4.19(d), associated with $\mathbf{T} = \mathbf{T}^*$ are unique.

4.7 Model experiments

The model we have developed provides a framework for investigating wound healing from a mechanical point of view. This can have particular value in the context of experiments in which the mechanical environment is explicitly altered. In this section we consider two such scenarios: rewounding and the application of pressure during healing.

4.7.1 Rewounding

The mechanical model predicts the stress state in the tissue at any point in space and time. In practice it is difficult to determine the stress profile experimentally, but the effect of stress can be apparent when it is relieved. Rewounding, i.e. recutting a wound in the same location, provides one means of accessing the mechanical state. In the same manner in which the degree of recoil upon initial wounding can be used to measure the residual tension in the healthy skin, measuring the degree of recoil upon rewounding gives a measure of the stress state in the skin during the healing process. Similar experiments have previously been used to determine whether the embryonic 'purse-string' mechanism is in tension [Davidson et al., 2002].

A hypothetical rewounding experiment also provides a means of calibrating our model. We have found that different balances of growth and contraction can generate similar healing profiles. Currently, most experimental data comprise time series of averaged wound areas. With such data it is not possible to distinguish between

different balances: additional information about the stress during healing is needed to calibrate the model and compare alternative hypotheses. In theory, a rewounding experiment could be repeated at regular intervals during healing to give a time series of spatially-averaged stress measurements.

Here, we simulate rewounding, using the model to predict the retraction of a wound in response to a second injury. By varying the radial growth and contraction coefficients, k and f, we compare two cases: (a) healing with high growth and low contraction and (b) healing with low growth and high contraction. While the evolution of the wound radius in each case is similar (see Figure 4.21), the stress generated in the tissue differs markedly. When the rate of contraction is high, the stress at the wound edge is much greater than when the contraction rate is low. In the absence of measurements of the stress profile, making a new wound and recording the retracted area would enable us to estimate the tension in the skin and to determine whether contraction or growth dominate healing. The retraction of the second injury in Figure 4.21(b), when the dermal tissue is subject to low growth and high contraction, is much greater than that in Figure 4.21(a) where the dermal tissue is subject to higher growth and lower contraction.

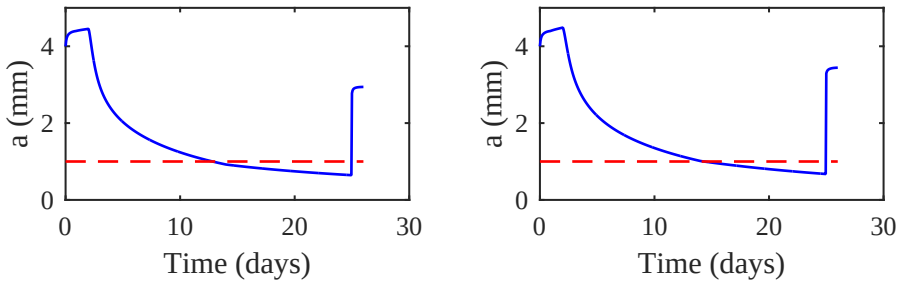

(a) High growth and low contraction (b) Low growth and high contraction

Figure 4.21: Predicted outcome of rewounding experiments. Equations (4.27) are solved numerically and at $t = 25$ days a wound of radius 1 mm is cut (dashed red). The wound radius is plotted as a function of time (solid blue) for (a) high growth and low contraction ($k = 0.8$, $f = 0.3$) and (b) low growth and high contraction ($k = 0.1$, $f = 0.5$). All other reference variables and parameters are specified using the default values in Table 4.1.

4.7.2 Pressure treatments

Pressure therapy involves the application of pressure to control wound healing. The most common application of pressure therapy for the management of hypertrophic scars is via pressure bandages [Kischer, 1975]. Despite their widespread use, the mechanism by which pressure bandages improve healing is not fully understood and the clinical effectiveness of this non-invasive therapy remains to be scientifically proven [Anzarut et al., 2009]. It has been suggested that mechanical pressure induces a hypoxic atmosphere resulting in death of fibroblasts and therefore reduced tissue synthesis [Kischer, 1975]. Alternatively mechanical pressure may inhibit the activity of fibroblasts by reducing the rate at which they secrete TGFβ, a growth factor which stimulates fibroblasts to contract and produce tissue [Martin, 1997].

As well as the application of pressure to retard the proliferative activity of fibroblasts during healing, negative pressure wound therapy (NPWT), or vacuum assisted closure (VAC), is used to stimulate tissue regeneration in non-healing wounds. NPWT and VAC have been shown to increase blood flow and granulation tissue formation, to decrease bacteria, and to stimulate tissue synthesis through increased mechanical tension [Mendez-Eastman, 2001, Huang et al., 2014].

The pressure needed for effective treatment is unknown, although values in the range 9-90 mm Hg (0.001-0.01 MPa) have been reported [Giele et al., 1997]. Alternatively NPWT tends to generate up to 125 mm Hg of suction in the wound area (approximately 0.017 MPa). In this section we use our mechanical model to investigate the effects of applying pressure to the surrounding dermal tissue during healing. Using Equation (4.27j) with a modelling domain of radius 20 mm, the pressures discussed here can be approximated by axial loads ranging from -12.5 to 21.5 N.

We simulate treatment for a period of 15 days. The wound begins to heal load-free ($N_z = 0$ N). On day 5 pressure is applied by assigning a non-zero axial load ($N_z = 10$ or $N_z = -10$ N). Pressure is released on day 20 and the wound continues to heal

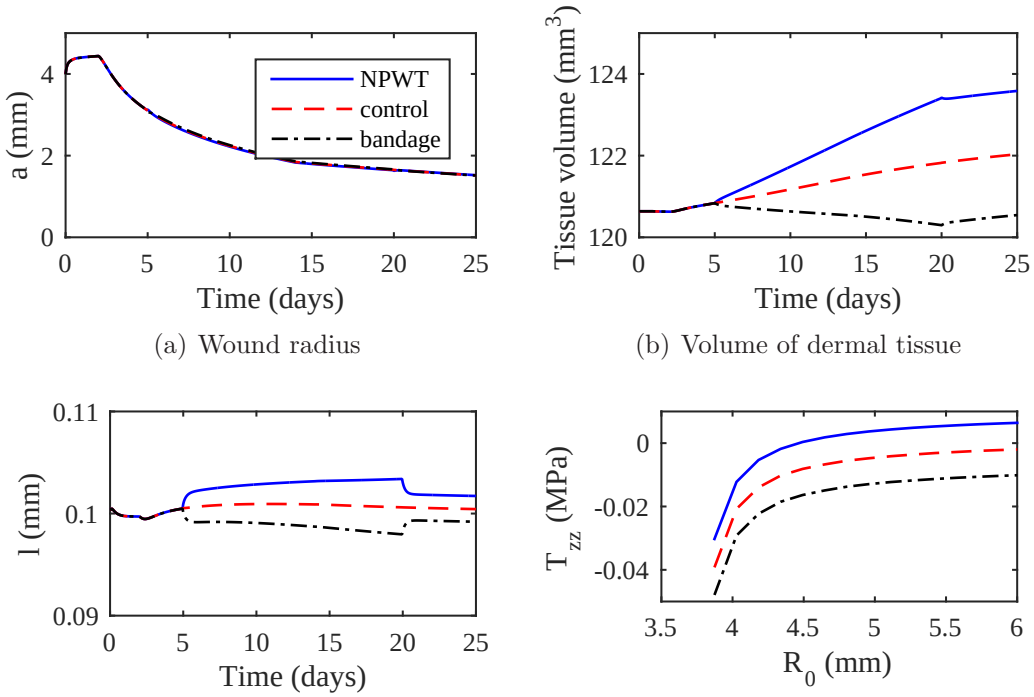

(a) Wound radius

(b) Volume of dermal tissue

(c) Thickness of dermal tissue

(d) Axial stress at $t = 25$ days

Figure 4.22: Effect of axial load on the healing dermis. Equations (4.27) are solved numerically. From day 5 to 20 and axial load is assigned for NPWT ($N_z = 10$ N, solid blue), control ($N_z = 0$ N, dashed red) and pressure bandage ($N_z = -10$ N, dash-dotted black). (a) The wound radius $a(t)$, (b) the total tissue volume and (c) the tissue thickness $l(t)$ are plotted as functions of time. (d) The axial stress, T_{zz}, at day 25 is plotted as a function of position. Reference variables and parameters are specified using the default values in Table 4.1.

load-free until day 25.

The results presented in Figure 4.22(a) show that the effect of axial load on the wound radius is negligible. However Figure 4.22(b) reveals that the tissue volume is greatly affected by applying a constant axial load. When the load is positive, for example corresponding to NPWT, the tissue mass added during the treatment period is three times greater than in the control case and could therefore be effective for slowly healing wounds. When the load is negative, for example in the application of a pressure bandage, there is a loss in total tissue volume, suggesting a use for reduced scarring. The plots in Figure 4.22(c) show that, although the changes in volume do not affect the wound radius, they contribute to the thickness of the tissue.

We also observe that when the load is released the thickness of the dermal tissue returns to a value closer to the control case but there is still a noticeable difference between the treated and untreated wounds. This discrepancy in dermal thickness is most likely due to the differences in tissue volume observed in Figure 4.22(b). The plot in Figure 4.22(d) shows the axial stress at day 25 as a function of position. We observe a lower axial stress profile (higher compression) when a higher pressure is applied to the tissue. These results suggest that although applying an axial load has negligible affect on the healing curve it could be used to control the total amount of tissue produced in the surrounding dermis during healing.

4.8 Conclusions

In this chapter we have developed a mechanical model of dermal wound healing in which closure is driven by contraction of the wound edge and mechanically induced volumetric growth in the surrounding tissue. Our first step was to establish the degree of residual tension in the pre-wounded tissue by analysing the recoil that is observed after circular punch biopsies are taken from mice. Volumetric tissue growth was motivated by the unrealistically high stresses that would be generated in the tissue surrounding the wound area if healing were to occur through contraction alone. A simple analysis of homogeneous growth revealed that normal healing should be characterised by anisotropic growth, with the addition of material in the radial direction and removal of material in the circumferential direction. In the full model, we have postulated simple mechanosensitive growth laws that enable us to isolate the effects of such anisotropy during healing simulations.

Typical solutions of the model revealed three distinct phases of healing. The wound quickly retracts and the radius plateaus in the absence of growth and active contraction at the wond margin (up to 2 days). The wound radius then decreases over

a period of approximately 14 days as a result of contraction and mechanosensitive growth. Finally, contraction and mechanosensitive growth slow down. Over a longer time period the dermal tissue remodels, and returns to its homoeostatic resting stress. We showed that there is only one steady state for the stress, corresponding to $\mathbf{T} = \mathbf{T}^*$, with one associated non-negative steady state growth profile. We estimated that the system takes approximately 120-150 days to remodel, depending on the choice of model parameters.

While our modelling framework neglects many features of the wound healing process, such as an explicit description of fibroblast activity, it has the advantage of characterising the wound healing of a non-linear elastic tissue in a simple manner and with a small number of parameters. We have shown that the model captures well the qualitative and dynamic features of healing curves obtained in mice. However, even while varying only four free parameters, we can identify multiple parameter sets consistent with the available data. For instance, we find that if one is only tracking the wound radius over time, two different parameter regimes – one with high growth and low contraction, and one with low growth and high contraction – can both produce the same healing curve for the wound radius. These results suggest that having access to only wound radius data will not uniquely determine the model parameters and, hence, the relative contributions of growth and contraction in healing. Fortunately, such cases can be distinguished if additional mechanical information is available. We have simulated rewounding experiments, in which the wound is recut before it is fully healed. The degree of recoil can be used to distinguish between alternative cases and to calibrate the model. Such experiments could provide useful information about the mechanical state of the healing tissue and the mechanosensitivity of the growing tissue.

Our framework is well suited to investigate pressure treatments. By applying an axial load to the healing dermis we observed that loads reported in the literature

do not change the behaviour of the healing curve but can have a significant effect on the total volume of tissue produced during healing. Therefore if the dermis is hyper-proliferative during healing, applying pressure to the area can normalise the overall tissue volume. Similarly, if the dermis in under-proliferative, applying suction can normalise the volume of tissue produced.

In order to focus on the mechanical environment in the tissue, we have restricted our study to mechanically stimulated growth, such that stress greater (less) than the residual stress results in addition (removal) of material. With the growth laws formulated in this manner, growth will not occur unless contraction is active. It is quite likely that basal or chemically stimulated growth occurs in the absence of contraction. Our sensitivity analysis in Section 4.5.1 showed that, to achieve a net gain in material, mechanosensitive growth should have a radial bias. This could be achieved with a growth factor gradient in the radial direction. A natural next step is to couple a mathematical description of fibroblast and growth factor activity to the contraction function and the evolution of growth laws providing a more mechanistic approach to the main processes driving dermal closure.

In Chapter 6 we will adapt the model presented in this chapter to account for such mechanistic behaviour. A more mechanistic approach will allow us to use the model to test clinically relevant pathologies and treatments, for example abnormally low fibroblast density in the dermal tissue and low detection of growth factors such as TGFβ. The aim is to describe both the chemical and mechanical tissue environment and to investigate their effects on dermal closure whilst maintaining our simplistic approach of a minimal number of unknown parameters.

Before extending our morphoelastic model, it is important to first validate its behaviour. We validated our model in Chapter 2 by comparing it with experimental data. We have shown, in this chapter, that the morphoelastic model reproduces normal healing behaviour similar to that observed in the wound healing data. Another

way in which we can validate the current model is to compare its behaviour with that of the ordinary differential equation model of wound healing from Chapter 2. Further by comparing the two models we can test the robustness of the conclusions of the phenomenological model. In the next chapter we simplify the morphoelastic model developed in this chapter so that it is directly comparable to the ordinary differential equation model of Chapter 2. We investigate the behaviour of the simplified model, fit it to the experimental data and compare the results with our conclusions from Chapter 2.

Chapter 5

A comparison of the two modelling approaches

5.1 Introduction

When developing a new mathematical model it is important to validate its behaviour and predictions. Often this is done by comparing results with experimental data. In Chapter 2 we compared our ordinary differential equation model of wound healing with wound healing data from our experimental collaborators. In developing our morphoelastic model in Chapter 4, we showed that our model can generate similar healing curves under different parameter regimes and, hence, comparing model behaviour with only wound radius data may be insufficient to identify well-defined parameter values. We therefore choose to test the robustness of our conclusions from the phenomenological model from Chapter 2 against the mechanistic model from Chapter 4. In this chapter we do this by first simplifying the morphoelastic model so that it is directly comparable to the ordinary differential equation one. In particular we assume that growth is homogeneous in a region close to the wound and comprises basal and mechanosensitive terms. By simplifying the model in this way we determine

a one-to-one map between the parameters of the two models.

5.2 Model simplifications

In this section we simplify our morphoelastic model of dermal wound healing. We consider the geometry of the dermal tissue, the balance of linear momentum and a spatially-averaged evolution law for the growth tensor.

5.2.1 Model geometry

Consistent with the model development in Chapter 2, we localise synthesis of new dermal tissue to a small proliferative annulus surrounding the wound. In this region we assume that growth is spatially homogeneous. Outside the proliferative region the tissue is assumed inactive but to be in mechanical contact with the growing region of the dermis. These assumptions have previously been used in a morphoelastic model of epidermal wound healing [Wu and Ben Amar, 2015].

We restrict the dermal tissue to 'in-plane' deformations so that the axial stretch and growth satisfy $\lambda = \gamma_z = 1$, and the tissue can be described as an annulus surrounding the wound, subject to radially symmetric deformations. The radial co-ordinate R in the stress-free reference configuration is deformed at time t to $r(R,t)$ in the current configuration.

In the reference configuration, the growing region occupies $A \leq R \leq B$, where $R = A$ is the initial wound radius, and the buffer region occupies $B \leq R \leq C$. In the current configuration, the growing region occupies $a \leq r \leq b$ and the buffer occupies $b \leq r \leq c$ (see Figure 5.1).

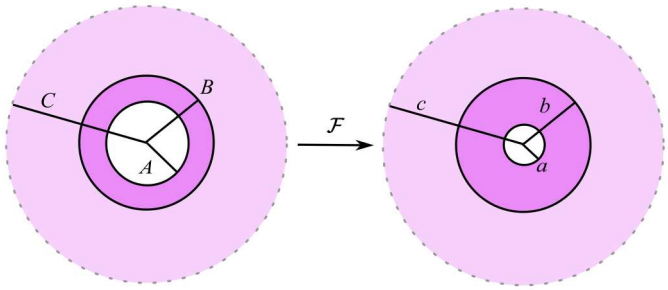

Figure 5.1: Proliferative region embedded in a non-growing buffer. The system comprises two attached tissues with the same mechanical properties. Distance from the wound centre is described by the independent variable R. Growth is localised to the region $A \leq R \leq B$ which is embedded in a non-growing buffer region $B \leq R \leq C$. Under the deformation $\mathcal{F}$, the reference configuration is mapped to the current configuration. The distance for the wound centre in the current configuration is described by the dependent variable $r(R,t)$. In the growing region of the dermis occupies $a \leq r \leq b$ and the buffer occupies $b \leq r \leq c$.

5.2.2 Tissue mechanics

Neglecting all body forces and viewing the tissue as incompressible, hyperelastic and neo-Hookean, the system mechanics can be described by the following equations:

$$\frac{\partial r}{\partial R} = \gamma_r \gamma_\theta \frac{R}{r}, \tag{5.1a}$$

$$\frac{\partial T_{rr}}{\partial r} = \frac{\alpha \hat{W}_\alpha}{r}, \tag{5.1b}$$

$$T_{\theta\theta} = T_{rr} + \alpha \hat{W}_\alpha, \tag{5.1c}$$

where

$$\hat{W}(\alpha) = \frac{\mu}{2}\left(\frac{1}{\alpha^2} + \alpha^2 - 2\right) \quad \text{and} \quad \alpha = \frac{r}{\gamma_\theta R}. \tag{5.2}$$

It remains to provide an evolution law for the growth (i.e. to specify γ_r and γ_θ) and appropriate boundary conditions for Equations (5.1).

5.2.3 Stress-free state and residual stress

In Chapter 4 we determined the residual stress of the dermis and its stress-free state by considering wound recoil measurements. A simplification of the model in this chapter is the assumption that there are no axial deformations, i.e. $\lambda = 1$. From our calculations in Section 4.2.3, assigning $\lambda = 1$ implies that the stress-free state (defined by R_0) is equivalent to the residually stressed state (defined by R) and the residual stress is given by the following equation

$$T_{\text{res}} = \frac{\mu}{2}\left[\log\left(\frac{C^2}{A^2}\right) - \log\left(\frac{C^2 - A^2 + a_R^2}{a_R^2}\right) + \left(A^2 - a_R^2\right)\left(\frac{1}{C^2 - A^2 + a_R^2} - \frac{1}{a_R^2}\right)\right], \tag{5.3}$$

where a_R is the radius of the recoiled wound.

5.2.4 A spatially-averaged growth law

In this section we develop a spatially-averaged growth law for the proliferative region of the dermis. We assume that growth occurs in the radial and circumferential directions so that the growth tensor is given by $\mathcal{G} = \text{diag}(\gamma_r, \gamma_\theta, 1)$.

In Section 4.2.7 we determined a relationship between radial and circumferential growth that is compatible with normal wound closure in the absence of boundary loads. We found that $\gamma_\theta < 1 < \gamma_r$, corresponding to addition of material in the radial direction and removal from the circumferential direction. For simplicity we will prescribe an evolution law for γ_r and choose γ_θ such that this relationship is satisfied.

Motivated by the functional form of dermal growth considered in Chapter 2, we consider a growth law consisting of basal and mechanosensitive growth. We assume that the mechanosensitive growth term is proportional to the mean radial stress over the active region of the dermis. This translates to an evolution equation for the radial

growth of the following form:

$$\frac{\mathrm{d}\gamma_r}{\mathrm{d}t} = \left[k_0 + k_1\left(\bar{T}_{rr} - T_{\mathrm{res}}\right)\right]\gamma_r, \tag{5.4}$$

where k_0 and k_1 are the basal and mechanosensitive growth rate constants, respectively, which we take to be non-negative, and $\bar{T}_{rr}$ is the mean radial stress over the proliferative zone of the dermal annulus, given by

$$\bar{T}_{rr} = \frac{2}{b^2 - a^2}\int_a^b T_{rr} r \ \mathrm{d}r. \tag{5.5}$$

The second term on the right hand side of Equation (5.4) represents mechanosensitive growth, so that $\bar{T}_{rr} > T_{\mathrm{res}}$ results in addition of material in the radial direction and $\bar{T}_{rr} < T_{\mathrm{res}}$ results in resorption. Circumferential growth is chosen such that, in the absence of boundary loads, the outer boundary of the annulus does not move (represented by points in $(\gamma_r, \gamma_\theta)$ space which lie on the dashed red line in Figure 4.8 and given by Equation (B.8) in Appendix B.2), therefore the system follows the constraints determined for normal healing. In the buffer region we assign $\gamma_r = \gamma_\theta = 1$. Initially no growth occurs so that $\gamma_r = \gamma_\theta = 1$ at $t = 0$.

5.2.5 Boundary and initial conditions

In order to close the system we must prescribe boundary conditions. We assume that the two tissues, representing the growing region of the dermis and the buffer region, are in perfect contact, that is, the radial stress and deformation are continuous at their common interface. Far from the wound, the dermis is in its residually stressed state and the wound edge is under tension caused by contraction. These biological

assumptions translate to the following boundary conditions

$$r|_{R=B_-} = r|_{R=B_+}, \quad T_{rr}|_{R=B_-} = T_{rr}|_{R=B_+},$$
$$T_{rr}|_{R=C} = T_{\text{res}}, \quad T_{rr}|_{R=A} = fa\mathcal{H}(t - t_c), \tag{5.6}$$

where B_- and B_+ are the positions as R approaches the interface $R = B$ from the left and right, respectively, and $\mathcal{H}$ is given by

$$\mathcal{H}(t - t_c) = \frac{1}{2}\left[\tanh\left(\frac{t - t_c}{\theta}\right) + 1\right], \tag{5.7}$$

with time delay t_c and switch gradient θ. We have assumed that the switch function approximating fibroblast activity is the continuous switch function used in Chapter 2 rather than the piecewise linear switch from Chapter 4. This choice facilitates our comparison between the two models later in this chapter.

5.3 A spatially-averaged morphoelastic model

In this section we state the full model. We present typical simulations and investigate the model behaviour by determining the sensitivity of the wound radius at steady state to model parameters. We fit the model to non-diabetic and diabetic data in the next section and then compare results with the model developed in Chapter 2.

We re-state the simplified system here for completeness in terms of the reference

variable R:

$$\frac{\partial r}{\partial R} = \begin{cases} \gamma_r \gamma_\theta \frac{R}{r} & \text{for } A \leq R \leq B \\ \frac{R}{r} & \text{for } B < R \leq C \end{cases}, \tag{5.8a}$$

$$\frac{\partial T_{rr}}{\partial R} = \begin{cases} \frac{\mu \gamma_r \gamma_\theta R}{r^2} \left[\frac{r^2}{\gamma_\theta^2 R^2} - \frac{\gamma_\theta^2 R^2}{r^2} \right] & \text{for } A \leq R \leq B \\ \frac{\mu R}{r^2} \left[\frac{r^2}{R^2} - \frac{R^2}{r^2} \right] & \text{for } B < R \leq C \end{cases}, \tag{5.8b}$$

$$T_{\theta\theta} = \begin{cases} T_{rr} + \mu \left[\frac{r^2}{\gamma_\theta^2 R^2} - \frac{\gamma_\theta^2 R^2}{r^2} \right] & \text{for } A \leq R \leq B \\ T_{rr} + \mu \left[\frac{r^2}{R^2} - \frac{R^2}{r^2} \right] & \text{for } B < R \leq C \end{cases}, \tag{5.8c}$$

$$\frac{\mathrm{d}\gamma_r}{\mathrm{d}t} = \left[k_0 + k_1 (\bar{T}_{rr} - T_{\text{res}}) \right] \gamma_r, \tag{5.8d}$$

where $\bar{T}_{rr}$ is given by

$$\bar{T}_{rr} = \frac{2\gamma_r \gamma_\theta}{B^2 - A^2} \int_A^B T_{rr} R \, \mathrm{d}R, \tag{5.8e}$$

and (from Equation (B.8) in Appendix B.2) γ_θ satisfies

$$\left(\frac{\gamma_r}{\gamma_\theta} \right)^2 = \frac{1}{\log\left(\frac{B^2}{A^2}\right)} \left[\log \left(\frac{B^2}{B^2 - \gamma_r \gamma_\theta (B^2 - A^2)} \right) + \frac{(\gamma_r \gamma_\theta - 1) \gamma_r \gamma_\theta (B^2 - A^2)}{B^2 - \gamma_r \gamma_\theta (B^2 - A^2)} \right]. \tag{5.8f}$$

The deformation and radial stress are subject to the following continuity and boundary conditions:

$$\begin{aligned} &r(B_-, t) = r(B_+, t), \quad T_{rr}(B_-, t) = T_{rr}(B_+, t), \\ &T_{rr}(C, t) = T_{\text{res}}, \quad T_{rr}(A, t) = fa\mathcal{H}(t - t_c), \end{aligned} \tag{5.8g}$$

with the following initial condition for the radial growth:

$$\gamma_r(0) = 1. \tag{5.8h}$$

5.3.1 Typical simulations

Equations (5.8) are solved numerically (details are given in Appendix C.1), however, we note that the deformation and the stress can be solved analytically and expressed in terms of the current wound radius a, which is determined by imposing the boundary condition at the wound edge ($T_{rr}(A,t)$ in Equations (5.8g)).

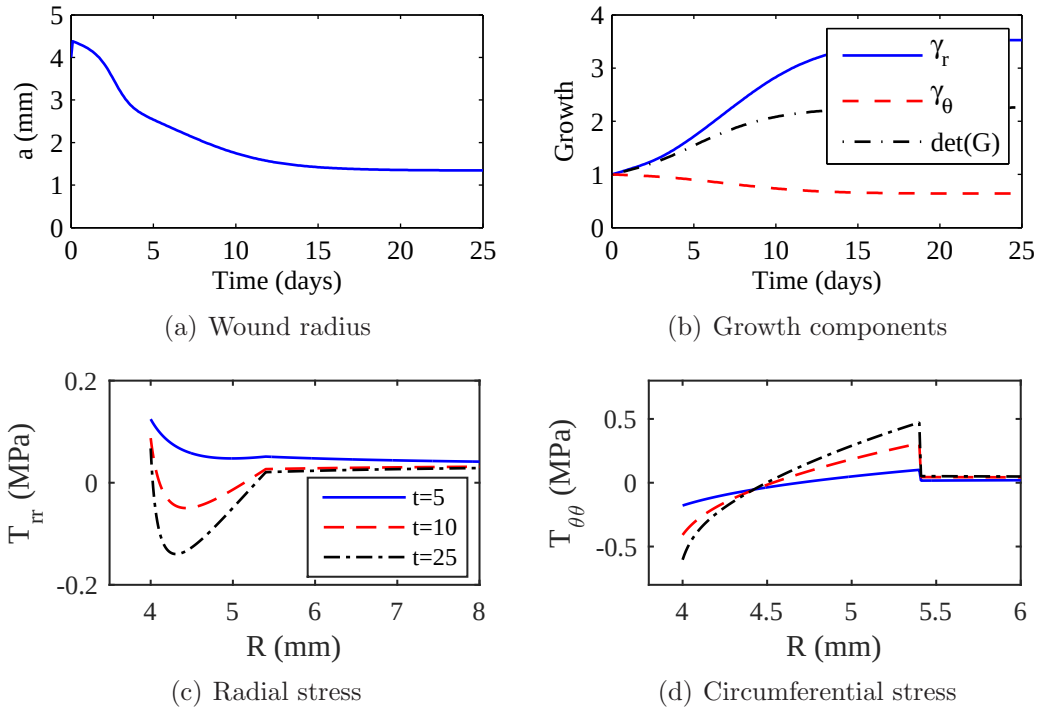

(a) Wound radius (b) Growth components

(c) Radial stress (d) Circumferential stress

Figure 5.2: Results for constant growth. Equations (5.8) are solved numerically. Reference variables are $A = 4$ mm, $B = 5.4$ mm and $C = 20$ mm with parameter values $k_0 = 0.1$ days^{-1}, $k_1 = 0.5$ MPa^{-1} days^{-1}, $f = 0.05$ N mm^{-3}, $t_c = 3$ days, $\theta = 1$, $\mu = 0.2$ MPa and $A_R = 4.4$ mm. See Appendix C.2 for the choice of parameters and reference variables.

In Figure 5.2 we plot the time evolution of the wound radius and growth components and the spatial profiles of the components of the stress tensor at days 5, 10 and 25. In Figure 5.2(a) we observe that the wound retracts immediately (in the first time step of the numerical method), and then the wound radius decreases between days 1 and 5. We remark that friction is neglected in this simplified model: with friction included, we would expect to see a more gradual retraction of the wound. The rate

of healing decreases between days 5 and 20 and eventually plateaus as the growth reaches a constant value around day 20. From Figure 5.2(b) we see that the growth components satisfy $\gamma_\theta < 1 < \gamma_r$, the relationship determined in Section 4.2.7, and the system gains mass (i.e. $\det(\mathcal{G}) > 1$). From the radial stress profiles in Figure 5.2(c) we observe that at $t = 5$ days the tissue is in radial tension due to contraction. As growth is activated in the proliferative region, radial tension decreases and the stress becomes compressive (see, for example, day 25). We would expect the dermal tissue to remain in tension to stimulate mechanosensitive growth. The compressive radial stress in the region close to the wound edge could be a result of prescribing constant growth in a fixed region and choosing circumferential growth such that the position $R = B$ does not move markedly. With little or no movement of the common interface the buffer does not act to absorb the newly synthesised material from the proliferative region.

In the next section we investigate the equilibrium points of the system before using the simplified model to compare normal and diabetic healing and test our conclusions from Chapter 2.

5.3.2 Steady states of the wound radius

Figure 5.2(a) shows that at long times the wound radius plateaus at a finite value and, hence, reaches an equilibrium. In Figure 5.2(b) we observe that the components of the growth tensor, γ_r and γ_θ, also reach an equilibrium. In this section we investigate how this equilibrium state depends on model parameters.

We are interested in the point at which the dermis stops growing, corresponding to

$$\dot{\gamma_r} = \dot{\gamma_\theta} = 0. \tag{5.9}$$

Since γ_θ is related to γ_r by Equation (5.8f), it follows that Equation (5.9) is satisfied

by considering the steady state of Equation (5.8d), given by

$$k_0 + k_1(\bar{T}_{rr} - T_{\text{res}}) = 0. \tag{5.10}$$

Recall from Equation (5.8e) that $\bar{T}_{rr}$ is the mean stress over the growing region of the dermis and is a function of A, B and γ_r (γ_θ can be eliminated using Equation (5.8f)). By integrating Equation (5.8b) and imposing the boundary conditions in Equation (5.8g) we can eliminate γ_r in the expression for $\bar{T}_{rr}$. In doing this, the unknown a and parameter f are introduced via $T_{rr}(A, t) = fa$ (we note, from Figure 5.2, that the equilibrium state is approached at late times, e.g. after day 20, by which time the contraction switch is turned on and therefore we take $\mathcal{H}(t - t_c) = 1$).

The wound radius, a, at equilibrium can therefore be expressed as a function of the model parameters only (k_0, k_1, f and μ). In Figure 5.3 we show how the equilibrium value of a changes as we vary the model parameters.

From Figure 5.3 we observe that, for the parameter values chosen, the model parameters that have the most influence on the steady state of the wound radius are f and μ. Increasing basal growth (k_0) has the least significant effect and varying mechanosensitive growth only has an effect at small values (for $0 < k_1 < 0.2$).

This analysis is important for our understanding of how the model parameters affect the final wound radius of the dermis. Since the analysis was performed at steady state it does not yield information about the rate of wound closure. In the next section we will use our model to investigate the differences between normal and diabetic healing.

5.4 Diabetic wound healing

We use a least squares method (see Appendix A.3) to fit the wound radius from Equations (5.8) to the data for non-diabetic and diabetic healing. To compare be-

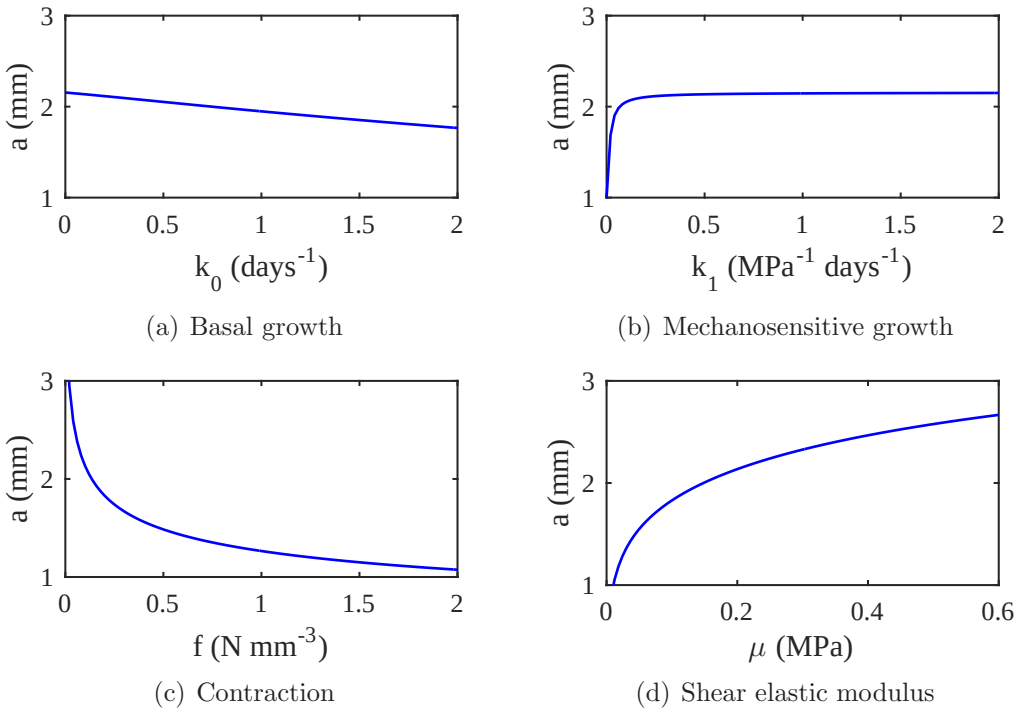

(a) Basal growth (b) Mechanosensitive growth

(c) Contraction (d) Shear elastic modulus

Figure 5.3: The steady state of the wound radius as a function of the model parameters. Equations (5.8b), (5.8e), (5.8f) and (5.10) and are solved simultaneously to find the steady state of the wound radius. The steady state of $a(t)$ is plotted as a function of (a) basal growth, k_0, (b) mechanosensitive growth, k_1, (c) contraction, f and (d) shear elastic modulus, μ. Reference variables are $A = 4$ mm, $B = 5$ mm and $C = 20$ mm. When not being varied, the model parameters are fixed at $k_0 = 0.1$ days^{-1}, $k_1 = 0.5$ MPa^{-1} days^{-1}, $f = 0.1$ N mm^{-3} and $\mu = 0.2$ MPa. See Appendix C.2 for the choice of parameters and reference variables.

tween the two data sets we non-dimensionalise by the maximum wound radius[1] (see Appendix C.2 for the choice of scaling and other parameter values used in the model).

In Figure 5.4 we plot the best fits of the model to the non-diabetic and diabetic dermal data. We observe that the model captures both data sets well (Figures 5.4(a) and (b)). The model suggests that there is more growth in the non-diabetic dermis and, as a consequence, the tissue is in compression in the proliferative region. This may be due to the fact that we have prescribed constant growth in a fixed region. Comparing the model parameters k_0, k_1 and f in Table 5.3 we observe that the basal growth, mechanosensitive growth and contraction parameters are lower in the

[1]Note that scaling r and R by the characteristic length does not affect Equations (5.8).

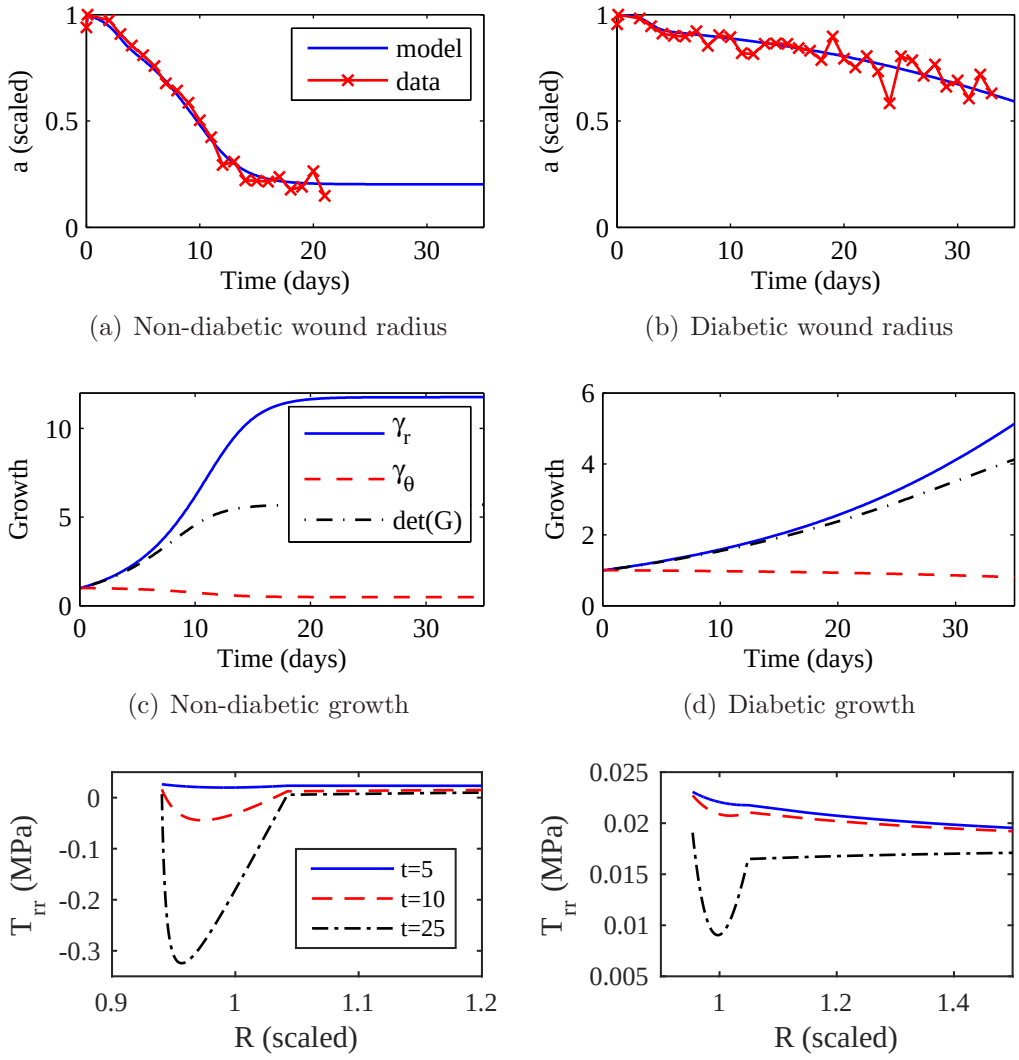

(a) Non-diabetic wound radius

(b) Diabetic wound radius

(c) Non-diabetic growth

(d) Diabetic growth

(e) Non-diabetic radial stress

(f) Diabetic radial stress

Figure 5.4: Best fits of the spatially-averaged morphoelastic model to data. Equations (5.8) are fit to the dermal wound data. Reference variables are $A = 0.9404$ ($A = 0.9542$ for diabetic), $B = 1/x$ and $C = 20/x$, where x is the maximum wound radius. Fixed parameter values are $\mu = 0.2$ MPa, $t_c = 3$ days, $\theta = 1$ and $a_R = 1$. Parameters optimised by the least squares fitting are displayed in Table 5.3. See Appendix C.2 for the choice of parameters and reference variables.

diabetic dermis (by approximately 75%, 70% and 25%, respectively) in comparison to the non-diabetic dermis. In Section 5.5 we discuss these conclusions together with those from the ordinary differential equation model developed in Chapter 2.

5.4.1 Mechanical properties of diabetic skin

It has been shown that mouse and human diabetic skin is biomechanically inferior to non-diabetic skin [Bermudez et al., 2011]. For example, skin samples from mice and humans with diabetes have a much lower maximum stress until failure than control samples.

It has also been observed, experimentally, that diabetic skin has a higher modulus of elasticity [Reihsner et al., 2000]. This means that the skin is stiffer and has a higher resistance to elastic deformation. Here we consider changing the mechanical properties in our model to see whether we are able to capture diabetic healing by varying the tissue stiffness only. In Figure 5.5 we plot the best fit of the wound radius to the non-diabetic data (solid blue). The parameters associated with this best fit are then fixed and the shear elastic modulus is optimised to give the best fit to the diabetic data, yielding $\mu = 9.1577$ MPa. Recall that a realistic range for μ was determined in Section 4.2.5, with values above $\mu = 0.52$ MPa generating unrealistic residual stresses when simulating wound recoil. For the degree of recoil observed in the diabetic data, $\mu = 9.1577$ MPa produces a residual stress of approximately 0.8 MPa. Stresses this high have been shown to tear tissue samples from diabetic mouse skin [Bermudez et al., 2011]. We plot the wound radius for $\mu = 0.5$ MPa (dash dotted green), a value within the determined biological range and observe that, although the final wound radius is larger than that for $\mu = 0.2$ MPa, the increase is not enough to describe the diabetic data. We conclude that increasing μ alone is not sufficient to capture the observed difference between the non-diabetic and diabetic healing curves. This suggests that other healing processes may be compromised in diabetic healing.

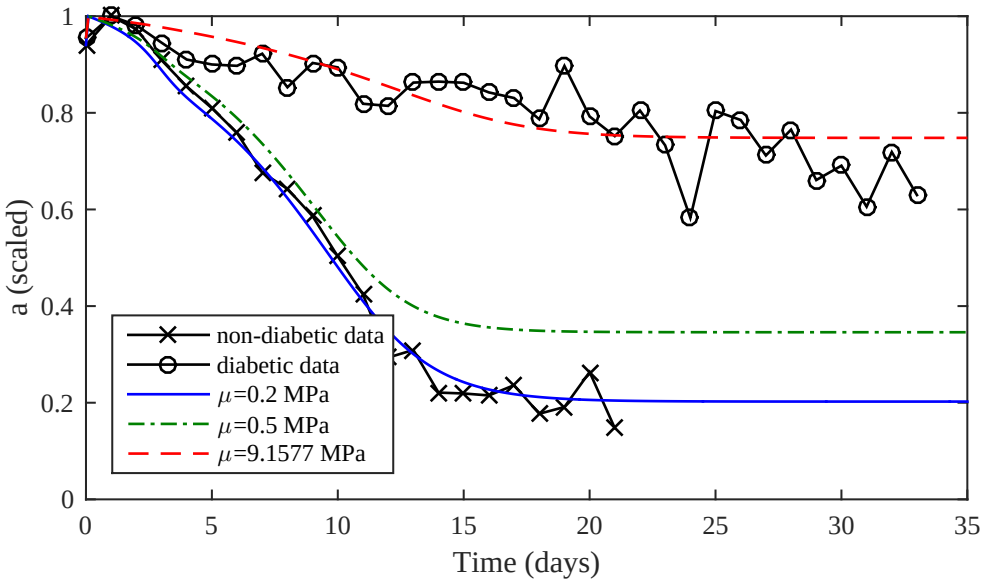

Figure 5.5: The effect of increasing the tissue stiffness on the healing curve. The dermal wound radius for the non-diabetic ($\times$) and diabetic ($\circ$) data are scaled by the maximum wound radius and plotted as functions of time. The parameters associated with the best fit of Equations (5.8) to the non-diabetic data (solid blue) are fixed. Equations (5.8) are then fitted to the diabetic data, allowing only the shear elastic modulus, μ, to vary and yielding $\mu = 9.1577$ MPa (dashed red). The wound radius for a realistic value of $\mu = 0.5$ MPa is plotted (dash-dotted green) showing that increasing the tissue stiffness within the realistic range is not sufficient to describe the diabetic data.

5.5 Comparison with the model from Chapter 2

We have developed a mechanical model that accounts for the contributions of growth and contraction to dermal healing. In Chapter 2 we developed a spatially-averaged ordinary differential equation model for healing of the epidermis and dermis and compared it to the experimental data. In this section we consider the strengths and limitations of each model, compare conclusions obtained by fitting the two models to the non-diabetic and diabetic data and discuss how the model variables and parameters may be used to compare with experimentally observed quantities.

For convenience, we will refer to the ODE model from Chapter 2 as Model A, and the simplified version of the morphoelastic model presented in this chapter as

Model B.

Recall the dermal healing equations from Model A, restated here for convenience, in dimensional form:

$$\frac{\mathrm{d}A_s}{\mathrm{d}t} = -\left(\hat{k}_0 + \hat{k}_1\left(\frac{A_s - A_d}{\hat{A}_R(1+\hat{\nu}) - A_d}\right)\right)(\hat{A}_R(1+\hat{\nu}) - A_s)\frac{A_s}{A_d}, \tag{5.11a}$$

$$\hat{q}\frac{\mathrm{d}A_d}{\mathrm{d}t} = \hat{E}(A_s - A_d) - \hat{c}\mathcal{H}(t - t_c)A_d, \tag{5.11b}$$

with the following initial conditions

$$A_s(0) = \hat{A}_R \quad \text{and} \quad A_d(0) = \hat{A}_0. \tag{5.11c}$$

In Equations (5.11) we have used $\hat{}$ to denote the parameters of Model A. The equation describing the change in epidermal wound area has been omitted as it decouples from the dermal equations and epidermal healing is not considered in this chapter. Equation (5.11a) describes the change in the dermal wound area due to growth only and has basal ($\hat{k}_0$) and mechanosensitive ($\hat{k}_1$) contributions. Equation (5.11b) represents a force balance on the dermal tissue accounting for drag, elastic recoil and contraction. It describes the change in dermal wound area, A_d, in relation to A_s.

Model B is given by Equations (5.8). The physical interpretations of the model parameters are summarised in Table 5.1. We note that, except for the friction term in Model A, there is a one-to-one mapping of the model parameters between the two systems. From our parameter estimation and sensitivity analysis of the friction coefficient in Chapters 2 and 4 we found that it was small in comparison to the other model parameters and that it only affects the initial recoil phase of the healing curve. We therefore proceed with our comparison despite having neglected friction in Model B.

Table 5.1: Parameters for the two models. The physical interpretation of each parameter for both Model A and B are presented. We state whether the parameter is estimated by fitting to the data using a least squares analysis, or fixed from observed experimental values and model behaviour (see Appendix C.2).

physical interpretation	Model A	dimension	Model B	dimension	est./fix
basal growth	$\hat{k_0}$	$\left[\frac{1}{time}\right]$	k_0	$\left[\frac{1}{time}\right]$	estimate
mechanosensitive growth	$\hat{k}_1$	$\left[\frac{1}{time}\right]$	k_1	$\left[\frac{area}{force \cdot time}\right]$	estimate
contraction	$\hat{c}$	$\left[\frac{force}{area}\right]$	f	$\left[\frac{force}{volume}\right]$	estimate
friction	$\hat{q}$	$\left[\frac{force \cdot time}{area}\right]$			fix
proliferative region	$\hat{\nu}$	$[area]$	$B - a_R$	$[length]$	fix
contraction delay	t_c	$[time]$	t_c	$[time]$	fix
contraction gradient	θ	$[time]$	θ	$[time]$	fix
Young's/shear modulus	$\hat{E}$	$[\frac{force}{area}]$	μ	$[\frac{force}{area}]$	fix
recoiled area/radius	$\hat{A}_R$	$[area]$	a_R	$[length]$	fix
initial area/radius	$\hat{A}_0$	$[area]$	A	$[length]$	fix

5.5.1 Representation of healing processes

In this section we generate synthetic data sets from Model A by individually varying the parameters for basal growth, mechanosensitive growth and contraction. We then fit Model B to each of the synthetic data sets to observe whether the correct enhanced or impaired process is detected.

A control data set is generated using the parameters found from the best fit of Model A to the non-diabetic data ($\beta_0 = 0.2950$, $\beta_1 = 0.0124$ and $\alpha = 0.2144$ in the non-dimensionalised version of Model A). In the first test, in order to simulate enhanced healing processes, we double each parameter, one at a time, and fit Model B to the resulting synthetic data curve using a least squares method. The estimated parameter values are presented in Table 5.2, where we have highlighted the parameter with the highest percentage increase from the control parameter set. We observe that Model B identifies correctly the process that has been enhanced in the case of basal growth and contraction. However, Model B fails to capture the increase in mechanosensitive growth. We note that the mechanosensitive growth term in Model B accounts for resorption of material when the tissue is in compression as

Table 5.2: Parameters associated with the best fits of Model B to synthetic data generated by Model A. (a) Individual processes in Model A are enhanced, one at a time, by doubling the associated parameter. The parameter with the highest percentage increase from fitting Model B to the synthetic data is highlighted in red. (b) Individual processes in Model A are impaired, one at a time, by halving the associated parameter. The parameter with the highest percentage decrease from fitting Model B to the synthetic data is highlighted in red. All MSEs are of order 10^{-4} or less except for enhanced basal growth which is 0.0037.

(a) Enhanced processes

sensitivity test	k_0	k_1	f
base values	0.1762	0.0758	0.0566
basal growth	0.3750 (+112%)	0.1114 (+47%)	0.1051 (+86%)
mechanosensitive growth	0.1773 (+0.6%)	0.0759 (+0.1%)	0.0571 (+0.8%)
contraction	0.1802 (+2%)	0.0712 (−6%)	0.1085 (+92%)

(b) Impaired processes

sensitivity test	k_0	k_1	f
base values	0.1762	0.0758	0.0566
basal growth	0.0883 (−50%)	0.3039 (+300%)	0.0385 (−32%)
mechanosensitive growth	0.1757 (−0.3%)	0.0757 (−0.2%)	0.0562 (−0.8%)
contraction	0.1749 (−0.8%)	0.0775 (+2%)	0.0336 (−41%)

well as addition of material when the tissue is in tension. This additional process, not accounted for in Model A, could explain the difference in the parameter ratios. Further, the sensitivity of the solutions of Model A to the mechanosensitive growth parameter was found to be very low and hence multiplying it by two does not change the data curve by much.

We perform the same analysis but half the test parameter: the same conclusions hold. We observe a low sensitivity of the solutions to the mechanosensitive growth parameter: the best fit parameters in Model B changed by less than 1% when mechanosensitive growth was enhanced or impaired in the synthetic data generated by Model A.

We conclude that, apart from mechanosensitive growth, the models are consistent in their representations of the healing processes. In the next section we compare the parameter values associated with diabetic and non-diabetic healing across the two models.

5.5.2 Best fits to the non-diabetic and diabetic data

In Section 5.4 we fitted the model to dermal data for non-diabetic and diabetic wounds. We now compare the estimates of the model parameters with those found from fitting Model A to the same data. In Table 5.3 we present results of the best fits. We note from Table 5.1 that while many of the model parameters are of the same dimensions, there are some that are not consistent between the two models. Therefore, rather than comparing the exact parameter values across the two models, we compare the percentage decrease, for each parameter, between the non-diabetic and diabetic value obtained from the best fits to the data.

Table 5.3: Parameters associated with the best fits of each model to the data. Best fit parameters for (a) Model A and (b) Model B to the non-diabetic and diabetic data. The percentage decreases between the non-diabetic and diabetic parameter values are presented. Mean squared errors are given in Table 5.4.

(a) Model A parameter estimates

physical interpretation	parameter	non-diabetic	diabetic	decrease
basal growth rate	β_0	0.2950	0.0715	76%
mechanosensitive growth rate	β_1	0.0124	0.0026	79%
contraction	α	0.2144	0.1593	26%

(b) Model B parameter estimates

physical interpretation	parameter	non-diabetic	diabetic	decrease
basal growth rate	k_0	0.1866	0.0462	75%
mechanosensitive growth rate	k_1	0.1701	0.0930	45%
contraction	f	0.0339	0.0256	24%

The percentage decreases from non-diabetic to diabetic parameter values for basal growth and contraction are similar for the best fits of both models to the experimental data (approximately 75% and 25%, respectively). However, the mechanosensitive growth parameter is decreased by 79% in Model A and only 45% in Model B. Again, this may be due to the mechanosensitive growth term in Model B accounting for resorption as well as addition of material.

5.5.3 Sensitivity of healing curve to growth parameters

From our sensitivity analysis of Model A in Chapter 2, we found that fitting the model to the non-diabetic data with mechanosensitive growth neglected ($\beta_1 = 0$), gave the same mean squared error as that with $\beta_1 > 0$. Further, by neglecting mechanosensitive growth, the model also showed the same qualitative healing behaviour when fit to the diabetic data.

In Table 5.4 we compare the mean squared errors for fitting Model B to the data with different combinations of the growth parameters. We find that Model B does not describe non-diabetic healing very well in the absence of basal growth (see Table 5.4) or in the absence of mechanosensitive growth. When fitting Model B to the diabetic data we observe that diabetic healing can be described equally well with either growth term neglected.

Table 5.4: Comparison of error when fitting Model B to the data with different growth terms active. The mean squared error is calculated from the best fit curves to the non-diabetic and diabetic data with either both k_0 and k_1 optimised, $k_1 = 0$ and k_0 optimised or $k_0 = 0$ and k_1 optimised. The parameter f is included in the optimisation.

	MSE	
type of growth	non-diabetic	diabetic
basal and mechanosensitive ($k_0, k_1 > 0$)	0.0011	0.0021
basal only ($k_1 = 0 < k_0$)	0.0370	0.0021
mechanosensitive only ($k_0 = 0 < k_1$)	0.0211	0.0021

We showed in Chapter 2 that the diabetic dermal healing curve could be described accurately by fixing the parameters found for the best fit to the non-diabetic data and decreasing only the basal growth parameter. In Figure 5.6 we present results obtained by fitting Model B in Equations (5.8) to the dermal data for diabetic wounds. We fix the parameters found for the best fit to the non-diabetic data and allow only the basal growth rate (k_0) to vary. In Figure 5.6 we observe a good fit to the diabetic data. We therefore conclude, as we did in Chapter 2, that the delay in diabetic healing can be mainly ascribed to a lower basal growth rate.

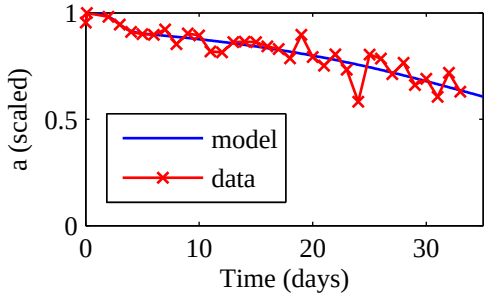

Figure 5.6: Best fit of Model B to the diabetic data described by lower basal growth only. The parameters are chosen for the best fit of Equations (5.8) to the data for non-diabetic wounds given in Table 5.3. Equations (5.8) are fit to the diabetic data by optimising k_0 only. A least squares optimisation gives $k_0 = 0.0422$ with MSE=0.0021.

5.5.4 Processes contributing to dermal healing

In Chapter 2 we used our model to decompose dermal healing into two processes: growth and contraction. To calculate the degree of healing experienced by the dermis due to growth alone in Model B we take $\gamma_r(t)$ and $\gamma_\theta(t)$ and calculate the deformation of the dermal annulus due to growth only. By construction, γ_r and γ_θ are such that $b = B$ in the absence of boundary loads, therefore we can solve Equation (5.8a) together with the boundary condition $r(B,t) = B$ to obtain

$$a_g(t) = \sqrt{B^2 - \gamma_r(t)\gamma_\theta(t)(B^2 - A^2)}, \tag{5.12}$$

where $a_g(t)$ is an approximation of the wound radius, at time t, due to dermal growth only. In Figure 5.7 we plot the proportion of the wound healed by growth and contraction as calculated by each model from the best fits to the non-diabetic and diabetic data. We plot only the proportion at the closure times (wound closure is defined by closure of the epidermis given in the data as day 14 in the non-diabetic wounds and day 33 in the diabetic wounds).

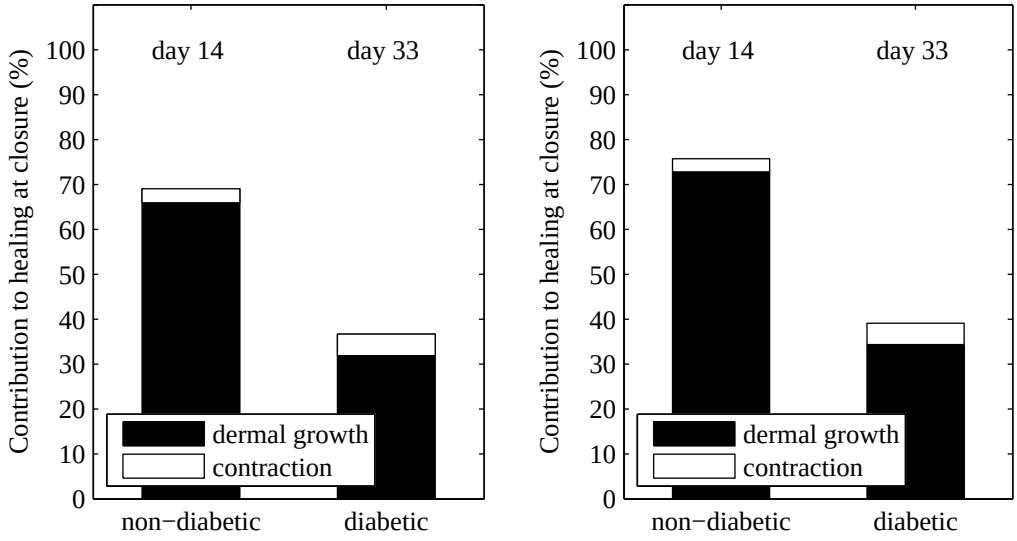

(a) Model A

(b) Model B

Figure 5.7: Contribution of growth and contraction to dermal healing at wound closure. The contributions of growth and contraction to dermal healing are calculated by the model at wound closure. Wound closure is defined by closure of the epidermis from the data, given by day 14 in the non-diabetic wounds and day 33 in the diabetic wounds. Contribution to closure from Model A is converted to percentage radius for comparison with Model B.

In Figure 5.7 we observe the same qualitative behaviour for both models. Although the estimated parameters are such that dermal growth and contraction are lower in the diabetic wounds (see Table 5.3), both models suggest that the percentage of the wound healed by contraction is greater in the diabetic wounds. This is because the decrease in basal growth is more marked than the decrease in contraction. Although we have only presented the proportion of growth and contraction to healing at wound

closure, the wound radius due to growth alone, $a_g(t)$, is a continuous, time-dependent function and therefore, at any time t, we can calculate the contribution of growth to dermal healing. In the previous chapter we discussed rewounding experiments that could help determine the breakdown of growth and contraction. These experiments could provide a validation of our predictions of diabetic healing and the relative contributions of each process.

5.5.5 Treatment intervention

We have suggested that the difference in the non-diabetic and diabetic data can be described by changing only the basal growth parameter. In Chapter 2, Model A was used to stage a treatment intervention in which basal growth was increased to observe the effects on the time to wound closure. In Figure 5.8 we present an analogous analysis of the treatment intervention using Model B. A characteristic of this model is that the dermal healing curve plateaus. Hence, rather than taking a specific value of the dermal wound radius as our marker, the time taken for the dermal gap to stop decreasing[2] and the radius of the dermal wound at this time point are recorded.

The model predicts that the dermal edge of the diabetic wounds will continue to advance into the wound space until day 86, by which time the intact dermis will have covered approximately 70% of the original wound radius. By increasing the basal growth rate from $k_0 = 0.0462$, as predicted by the best fit of the model to the diabetic data, to $k_0 = 0.108$, the dermal gap will stop decreasing at day 43 (half of the time taken without treatment), with the intact dermis covering approximately 80% of the original wound radius, the same as for the control wounds. Further, the proportions of growth and contraction contributing to dermal healing are normalised by this increased value of basal growth (see Figure 5.8(c)).

[2]Numerically this is calculated by choosing the time point for which the gradient of the healing curve is less than some threshold. We take the smallest t such that $\frac{\mathrm{d}}{\mathrm{d}t}(a(t)) < 10^{-5}$.

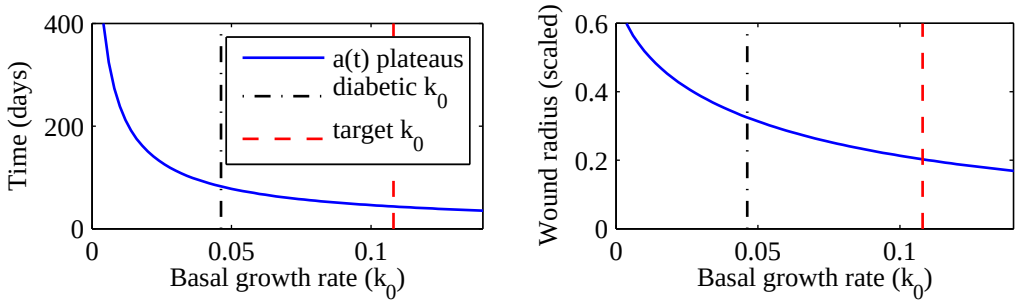

(a) Time until dermis halts for increasing k_0 (b) Minimum wound radius for increasing k_0

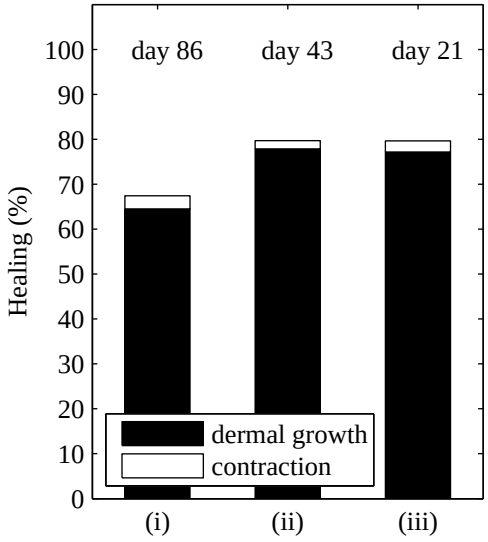

(c) Contribution to dermal healing

Figure 5.8: Increasing the basal growth rate in Model B as a treatment strategy. The basal growth parameter, k_0, is held at its elevated value for $t > 0$ with all other parameters fixed according to the best fit to the diabetic data. (a) Parameter sensitivity showing how, for the diabetic tissue, the time for the dermal curve to plateau decreases as k_0 increases (solid blue). (b) Parameter sensitivity showing the final dermal wound radius as a function of k_0 (solid blue). As k_0 increases, the final wound radius decreases. The value of k_0 as estimated by the best fit of Equations (5.8) to the diabetic data is 0.0462 (dash-dotted black) and the target treatment value is $k_0 = 0.108$ (dashed red). By increasing k_0 to 0.108 the diabetic dermis is predicted to plateau by day 43 to the same wound radius as that observed in the non-diabetic data. (c) Comparison of the contributions to healing at the time of dermal closure (defined by the dermal curve reaching a plateau) for (i) the diabetic case, (ii) the diabetic case with elevated k_0 to the target value, and (iii) the non-diabetic case.

5.5.6 A mechanistic approach

The model developed in Chapter 4 and simplified in this chapter provides a more mechanistic description than the phenomenological model from Chapter 2. Therefore many of the model parameters represent experimentally measurable values such as the residual stress and shear elastic modulus. Further, the model solution encompasses the heterogeneous radial stress experienced by the healing dermis, allowing us to compare model predictions with realistic stresses experienced by dermal tissue *in vivo*. In our model development we made a constitutive assumption about the mechanical properties of the material. We assumed that the tissue is incompressible and hyperelastic and chose a neo-Hookean strain-energy function. If more detailed stress-strain information were available, then the model could be adapted to more accurately represent dermal tissue from different species, such as mouse or human, or different pathological conditions, such as diabetes [Reihsner et al., 2000].

We note that the steady states of Model A are $A_s = A_d = 0$, corresponding to the dermis completely closing and being relieved of all tension. However, from experimental observations the dermis never fully closes. In Chapter 4 we showed that the morphoelastic model, with mechanosensitive growth laws, predicted that the tissue returns to its residually stressed state. Therefore the morphoelastic approach is better suited to investigate dermal closure, under what conditions the dermis stops advancing into the wound, and the stresses experienced by the dermis during healing.

5.6 Conclusions

In this chapter we assumed that, close to the wound, growth was constant and that elsewhere it was negligible. Under these assumptions the governing equations were analytically tractable. We proposed a growth law for the radial component of the growth tensor that includes a basal growth term and a spatially-averaged, stress-

induced, growth term. We specified circumferential growth such that it satisfied the wound filling region of Figure 4.8 determined by our growth analysis in Section 4.2.7. Contraction was modelled by imposing a radial tension at the wound boundary with the temporal behaviour of the fibroblasts approximated by a switch function. To facilitate comparison, we used the continuous switch function introduced in Chapter 2.

In practice, tissue growth is localised close to the wound edge [Bullough and Laurence, 1960]. By restricting growth to a small region it was reasonable to assume constant growth within this area. By adopting an isotropic, but spatially homogeneous growth law, addition of mass in the active dermal region caused a build up of material, creating a compressive stress. We would expect growth to be higher in regions of high stress and growth factor concentration, that is, close to the wound edge. We observed this behaviour in the spatially-resolved morphoelastic model in Chapter 4 where growth depended on the local mechanical environment. However, we would also expect growth to be stimulated by biochemical stimuli.

With the exception of friction (which was neglected in the simplified model so that analytical solutions could be constructed), we noted that there was a one-to-one mapping of model parameters between the two systems which facilitated their comparison. Basal growth and contraction parameters obtained from the best fits of the two models to the data showed similar percentage decreases between the non-diabetic and diabetic estimates. Although the mechanosensitive growth parameter was also lower in the diabetic case, the percentage decrease was not consistent across both models. We speculated that this discrepancy could be the result of mechanosensitive growth in Model B also accounting for resorption of material, concluding that mechanosensitive growth was not necessarily directly comparable across the two models.

The main focus of the model comparison in this chapter was to test the robustness of the conclusions of Model A. The ODE model, together with the data, suggested that mechanosensitive growth is negligible. This was not the case when fitting Model B

to the data where we found that both basal and mechanosensitive terms contributed significantly to healing. Further, the growth laws for the spatially-averaged morphoelastic model in Chapter 4 were entirely stress dependent and yielded solutions qualitatively similar to wound healing curves in rodents (see McGrath and Simon [1983] and Figure 2.2). These results suggest that our phenomenological model from Chapter 2 may not be appropriate for incorporating mechanically induced growth.

In this chapter the epidermis was neglected since our conclusions from Chapter 2 implied that dermal healing was most compromised in diabetic wounds. Although re-epithelialisation may not be greatly affected by diabetes, the epidermis may influence dermal healing (and *vice versa*). These interactions may be mediated by growth factors that allow communication between the two layers [Werner et al., 2007] or mechanical interactions, such as the spring load assumed in Chapter 4.

In Chapters 2 and 4 we found that the friction term had negligible effect after the recoil phase of healing. In our spatially-averaged morphoelastic model we neglected friction so that analytical solutions for the deformation and stress could be obtained. With explicit analytical solutions, the process of fitting the model to the data was more efficient than fitting the spatially-resolved morphoelastic model.

In Section 5.5.6 we noted that the parameters of the morphoelastic model represent biomechanical quantities that can be determined experimentally and therefore the morphoelastic approach is better suited to modelling dermal healing. Models A and B, together with the data, suggested that the most compromised process in diabetic healing is dermal growth. Therefore, in the next chapter we extend the spatially-resolved morphoelastic model to include a more mechanistic description of growth. Growth and contraction are regulated by fibroblasts which in turn are regulated by growth factors released from the wound. To incorporate such activity we introduce fibroblast and growth factor species, coupling their activity to growth and contraction of the dermal tissue, these processes being described in the morphoelastic framework.

Chapter 6

A morpho-mechano-chemical model

6.1 Introduction

Thus far we have developed two distinct forms of wound healing models. In Chapter 2, a simple, time-dependent, ordinary differential equation model described changes in the epidermal and dermal wound areas. Growth was assumed to follow a modified logistic growth law in both the epidermis and dermis, with growth in the dermis enhanced by 'stretch' of the tissue. A phenomenological force balance assumed the elastic, contractile and frictional forces acting on the dermis to be in equilibrium yielding the dermal wound area. In Chapter 4 we used morphoelasticity theory to develop a mechanical model of dermal wound healing. This approach allowed for position-dependent and stress-induced growth. The morphoelastic model provides a theoretical framework with which to investigate possible growth laws and devise mechanically motivated experiments. However, our growth laws depended only on stress, and contraction was modelled phenomenologically, with the migratory and contractile behaviour of fibroblasts being represented by a time-dependent switch function. The

switch function was characterised by a time delay for fibroblast migration and a time for maximal fibroblast contraction. In practice, we expect growth to be influenced by biochemical and mechanical stimuli [Roberts et al., 1992, Murata et al., 1997, Kessler et al., 2001]. Furthermore, for a more mechanistic approach to both growth and contraction we must consider explicitly the activity of the cells and chemicals that regulate these processes.

In this chapter we develop a novel mechano-chemical model of dermal wound healing. Our model in Chapter 4 comprised two components: growth and mechanics. Here we introduce an extra component by coupling advection-diffusion equations for fibroblast cells and a diffusible growth factor to the morphoelastic model. This third component enables us explicitly to introduce physical regulators of growth and contraction. We must revisit how evolution of growth and wound contraction are formulated so that the phenomenological laws can be replaced by mechanistic ones.

A review of previous mechano-chemical models for dermal wound healing was included in Chapter 1. Typically such models consist of advection-diffusion equations for mass conservation of cells, growth factors and/or ECM and a phenomenological momentum balance combined with a constitutive assumption about the mechanical properties of the ECM enabling for the ECM displacement, stress and strain to be determined. Most models assume linear elasticity and are, therefore, unable to reproduce the large degree of wound contraction observed experimentally [Catty, 1965, McGrath and Simon, 1983]. We have developed a morphoelastic framework for modelling dermal wound healing which accounts for the non-linear elastic properties of the dermis and position-dependent, mechanically influenced tissue growth.

By explicitly accounting for the fibroblast cells and a regulating growth factor, we can ask questions about specific wound healing pathologies. For example, diabetic wounds are known to have a lower fibroblast density than non-diabetic wounds [Desta et al., 2010]. Could this be due to lower rates of cell proliferation or higher rates of

cell death? Further, as cell proliferation is regulated by growth factors, could changes in proliferation rates be due to lower rates of growth factor production or reduced cell sensitivity to the growth factor? By investigating the behaviour of the mathematical model, we aim to determine possible explanations for different healing pathologies.

The remainder of this chapter is organised as follows. In Section 6.2 we develop mass conservation equations for the growth factor and fibroblast species. We assume that the growth factor diffuses from the wound space where it is produced and undergoes natural decay within the normal dermal tissue, while the fibroblasts migrate and proliferate in response to the growth factor. Both species are passively advected by the moving dermal tissue. We pay particular attention to the advection term in Lagrangian coordinates. By construction of the PDEs in a fixed reference configuration, the typical advection terms due to material velocities are absent. However, growth of the tissue introduces growth advection. In Section 6.3 we propose an evolution law for the growth of the dermal tissue. The growth rate is assumed to depend on fibroblast density, with new material being distributed in the direction of greatest tension (see, for example, Araujo and McElwain [2004]). Following Chapters 3 - 5, the dermal tissue is viewed as a hyperelastic cylinder surrounding the wound. In Section 6.4 the tissue mechanics are described in the morphoelastic framework together with our proposed mechanistic approach for contraction of the wound edge. We present the full model in Section 6.5 where we also non-dimensionalise by considering realistic parameter values from the biological literature. Typical model behaviour and a consideration of different healing pathologies are the focus of Section 6.6. Finally, in Section 6.7 we summarise our results, leaving a discussion of our ideas for future work to Chapter 7.

6.2 Mass conservation equations

In this section we develop equations for the fibroblasts and a regulating growth factor, TGFβ, a key growth factor in dermal healing influencing cell behaviour in processes such as angiogenesis, granulation tissue formation, collagen synthesis, wound contraction and remodelling [Roberts et al., 1992, Desmoulière et al., 1993, Murata et al., 1997, Rhett et al., 2008]. TGFβ is present across many of the wound healing phases. Platelets and macrophages, present in the wound space, are the primary source of TGFβ synthesis [Barrientos et al., 2008]. We therefore consider a source of TGFβ diffusing from the wound space into the surrounding tissue. Fibroblasts are present at low density in unwounded dermal tissue [Randolph and Simon, 1998, Miller et al., 2003]. Upon injury, growth factors stimulate proliferation and directed migration of fibroblasts towards the wound [Cordeiro et al., 2000]. The spatial distribution of fibroblasts influences the locally defined tissue growth and contraction of the wound edge.

To describe the spatio-temporal evolution of the growth factor and fibroblast populations we appeal to mass conservation laws. In general, the conservation of a cellular or chemical species $q = q(\mathbf{x}, t)$, defined in the current (Eulerian) configuration, can be written

$$\frac{\partial q}{\partial t} + \nabla \cdot \mathbf{J}_q = S_q, \tag{6.1}$$

where $\mathbf{J}_q$ is the net flux of species q, S_q its net rate of production and ∇ denotes the gradient operator with respect to $\mathbf{x}$. For example, on a moving domain, one may write $\mathbf{J}_q = \mathbf{v}q - D\nabla q$, where $\mathbf{v} = \frac{\mathrm{d}\mathbf{x}}{\mathrm{d}t}$ is the velocity of a material point $\mathbf{x}$. The first term represents the flux of the species due to advection of the material and the second term the flux due to diffusion, where D denotes the diffusion coefficient, which is assumed to be constant and non-negative.

When using morphoelasticity, it is computationally convenient (as we have done

in Chapters 3 - 5) to write all dependent variables in terms of the reference variable $\mathbf{X}$. We explain how this is done in the following section for the general species $q(\mathbf{x}, t)$, before developing our equations for TGFβ and fibroblasts.

6.2.1 Transformation to Lagrangian coordinates

We define $Q(\mathbf{X}, t) = q(\mathbf{x}(\mathbf{X}, t), t)$ and let 'Grad' and 'Div' define the gradient and divergence in the reference configuration (with respect to $\mathbf{X}$) and 'grad' and 'div' in the current configuration (with respect to $\mathbf{x}$). To facilitate mapping from the current to the reference configuration, the following relationships will be useful (see Ogden [1997] for details):

$$\operatorname{grad} q = \mathcal{F}^{-T}\operatorname{Grad} Q \quad \text{and} \quad \operatorname{div} \mathbf{u} = \frac{1}{\det(\mathcal{F})}\operatorname{Div}(\det(\mathcal{F})\,\mathcal{F}^{-1}\mathbf{u}), \tag{6.2}$$

where q is a scalar, $\mathbf{u}$ a vector and $\mathcal{F}$ the deformation gradient tensor. We note that $\mathcal{F}$ is non-singular and, hence, its inverse exists.

Equation (6.1), with advective and diffusive fluxes included, can be written as

$$\frac{\partial q}{\partial t} + \operatorname{grad} q \cdot \mathbf{v} + q\operatorname{div} \mathbf{v} = \operatorname{div}(D\operatorname{grad} q) + S_q. \tag{6.3}$$

Differentiating Q with respect to time and using the chain rule for partial derivatives we obtain the material derivative:

$$\frac{\partial Q}{\partial t} = \frac{\partial q}{\partial t} + \operatorname{grad} q \cdot \mathbf{v}. \tag{6.4}$$

Substituting Equation (6.4) into (6.3) and using the relationships in Equation (6.2) gives

$$\frac{\partial Q}{\partial t} + Q\operatorname{div} \mathbf{v} = \frac{1}{\det(\mathcal{F})}\operatorname{Div}(D\det(\mathcal{F})\mathcal{F}^{-1}\mathcal{F}^{-T}\operatorname{Grad} Q) + S_Q. \tag{6.5}$$

In Equation (6.5), which is defined in Lagrangian variables, we retain a growth advection term. It remains to find a relationship between material growth and $\operatorname{div}\mathbf{v}$.

Consider a tissue, with density ρ and velocity $\mathbf{v}$. The growth rate function $\hat{\gamma}$, describes position-dependent volumetric growth of the tissue. Under the slow growth assumption of morphoelasticity, material fluxes through the boundary are assumed to be negligible and conservation of tissue mass supplies [Goriely and Moulton, 2011]

$$\frac{\partial \rho}{\partial t} + \rho \operatorname{div}\mathbf{v} = \hat{\gamma}. \tag{6.6}$$

In Equation (6.6) we have assumed that both cells and growth factor occupy negligible volume. For a material with constant density, Equation (6.6) simplifies to

$$\operatorname{div}\mathbf{v} = \frac{\hat{\gamma}}{\rho}. \tag{6.7}$$

It can be shown that the growth rate function, $\hat{\gamma}$, is related to the growth tensor, $\mathcal{G}$, by the following relationship [Goriely and Moulton, 2011],

$$\hat{\gamma} = \rho \operatorname{tr}(\mathcal{G}^{-1}\dot{\mathcal{G}}), \tag{6.8}$$

where the dot represents differentiation with respect to time. Equations (6.7) and (6.8) can be combined to give

$$\operatorname{div}\mathbf{v} = \operatorname{tr}(\mathcal{G}^{-1}\dot{\mathcal{G}}), \tag{6.9}$$

where specification of the form of the growth tensor, $\mathcal{G}$, will be given in Section 6.3.

For notational simplicity, we introduce the tensor $\mathcal{C} = \det(\mathcal{F})\mathcal{F}^{-1}\mathcal{F}^{-T}$ for substitution into Equation (6.5) and ∇ will be used, from now on, to denote differentiation with respect to the Lagrangian coordinate, $\mathbf{X}$.

6.2.2 Growth factor concentration

We consider a single growth factor, such as TGFβ, whose concentration at position $\mathbf{X}$ and time t is denoted $\beta(\mathbf{X}, t)$. The growth factor is produced in the wound space and regulates fibroblast activity.

The growth factor is assumed to diffuse from the wound space into the surrounding dermal tissue with linear diffusion coefficient D_β so that the total flux has advective and diffusive terms. The growth factor is removed at a rate linearly proportional to the growth factor concentration, with rate d. By considering the Lagrangian advection-diffusion equation in Equation (6.5), the concentration of growth factor in the dermal tissue can be written

$$\frac{\partial \beta}{\partial t} + \beta \mathrm{tr}(\mathcal{G}^{-1}\dot{\mathcal{G}}) = \frac{D_\beta}{\det(\mathcal{F})} \nabla \cdot (\mathcal{C} \nabla \beta) - d\beta. \tag{6.10}$$

Assuming, as in previous chapters, a cylindrical geometry of the dermal tissue and restricting attention to symmetrical deformations, we express the growth factor concentration as a function of the independent variables R_0 and t. The gradient and divergence are defined in the one-dimensional polar coordinate system and, hence, only the radial component of $\mathcal{C}$ ($\mathcal{C}_1$, say) appears in Equation (6.10). Here, we allow for axial deformations and, thus, the growth factor concentration at a point R_0 in the reference configuration will be diluted, or concentrated, according to the current dermal thickness. In particular, the concentration of TGFβ, when the tissue has been subject to axial deformation, is given by β/λ, where λ is the axial stretch.

6.2.2.1 Boundary and initial conditions

We assume that initially, there is no TGFβ present in the unwounded dermis. Upon injury, growth factor is released by platelets located in the wound space. During healing, other sources within the wound, such as macrophages, also produce growth

factor. We assume that the main source of TGFβ is the wound space and, hence, prescribe the concentration of TGFβ on the wound margin, $R_0 = A_0$, taking it to be proportional to the wound area. From there, it diffuses into the surrounding tissue. The domain is taken to be sufficiently large that far from the wound we can assume that the growth factor concentration is zero. For a dermal cylinder occupying $A_0 \leq R_0 \leq B_0$ (in the reference configuration) the initial and boundary conditions for the TGFβ concentration are given by

$$\beta(R_0, 0) = 0 \tag{6.11a}$$

$$\beta(A_0, t) = \beta_0 a^2(t) \tag{6.11b}$$

$$\beta(B_0, t) = 0, \tag{6.11c}$$

where β_0 is a non-negative constant of proportionality for the concentration of growth factor at the wound boundary and $a(t)$ is the wound radius at time t.

6.2.3 Fibroblast population

We consider a single population of fibroblasts, with density $\phi(\mathbf{X}, t)$, whose activity is determined by the local mechano-chemical environment. Since fibroblasts are motile cells that are chemotactically attracted to the growth factor [Pierce et al., 1989, Cordeiro et al., 2000], we consider the total flux to have advective, diffusive and chemotactic terms, with non-negative constant coefficients of diffusion and chemotaxis, D_ϕ and χ, respectively. Assuming that, in normal conditions, the rate of cell proliferation and cell death balance, we write the enhanced proliferation term as

$$S_\phi = \hat{k}\phi\left(1 - \frac{\phi}{\phi_{\max}}\right), \tag{6.12}$$

where $\phi_{\max}$ is the maximal fibroblast density and $\hat{k} = \hat{k}(\beta)$ is the enhanced proliferation rate. Cell proliferation is enhanced in the presence of TGFβ [Cordeiro et al., 2000, Kessler et al., 2001] and, hence, we consider the proliferation rate to be an increasing function of growth factor concentration such that

$$\hat{k}(\beta) = k \left[\frac{\left(\frac{\beta}{\beta^*}\right)^{s_\beta}}{\left(\frac{\beta}{\beta^*}\right)^{s_\beta} + 1} \right], \tag{6.13}$$

where k is the proliferation coefficient, β^* is the value of growth factor such that proliferation is half-maximal and s_β is the sensitivity of the fibroblasts to the growth factor concentration.

In the axisymmetric cylindrical geometry, the fibroblast density is a function of the independent variables R_0 and t, and the Lagrangian advection-diffusion equation in Equation (6.5) can be written as

$$\begin{aligned} \frac{\partial \phi}{\partial t} + \phi \mathrm{tr}(\mathcal{G}^{-1}\dot{\mathcal{G}}) = \frac{1}{\det(\mathcal{F})} \nabla \cdot [\mathcal{C}_1 (D_\phi \nabla \phi - \chi \phi \nabla \beta)] \\ + k \left[\frac{\left(\frac{\beta}{\beta^*}\right)^{s_\beta}}{\left(\frac{\beta}{\beta^*}\right)^{s_\beta} + 1} \right] \phi \left(1 - \frac{\phi}{\phi_{\max}}\right). \end{aligned} \tag{6.14}$$

Since the dermal cylinder experiences axial deformations, the fibroblast density at a given point R_0 is ϕ/λ.

6.2.3.1 Boundary and initial conditions

The initial fibroblast density is assumed to be uniform across the unwounded dermal tissue. As we do not model the central granulation tissue we assume that fibroblasts migrating towards the wound stop at the wound edge. The domain is taken to be sufficiently large that we can neglect fibroblast movement at the outer boundary. We therefore assume zero flux of fibroblasts at $R_0 = A_0$ and $R_0 = B_0$. The initial and

boundary conditions for the fibroblast density are written as

$$\phi(R_0, 0) = \phi_0, \tag{6.15a}$$

$$D_\phi \nabla\phi(A_0, t) - \chi\phi(A_0, t)\nabla\beta(A_0, t) = 0, \tag{6.15b}$$

$$D_\phi \nabla\phi(B_0, t) - \chi\phi(B_0, t)\nabla\beta(B_0, t) = 0, \tag{6.15c}$$

where ϕ_0 is the fibroblast density in the unwounded tissue with $0 < \phi_0 < \phi_{\max}$.

Taken together, Equations (6.10), (6.11), (6.14) and (6.15) define the spatio-temporal evolution of the growth factor and fibroblast species. In the next section we consider growth of the dermal tissue by postulating a form for the evolution of the growth tensor.

6.3 Growth of the dermal tissue

In Chapter 4, growth of the dermal tissue was formulated such that stress higher (lower) than the residual stress induced growth (resorption). We found that, due to the circular wound geometry, anisotropic growth was needed to reproduce the observed healing behaviour. Our sensitivity analysis also revealed that axial growth had a negligible effect on the model solutions. Therefore, in this chapter, we neglect growth in the axial direction and consider anisotropic growth such that $\mathcal{G} = \text{diag}(\gamma_r, \gamma_\theta, 1)$. In this section we formulate an evolution law for the total growth of the dermis, which locally defines the net addition or loss of material. This growth is then distributed in the radial and circumferential directions according to the local mechanical environment.

6.3.1 Locally defined net growth

Net growth is defined point-wise and depends on the synthesis and degradation of collagen by fibroblasts. We assume that, in normal conditions, i.e. $\phi = \phi_0$, production and degradation of collagen balance. The total net growth is described by the determinant of the growth tensor

$$\begin{aligned}\det(\mathcal{G}) &= \frac{\text{current tissue volume}}{\text{initial tissue volume}} \\ &= \frac{\text{initial tissue volume + volume of new cell-derived material}}{\text{initial tissue volume}} \\ &= 1 + \int_0^t \frac{V_\text{c}}{\lambda}(\phi - \phi_0)\ \mathrm{d}t, \end{aligned} \tag{6.16}$$

where V_c is the volume of material synthesised per cell. We note also that the rate of tissue synthesis is scaled by $1/\lambda$ since the fibroblast density depends on the current thickness of the dermis.

6.3.2 Isotropic growth

Following the form of the growth evolution in Chapters 4 and 5, we assume that, in the case of isotropic growth ($\gamma_r = \gamma_\theta = \gamma$), growth satisfies

$$\frac{\partial \gamma}{\partial t} = n\gamma, \tag{6.17}$$

where the growth rate n may be a function of fibroblast density, growth factor concentration and/or stress. Our aim in this section is to determine the form of the isotropic growth rate, n, given Equations (6.16) and (6.17). Since we consider growth to be anisotropic in wound healing, we then map the isotropic growth rate to anisotropic rates according to the mechanical stress.

At any point in space, the total growth is given by the determinant of the growth

tensor

$$\det(\mathcal{G}) = \gamma^2. \tag{6.18}$$

Differentiating Equation (6.18) with respect to time gives

$$\frac{\partial}{\partial t}\det(\mathcal{G}) = 2\gamma\frac{\partial \gamma}{\partial t} = 2n\gamma^2 = 2n\det(\mathcal{G}). \tag{6.19}$$

Rearranging Equation (6.19) yields an expression for the isotropic growth rate

$$n = \frac{1}{2\det(\mathcal{G})}\frac{\partial}{\partial t}\det(\mathcal{G}). \tag{6.20}$$

For anisotropic growth, the total growth must be distributed between the radial and circumferential directions appropriately.

6.3.3 Anisotropic radial and circumferential growth

We return now to anisotropic growth ($\mathcal{G} = \mathrm{diag}(\gamma_r, \gamma_\theta, 1)$) and seek evolution laws for radial and circumferential growth in the form

$$\frac{\partial \gamma_r}{\partial t} = n_r\gamma_r, \tag{6.21a}$$

$$\frac{\partial \gamma_\theta}{\partial t} = n_\theta\gamma_\theta, \tag{6.21b}$$

where n_r and n_θ are the radial and circumferential growth rates, respectively. The total growth is given by the determinant of the growth tensor:

$$\det(\mathcal{G}) = \gamma_r\gamma_\theta. \tag{6.22}$$

It remains to relate n_r and n_θ to the isotropic growth rate, n.

Taking the time derivative of Equation (6.22), and following the same argument

as for isotropic growth, we have

$$\frac{\partial}{\partial t}\det(\mathcal{G}) = (n_r + n_\theta)\det(\mathcal{G}). \tag{6.23}$$

By equating Equations (6.19) and (6.23), we obtain

$$n_r + n_\theta = 2n. \tag{6.24}$$

We must now determine how to distribute the total growth between its radial and circumferential components. Following Araujo and McElwain [2004], we assume that the highest addition of material will occur in the direction of highest tension and that resorption of material will occur in the direction of highest compression. Letting $n_r = 2n\upsilon_r$ and $n_\theta = 2n\upsilon_\theta$, Equation (6.24) can be written

$$\upsilon_r + \upsilon_\theta = 1, \tag{6.25}$$

where υ_r and υ_θ are the radial and circumferential strain multipliers, respectively. Since the position-dependent net growth in Equation (6.16) accounts for both addition of material due to collagen synthesis and removal of material due to degradation, the strain multipliers will take different forms depending on whether net growth is positive or negative. Supposing that material will be added and removed according to the relative sizes and signs of the radial and circumferential stresses, we introduce the stress difference $\hat{T} = T_{rr} - T_{\theta\theta}$ and propose the following form for the radial strain multiplier

$$\upsilon_r = \frac{1}{2}\left[1 + 3\mathrm{sgn}(n)\tanh(s_T\hat{T})\right], \tag{6.26}$$

where $\mathrm{sgn}(n) = 1$ for $n > 0$ and $\mathrm{sgn}(n) = -1$ for $n < 0$ and s_T characterises the sensitivity of growth direction to the stress. In Figure 6.1 we plot the radial strain multiplier as a function of the stress difference measure $\hat{T}$.

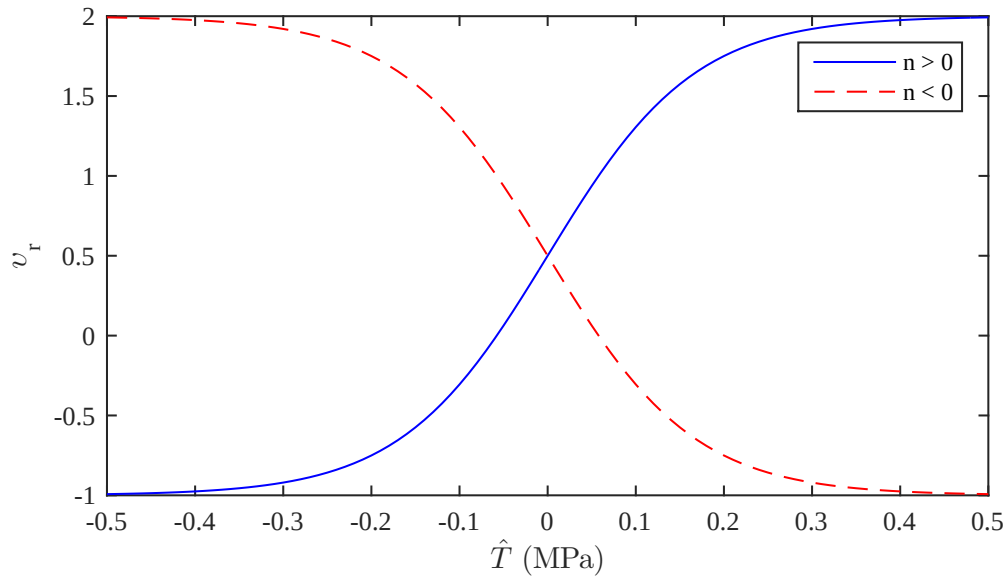

Figure 6.1: Functional form for the radial strain multiplier. The radial strain multiplier is plotted as a function of $\hat{T} = T_{rr} - T_{\theta\theta}$, according to Equation (6.26), with sensitivity parameter $s_T = 6$. For a positive volumetric growth rate ($n > 0$), material is distributed preferentially in the direction of greatest tension (solid blue). For example, if radial stress is greater than circumferential stress ($\hat{T} > 0$) then $\upsilon_r > 0.5 > \upsilon_\theta$ and more material is distributed in the radial than the circumferential direction. For a negative volumetric growth rate ($n < 0$), material is removed preferentially from the direction of highest compression (dashed red). For example, if radial stress is greater than circumferential stress ($\hat{T} > 0$) then $\upsilon_r < 0.5 < \upsilon_\theta$ and more material is removed from the circumferential than the radial direction.

Equations (6.25) and (6.26) imply that when the radial and circumferential stresses are equal, the distribution of material will be isotropic. At a given position and time, if material is added ($n > 0$), it will be distributed preferentially in the direction of highest tension. For example, if $T_{rr} > T_{\theta\theta}$, then $\upsilon_r > \upsilon_\theta$, and new material will be biased in the radial direction. If the fibroblast density drops below the normal density, then there will be net loss of material due to higher rates of degradation than production. In this case, $n < 0$, and more material is removed from the direction of highest compression. We note that Equations (6.25) and (6.26) allow for remodelling of material from one direction to another if the stress difference is high enough.

6.3.4 Growth evolution equations

Defining $Y = \det(\mathcal{G})$ and combining Equations (6.16), (6.20), (6.21) and (6.24)-(6.26), the growth evolves according to the following equations

$$\frac{\partial Y}{\partial t} = \frac{V_c}{\lambda}(\phi - \phi_0), \tag{6.27a}$$

$$\frac{\partial \gamma_r}{\partial t} = \frac{1}{Y}\frac{\partial Y}{\partial t}\upsilon_r \gamma_r, \tag{6.27b}$$

$$\frac{\partial \gamma_\theta}{\partial t} = \frac{1}{Y}\frac{\partial Y}{\partial t}\upsilon_\theta \gamma_\theta, \tag{6.27c}$$

where

$$\upsilon_r = \frac{1}{2}\left[1 + 3\mathrm{sgn}(\phi - \phi_0)\tanh(s_T \hat{T})\right] \quad \text{and} \quad \upsilon_\theta = 1 - \upsilon_r. \tag{6.28}$$

In Equations (6.28), $\mathrm{sgn}(\phi - \phi_0) = 1$ for $\phi \geq \phi_0$ and $\mathrm{sgn}(\phi - \phi_0) = -1$ for $\phi < \phi_0$ and the stress measure $\hat{T}$ is defined as $\hat{T} = T_{rr} - T_{\theta\theta}$. We assume that no growth occurs initially so that

$$\gamma_r(R_0, 0) = \gamma_\theta(R_0, 0) = Y(R_0, 0) = 1. \tag{6.29}$$

Remark (Growth advection)**.** Recall from Section 6.2.1 that $\mathrm{div}\,\mathbf{v} = \mathrm{tr}(\mathcal{G}^{-1}\dot{\mathcal{G}})$. With $\mathcal{G} = \mathrm{diag}(\gamma_r, \gamma_\theta, 1)$, we note from Equations (6.27) that

$$\mathrm{div}\,\mathbf{v} = \mathrm{tr}(\mathcal{G}^{-1}\dot{\mathcal{G}}) = \frac{\dot{\gamma_r}}{\gamma_r} + \frac{\dot{\gamma_\theta}}{\gamma_\theta} = \frac{1}{Y}\frac{\partial Y}{\partial t}. \tag{6.30}$$

6.4 Tissue mechanics

We next turn to the mechanical description of the tissue. The mechanical framework proceeds as in Equations (4.27) from Chapter 4, but with one change. We found that the friction term in the balance of linear momentum affected only the recoil phase of the healing curve, hence in this chapter we neglect friction and assume that the tissue

is in mechanical equilibrium. Neglecting all body forces and assuming that the tissue is incompressible, hyperelastic and can be described by a neo-Hookean strain-energy function, we deduce that the system mechanics can be described by the following equations:

$$\frac{\partial r}{\partial R_0} = \frac{\gamma_r \gamma_\theta R_0}{\lambda r}, \tag{6.31a}$$

$$\frac{\partial T_{rr}}{\partial r} = \frac{\alpha \hat{W}_\alpha}{r}, \tag{6.31b}$$

$$T_{\theta\theta} = T_{rr} + \alpha \hat{W}_\alpha, \tag{6.31c}$$

$$T_{zz} = T_{rr} + \lambda \hat{W}_\lambda, \tag{6.31d}$$

where

$$\hat{W}(\alpha, \lambda) = \frac{\mu}{2}\left(\frac{1}{\alpha^2\lambda^2} + \alpha^2 + \lambda^2 - 3\right) \quad \text{and} \quad \alpha = \frac{r}{\gamma_\theta R_0}. \tag{6.32}$$

In Equation (6.32), $\hat{W}_\alpha$ and $\hat{W}_\lambda$ are the partial derivatives of the auxiliary strain-energy function with respect to the strain α and axial stretch λ, respectively.

Remark (Lagrangian conversion factor)**.** In Equations (6.10) and (6.14) the term $\mathcal{C} = \det(\mathcal{F})\mathcal{F}^{-1}\mathcal{F}^{-T}$ appears as a result of a transformation to the Lagrangian coordinate system. Since $\mathcal{F} = \mathrm{diag}(\frac{\partial r}{\partial R_0}, \frac{r}{R_0}, \lambda)$ is symmetric, and the tissue is incompressible, it follows that $\mathcal{F}^{-T} = \mathcal{F}^{-1}$ and $\det(\mathcal{F}) = \det(\mathcal{G})$. Considering Equation (6.31a), $\mathcal{C}$ can be written as follows:

$$\mathcal{C} = \gamma_r \gamma_\theta \,\mathrm{diag}\left(\left(\frac{\lambda r}{\gamma_r \gamma_\theta R_0}\right)^2, \frac{R_0^2}{r^2}, \frac{1}{\lambda^2}\right).$$

Since β and ϕ are functions of R_0 and t, only the radial component of $\mathcal{C}$ is required, which can be simplified to

$$\mathcal{C}_1 = \frac{1}{\det(\mathcal{G})}\left(\frac{\lambda r}{R_0}\right)^2.$$

6.4.1 Contraction

In Chapters 4 and 5, contraction was defined by imposing the radial stress at the wound edge, i.e.

$$T_{rr}(A_0, t) = f_c.$$

In the absence of explicit fibroblast and growth factor behaviours we have previously defined the contraction function to be

$$f_c = fa(t)\mathcal{H}(t; t_c, t_m), \tag{6.33}$$

where f is the contraction coefficient, a is the current wound radius and $\mathcal{H}(t; t_c, t_m)$ is a linear switch function, characterised by a delay, t_c, representing the time at which the switch turns on, and t_m, the time at which the fibroblasts exert their maximum contractile effect. Typically, t_c is approximately 2-5 days post wounding and t_m is approximately 2 weeks after contraction begins.

With the additional biochemical components we now consider a more mechanistic approach, by taking the magnitude of contraction to be proportional to the density of fibroblasts on the wound edge. Since $\phi(A_0, t)/\lambda$ is the density of fibroblasts at the wound edge and the wound circumference is proportional to $a(t)$, we now write

$$f_c = fa(t)\frac{\phi(A_0, t)}{\lambda}, \tag{6.34}$$

where f is the contraction coefficient with dimensions N cell^{-1}.

6.4.2 Boundary conditions

As before, far from the wound the tissue remains residually stressed. At the wound edge the radial stress is assigned according to the contraction function in Equation (6.34). In Chapter 4 we simulated mechanical experiments in which the axial

load was varied. Although our results showed that varying the axial load, N_z, had a significant effect on the total volumetric growth in the tissue, here we are interested in perturbing the biochemical environment and will therefore take $N_z = 0$ so that the dermis is assumed to be unloaded in the axial direction. The boundary conditions that close Equations (6.31) can be written as follows

$$T_{rr}(A_0, t) = fa(t)\frac{\phi(A_0, t)}{\lambda}, \tag{6.35a}$$

$$T_{rr}(B_0, t) = T_{\text{res}}, \tag{6.35b}$$

$$\frac{2\pi}{\lambda(t)}\int_{A_0}^{B_0} \gamma_r\gamma_\theta T_{zz} R_0 \, \mathrm{d}R_0 = 0. \tag{6.35c}$$

6.5 The full model

The full morpho-mechano-chemical model is determined by considering the growth factor and fibroblast species in Equations (6.10) and (6.14), the growth evolution of the dermal tissue in Equations (6.27) and the deformation and stress in Equations (6.31). Here we state all the equations, in terms of the reference variable R_0

and time t:

$$\frac{\partial \beta}{\partial t} + \frac{\beta}{Y}\frac{\partial Y}{\partial t} = \frac{1}{Y}\nabla \cdot \left[\frac{1}{Y}\left(\frac{\lambda r}{R_0}\right)^2 D_\beta \nabla \beta\right] - d\beta, \tag{6.36a}$$

$$\frac{\partial \phi}{\partial t} + \frac{\phi}{Y}\frac{\partial Y}{\partial t} = \frac{1}{Y}\nabla \cdot \left[\frac{1}{Y}\left(\frac{\lambda r}{R_0}\right)^2 (D_\phi \nabla \phi - \chi \phi \nabla \beta)\right] + k\left[\frac{\left(\frac{\beta}{\beta^*}\right)^{s_\beta}}{\left(\frac{\beta}{\beta^*}\right)^{s_\beta} + 1}\right]\phi\left(1 - \frac{\phi}{\phi_{\max}}\right), \tag{6.36b}$$

$$\frac{\partial r}{\partial R_0} = \gamma_r \gamma_\theta \frac{R_0}{\lambda r}, \tag{6.36c}$$

$$\frac{\partial T_{rr}}{\partial R_0} = \frac{\gamma_r \gamma_\theta R_0}{\lambda r^2}\alpha \hat{W}_\alpha, \tag{6.36d}$$

$$T_{\theta\theta} = T_{rr} + \alpha \hat{W}_\alpha, \tag{6.36e}$$

$$T_{zz} = T_{rr} + \lambda \hat{W}_\lambda, \tag{6.36f}$$

$$\frac{\partial Y}{\partial t} = \frac{V_c}{\lambda}(\phi - \phi_0), \tag{6.36g}$$

$$\frac{\partial \gamma_r}{\partial t} = \frac{1}{Y}\frac{\partial Y}{\partial t}\upsilon_r \gamma_r, \tag{6.36h}$$

$$\frac{\partial \gamma_\theta}{\partial t} = \frac{1}{Y}\frac{\partial Y}{\partial t}\upsilon_\theta \gamma_\theta, \tag{6.36i}$$

where

$$\hat{W}(\alpha, \lambda) = \frac{\mu}{2}\left(\frac{1}{\lambda^2 \alpha^2} + \alpha^2 + \lambda^2 - 3\right), \quad \alpha = \frac{r}{\gamma_\theta R_0}, \tag{6.37a}$$

$$\upsilon_r = \frac{1}{2}\left[1 + 3\mathrm{sgn}(\phi - \phi_0)\tanh(s_T(T_{rr} - T_{\theta\theta}))\right] \quad \text{and} \quad \upsilon_\theta = 1 - \upsilon_r. \tag{6.37b}$$

Equations (6.36) are closed by imposing the boundary and initial conditions given by Equations (6.11), (6.15), (6.29) and (6.35),

$$\beta(A_0,t) = \beta_0\ a^2(t) \quad \text{and} \quad \beta(B_0,t) = 0, \tag{6.38a}$$

$$D_\phi \nabla\phi - \chi\phi\nabla\beta = 0 \quad \text{at } R_0 = A_0 \text{ and } R_0 = B_0, \tag{6.38b}$$

$$T_{rr}(A_0,t) = fa(t)\frac{\phi(A_0,t)}{\lambda} \quad \text{and} \quad T_{rr}(B_0,t) = T_{\text{res}}, \tag{6.38c}$$

$$\frac{2\pi}{\lambda(t)}\int_{A_0}^{B_0} \gamma_r\gamma_\theta T_{zz} R_0\ \mathrm{d}R_0 = 0, \tag{6.38d}$$

$$\beta(R_0,0) = 0, \quad \phi(R_0,0) = \phi_0, \quad \gamma_r(R_0,0) = \gamma_\theta(R_0,0) = Y(R_0,0) = 1. \tag{6.38e}$$

6.5.1 Dimensional analysis

In this section we non-dimensionalise Equations (6.36). We are interested in the system dynamics on the timescale of tissue growth and, hence, by considering the growth rate of the dermal tissue in Equation (6.36g), we introduce the following scalings for the model variables

$$t' = V_c\phi_{\max}t, \quad R_0' = \frac{R_0}{[r]}, \quad r' = \frac{r}{[r]}, \quad \beta' = \frac{\beta}{\beta^*}, \quad \phi' = \frac{\phi}{\phi_{\max}} \quad \text{and} \quad \mathbf{T}' = \frac{\mathbf{T}}{\mu}, \tag{6.39}$$

where $[r]$ is a typical length scale. Details of the choice of scalings are discussed in Appendix D.2. Substituting the scaled variables from Equation (6.39) into Equations (6.36)-(6.38) and omitting the primes for notational simplicity, we arrive at the

following dimensionless system

$$\frac{\partial \beta}{\partial t} + \frac{\beta}{Y}\frac{\partial Y}{\partial t} = \frac{1}{Y}\nabla \cdot \left[\frac{\bar{D}_\beta}{Y}\left(\frac{\lambda r}{R_0}\right)^2 \nabla \beta\right] - \bar{d}\beta, \tag{6.40a}$$

$$\frac{\partial \phi}{\partial t} + \frac{\phi}{Y}\frac{\partial Y}{\partial t} = \frac{1}{Y}\nabla \cdot \left[\frac{1}{Y}\left(\frac{\lambda r}{R_0}\right)^2 \left(\bar{D}_\phi \nabla \phi - \bar{\chi}\phi \nabla \beta\right)\right] + \bar{k}\left[\frac{\beta^{s_\beta}}{\beta^{s_\beta}+1}\right]\phi(1-\phi), \tag{6.40b}$$

$$\frac{\partial r}{\partial R_0} = \gamma_r \gamma_\theta \frac{R_0}{\lambda r}, \tag{6.40c}$$

$$\frac{\partial T_{rr}}{\partial R_0} = \frac{\gamma_r \gamma_\theta R_0}{\lambda r^2}\alpha \bar{W}_\alpha, \tag{6.40d}$$

$$T_{\theta\theta} = T_{rr} + \alpha \bar{W}_\alpha, \tag{6.40e}$$

$$T_{zz} = T_{rr} + \lambda \bar{W}_\lambda, \tag{6.40f}$$

$$\frac{\partial Y}{\partial t} = \frac{\phi - \phi^*}{\lambda}, \tag{6.40g}$$

$$\frac{\partial \gamma_r}{\partial t} = \frac{1}{Y}\frac{\partial Y}{\partial t}\upsilon_r \gamma_r, \tag{6.40h}$$

$$\frac{\partial \gamma_\theta}{\partial t} = \frac{1}{Y}\frac{\partial Y}{\partial t}\upsilon_\theta \gamma_\theta, \tag{6.40i}$$

where

$$\bar{W}(\alpha, \lambda) = \frac{1}{2}\left(\frac{1}{\lambda^2 \alpha^2} + \alpha^2 + \lambda^2 - 3\right), \quad \alpha = \frac{r}{\gamma_\theta R_0}, \tag{6.41a}$$

$$\upsilon_r = \frac{1}{2}\left[1 + 3\mathrm{sgn}(\phi - \phi^*)\tanh(s_T(T_{rr} - T_{\theta\theta}))\right] \quad \text{and} \quad \upsilon_\theta = 1 - \upsilon_r. \tag{6.41b}$$

Equations (6.40) are subject to the following boundary and initial conditions

$$\beta(A_0,t) = \bar{\beta}_0\, a^2(t) \quad \text{and} \quad \beta(B_0,t) = 0, \tag{6.42a}$$

$$\bar{D}_\phi \nabla\phi - \bar{\chi}\phi\nabla\beta = 0 \quad \text{at } R_0 = A_0 \text{ and } R_0 = B_0, \tag{6.42b}$$

$$T_{rr}(A_0,t) = \bar{f}a(t)\frac{\phi(A_0,t)}{\lambda} \quad \text{and} \quad T_{rr}(B_0,t) = T^*, \tag{6.42c}$$

$$\frac{2\pi}{\lambda(t)}\int_{A_0}^{B_0} \gamma_r\gamma_\theta T_{zz} R_0 \, \mathrm{d}R_0 = 0, \tag{6.42d}$$

$$\beta(R_0,0) = 0, \quad \phi(R_0,0) = \phi^*, \quad \gamma_r(R_0,0) = \gamma_\theta(R_0,0) = Y(R_0,0) = 1. \tag{6.42e}$$

In Equations (6.40)-(6.42) we have introduced the following dimensionless parameter groupings

$$\bar{D}_\beta = \frac{D_\beta}{[r]^2 V_\mathrm{c}\phi_\mathrm{max}}, \quad \bar{d} = \frac{d}{V_\mathrm{c}\phi_\mathrm{max}}, \quad \bar{D}_\phi = \frac{D_\phi}{[r]^2 V_\mathrm{c}\phi_\mathrm{max}}, \quad \bar{\chi} = \frac{\chi\beta^*}{[r]^2 V_\mathrm{c}\phi_\mathrm{max}},$$
$$\bar{k} = \frac{k}{V_\mathrm{c}\phi_\mathrm{max}}, \quad \bar{\beta}_0 = \frac{[r]^2\beta_0}{\beta^*}, \quad \bar{f} = \frac{f\phi_\mathrm{max}[r]}{\mu}, \quad \phi^* = \frac{\phi_0}{\phi_\mathrm{max}}, \quad T^* = \frac{T_\mathrm{res}}{\mu}.$$

6.6 Numerical results

In this section we present results obtained by solving Equations (6.40)-(6.42) for parameter values associated with normal healing. We validate the model behaviour by comparing these solutions to our previous results. We then perform a parameter sensitivity analysis, focussing on parameters associated with processes thought to be compromised in diabetic healing and other healing pathologies. For example, decreased collagen synthesis and abnormal production of TGFβ.

6.6.1 Numerical computation

The dependent variables in Equations (6.40) are functions of the stress-free state, R_0. However, the known measurements are taken from the observed, residually stressed

state, R. The stress-free state, R_0, and the residual stress, T_{res}, are calculated as in Section 4.2.3 by solving Equations (4.11), (4.14) and (4.15). The inputs are the known measurements A, B, L and a_R, returning the stress-free state, $\{A_0, B_0, L_0\}$, and the residual stress, T_{res}.

The numerical method outlined below is implemented in MATLAB. All dependent variables are stored as functions of R_0, with spatial discretisation $\mathrm{d}x = 0.05$. Equations (6.40g), (6.40h) and (6.40i) are discretised in time subject to Equations (6.42e) using a forward Euler approximation. For each time increment ($\mathrm{d}t = 0.05$), the variable quantities in Equations (6.40) are updated in the following order:

1. The TGFβ and fibroblast species (β and ϕ) are updated by solving Equations (6.40a) and (6.40b) using the function `pdepe` with the boundary and initial conditions specified by Equations (6.42a), (6.42b) and (6.42e).

2. The total, radial and circumferential growth (Y, γ_r and γ_θ) are updated by solving the forward Euler approximations to Equations (6.40g), (6.40h) and (6.40i) subject to Equations (6.42e).

3. The deformation and radial stress (r and T_{rr}) are updated by solving Equations (6.40c) and (6.40d) together with the boundary conditions in Equations (6.42c) and (6.42d) using the function `bvp4c`.

4. The circumferential and axial stress ($T_{\theta\theta}$ and T_{zz}) are evaluated via Equations (6.40e) and (6.40f).

5. All dependent variables are stored as functions of R_0.

Full details of the numerical method are provided in Appendix D.3. The numerical method was validated by comparing simulations with pseudo-analytical solutions of a simplified version of the model obtained by neglecting the TGFβ dependence in the fibroblast equation ($\bar{\chi} = \beta^* = 0$ in Equation (6.40b)) and assuming isotropic growth

($s_T = 0$ in Equation (6.41b)). Simplifying the model in this way allows the deformation and radial stress in Equations (6.40c) and (6.40d) to be solved analytically while the fibroblasts in Equation (6.40b) are updated via a forward Euler method. Details of this comparison are presented in Appendix D.3.1.

6.6.2 Typical simulations and model behaviour

In this section we present results of a typical simulation of Equations (6.40)-(6.42) (see Figure 6.2). Parameter values are chosen to be representative of normal healing and, where possible, taken from the literature. A list of dimensionless model parameters is given in Table 6.1. Justification for these parameter values and their dimensional counterparts is provided in Appendix D.1.

Table 6.1: List of normalised parameters for the morpho-mechano-chemical model. The table lists the parameters of the non-dimensionalised model in Equations (6.40) and their physical interpretation. We state the approximate range for each parameter, calculated from the experimental literature (see Appendix D.1) and the default value used in model simulations.

parameter	physical interpretation	range	default value
$\bar{\beta}_0$	TGFβ supply	$\mathcal{O}(1)$	1
$\bar{D}_\beta$	TGFβ diffusion	$\mathcal{O}(10)$	50
$\bar{d}$	TGFβ decay	$\mathcal{O}(10^3)$	1000
$\bar{D}_\phi$	fibroblast diffusion	$\mathcal{O}(1)$	2
$\bar{\chi}$	fibroblast chemotaxis	unknown	0.1
$\bar{k}$	fibroblast proliferation	$\mathcal{O}(1)$	3
s_β	sensitivity to TGFβ	unknown	5
ϕ^*	normal to max fibroblast ratio	$\mathcal{O}(10^{-2})$	0.01
$\bar{f}$	contraction coefficient	$f < 8$	0.5
s_T	growth directional sensitivity	unknown	1
A	initial wound radius		4
B	initial external radius		20
L	initial dermal thickness		0.1
a_R	recoiled wound radius		4.4

The time dynamics of the wound radius, $a(t)$, are plotted in Figure 6.2(a). We observe an immediate recoil of the wound, followed by a reduction in wound radius

and, at later times, the radius plateaus. This behaviour is similar to our simulations from Chapter 4 (see Figure 4.11). However, we do not observe a delay in the onset of healing in the current model. This is because TGFβ is released from $t = 0$, stimulating fibroblast activity and, hence, growth and contraction. In the previous model, only mechanosensitive growth was considered, with contraction switching on at day 2.

The radial stress at the wound edge, $T_{rr}(A_0, t)$, is plotted in Figure 6.2(b) for two choices of contraction function: the one introduced in this chapter (see Equation (6.42c)), depending on the fibroblast density at the wound edge (solid blue); and the phenomenological contraction function used in Chapter 4 (see Equation (6.33)), where the behaviour of the fibroblasts is approximated by the piecewise linear switch function, $\mathcal{H}(t; t_c, t_m)$ (dashed green). The latter is plotted for comparison only, while all other results in Figure 6.2 correspond to the former. Explicitly including the growth factor and fibroblasts in the extended model enables us to reproduce the qualitative behaviour associated with the phenomenological contraction switch. These results suggest that the extended model, with the new, physically-based contraction function (Equation (6.34)), can reproduce the expected healing behaviour. Furthermore, the agreement in Figure 6.2(b) validates the choice of switch functions used in the previous chapters.

Plots showing how the spatial distributions of the growth factor, β, and fibroblast species, ϕ, evolve over time are presented in Figures 6.2(c) and (d), respectively. TGFβ diffuses from the wound space and decreases monotonically with distance from the wound edge. Due to a high rate of decay, TGFβ is only present in a band of approximately 1 mm from the wound (in the current configuration). As a result, TGFβ stimulated fibroblast proliferation is concentrated close to the wound edge, resulting in high cell numbers there. At a distance of more than 10 mm from the wound, the fibroblast density falls to values more representative of the initial, unwounded value.

Plots showing how the spatial distributions of the radial and circumferential com-

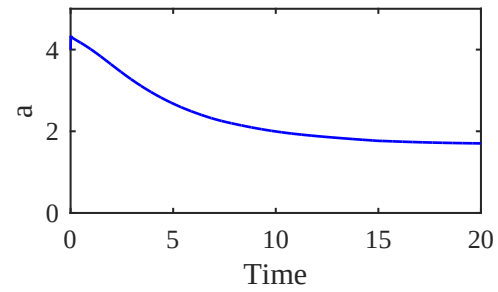

(a) Wound radius

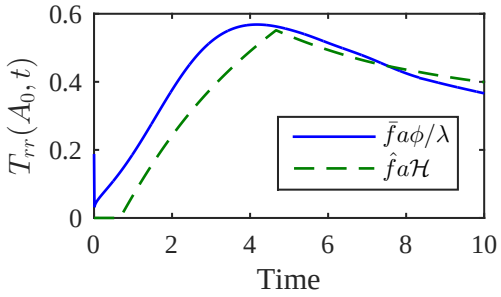

(b) Comparison of contraction functions

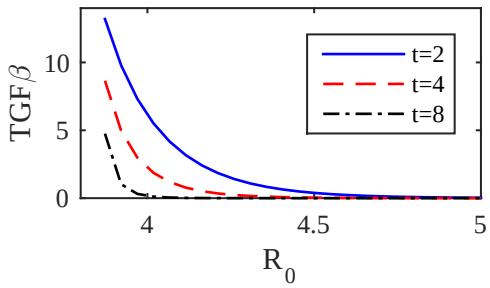

(c) TGFβ

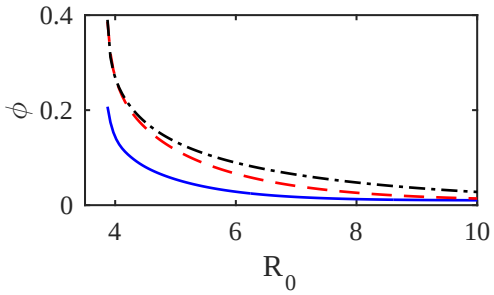

(d) Fibroblasts

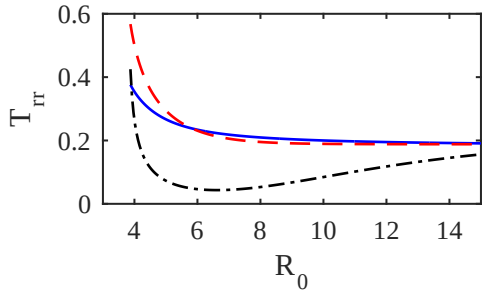

(e) Radial stress

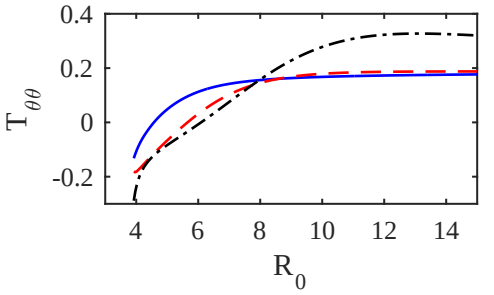

(f) Circumferential stress

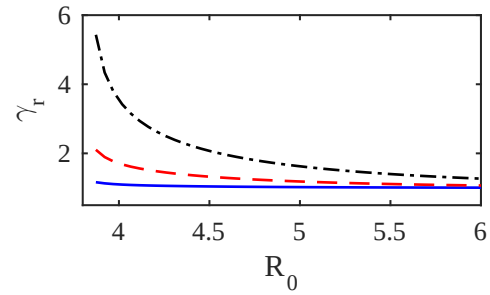

(g) Radial growth

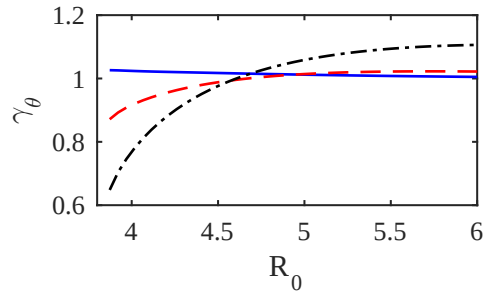

(h) Circumferential growth

Figure 6.2: Numerical results for normal healing behaviour. Continued on the following page.

Figure 6.2: Numerical results for normal healing behaviour. Equations (6.40)-(6.42) are solved numerically. (a) The wound radius, $a(t)$, is plotted as a function of time. (b) The radial stress at the wound edge, $T_{rr}(A_0, t)$, determined by the boundary condition in Equation (6.42c) is compared with the radial stress with the phenomenological contraction function in Equation (6.33) is used. (c) TGFβ, $\beta(R_0, t)$, (d) the fibroblasts, $\phi(R_0, t)$, (e) radial stress, $T_{rr}(R_0, t)$, (f) circumferential stress, $T_{\theta\theta}(R_0, t)$, (g) radial growth, $\gamma_r(R_0, t)$, and (h) circumferential growth, $\gamma_\theta(R_0, t)$, are plotted as functions of position, R_0, at $t = 2$, 4 and 8. Parameter values: see Table 6.1. Parameters for the phenomenological contraction switch: $\hat{f} = 0.2$, $t_c = \frac{2}{3}$ and $t_m = \frac{14}{3}$, consistent with values used in Chapter 4. A dimensionless unit of time corresponds to approximately 3 days.

ponents of the stress and growth tensors evolve over time are presented in Figures 6.2(e)-(h). We note that the radial and circumferential stresses have the same qualitative behaviour as those presented in Chapter 4 (see Figures 4.12(a) and (b)). Consequently, the distribution of growth close to the wound edge is such that material is added in the radial direction and removed from the circumferential direction, behaviour which is consistent with the growth analysis in Section 4.2.7 and numerical simulations in Chapter 4 (see Figures 4.12(d) and (e)). These results suggest that assuming growth is distributed in the direction of greatest tension (see Equations (6.40g)-(6.40h) and (6.41b)) yields behaviour that is consistent with normal healing.

Having established the basic model behaviour, in the next section we consider perturbations from 'normal' healing by varying parameters that are thought to be affected in wound healing pathologies.

6.6.3 Pathological healing

In this section we perform a parameter sensitivity analysis focussing on parameters which may be altered in pathology. Typically, when diagnosing a pathological wound, the measurement most easily accessible to clinicians is the size of the wound. In this section we determine how the wound radius changes in response to different simulated

pathologies. We consider abnormal values of TGFβ supply and decay rate, fibroblast proliferation and collagen synthesis rates and the force exerted by fibroblasts.

Equations (6.40)-(6.42) are solved numerically and each parameter is varied individually by $\pm 50\%$ of its default value while all other parameters are held fixed at the values specified in Table 6.1. The wound radius, $a(t)$, is recorded at $t = 20$, which is equivalent to approximately 60 days post wounding. In Figure 6.3 we show how $a(t = 20)$ changes as specific model parameters are varied. We observe that the wound radius is smaller for increased TGFβ supply, $\bar{\beta}_0$, fibroblast proliferation rate, $\bar{k}$, and contraction coefficient, $\bar{f}$ and increasing the TGFβ decay rate, $\bar{d}$, results in larger wound radius than in the control case. These results are as we might expect. However, the sensitivity of $a(t = 20)$ to the rate of material synthesis, V_c, is very small, suggesting that tissue growth has little influence on the wound radius.

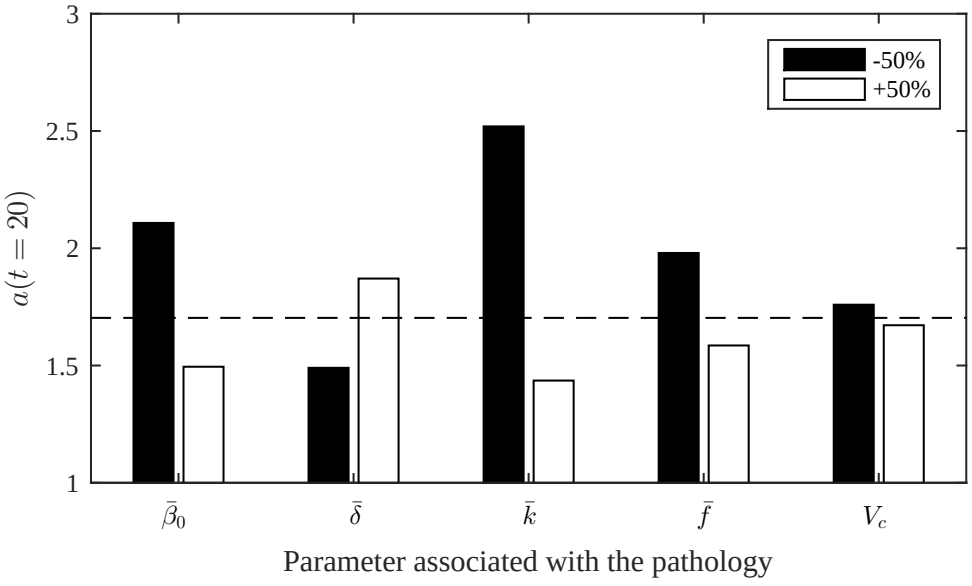

Figure 6.3: Effect of pathologies on the wound radius. Equations (6.40)-(6.42) are solved numerically. Each model parameter is varied by $\pm 50\%$ of its default value and the wound radius, a, is recorded at $t = 20$. The dashed lines indicate the wound radius/dermal thickness when all parameters are fixed at their default values. All reference variables and parameters are specified using the default values in Table 6.1. Increasing the TGFβ supply, $\bar{\beta}_0$, fibroblast proliferation rate, $\bar{k}$, contraction coefficient, $\bar{f}$, and material synthesis rate, V_c, decrease the wound radius. Increasing the TGFβ decay rate, $\bar{d}$, increases the wound radius.

6.6.4 Treatment intervention

In Chapters 2 and 5 our modelling, together with wound healing data, suggested that the rate of closure of diabetic wounds could be normalised by increasing the basal growth rate. This theoretical treatment was carried out on spatially-averaged models of wound healing by increasing the dermal growth parameter. In the current model, TGFβ stimulates migration and proliferation of fibroblasts which, in turn, influence dermal growth and contraction. Reduced dermal growth could arise from a variety of pathologies, which can be discriminated in the extended biochemical model.

In this section we investigate whether treatment with a single application of TGFβ into the wound space can correct for any of the pathologies discussed in the previous section. When administering the theoretical treatment, we consider the dosage and the duration of treatment. For simplicity, we fix the time of application, assuming that if treatment were administered it would be given as soon as possible after diagnosis.

To apply TGFβ into the wound space we assign an elevated value of TGFβ at the wound edge

$$\beta(A_0,t) = \begin{cases} \bar{\beta}_0\ a^2(t) & \text{for } 0 \leq t < t_1 \\ \bar{\beta}_0\ a^2(t) + \beta_{\text{dose}} & \text{for } t_1 \leq t \leq t_2\ , \\ \bar{\beta}_0\ a^2(t) & \text{for } t > t_2 \end{cases} \tag{6.43}$$

where β_{dose} is the amount of TGFβ applied, t_1 is the time of treatment and $t_2 - t_1$ is the treatment duration. We take $t_1 = 5$ (corresponding to approximately day 15 post wounding). The TGFβ concentration satisfies Equation (6.40a) with the boundary condition on the wound edge replaced by Equation (6.43).

We will first consider a wound with low TGFβ production and determine a suitable treatment duration and dose for normalising healing in this case. We then test this treatment on the remaining healing pathologies discussed in the previous section.

6.6.4.1 Decreased production of TGFβ

Low TGFβ production is simulated by taking $\bar{\beta}_0 = 0.5$. We observe in Figure 6.3 that this causes a larger wound radius than the control case. To simulate treatment, Equations (6.40)-(6.42) are solved numerically with the boundary condition for β at the wound edge replaced by Equation (6.43).

In Figure 6.4 we plot the time evolution of the wound radius for a control wound, an untreated pathological wound, and a pathological wound for which the treatment has been applied continuously from $t_1 = 5$ until $t_2 = 15$ at a dose of $\beta_{\text{dose}} = 5$. We observe a sharp decrease in the wound radius at the time of application. The wound radius then decreases at a faster rate than the normal wound. When the treatment is removed, the wound radius increases slightly and plateaus at a value similar to the normal wound.

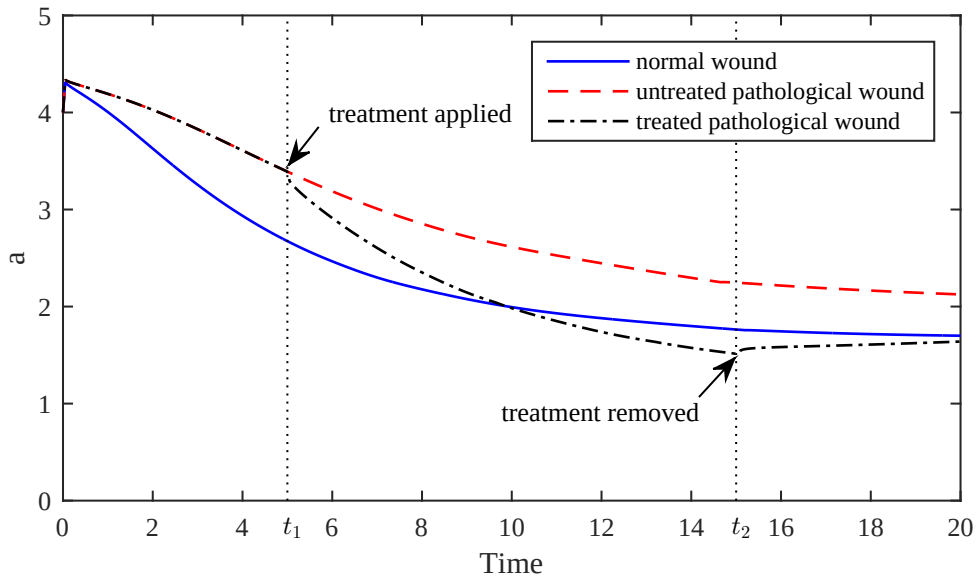

Figure 6.4: The effect of treatment on the time evolution of the wound radius. Equations (6.40)-(6.42) are solved numerically with the boundary condition for β at the wound edge replaced by Equation (6.43). Treatment is applied continuously from $t_1 = 5$ to $t_2 = 15$ at a dose of $\beta_{\text{dose}} = 5$. The evolution of the wound radius, $a(t)$, is plotted for a normal wound corresponding to the parameters in Table 6.1 (solid blue), an untreated pathological wound for which $\bar{\beta}_0 = 0.5$ (dashed red) and a pathological wound with treatment (dash-dotted black).

As well as the rate of closure, we are interested in the quality of the healed tissue. In the previous chapters this has been characterised by the relative contributions of growth and contraction to healing. To determine a suitable treatment we need to consider the effects that different durations and doses have on the growth of the tissue and the stress caused by contraction. An imbalance of these two processes could result in mechanically inferior healed tissue.

In Figure 6.5 we present bar charts for (a) the wound radius at $t = 20$, (b) the total volume increase of tissue at $t = 20$ and (c) the maximum radial stress experienced by the tissue during healing. Results are given for different treatment durations and doses.

In Figure 6.5(b) we observe that the behaviour for the total tissue volume as a function of the dose is non-monotonic. From Equations (6.40b) and (6.40g), we would expect that more TGFβ results in higher fibroblast densities and, therefore, more collagen synthesis. However, when the concentration of TGFβ in the wound space is very high, the chemotaxis term in Equation (6.40b) is large. This causes the region of high fibroblast density surrounding the wound to decrease in size and, hence, volumetric growth is reduced. We further note that our assumption of linear chemotaxis implies that, for very large concentration gradients, the model is invalid.

We observe in Figure 6.5(c) that for a fixed dose, the maximum radial stress during healing is very similar for different treatment durations. This is because the maximum radial stress occurs very close to the time of application ($t_1 = 5$), therefore the duration has no significant effect on the maximum radial stress. The stress for a discrete application (treatment is only applied for one time step of the numerical method) is lower than for longer durations because the fibroblasts do not have enough time to respond to the elevated value of TGFβ.

With the exception of the maximum radial stress, a discrete application of TGFβ into the wound space, for example a single injection, has negligible effect on healing.

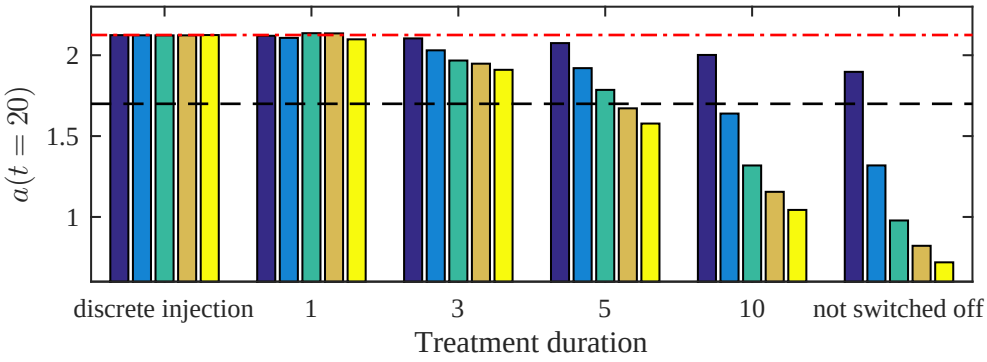

(a) Wound radius at $t = 20$

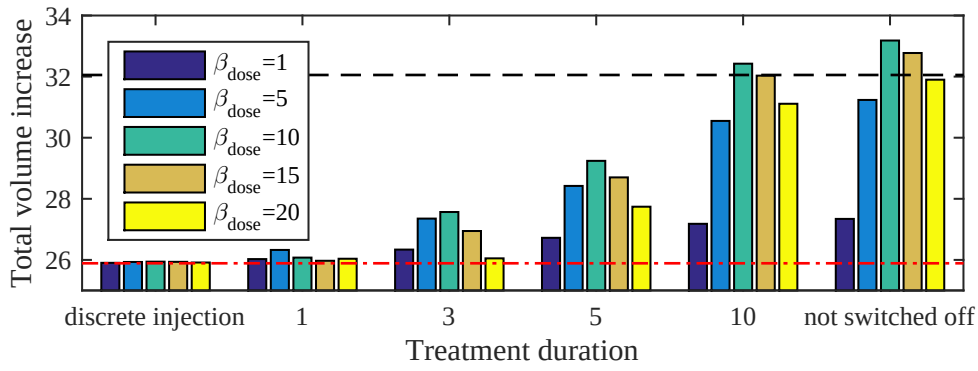

(b) Total volume increase at $t = 20$

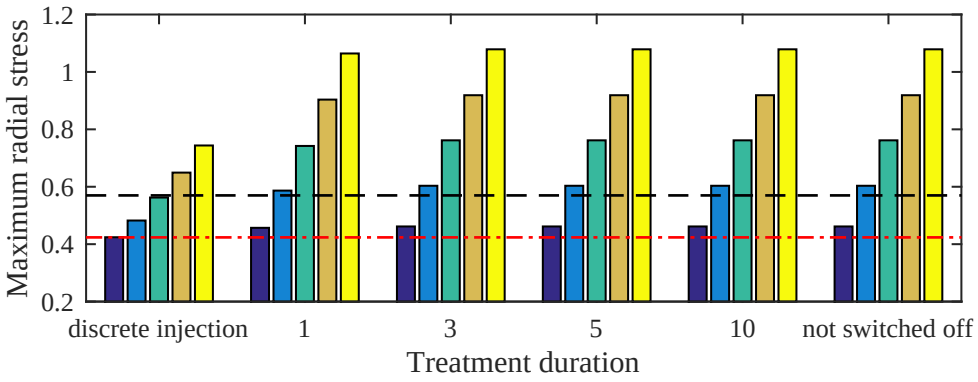

(c) Maximum radial stress during healing

Figure 6.5: The effects of different treatment protocols on healing outcomes. Equations (6.40)-(6.42) are solved numerically with the wound edge boundary condition for β replaced by Equation (6.43). The treatment duration and dose are varied and bar graphs for (a) the wound radius, a, at $t = 20$, (b) the total volume increase at $t = 20$ and (c) the maximum radial stress over the duration of healing are presented. Values for a normal wound corresponding to the parameters in Table 6.1 (dashed black) and an untreated pathological wound for which $\bar{\beta}_0 = 0.5$ (dash-dotted red) are plotted. All treated wounds are such that $\bar{\beta}_0 = 0.5$. Treatment is applied continuously from $t_1 = 5$ until t_2, where the duration is given by $t_2 - t_1$.

Similarly, a duration of $t_2 - t_1 = 1$ (1 dimensionless time unit, corresponding to approximately 3 days) has no significant effect on the wound radius or total tissue growth. Some treatments that perform well for the wound radius perform less well for normalising the total tissue growth and *vice versa*.

In order to characterise the effects of the treatment on all three model observables, we define the following measure which captures the error between a normal wound and a treated pathological wound

$$\text{measure} = \left| \frac{a_{\text{normal}} - a_{\text{treated}}}{a_{\text{normal}}} \right| + \left| \frac{G^V_{\text{normal}} - G^V_{\text{treated}}}{G^V_{\text{normal}}} \right| + \left| \frac{T^{\max}_{\text{normal}} - T^{\max}_{\text{treated}}}{T^{\max}_{\text{normal}}} \right|, \quad (6.44)$$

where a_{normal} and a_{treated} are the wound radii of the normal and treated wounds at $t = 20$, respectively, G^V_{normal} and G^V_{treated} denote the total volume increases at $t = 20$ and $T^{\max}_{\text{normal}}$ and $T^{\max}_{\text{treated}}$ the maximum radial stress over the duration of healing.

Equation (6.44) is evaluated for each of the treatments presented in Figure 6.5. We choose the protocol which minimises Equation (6.44), yielding a time duration of 10 (corresponding to approximately 30 days) and a dose of $\beta_{\text{dose}} = 5$ (corresponding to approximately 250 pg mm^{-3}). In the next section we test how this treatment protocol performs when applied to the other pathologies presented in Figure 6.3.

6.6.4.2 One treatment multiple pathologies

Identifying a single treatment that is effective for multiple pathologies would be extremely valuable from an economic and healthcare point of view. In this section we test how the most suitable treatment combination, determined in the previous section, affects other healing abnormalities. TGFβ is applied to different pathological wounds from $t_1 = 5$ to $t_2 = 15$, with a dose of $\beta_{\text{dose}} = 5$. Figure 6.6 shows how this treatment affects (a) the wound radius at $t = 20$, (b) total volume increase of the dermal tissue at $t = 20$ and (c) the maximum radial stress at the wound edge for each

pathology.

We observe that the treatment improves all three measures for only impaired TGFβ supply, $\bar{\beta}_0$, and impaired fibroblast proliferation rate, $\bar{k}$. For decreased contraction, $\bar{f}$, treatment normalises the wound area and increases the stress lifting it closer to the value in the normal wound, however, the total tissue volume is increased, resulting in a value that is even further from normal. Treatment applied to a wound with reduced collagen synthesis, V_c, has negligible effect on the maximum radial stress and only a slight increase in tissue volume. These results suggest that no single treatment is likely to correct all of the pathologies simulated in this chapter.

6.7 Conclusions

In this chapter we have extended the morphoelastic model developed in Chapter 4 to include a more physically-based description of tissue growth and contraction. We included separate equations for TGFβ, a potent growth factor, and fibroblasts, the main cell type in the dermis. The resulting PDEs were constructed in the Lagrangian configuration so that all dependent variables could be described as functions of the reference variable R_0, and time t. Since the tissue experiences growth, this led to the appearance of an advection term in the reference frame. We related this advection term to the growth tensor by considering conservation of tissue mass (see Equation (6.9)). Growth in the dermis was assumed to be directly proportional to the fibroblast density and distributed in the direction of highest tension. We adapted the distribution laws of Araujo and McElwain [2004] to allow for 'remodelling' of material in the case where the difference between the radial and circumferential stresses was very large. Wound contraction was modelled by imposing a radial tension at the wound edge proportional to the density of fibroblasts there; this boundary condition replaced the phenomenological switch used in previous chapters.

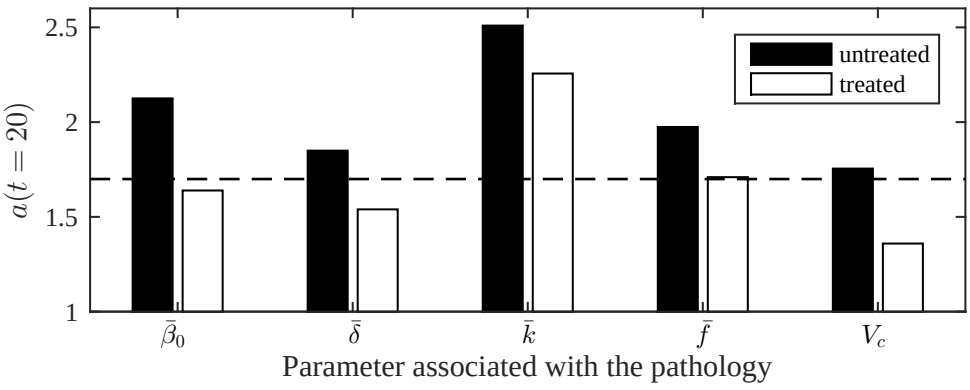

(a) Wound radius at $t = 20$

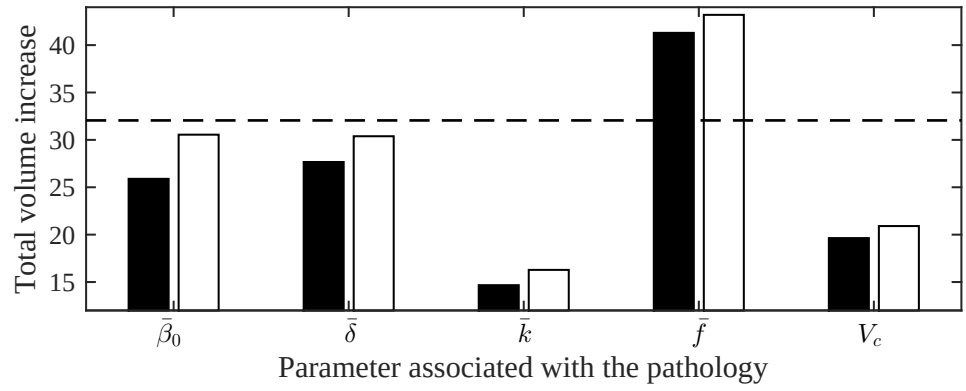

(b) Total volume increase at $t = 20$

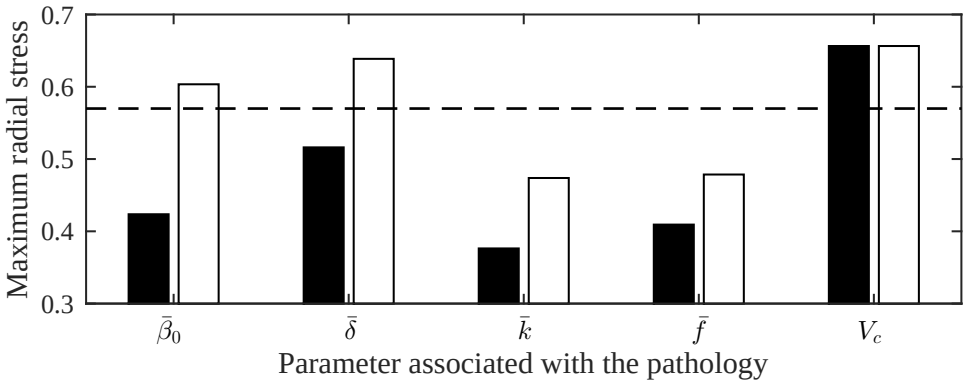

(c) Maximum radial stress during healing

Figure 6.6: The effect treatment on different pathologies. Equations (6.40)-(6.42) are solved numerically with the boundary condition for β at the wound edge replaced by Equation (6.43) with $t_1 = 5$, $t_2 = 15$ and $\beta_{\text{dose}} = 5$. (a) The wound radius, a, at $t = 20$, (b) the total volume increase at $t = 20$ and (c) the maximum radial stress over the duration of healing are presented for each untreated and treated pathology. Values for a normal wound corresponding to the parameters in Table 6.1 are plotted (dashed black). The pathologies correspond to individually varying each parameter. When varied the parameter of interest takes the following value: $\bar{\beta}_0 = 0.5$, $\bar{d} = 1500$, $\bar{k} = 1.5$, $\bar{f} = 0.25$ and collagen production, V_c, is halved.

Typical model simulations showed that the spatial distributions of the components of the stress and growth tensors were qualitatively similar to the results from Chapter 4, suggesting that distributing material in the direction of highest tension during wound healing is a feasible mechanism for growth. However, the wound healing curve is no longer subject to a delay immediately after the recoil, a feature of our previous results. We concluded that this was because, in the new model, TGFβ is released from $t = 0$, stimulating growth and contraction from the outset. By explicitly accounting for TGFβ and fibroblasts, and assuming dependence of wound contraction on the fibroblast density, the model was able to reproduce the qualitative behaviour of the phenomenological contraction switch, suggesting that our formulation of the growth factor, fibroblasts and wound edge boundary condition are reasonable.

We simulated wound healing pathologies and showed how the wound radius at $t = 20$ (corresponding to approximately 60 days post wounding) changed as we varied specific model parameters. In Chapters 2 and 5 the rate of closure and growth in diabetic wounds was normalised by increasing the basal growth rate. We hypothesised that by adding TGFβ to the wound the simulated pathologies could be corrected. We showed that this was the case for low TGFβ supply if treatment lasted for approximately 30 days with a dose of 250 pg mm^{-3}. When this treatment was applied to other simulated pathologies, it improved healing for impaired fibroblast proliferation. However, our results suggest that different protocols are needed to normalise other healing abnormalities. Indeed it is possible that application of TGFβ into the wound space of any duration or dose can not correct for certain pathologies.

Our model represents a first attempt to incorporate biochemical realism into our morphoelastic framework. As such, several interactions were neglected that could be included in future models. In the next chapter we will discuss the limitations of the current model and provide possible future directions and extensions.

Chapter 7

Discussion and future work

7.1 Introduction

Normal wound healing requires the careful synchronisation of a range of biochemical and biomechanical processes. For some patients underlying pathologies or other factors can result in the wound failing to heal in an orderly and timely manner. For example, diabetes can have a significant effect on wound healing [Brem and Tomic-Canic, 2007]. It is one of the main causes of lower limb amputations world-wide [Unwin, 2000]. The reduced quality of life for wound patients and the alarming impact that wound care has on the economy highlight the need for improved treatments and methods of application. Only by understanding the mechanisms that underpin wound healing and the impact of disrupting those mechanisms will we make significant advances in wound care development. Mathematical modelling offers a powerful tool for accelerating progress in many biological applications.

In this thesis we developed a series of mathematical models that were used to investigate the mechanisms driving the healing of a full thickness circular wound. The current theoretical literature focusses mainly on remodelling of the central granulation tissue and scar formation. However, during healing, wound contraction influences the

surrounding dermal tissue which is subject to mechanical forces and growth. The primary aims of this thesis were to:

1. Develop simple models of wound healing easily comparable with data.
2. Determine major differences between normal and diabetic healing.
3. Determine the influence of the biomechanical and biochemical environment on dermal wound healing.

In this chapter we draw together the important results generated in the thesis, comparing the results of our mathematical models with the current biological and mathematical literature. We highlight the limitations of our work and provide possible directions for its continuation.

7.2 Conclusions

We began, in Chapter 2, by developing a simple ordinary differential equation model of wound healing. The choice of framework was motivated by data provided by our experimental collaborators. The data comprised time courses of averaged wound areas for the epidermis and dermis in both non-diabetic and diabetic mouse wounds. Given that the initial wounds created were circular, remained approximately circular during healing and the measurements were spatially-averaged, it was appropriate to restrict our modelling to a radially symmetric geometry. This simplistic model was developed with a view to addressing the first two of the primary aims stated above.

Asymptotic analysis of the model revealed which processes are dominant during each healing phase and how each phase progressed over time. By perturbing certain model parameters, this analysis could be used to guide the development of more effective treatments for normalising aberrant wound healing.

Numerical results, obtained by fitting the model to the data, suggested that both the dermal growth rate and contractile force were lower in the diabetic wounds. The model was used to determine the relative contributions of growth and contraction to dermal healing, revealing that the percentage of the wound healed by contraction is greater in diabetic than non-diabetic wounds. This is because the reduction in dermal growth rate is more pronounced than the reduction in contraction, resulting in significantly lower growth in the diabetic than the non-diabetic dermis. Based on this conclusion we staged a treatment intervention by increasing dermal growth in the diabetic wounds. The corresponding numerical simulations showed that the healing time and proportions healed by growth and contraction in the diabetic wound could be normalised by this theoretical treatment. Our model predictions highlight the need for additional, more detailed experiments that can distinguish between contraction and dermal growth during wound healing.

The simple ODE model further suggested that mechanosensitive growth in the dermis is negligible. However, it has been shown that cells are stimulated to proliferate and synthesise material at higher rates under mechanical stress [Kessler et al., 2001]. We therefore turned to a more mechanically sophisticated framework in order to describe this phenomenon, the relevant theoretical background being outlined in Chapter 3.

In Chapter 4 we developed a mechanical model of dermal wound healing using morphoelasticity. Results from Chapter 2 suggested that there were no significant differences in epidermal healing between non-diabetic and diabetic wounds and, therefore, the epidermis was omitted from this model. By using a continuum mechanics framework we were able to establish the degree of residual tension in the pre-wounded tissue. The model was used to quantify the amount of stress experienced by the tissue when closure is driven by contraction only. Unrealistically high radial stresses were generated in this scenario, motivating the need for volumetric growth. We explored

possible growth laws and showed that for a circular wound to shrink, material must be added in the radial direction and removed from the circumferential direction, i.e. growth must be anisotropic. We restricted attention to mechanically induced, but inhomogeneous growth, with simulations yielding results qualitatively similar to the healing curves obtained in mice. These results suggest that mechanosensitive growth could play an important role in wound healing, contrary to our conclusions from Chapter 2.

The morphoelastic framework generated predictions beyond the scope of the previous model. Knowledge of the stresses experienced by the dermal tissue allowed for investigations on mechanical interventions, such as pressure treatments. We found that treatment via pressure bandages or vacuum assisted closure had no significant impact on the rate of wound closure but did influence the volume of tissue synthesised. We designed rewounding experiments that could be used to determine the balance of contraction and growth in healing, a feature that the model from Chapter 2 recognised as important for correcting diabetic healing.

Given that the two models disagree in terms of the significance of mechanically induced growth we chose to test the robustness of our other conclusions from Chapter 2 using the morphoelastic model. In order to make a reliable and fair comparison between the two modelling frameworks we first simplified the morphoelastic model. By restricting attention to homogeneous growth in an annulus close to the wound edge and formulating a growth law comprising basal and mechanosensitive parts, we identified a one-to-one map for parameters associated with the two models. By fitting the spatially-averaged morphoelastic model to the wound healing data, our conclusions regarding non-diabetic and diabetic healing were found to be consistent with the time-dependent ODE model.

Returning to the spatially-resolved morphoelastic model, there are certain features that are missing. In order to focus on the mechanical environment in the tissue,

we restricted attention to mechanically stimulated growth. With the growth laws formulated in this manner, growth will not occur unless contraction is active. Of course, growth is also stimulated by the biochemical environment. Wound healing is orchestrated by fibroblasts; their behaviour determined by the combined effects of biomechanical and biochemical stimuli. Thus, in Chapter 6 we extended the morphoelastic framework to explicity include fibroblasts and a potent growth factor, TGFβ. We restricted attention to TGFβ induced cell proliferation, with growth of the tissue directly proportional to the fibroblast density. The newly synthesised material was distributed according to the local stress, with more material deposited in the direction of greatest tension. When constructing the PDEs for the growth factor and fibroblast species in the Lagrangian configuration we obtained a growth advection term, relating it to the growth tensor by considering conservation of tissue mass. While the model extensions proposed introduced more parameters, many of these were related to measurable quantities found in the experimental literature.

Typical simulations revealed similar qualitative behaviour to the mechanical model. However, accounting for the biochemistry allowed for a more biophysical description of growth and contraction and the opportunity to investigate realistic healing pathologies. As in Chapters 2 and 5 we considered the effects of treatment on the wound radius, tissue growth and stress in the tissue. Identifying a specific treatment for various pathologies could have a substantial impact on the cost of wound care and, hence, we aimed to find one treatment to correct multiple pathologies. We showed that the application of TGFβ could improve healing in a wound with lower than normal TGFβ supply and fibroblast proliferation rate. However, we found that this treatment was not sufficient for the other pathologies simulated.

7.3 Future work

7.3.1 Comparison with the classical mechano-chemical models

Our morpho-mechano-chemical model in Chapter 6 includes the biochemical and the biomechanical environment. The are two main differences between our model and previous mechano-chemical models of wound healing [Tranquillo and Murray, 1992]. The first is that we focussed on the dermal tissue surrounding the wound rather than synthesis and remodelling of the wound contents. The second is that we have modelled the tissue as a non-linear hyperelastic material. Most previous mechano-chemical models assume linear viscoelasticity. We have argued that the large recoil observed upon wounding merits a non-linear elastic framework and the assumption of linear elasticity fails to reproduce the degree of wound contraction observed in murine or human wounds.

However, there are many similarities between the two modelling frameworks. Both approaches formulate the biochemical environment by explicitly accounting for cell and chemical species using PDEs. It would be interesting in future work to compare the two mechanical approaches by considering the same equations for the cell and chemical species.

7.3.2 Extensions to the morpho-mechano-chemical model

We have extended a mechanical model of dermal wound healing, described in a morphoelastic framework, to account for biochemical stimuli. In doing so, many interactions were neglected: these could be incorporated into future models. For example, we assumed the growth factor supply, diffusing from the wound space into the dermal tissue, was proportional to the wound area. Time series data for the concentration of TGFβ in the wound space, although out-dated and noisy, have been measured by

Cromack et al. [1987] and Yang et al. [1999]. These data could be used to determine a realistic functional form for the source of TGFβ on the wound boundary. Equally, fibroblast proliferation and migration have been shown to exhibit biphasic dependence on TGFβ levels [Cordeiro et al., 2000]: a more realistic model might assume that both the chemotaxis coefficient and fibroblast proliferation rates are non-monotonic functions of TGFβ levels. Finally, the growth law for the dermal tissue could be superseded by one which depends on local levels of TGFβ and stress to reflect their impact on the rate at which fibroblasts synthesise collagen [Cordeiro et al., 2000, Kessler et al., 2001].

The current formulation of the fibroblast equation requires further consideration. A limitation is that only net proliferation of fibroblasts is considered. Therefore, after wound closure, the fibroblast density does not return to its initial distribution or reach a biologically realistic steady state. Thus, in its current form, the model is only valid on the timescale of wound closure. By introducing a fibroblast death term or allowing for cell movement into the granulation tissue, we could ensure that the fibroblast distribution eventually returns to its initial, unwounded state.

We assumed that the fibroblasts do not occupy significant volume. Under certain conditions, for example large chemotactic or proliferative terms, the fibroblast density at the wound edge is very high. Therefore, the volume that the fibroblasts occupy may become significant, warranting their inclusion in the growth evolution equations.

7.3.3 Symmetry breaking

In many of our simulations of wound healing, when contraction is high in comparison to tissue growth, we observe a highly compressive circumferential stress at the wound edge. A high compressive circumferential stress can induce instabilities in the circular geometry [Moulton and Goriely, 2011, Wu and Ben Amar, 2015]. The balance between growth and contraction in the context of instabilities would be an interesting addition

to our morphoelastic models of dermal wound healing.

7.3.4 A model of human wound healing

It is important to note the differences between healing in mice and humans. Mice have thinner, looser skin, whereas human skin is thick, relatively stiff and adherent to the underlying tissues [Wong et al., 2011]. As a consequence of a muscular layer underneath the skin, which is absent in humans, murine wounds heal mainly by contraction. Although contraction contributes to human healing, re-epithelialisation is believed to be the dominant process. Despite these differences, mouse models have contributed greatly to our understanding of wound healing. Further, our awareness of the differences will allow us to better evaluate the data and make predictions about human healing.

Due to the lack of wound healing data in adult humans, the work presented in this thesis focussed on data from wound healing in mice. However, the ultimate aim would be to develop a model of human wound healing that could be used to test treatments for wound healing patients.

In this thesis we have assumed that the tissue is mechanically homogeneous and isotropic, following a neo-Hookean strain-energy function. This is a good first approximation in the absence of more detailed information about the stress-strain characteristics of the material. Assuming an isotropic tissue in the simplified geometry yields a model with fewer degrees of freedom and therefore we could infer more through comparing our results with experimental data. However, there is experimental evidence that skin is anisotropic and inhomogeneous. For example, the skin is more deformable along certain axis known as Langer's lines [Langer, 1978, Reihsner et al., 2000]. Constitutive laws for human dermal tissue have been developed and would provide a more accurate description of the mechanical properties of the dermis [Annaidh et al., 2012, Yang et al., 2013].

7.3.5 Experimental work

Experimental work that could validate some of our model predictions would be essential. We discuss some possibilities in the following sections.

7.3.5.1 Rewounding experiments

More detailed experimental data are required to distinguish between growth and contraction processes in dermal wound healing. In Chapter 4 we simulated experiments to demonstrate how this could be done. Using our proposed method, initial experimental work from our collaborators suggests a large contribution from contraction. However, data have only been collected from wounds in diabetic mice. To determine whether our predictions about the difference in relative contributions of growth and contraction between the non-diabetic and diabetic wounds, data from wounds in non-diabetic mice would also be required. Alternatively, if a non-invasive method of determining stress levels were available, this could prove useful.

7.3.5.2 Pressure treatments

The clinical effectiveness of the application of pressure to control healing remains to be scientifically proven [Anzarut et al., 2009]. Our results from Chapter 4 suggested that varying the axial load (to simulate different pressure treatments) had no significant effect on the rate of wound closure. However, the net change in volume of tissue could be controlled. Experiments demonstrating the effects of pressure on the tissue surrounding a wound would be valuable in testing our model predictions.

7.3.5.3 Treatment strategies

Throughout this thesis we have shown that increasing dermal growth could normalise healing in diabetic mouse wounds. We determined strategies for correcting the imbalance between growth and contraction in aberrant wounds. Of considerable interest

would be testing these predictions, in particular the results from Chapter 6, by applying TGFβ into the wound space. Further, it would be interesting to compare our treatment results from the mechano-chemical model with those of an extended version accounting for the interactions discussed in Section 7.3.2. The effects of applying TGFβ would not be trivial with more complicated feedback between TGFβ, stress and fibroblast activity.

7.3.6 Final words

We have developed a series of mathematical models with increased complexity for healing of full thickness circular wounds. Our initial focus on developing a model comparable to the data revealed that, even with a simple model, more detailed data are needed to test our predictions. We have demonstrated that the balance between growth and contraction in dermal healing is key. Our morphoelastic approach offers a sophisticated framework for investigating these processes and how they are influenced by a combination of biochemical and biomechanical stimuli.

Appendix A

The ODE model

In this appendix we discuss the parameter values and numerical methods used in Chapter 2.

A.1 Parameter estimation

In this section we explain how we estimate A_R, T and the dimensionless parameters which are held fixed during the least squares analysis in Section 2.4.1. The value A_R is the maximum area of the wound, which, from the data, is 47.6816 mm^2 in the non-diabetic and 59.0705 mm^2 in the diabetic wounds. The typical time scale, T, is taken to be 1 day, which is approximately the doubling time for both epithelial cells and fibroblasts [Shi and King, 2005, Ghosh et al., 2007].

The dimensionless parameter ϵ represents the relative importance of the frictional and elastic responses of the dermal tissue. We assume that the elastic response is much faster than the timescale of friction, so that the wound rapidly springs open to its relaxed size and, hence, $\epsilon \ll 1$. The recoil data presented in Figure 2.2 are limited to time points at days 0 and 1 only, hence an accurate estimate of ϵ can not be obtained. Accordingly, we fix $\epsilon = 0.01$ (corresponding to recoil occurring within hours) and note that this choice of ϵ does not affect our analysis, influencing the

speed of recoil only. For a more accurate value, finer resolved temporal data between days 0 and 1 would be needed. The delay for contraction has been estimated to be approximately 2 to 5 days post wounding [Monaco and Lawrence, 2003]. The parameter t_c represents the time (in days) at which $\mathcal{H}(t - t_c) = 0.5$. We therefore assume that $t_c = 3$ and fix θ as follows. We consider the gradient of the contraction switch and assign $\theta = 1$ such that the continuous switch represents a period of 4 days from which contraction begins to activate until it has reached close to its maximum. This 4 day period (day 1 to 5) represents the time taken for the fibroblasts to reach the wound edge.

A.2 Numerical solution

In order to numerically solve the non-linear system defined by Equations (2.18) we use MATLAB's stiff ODE solver `ode15s` [Shampine and Reichelt, 1997]. The solver implements a backward difference scheme of order k, where k represents the number of previous solutions needed to compute the solution at the $(k + 1)$th step. The method chooses the time-step, h, to be the largest h for which the truncation error is less than a given tolerance. For each step, the backward difference scheme generates non-linear equations which are solved by Newton's method.

A.3 Least squares method

Given the model solutions $A_e(t; \Phi)$ and $A_d(t; \Phi)$, where Φ is the set of model parameters, and the data sets $\mathbf{x_e}(t_i)$ and $\mathbf{x_d}(t_i)$, we aim to find $\Phi^* \subseteq \Phi$ that minimises the sum of errors squared (MSE),

$$\text{MSE} = \min_{\Phi^*} \left[\frac{1}{k} \sum_{i=1}^{k} \left(\, |x_e(t_i) - A_e(t_i, \Phi)| + |x_d(t_i) - A_d(t_i, \Phi)| \, \right)^2 \right], \tag{A.1}$$

where k is the number of time points in the data. This least squares method is implemented using the `lsqnonlin` function in MATLAB and requires an initial estimate of the parameters, Φ_0.

A.4 Numerical parameter sensitivity analysis

Given Equations (2.18), with parameter set $\Phi = \{\phi_1, \phi_2, ..., \phi_n\}$, we define the sensitivity $S(t, \phi_j)$, of the solution $A(t, \Phi)$, with respect to the parameter ϕ_j by,

$$S(t, \phi_j) = \left| \frac{\text{normalised change in } A(t;\Phi)}{\text{normalised change in } \phi_j} \right| = \left| \frac{\Delta A(t;\Phi)}{\Delta \phi_j} \frac{\phi_j}{A(t;\Phi)} \right|. \tag{A.2}$$

If ϕ_j is varied between ϕ_j^+ and ϕ_j^- then $\Delta\phi_j = \phi_j^+ - \phi_j^-$ and $\Delta A(t;\Phi) = A(t;\Phi,\phi_j^+) - A(t;\Phi,\phi_j^-)$.

Since we have obtained numerical solutions, Equation (A.2) is a discretised analogue of the expression often used in parameter sensitivity analysis [Dickinson and Gelinas, 1976], where partial derivatives of the solutions with respect to the parameters are calculated. In Figure A.1 we present the average (over time) sensitivity of A_e and A_d to each of the parameters,

$$\bar{S}(\phi_j) = \frac{1}{k} \sum_{i=0}^{i=k} S(t_i, \phi_j), \tag{A.3}$$

where k is the number of time points in the solution.

We are interested in model parameters which represent proliferation in the epidermis (λ) and growth (β_0, β_1) and contraction (α) in the dermis. We therefore fix $\theta = 1, t_c = 3$ and $\epsilon = 0.01$, since they have a low sensitivity in comparison to the other parameters (see Appendix A.1). Given the relatively high sensitivity of the solutions to γ and ν, these parameters are included in the least squares analysis. The parameter set optimised in the least squares analysis is therefore $\Phi^* = \{\lambda, \beta_0, \beta_1, \alpha, \gamma, \nu\}$.

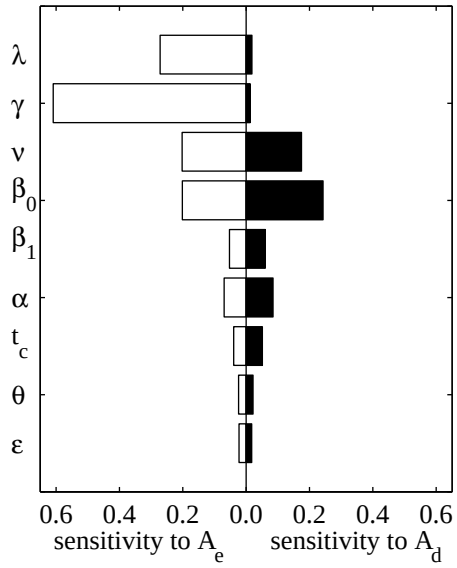

Figure A.1: Average sensitivity of the solutions to the model parameters. Numerical parameter sensitivity to the solutions $A_e(t)$ and $A_d(t)$ of Equation (2.18) are averaged using Equations (A.2) and (A.3) for the parameter set $\Phi = \{\lambda, \beta_0, \beta_1, \alpha, \gamma, \theta, t_c, \epsilon, \nu\} = \{0.5, 0.2, 0.1, 0.2, 0.1, 1, 3, 0.01, 0.1\}$. Each parameter, ϕ_j, is varied by $\pm 60\%$.

A.5 Comparison of epidermal growth rates

When developing the mass conservation equation for the epidermis in Section 2.2.1 we discusses two different functional forms which could be used for the growth rate. Results were presented for a growth rate proportional to the area of new epidermal tissue, a functional form consistent with experimental observations by Usui et al. [2008]. However, Bullough and Laurence [1960] found that mitotic activity was high in a region of width 1 mm surrounding the wound suggesting that the epidermal growth rate could, instead, be proportional to the wound circumference. In this section we consider these two choices for the epidermal growth rate and see how well each of them describes the experimental data.

Assuming that the growth rate is proportional to the circumference of the wound

we write the change in epidermal wound area as

$$\frac{\mathrm{d}A_e}{\mathrm{d}t} = -\lambda\sqrt{\frac{A_e}{A_R}}\left(\frac{A_e - \gamma A_d}{1 - \gamma A_d}\right), \tag{A.4}$$

where λ is the growth rate coefficient and γ is the dependence of epidermal growth on the dermis. The equations for the change in dermal wound areas (A_s and A_d) remain unchanged and are given in Equations (2.18) along with the change in epidermal wound area for which the growth rate is proportional to the area of new tissue.

In Figure A.2(a) we present the best fits of $A_e(t)$ to the epidermal data for non-diabetic wounds. We observe that Equation (2.18a) describes the data better than Equation (A.4). By fitting to the diabetic data, both models also predict that the epidermal growth rate is lower in the diabetic wounds (see Figure A.2). We conclude that changing the form of the growth rate has no impact on our results and conclusions for normal and diabetic healing.

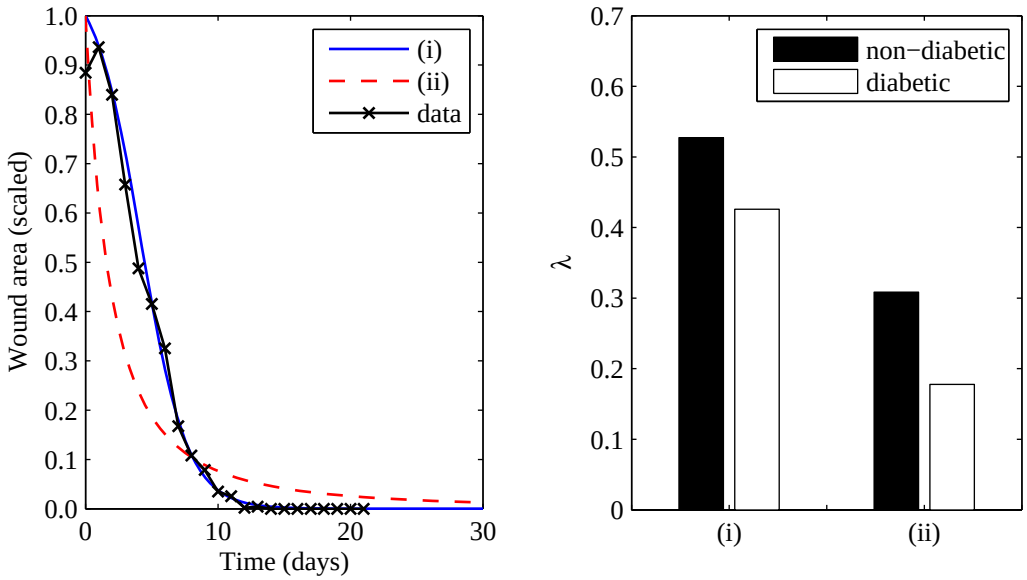

(a) Epidermal healing curves

(b) Epidermal growth parameter

Figure A.2: Comparison of different epidermal growth rates. Equations (2.18) are fit to the data in Figure 2.2 by optimising the parameter set $\Phi^* = \{\lambda, \beta_0, \beta_1, \alpha, \gamma, \nu\}$ using a least squares analysis. The parameters $\theta = 1, t_c = 3$ and $\epsilon = 0.01$ are fixed. (a) The epidermal healing curves are compared for: (i) the experimental data ($\times$); (ii) the best fit of Equation (2.18a) to the data (solid blue) – the growth rate is proportional to the area of new tissue; and (iii) the best fit of Equation (A.4) to the data (dashed red) – the growth rate is proportional to the wound circumference. Best fit parameters for (ii) are given in Table 2.1 and for (iii) are $\lambda = 0.3083$, $\beta_0 = 0.3480$, $\beta_1 = 0.2767$, $\alpha = 0.1961$, $\gamma = 0.0023$ and $\nu = 0.0372$. (b) The parameter, λ, associated with the best fits to the non-diabetic and diabetic data are compared for the two functional forms of epidermal growth rate.

Appendix B

The morphoelastic model

In this appendix we present details of the numerical methods for solving the morphoelastic model in Chapter 4. We also present asymptotic analysis of an annulus subject to homogeneous growth from Section 4.2.7, details of how the residual stress is calculated for variations of the model (different strain-energy functions and external boundary conditions) and discussion of the value of the contraction parameter used in the model simulations.

B.1 Numerical methods

B.1.1 Root-finding algorithm

In Section 4.2.7 we determined implicit equations for the current wound radius a and outer radius of the annulus b. These are plotted in Figure 4.8 for $a = A_0$ and $b = B_0$ in Equations (4.18) and (4.19), respectively.

The curve $a = A_0$ is solved in MATLAB using the built-in function `fsolve`. This function takes the following inputs: a vector of values for γ_r and an initial guess for the associated values of γ_θ. The function outputs the values of γ_θ which satisfies Equation (4.18) with $a = A_0$ for the given γ_r. We take the initial guess for γ_θ to be

γ_r.

The function `fsolve` uses a trust region reflective algorithm. This method is based on the interior reflective Newton method [Coleman and Li, 2006]. Each iteration involves the approximate solution of a large linear system using preconditioned conjugate gradients.

B.1.2 Arc length continuation method

If the initial guess is not sufficiently accurate, `fsolve` can return the wrong root or fall into a minimum, failing to return any root. This is the case for Equation (4.19) with $b = B_0$. In order to supply a more accurate initial guess for γ_θ we implement an arc length continuation method. A more accurate initial guess for γ_θ increases the chances of the root-finding algorithm returning the correct root.

Equation (4.19), with $b = B_0$, is a curve $f(\gamma_r, \gamma_\theta) = 0$ which defines a path in $(\gamma_r, \gamma_\theta)$ space. Given two points on the curve $\mathbf{f}_0 = (\gamma_r^0, \gamma_\theta^0)$ and $\mathbf{f}_1 = (\gamma_r^1, \gamma_\theta^1)$, we define the tangent vector $\mathbf{t}$ and a small step size ds. For the next point we take a step of size ds in the tangent direction and a corrector step of size ds in the orthogonal direction. The new point is the updated initial guess for γ_θ, which is an input of the function `fsolve`.

B.1.3 Numerical solution to the full model

The stress-free state, R_0, and the residual stress, T_{res}, are calculated as in Section 4.2.3 by solving Equations (4.11), (4.14) and (4.15). The inputs are the known measurements A, B, L and a_R, returning the stress-free state, $\{A_0, B_0, L_0\}$, and the residual stress, T_{res}.

Equations (4.27) are solved numerically in MATLAB. All dependent variables are stored as functions of R_0 with spatial discretisation $\mathrm{d}x = 0.1$. The growth in Equations (4.27e)-(4.27g) are discretised in time using a forward Euler approximation

[Press et al., 1994]. The integral boundary condition in Equation (4.27j) is re-written as a differential equation by letting

$$\frac{\partial I}{\partial R_0} = \gamma_r \gamma_\theta \gamma_z T_{zz} R_0, \tag{B.1a}$$

with

$$I(B_0) = \frac{N_z}{2\pi} \quad \text{and} \quad I(A_0) = 0. \tag{B.1b}$$

For each time increment ($\mathrm{d}t = 0.05$ days), the variable quantities in Equations (4.27) are updated in the following order:

1. The growth is updated by solving the forward Euler approximations to Equations (4.27e)-(4.27g) subject to the initial conditions in Equation (4.27k).

2. The deformation and the radial stress are updated using the boundary value problem solver `bvp4c` for a system of three differential equations given by Equations (4.27a), (4.27b) and (B.1a) subject to boundary conditions in Equations (4.27h), (4.27i) and (B.1b). The unknowns a and λ are included in the boundary value problem solver as free parameters.

3. The circumferential and axial stress are updated according the Equations (4.27c) and (4.27d).

The function `bvp4c` in MATLAB is a boundary value problem solver. It numerically integrates a system of first order ordinary differential equations using Simpson's method, subject to two boundary conditions. The approximate solution is discretised on a chosen mesh such that it is a cubic polynomial on each interval, satisfying the differential equation at both ends and the middle of the interval. If there are unknown parameters in the system then for every parameter an additional boundary condition must be specified. Since boundary value problems can have multiple solutions, `bvp4c`

requires an initial guess for the mesh and solution so that the method returns the desired solution.

B.2 Asymptotic analysis

In Section 4.2.7 we found implicit equations for the current configuration of an unloaded annulus subject to homogeneous growth in terms of the reference configuration and the growth components. The equations were solved numerically using a root-finding algorithm as described in Appendix B.1.3.

Asymptotics provides a check on our numerical calculations and can yield information on how the radial and circumferential growth laws should be inter-related at extreme values of $\gamma_r\gamma_\theta$. We seek the limits of the curves $a = A_0$ and $b = B_0$ as $\gamma_r \to 0$ and $\gamma_r \to \infty$. By finding these limits we will determine the points to which we would expect our growth functions to tend for large times.

B.2.1 Stalled healing: $a = A_0$

We first investigate the limits of γ_r and γ_θ along the curve $a = A_0$ in Figure 4.8, given by Equation (4.18). We let $a = A_0$ in Equation (4.18) and rearrange to obtain

$$\left(\frac{\gamma_r}{\gamma_\theta}\right)^2 = \frac{1}{\log\left(\frac{B_0^2}{A_0^2}\right)}\left[\log\left(1+\gamma_r\gamma_\theta\left(\frac{B_0^2}{A_0^2}-1\right)\right) + (\gamma_r\gamma_\theta - 1)\left(1 - \frac{1}{1+\gamma_r\gamma_\theta\left(\frac{B_0^2}{A_0^2}-1\right)}\right)\right]. \tag{B.2}$$

From Equation (B.2) we deduce that γ_r and γ_θ appear in two combinations: $\gamma_r\gamma_\theta$ and γ_r/γ_θ. Motivated by Figure 4.8 we perform an asymptotic expansion for γ_r/γ_θ in terms of $\gamma_r\gamma_\theta$.

B.2.1.1 (i) Limit as $\gamma_r \to 0$

Guided by Figure 4.8, we anticipate that as $\gamma_r \to 0$ along the curve $a = A_0$, γ_θ remains finite. Accordingly we fix $\gamma_r\gamma_\theta = \epsilon \ll 1$ in Equation (B.2) and perform an asymptotic expansion for γ_r/γ_θ in powers of ϵ to obtain

$$\left(\frac{\gamma_r}{\gamma_\theta}\right)^2 = \frac{\left(\frac{B_0^4}{A_0^4} - 1\right)}{2\log\left(\frac{B_0^2}{A_0^2}\right)}\epsilon^2 + \mathcal{O}(\epsilon^3). \tag{B.3}$$

Combining Equation (B.3) with $\gamma_r\gamma_\theta = \epsilon$ we deduce that, in the limit as $\gamma_r \to 0$,

$$\gamma_r \approx \left(\frac{\frac{B_0^4}{A_0^4} - 1}{2\log\left(\frac{B_0^2}{A_0^2}\right)}\right)^{\frac{1}{4}} \epsilon \quad \text{and} \quad \gamma_\theta \approx \left(\frac{\frac{B_0^4}{A_0^4} - 1}{2\log\left(\frac{B_0^2}{A_0^2}\right)}\right)^{-\frac{1}{4}}. \tag{B.4}$$

We plot γ_θ from Equation (B.4) for $\gamma_r \to 0$ along the curve $a = A_0$ in Figure B.1 and observe that the asymptotic approximation is in agreement with the limit of the numerical solution.

B.2.1.2 (ii) Limit as $\gamma_r \to \infty$

From Figure 4.8 we anticipate that along the curve $a = A_0$, $\gamma_\theta \to \infty$ as $\gamma_r \to \infty$, and so we set $\gamma_r\gamma_\theta = 1/\epsilon \gg 1$ in Equation (B.2) to obtain,

$$\left(\frac{\gamma_r}{\gamma_\theta}\right)^2 = \frac{1}{\log\left(\frac{B_0^2}{A_0^2}\right)}\left[\log\left(1 + \frac{1}{\epsilon}\left(\frac{B_0^2}{A_0^2} - 1\right)\right) + \left(\frac{1}{\epsilon} - 1\right)\left(1 - \frac{1}{1 + \frac{1}{\epsilon}\left(\frac{B_0^2}{A_0^2} - 1\right)}\right)\right]. \tag{B.5}$$

In Equation (B.5) the dominant term on the right hand side is $\mathcal{O}(1/\epsilon)$, leading to

$$\left(\frac{\gamma_r}{\gamma_\theta}\right)^2 \approx \frac{1}{\log\left(\frac{B_0^2}{A_0^2}\right)}\frac{1}{\epsilon}. \tag{B.6}$$

Combining Equation (B.6) with $\gamma_r\gamma_\theta = 1/\epsilon$ we deduce

$$\gamma_r \approx \left(\log\left(\frac{B_0^2}{A_0^2}\right)\right)^{-\frac{1}{4}} \epsilon^{-\frac{3}{4}} \quad \text{and} \quad \gamma_\theta \approx \left(\log\left(\frac{B_0^2}{A_0^2}\right)\right)^{\frac{1}{4}} \epsilon^{-\frac{1}{4}}. \tag{B.7}$$

B.2.2 Normal healing: $b = B_0$

Similar to the case for which $a = A_0$, to determine the behaviour of γ_r and γ_θ along the curve $b = B_0$, we rearrange Equation (4.19) to obtain

$$\begin{aligned}\left(\frac{\gamma_r}{\gamma_\theta}\right)^2 =& \frac{1}{\log\left(\frac{B_0^2}{A_0^2}\right)}\left[\log\left(\frac{1}{1-\gamma_r\gamma_\theta\left(1-\frac{A_0^2}{B_0^2}\right)}\right)\right. \\ &\left. + (1-\gamma_r\gamma_\theta)\left(1-\frac{1}{1-\gamma_r\gamma_\theta\left(1-\frac{A_0^2}{B_0^2}\right)}\right)\right].\end{aligned} \tag{B.8}$$

We perform an asymptotic expansion for γ_r/γ_θ in terms of $\gamma_r\gamma_\theta$.

B.2.2.1 (i) Limit as $\gamma_r \to 0$

Guided by Figure 4.8, we anticipate that as $\gamma_r \to 0$ along the curve $b = B_0$, γ_θ remains finite. Accordingly we fix $\gamma_r\gamma_\theta = \epsilon \ll 1$ in Equation (B.8) and perform an asymptotic expansion for γ_r/γ_θ in powers of ϵ to obtain

$$\left(\frac{\gamma_r}{\gamma_\theta}\right)^2 = \frac{\left(1-\frac{A_0^4}{B_0^4}\right)}{2\log\left(\frac{B_0^2}{A_0^2}\right)}\epsilon^2 + \mathcal{O}(\epsilon^3). \tag{B.9}$$

Combining Equation (B.9) with $\gamma_r\gamma_\theta = \epsilon$ we deduce that, as $\gamma_r \to 0$,

$$\gamma_r \approx \left(\frac{1-\frac{A_0^4}{B_0^4}}{2\log\left(\frac{B_0^2}{A_0^2}\right)}\right)^{\frac{1}{4}} \epsilon \quad \text{and} \quad \gamma_\theta \approx \left(\frac{1-\frac{A_0^4}{B_0^4}}{2\log\left(\frac{B_0^2}{A_0^2}\right)}\right)^{-\frac{1}{4}}. \tag{B.10}$$

We plot γ_θ from Equation (B.10) for $\gamma_r \to 0$ along the curve $b = B_0$ in Figure B.1 and observe that the asymptotic approximation is in agreement with the limit of the numerical solution.

B.2.2.2 (ii) Limit as $\gamma_r \to \infty$

We anticipate that as $\gamma_r \to \infty$ along the curve $b = B_0$, γ_θ remains finite. We choose the ansatz $\gamma_r\gamma_\theta = (1-\epsilon)/\beta$, where $\beta = (1 - A^2/B^2)$ and $0 < \beta < 1$ since $B_0 > A_0$. Substituting this into Equation (B.8) gives,

$$\begin{aligned}\left(\frac{\gamma_r}{\gamma_\theta}\right)^2 =& \frac{1}{\log\left(\frac{B_0^2}{A_0^2}\right)}\left[\log\left(\frac{1}{1-(1-\epsilon)}\right)\right. \\ &\left. + \left(1 - \frac{(1-\epsilon)}{\beta}\right)\left(1 - \frac{1}{1-(1-\epsilon)}\right)\right]. \end{aligned} \tag{B.11}$$

The dominant term on the right hand side is $\mathcal{O}(1/\epsilon)$, therefore

$$\left(\frac{\gamma_r}{\gamma_\theta}\right)^2 \approx \frac{1}{\log\left(\frac{B_0^2}{A_0^2}\right)}\left(\frac{1}{\beta} - 1\right)\frac{1}{\epsilon}. \tag{B.12}$$

Combining Equation (B.12) with $\gamma_r\gamma_\theta = (1-\epsilon)/\beta$ we obtain, to leading order in ϵ,

$$\gamma_r \approx \left(\frac{\frac{A_0^2}{B_0^2}}{\left(1 - \frac{A_0^2}{B_0^2}\right)^2 \log\left(\frac{B_0^2}{A_0^2}\right)}\right)^{\frac{1}{4}} \epsilon^{-\frac{1}{4}} \quad \text{and} \quad \gamma_\theta \approx \left(\frac{\log\left(\frac{B_0^2}{A_0^2}\right)}{\left(1 - \frac{A_0^2}{B_0^2}\right)^2 \frac{A_0^2}{B_0^2}}\right)^{\frac{1}{4}} \epsilon^{\frac{1}{4}}. \tag{B.13}$$

We note that, if we require the dermal wound to fully heal, i.e. $a = 0$, along $b = B_0$, then from $b^2 = a^2 + \gamma_r\gamma_\theta(B_0^2 - A_0^2)$ we have that $\gamma_r\gamma_\theta = 1/\beta$. Therefore the dermal wound will only fully heal along $b = B_0$ in the limit as $\gamma_r \to \infty$.

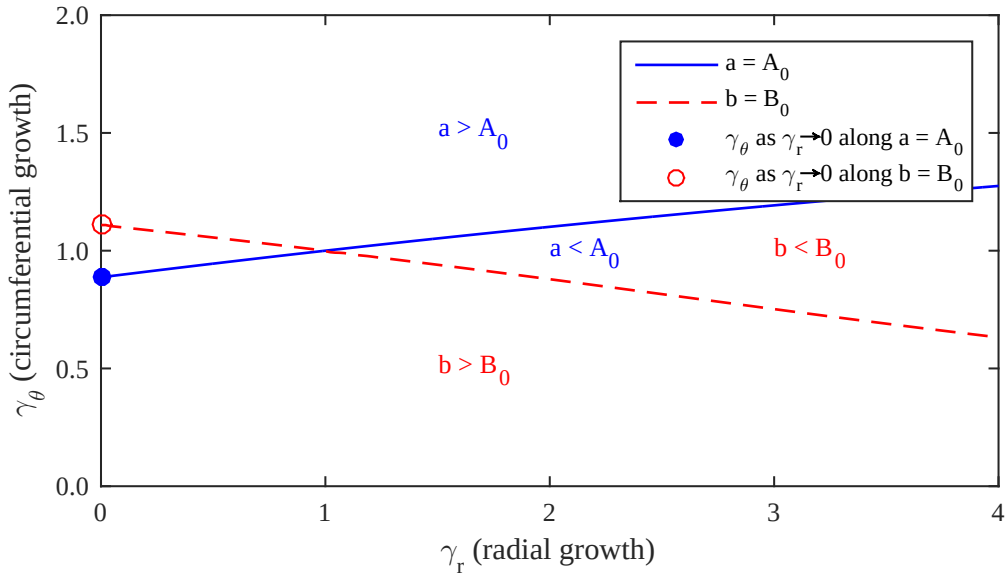

Figure B.1: Asymptotic analysis of compatible growth laws and numerical approximation. Equations (4.18) and (4.19) are solved numerically to find the curves in $(\gamma_r, \gamma_\theta)$-space such that $a = A_0$ (solid blue) and $b = B_0$ (dashed red). The asymptotic values of γ_θ as $\gamma_r \to 0$ are plotted for $a = A_0$ (filled blue circle) from Equation (B.4) and $b = B_0$ (red circle) from Equation (B.10). Reference variables are $A_0 = 4$ mm and $B_0 = 5$ mm corresponding to a proliferative band of width 1 mm surrounding the wound.

B.2.3 Conclusion

By performing asymptotic expansions we found the limits of the curves $a = A_0$ and $b = B_0$ as $\gamma_r \to 0$ and $\gamma_r \to \infty$. We can use these to check that the growth laws we prescribe to the system behave as we would expect and that the numerical solutions are accurate.

B.3 Calculation of the stress-free state

Analogous to Section 4.2.3 we calculate the stress-free state under the assumptions of Hooke's law, a Fung elastic material and for the comparison of boundary conditions

in Section 4.4.4. The deformation $\mathcal{F}_1$ is given by

$$R = \frac{B}{B_0} R_0, \tag{B.14}$$

and $\mathcal{F}_2$ by

$$r^2 = \frac{R_0^2 - A_0^2}{\lambda^2} + a_R^2, \tag{B.15}$$

where A_0 and B_0 are, respectively, the inner and outer radii of the stress-free state, a_R is the recoiled wound radius and λ is the axial stretch associated with the deformation $\mathcal{F}_2$. The balance of linear momentum gives

$$\frac{\partial T_{rr}}{\partial r} = \frac{1}{r}(T_{\theta\theta} - T_{rr}), \tag{B.16}$$

and the axial boundary condition is

$$N_z = 2\pi \int_a^b T_{zz} r \, \mathrm{d}r. \tag{B.17}$$

In the following sections we calculate the stress-free state $\{A_0, B_0, L_0\}$ and the residual stress for a Hookean solid and a Fung elastic material.

B.3.1 A Hookean solid

The stress-strain relationship for an incompressible Hookean solid is given by

$$e_{rr} = \frac{1}{E}\left(T_{rr} - \frac{1}{2}(T_{\theta\theta} + T_{zz})\right), \tag{B.18a}$$

$$e_{\theta\theta} = \frac{1}{E}\left(T_{\theta\theta} - \frac{1}{2}(T_{rr} + T_{zz})\right), \tag{B.18b}$$

$$e_{zz} = \frac{1}{E}\left(T_{zz} - \frac{1}{2}(T_{rr} + T_{\theta\theta})\right), \tag{B.18c}$$

where $E = 3\mu$ is Young's modulus and $\mathcal{E} = \text{diag}(e_{rr}, e_{\theta\theta}, e_{zz})$ is the stretch, related to the deformation by $\mathcal{E} = \mathcal{F} - \mathbb{I}$.

Substituting Equations (B.18) into (B.16), integrating and imposing $T_{rr}|_{R_0=B_0} = T_{\text{res}}$ gives $T_{rr} = T_{\theta\theta} = T_{\text{res}}$. Therefore

$$T_{\text{res}} = E\left(1 - \frac{B_0^2}{B^2}\right). \tag{B.19}$$

Substituting Equations (B.15) and (B.18) into (B.16) and solving subject to $T_{rr}|_{R_0=A_0} = 0$ and $T_{rr}|_{R_0=B_0} = T_{\text{res}}$ gives

$$T_{\text{res}} = \frac{2E}{3\lambda}\left(\frac{B_0}{\sqrt{\lambda(B_0^2 - A_0^2) + a_R^2}} - \frac{A_0}{a_R}\right). \tag{B.20}$$

Equations (B.17), (B.19) and (B.20) are solved simultaneously to find T_{res}, B_0 and λ.

B.3.2 A Fung elastic solid

The strain-energy function for a Fung material is given by

$$W(\alpha_r, \alpha_\theta, \alpha_z) = \frac{\mu}{2c}\left(\exp^{c(\alpha_r^2+\alpha_\theta^2+\alpha_z^2-3)} - 1\right), \tag{B.21}$$

and the components of the Cauchy stress tensor are

$$T_{rr} = \alpha_r W_r - p, \quad T_{\theta\theta} = \alpha_\theta W_\theta - p \quad \text{and} \quad T_{zz} = \alpha_z W_z - p. \tag{B.22}$$

Substituting Equations (B.22) into (B.16), integrating and imposing $T_{rr}|_{R_0=B_0} = T_{\text{res}}$ gives $T_{rr} = T_{\theta\theta} = T_{\text{res}}$. By imposing the axial boundary condition in Equation (B.17) with $N_z = 0$ we find that $T_{zz} = 0$ and therefore

$$0 = T_{\text{res}} + \mu \exp\left[c\left(2\frac{B^2}{B_0^2} + \frac{B_0^4}{B^4} - 3\right)\right]\left(\frac{B_0^4}{B^4} - \frac{B^2}{B_0^2}\right). \tag{B.23}$$

Substituting Equations (B.15) and (B.22) into (B.16) and solving subject to $T_{rr}|_{r=A_R} = 0$ and $T_{rr}|_{r=b_R} = T_{\text{res}}$ gives

$$T_{\text{res}} = \int_{a_R}^{b_R} \mu \left(\frac{r}{\lambda(r^2 - a_R^2) + A_0^2} - \frac{\lambda(r^2 - a_R^2) + A_0^2}{\lambda^2 r^3} \right) \times \exp\left[c \left(\frac{r}{\lambda(r^2 - a_R^2) + A_0^2} + \frac{\lambda(r^2 - a_R^2) + A_0^2}{\lambda^2 r^3} + \lambda^2 - 3 \right) \right] \, \mathrm{d}r. \tag{B.24}$$

Equations (B.17), (B.23) and (B.24) are solved simultaneously to find T_{res}, B_0 and λ.

B.3.3 Different external boundary conditions

To calculate the stress-free state for different external boundary conditions with a neo-Hookean strain-energy function we substitute Equations (4.3) and (4.4) and into (B.16). Solving with $T_{rr}|_{R_0=B_0} = T_{\text{res}}$ gives $T_{rr} = T_{\theta\theta} = T_{\text{res}}$. By imposing the axial boundary condition in Equation (B.17) with $N_z = 0$ we find that $T_{zz} = 0$ and therefore

$$0 = T_{\text{res}} + \mu \left(\frac{B_0^4}{B^4} + \frac{B^2}{B_0^2} \right). \tag{B.25}$$

Imposing $r|_{R_0=B_0} = B$ in Equation (B.15) determines the axial stretch

$$\lambda = \frac{B_0^2 - A_0^2}{B^2 - a_R^2}. \tag{B.26}$$

Substituting Equations (4.3), (4.4) and (B.15) into (B.16) and solving subject to $T_{rr}|_{r=A_R} = 0$ gives

$$T_{rr} = \frac{\mu}{2\lambda} \left[\log\left(\frac{\lambda(r^2 - a_R^2) + A_0^2}{A_0^2} \right) - \log\left(\frac{r^2}{a_R^2} \right) + \left(\frac{A_0^2}{\lambda} - a_R^2 \right) \left(\frac{1}{r^2} - \frac{1}{a_R^2} \right) \right]. \tag{B.27}$$

For fixed position boundary condition, B_0 is determined by solving Equation (B.17) with integration over $r \in [a_R, B]$.

For both fixed position and fixed stress, B_0 is determined by imposing $T_{rr}|_{R_0=B_0} = T_{\text{res}}$ in Equation (B.27) and equating with (B.25).

B.4 Estimation of the contraction coefficient

The contraction force is phenomenological: we use Equation (4.27h) to prescribe the radial stress at the wound edge. Since contraction of the dermis causes tension at the wound edge we expect the contraction parameter, f, to be positive. In this section we derive an upper bound on f based on published information about fibroblast cells.

The range of forces exerted by fibroblasts varies from $0.138\,\mu$N to $2.65\,\mu$N per cell, with the discrepancy due to different techniques used to measure the force exerted by a fibroblast.

Given that the volume of a fibroblast is approximately $2000\mu\text{m}^3$ [Uhal et al., 1998], as an upper bound we approximate the dermal tissue at the wound edge as a fully confluent population of fibroblasts. From Table 4.1, f is a force per volume, hence

$$\begin{aligned}\frac{\text{maximum force}}{\text{cell volume}} &= \frac{2.65\,\mu\text{N}}{2000\,\mu\text{m}^3},\\ \frac{\text{force}}{\text{tissue volume}} &\leq 1.325\,\frac{\text{N}}{\text{mm}^3},\\ \implies f &\leq 1.325\,\frac{\text{N}}{\text{mm}^3}.\end{aligned}$$

This calculation imposes an upper bound on the contraction parameter f, where we have used the maximum force exerted by a single fibroblast cell found in the literature and assumed that the wound edge consists entirely of fibroblasts. The inequality appears since the maximum volume of fibroblasts is bounded by the volume of dermal tissue.

B.5 Sensitivity of remodelling time to parameters

In Section 4.6.1 we presented a numerical sensitivity of the time taken for the tissue to reach a steady state as the model parameters were varied. Results showed that the sensitivity to the axial growth parameter was larger than expected. We postulated that this was because the axial deformation was fixed during the remodelling period and hence small changes in axial growth had a big effect on the time taken to reach steady state. To test this we present an analogous sensitivity analysis where the axial deformation satisfies the spring condition in Equation (4.27j). Results are given in Figure B.2 and we observe that the sensitivity of remodelling time to the axial growth parameter is much lower in this case in comparison to in Figure 4.20.

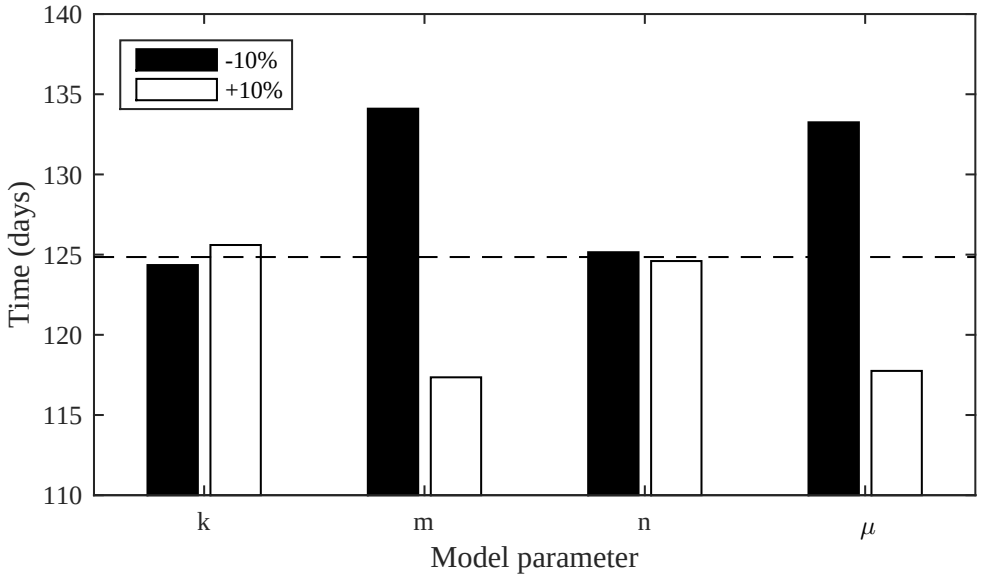

Figure B.2: Effect of model parameters on remodelling time. Equations (4.27) are solved numerically for $0 < t < 25$. At $t = 25$ the position of the wound edge is fixed by switching the boundary condition from a fixed load (Equations (4.27h)-(4.27j)) to a fixed radial displacement specified by Equation (4.34) with λ satisfying Equation (4.27j). During the remodelling phase, each model parameter is varied by $\pm 10\%$ of its default value and the time taken to reach steady state is recorded. The dashed line indicates the remodelling time when all parameters are fixed at their default values. Reference variables and parameters are specified using the default values in Table 4.1.

Appendix C

The model comparison

In this appendix we present the numerical method used to solve the simplified morphoelastic model in Equations (5.8) and discuss the parameters used in our comparison of the spatially-averaged morphoelastic model with the time-dependent ODE model in Equations (2.18).

C.1 Numerical method for constant growth

Equations (5.8) are solved numerically in MATLAB. All dependent variables are stored as functions of R with spatial discretisation $\mathrm{d}x = 0.01$. For each time increment ($\mathrm{d}t = 0.1$ days) Equations (5.8) are updated in the following order:

1. The residual stress is calculated according to Equation (5.3).

2. Equation (5.8e) is integrated numerically using the `trapz` function to find the mean radial stress.

3. Equation (5.8d) is solved using a forward Euler method to find the radial growth γ_r subject to $\gamma_r(0) = 1$.

4. Equation (5.8f) is solved using the `fsolve` function to find the circumferential

growth γ_θ.

5. Equations (5.8a) and (5.8b) are integrated exactly subject to the boundary conditions in Equation (5.8g).

6. The unknown, a, is found be imposing the boundary condition $T_{rr}|_{R=A} = fa\mathcal{H}(t - t_c)$ and using the `fsolve` function.

7. The circumferential stress is given by Equation (5.8c).

C.2 Parameter estimation

In this section we discuss the estimation of the parameters that are fixed for the least squares analysis. The reference variable A is the initial wound radius which, unless specified otherwise, is given by the experimental data (3.664 mm for non-diabetic and 4.1373 mm for diabetic). The recoiled wound radius a_R is also taken from the data (3.896 mm for non-diabetic and 4.2262 mm for diabetic). The reference variable B is chosen to be $a_R + \nu$ where ν is the radius of the proliferative region of the dermis. We take $\nu = 1$ mm [Bullough and Laurence, 1960] and when comparing with Model A we take ν to be consistent with the area of the proliferative region found from fitting Model A to the data (non-diabetic $\nu = 0.1723$ mm, diabetic $\nu = 0.2169$ mm). The reference variable C is fixed at 20 mm and is estimated in Section 4.2.4.

Other parameters which are fixed in the least squares optimisation are the shear stress, μ, the delay for contraction, t_c, and the gradient of the contraction switch, θ. We set $\mu = 0.2$ MPa, consistent with Annaidh et al. [2012] and discussed in Section 4.2.5. Following our discussion of parameters in Appendix A.1 we take $t_c =$ 3 days and $\theta = 1$.

Appendix D

The morpho-mechano-chemical model

In this appendix we discuss the choice of model parameters and typical scalings used in the non-dimensionalisation and the numerical method implemented to solve Equations (6.40).

D.1 Dimensional model parameters

The dimensional model parameters are discussed below and summarised in Tables D.1-D.3:

- The diffusion rate of a growth factor through a fibrin gel is approximately 1.59×10^{-6} cm^2 s^{-1} [Nauman et al., 2007]. We therefore take $D_\beta = 14$ mm^2 days^{-1}.
- The half-life of active TGFβ, which we will denote $t_{1/2}$, is $2-3$ minutes [Wakefield et al., 1990]. The decay rate is related to the half-life by $d = \frac{\log(2)}{t_{1/2}}$. We therefore take the TGFβ decay rate to be $d = 330 - 495$ days^{-1}.
- The half-maximal proliferation threshold value of TGFβ should be positive. We choose a default value of $\beta^* = 50$ pg mm^{-3}.

- Data for TGFβ concentration in the wound gives values on the order of 100 [Yang et al., 1999]. We take $\beta_0 = 50$ pg mm^{-3} with $\beta(A_0, t) = \beta_0 a^2(t)$, where $a(t = 0) = 4$ mm.

- The fibroblast diffusion coefficient is 2×10^{-2} cm^2 days^{-1} [Ghosh et al., 2007]. We therefore take $D_\phi = 2$ mm^2 day^{-1}.

- The fibroblast proliferation rate is $k = 0.832$ days^{-1} [Ghosh et al., 2007].

- The maximum fibroblast density in the dermis has been shown to be 10^5 cells mm^{-3}. The physical capacity of the tissue can be calculated using the volume of a fibroblast cell resulting in 5×10^5 cells mm^{-3}, where the volume of a human fibroblast cell is approximately 2260 μm^3 [Mitsui and Schneider, 1976]. We therefore take $\phi_{\max} = 10^5$ cells mm^{-3}.

- The fibroblast density in unwounded dermal tissue is $\phi_0 = 10^3$ cells mm^{-3} found from experimental data [Randolph and Simon, 1998, Miller et al., 2003].

- The maximum volume of cell-derived material produced per cell per day is $V_{\text{col}} = 3.6 \times 10^{-6}$ mm^3 cell^{-1} day^{-1} [Mitsui and Schneider, 1976].

- The maximum force exerted by a single fibroblast cell has been shown to be 2.65 μN [Fray et al., 1998, Wrobel et al., 2002]. Assuming that the force exerted on the tissue is proportional to the circumference of the wound it follows that $f \leq 2.65 \times 10^{-6}\pi = 1.665 \times 10^{-5}$ N cell^{-1}.

- The shear elastic modulus was estimated in Section 4.2.5 giving $\mu = 0.2$ MPa.

- The observed, *in vivo*, dimensions of the tissue are taken from data [McGrath and Simon, 1983], with $A = 4$ mm, $a_R = 4.4$ mm, $L = 0.1$ mm and the outer radius was estimated in Section 4.2.4 giving $B = 20$ mm.

Table D.1: Model parameters for transforming growth factor β. The dimensional parameters for Equations (6.36a) and (6.38a) are presented. The approximate values are discussed in Section D.1.

parameter	physical interpretation	units	approximate value
D_β	diffusion coefficient	$\text{mm}^2\ \text{days}^{-1}$	14
d	decay rate	days^{-1}	$330 - 495$
β^*	threshold concentration	pg mm^{-3}	50
s_β	cell sensitivity to TGFβ		unknown

Table D.2: Model parameters for the fibroblasts. The dimensional parameters for Equations (6.36b), (6.36g) and (6.38b) are presented. The approximate values are discussed in Section D.1.

parameter	physical interpretation	units	approximate value
D_ϕ	diffusion coefficient	$\text{mm}^2\ \text{days}^{-1}$	2
χ	chemotaxis coefficient	$\text{mm}^5\ \text{days}^{-1}\ \text{pg}^{-1}$	unknown
k	maximum proliferation rate	days^{-1}	0.832
V_c	cell derived material	$\text{mm}^3\ \text{cell}^{-1}\ \text{day}^{-1}$	3.6×10^{-6}
ϕ_0	initial density	cells mm^{-3}	10^3
ϕ_max	maximum density	cells mm^{-3}	10^5

Table D.3: Model parameters for the dermal tissue. The dimensional parameters for Equations (6.36d)-(6.36f), (6.37) and (6.38c) and the residually stressed state are presented. The approximate values are discussed in Section D.1.

parameter	physical interpretation	units	approximate value
s_T	growth distribution sensitivity		unknown
f	contraction	N cell^{-1}	$f < 1.665 \times 10^{-5}$
μ	shear elastic modulus	MPa	0.2
A	initial wound radius	mm	4
a_R	recoiled wound radius	mm	4.4
B	domain size	mm	20
L	tissue thickness	mm	0.1

D.2 Non-dimensionalisation

Typical scalings used in the non-dimensionalisation are

- Length: The wound radius is measured in mm hence we take the typical length scale to be $[r] = 1$ mm.
- Time: The healing of the wound occurs on the timescale of tissue growth so we take the typical timescale to be the rate of growth in the dermis, given by $\frac{1}{V_{\text{col}}\phi_{\max}}$.
- TGFβ: The half-maximal proliferation threshold concentration of TGFβ is $\beta^* = 50$ pg mm^{-3} [Yang et al., 1999].
- Fibroblasts: The maximum fibroblast density in the dermis is $\phi_{\max} = 10^5$ cells mm^{-3}.
- Stress: From the strain-energy function, the Cauchy stress tensor scales with the shear elastic modulus μ.

The parameters of the non-dimensionalised model are summarised in Table 6.1.

D.3 Numerical method

In this section we detail the numerical method employed to solve Equations (6.40). The method is implemented in MATLAB. The stress free state, R_0, and the residual stress, T_{res}, are calculated as in Section 4.2.3 by solving Equations (4.11), (4.14) and (4.15). The inputs are the known measurements A, B, L and a_R, returning the stress-free state, $\{A_0, B_0, L_0\}$, and the residual stress, T_{res}. All dependent variables are stored as functions of R_0 with spatial discretisation $\mathrm{d}x = 0.05$. Equations (6.40g), (6.40h) and (6.40i) are discretised in time using a forward Euler approximation.

For each time increment ($\mathrm{d}t = 0.05$), the variable quantities in Equations (6.40) are updated in the following order:

1. The TGFβ and fibroblast species are updated by solving Equations (6.40a) and (6.40b) using the function `pdepe`. The boundary and initial conditions specified in Equations (6.42a), (6.42b) and (6.42e) are supplied via function handles. Function inputs are the dimensions (radial symmetry), a mesh for R_0, time points for the solution to be specified, β, ϕ, Y and r from the previous time step and the model parameters. Function outputs are current values of β and ϕ, on the chosen mesh and at the specified time points.

2. The growth of the tissue is updated by solving the forward Euler approximations to Equations (6.40g), (6.40h) and (6.40i).

3. The deformation and radial stress are updated by solving Equations (6.40c) and (6.40d) together with the boundary conditions in Equations (6.42c) and (6.42d) using the function `bvp4c`. The two unknowns a and λ are included as unknown parameters. Equation (6.42d) is dealt with in the same manner as in Appendix B.1.3.

4. The circumferential and axial stresses in Equations (6.40e)-(6.40f) are evaluated.

5. All dependent variables are stored as functions of R_0.

The function `pdepe` in MATLAB is an initial-boundary value problem solver dealing with systems of parabolic and elliptic PDEs. The PDEs are discretised in space and the resulting ODEs are solved using `ode15s` to obtain approximate solutions at the times specified by the user. The initial conditions and boundary conditions are specified via function handles. The function selects its own time step when solving the system of ODEs, whereas the spatial mesh is defined by the user. The function `ode15s` is detailed in Appendix A.2.

D.3.1 Testing the numerical method

To test our numerical method we simplify the model so that analytical progress can be made and we can compare analytical solutions with the numerical solutions. We make the following simplifications:

1. Assume the fibroblasts have no growth factor dependence by setting $\bar{\chi} = s_\beta = 0$ in Equation (6.40b).

2. Assume that growth is distributed isotropically by setting $s_T = 0$ in Equation (6.41b).

These simplifications result in spatially homogeneous fibroblast and growth distributions so that the deformation and radial stress can be integrated exactly to obtain analytical expressions. Since growth is isotropic we let $\gamma = \gamma_r = \gamma_\theta$ and Equations (6.40) reduce to

$$\frac{\mathrm{d}\phi}{\mathrm{d}t} = \frac{\bar{k}}{2}\phi(1-\phi) - \frac{\phi}{\gamma^2}\left(\frac{\phi-\phi^*}{\lambda}\right), \tag{D.1a}$$

$$\frac{\mathrm{d}\gamma}{\mathrm{d}t} = \frac{1}{\gamma}\left(\frac{\phi-\phi^*}{2\lambda}\right), \tag{D.1b}$$

$$r^2 = a^2 + \frac{\gamma^2}{\lambda}(R_0^2 - A_0^2), \tag{D.1c}$$

$$T_{rr} = \frac{\bar{f}a\phi}{\lambda} + \frac{1}{2\lambda}\left[\log\left(\frac{R_0^2}{A_0^2}\right) - \log\left(\frac{\gamma^2(R_0^2-A_0^2)+\lambda a^2}{\lambda a^2}\right) + (\gamma^2 A_0^2 - \lambda a^2)\left(\frac{1}{\gamma^2(R_0^2-A_0^2)+\lambda a^2} - \frac{1}{\lambda a^2}\right)\right], \tag{D.1d}$$

$$T_{\theta\theta} = T_{rr} + \frac{\gamma^2 R_0^2}{r^2} - \frac{\gamma^2 R_0^2}{\lambda^2 r^2}, \tag{D.1e}$$

$$T_{zz} = T_{rr} + \lambda^2 - \frac{\gamma^2 R_0^2}{\lambda^2 r^2}, \tag{D.1f}$$

where a and λ are determined by evaluating

$$T_{rr}(B_0, t) = T_{\mathrm{res}} \quad \text{and} \quad 0 = \int_{A_0}^{B_0} T_{zz} R_0 \, \mathrm{d}R_0. \tag{D.1g}$$

Equations (D.1) are solved by updating ϕ and γ in Equations (D.1a) and (D.1b) via a forward Euler method, solving for a and λ using a root-finding algorithm and then evaluating Equations (D.1c)-(D.1f) for the deformation and stress. Although there are numerical approximations required to solve this simplified version of the model, they are methods that have been used in previous chapters and can be used to compare with the full numerical method.

In Figure D.1 we plot the wound radius, fibroblast density and isotropic growth as functions of time, and the radial stress at $t = 8$ as a function of position, R_0. We observe that, for the chosen parameter values, there is good agreement between the two different methods.

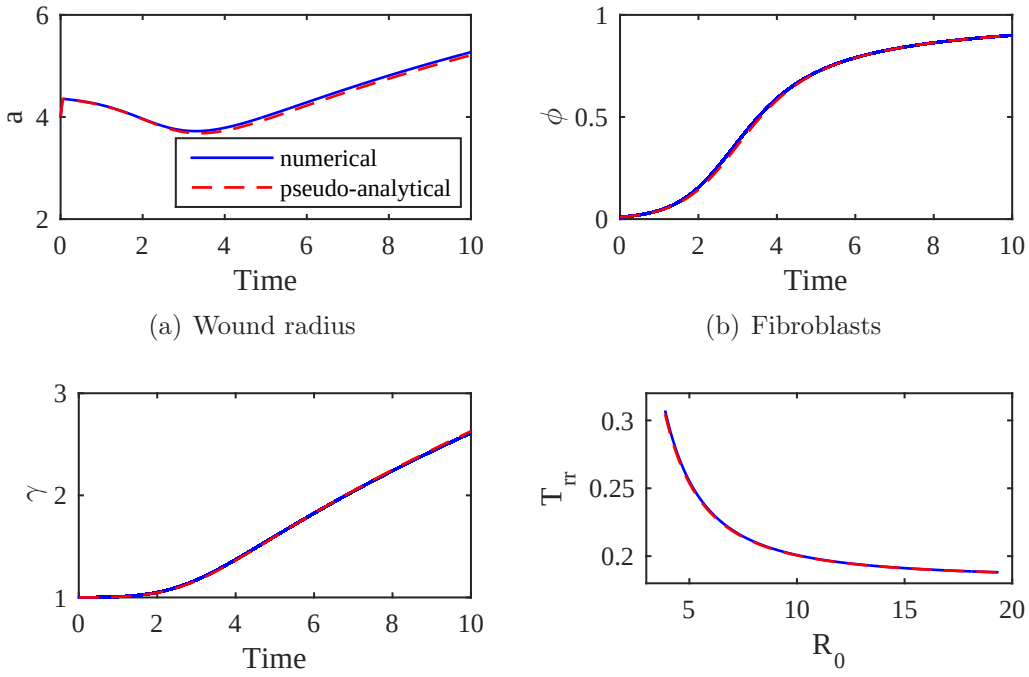

(a) Wound radius (b) Fibroblasts

(c) Growth (d) Radial stress

Figure D.1: Comparison of numerical and pseudo-analytical solutions. Equations (6.40) are solved numerically (solid blue) and compared to the solutions of Equations (D.1) (dashed red). (a) The wound radius, a, (b) the fibroblasts, ϕ, and (c) the isotropic growth, γ, are plotted as a functions of time. (d) The radial stress, T_{rr}, is plotted as a function of position, R_0, at $t = 8$. The TGFβ dependence is turned off and growth is isotropic by setting $\bar{\chi} = s_\beta = s_T = 0$. All other parameters are given in Table 6.1. We observe that the two methods agree.

Bibliography

S Aarabi, KA Bhatt, Y Shi, J Paterno, EI Chang, SA Loh, JW Holmes, MT Longaker, H Yee, and GC Gurtner. Mechanical load initiates hypertrophic scar formation through decreased cellular apoptosis. *Fed. Am. Soc. Exp. Biol. J.*, 21(12):3250–61, 2007.

M Abercrombie, MH Flint, and DW James. Wound contraction in relation to collagen formation in scorbutic guinea-pigs. *J. Embryol. Exp. Morphol.*, 4(2):167–75, 1956.

AI Adler, EJ Boyko, JH Ahroni, and DG Smith. Lower-extremity amputation in diabetes. The independent effects of peripheral vascular disease, sensory neuropathy, and foot ulcers. *Diabetes Care*, 22(7):1029–35, 1999.

PW Alford, JD Humphrey, and LA Taber. Growth and remodeling in a thick-walled artery model: effects of spatial variations in wall constituents. *Biomech. Model. Mechan.*, 7(4):245–62, 2008.

OM Alvarez, PM Mertz, and WH Eaglstein. The effect of occlusive dressings on collagen synthesis and re-epithelialization in superficial wounds. *J. Surg. Res.*, 35 (2):142–8, 1983.

D Ambrosi and F Mollica. The role of stress in the growth of a multicell spheroid. *J. Math. Biol.*, 48(5):477–99, 2004.

American Diabetes Association. Diagnosis and classification of diabetes mellitus. *Diabetes Care*, 29(S):S43–8, 2006.

AN Annaidh, K Bruyère, M Destrade, MD Gilchrist, C Maurini, M Otténio, and G Saccomandi. Automated estimation of collagen fibre dispersion in the dermis

and its contribution to the anisotropic behaviour of skin. *Ann. Biomed. Eng.*, 40 (8):1666–78, 2012.

A Anzarut, J Olson, P Singh, BH Rowe, and EE Tredget. The effectiveness of pressure garment therapy for the prevention of abnormal scarring after burn injury: a meta-analysis. *J. Plast. Reconstr. Aes.*, 62(1):77–84, 2009.

RP Araujo and SDL McElwain. A linear-elastic model of anisotropic tumour growth. *Eur. J. Appl. Math.*, 15(03):365–84, 2004.

J Arciero and D Swigon. Equation-based models of wound healing and collective cell migration. In *Complex Systems and Computational Biology Approaches to Acute Inflammation*, pages 185–207. Springer, 2013.

A Barbul, SA Lazarou, DT Efron, HL Wasserkrug, and G Efron. Arginine enhances wound healing and lymphocyte immune responses in humans. *Surgery*, 108(2): 331–7, 1990.

S Barrientos, O Stojadinovic, MS Golinko, H Brem, and M Tomic-Canic. Growth factors and cytokines in wound healing. *Wound Repair Regen.*, 16(5):585–601, 2008.

E Bell, B Ivarsson, and C Merrill. Production of a tissue-like structure by contraction of collagen lattices by human fibroblasts of different proliferative potential in vitro. *P. Natl. Acad. Sci. USA*, 76(3):1274–8, 1979.

YM Bello, AF Falabella, and WH Eaglstein. Tissue-engineered skin: current status in wound healing. *Am. J. Clin. Derm.*, 2(5):305–13, 2001.

DM Bermudez, BJ Herdrich, J Xu, R Lind, DP Beason, ME Mitchell, LJ Soslowsky, and KW Liechty. Impaired biomechanical properties of diabetic skin implications in pathogenesis of diabetic wound complications. *Am. J. Pathol.*, 178(5):2215–23, 2011.

A Bianchi, KJ Painter, and JA Sherratt. A mathematical model for lymphangiogenesis in normal and diabetic wounds. *arXiv:1501.00421v1 [q-bio.TO]*, 2015.

H Brem and M Tomic-Canic. Cellular and molecular basis of wound healing in diabetes. *J. Clin. Invest.*, 117(5):1219–22, 2007.

WS Bullough and EB Laurence. The control of epidermal mitotic activity in the mouse. *P. R. Soc. B.*, 151(945):517–36, 1960.

MA Carlson and MT Longaker. The fibroblast-populated collagen matrix as a model of wound healing: a review of the evidence. *Wound Repair Regen.*, 12(2):134–47, 2004.

RHC Catty. Healing and contraction of experimental full-thickness wounds in the human. *Brit. J. Surg.*, 52(7):542–8, 1965.

C Cherubini, S Filippi, P Nardinocchi, and L Teresi. An electromechanical model of cardiac tissue: Constitutive issues and electrophysiological effects. *Prog. Biophys. Mol. Biol.*, 97(2):562–73, 2008.

CC Chipev and M Simon. Phenotypic differences between dermal fibroblasts from different body sites determine their responses to tension and tgfβ1. *BMC Dermatol.*, 2(1):13, 2002.

M Chiquet. Regulation of extracellular matrix gene expression by mechanical stress. *Matrix Biol.*, 18(5):417–26, 1999.

CY Chung, S Funamoto, and RA Firtel. Signaling pathways controlling cell polarity and chemotaxis. *Trends Biochem. Sci.*, 26(9):557–66, 2001.

P Ciarletta and M Ben Amar. Papillary networks in the dermal–epidermal junction of skin: a biomechanical model. *Mech. Res. Commun.*, 42:68–76, 2012.

P Ciarletta, L Foret, and M Ben Amar. The radial growth phase of malignant melanoma: multi-phase modelling, numerical simulations and linear stability analysis. *J. R. Soc. Interface*, 8(56):345–68, 2011.

RAF Clark. *The Molecular and Cellular Biology of Wound Repair*. Plenum, New York, 1988.

DL Coleman. Obese and diabetes: Two mutant genes causing diabetes-obesity syndromes in mice. *Diabetologia*, 14(3):141–8, 1978.

TF Coleman and Y Li. An interior trust region approach for nonlinear minimization subject to bounds. *SIAM J. Optimiz.*, 6(2):418–45, 2006.

MF Cordeiro, SS Bhattacharya, GS Schultz, and PT Khaw. Tgf-β_1, -β_2 and -β_3 in vitro: biphasic effects on tenons fibroblast contraction, proliferation, and migration. *Invest. Ophthalmol. Vis. Sci.*, 41(3):756–63, 2000.

SC Cowin and K Firoozbakhsh. Bone remodeling of diaphysial surfaces under constant load: Theoretical predictions. *J. Biomech.*, 14(7):471–84, 1981.

DT Cromack, MB Sporn, AB Roberts, MJ Merino, LL Dart, and JA Norton. Transforming growth factor β levels in rat wound chambers. *J. Surg. Res.*, 42(6):622–8, 1987.

GC Cruywagen and JD Murray. On a tissue interaction model for skin pattern formation. *J. Nonlinear Sci.*, 2(2):217–40, 1992.

GC Ctercteko, M Dhanendran, WC Hutton, and LP Le Quesne. Vertical forces acting on the feet of diabetic patients with neuropathic ulceration. *Brit. J. Surg.*, 68(9): 608–14, 1981.

D Cukjati, S Reberŝek, R Karba, and D Miklavĉiĉ. Modelling of chronic wound healing dynamics. *Med. Biol. Eng. Comput.*, 38(3):339–47, 2000.

BD Cumming, SDL McElwain, and Z Upton. A mathematical model of wound healing and subsequent scarring. *J. R. Soc. Interface*, 7(42):19–34, 2010.

JC Dallon. Biological implications of a discrete mathematical model for collagen deposition and alignment in dermal wound repair. *Math. Med. Biol.*, 17(4):379–93, 2000.

JC Dallon and PH Ehrlich. A review of fibroblast-populated collagen lattices. *Wound Repair Regen.*, 16(4):472–9, 2008.

JC Dallon, JA Sherratt, and PK Maini. Mathematical modelling of extracellular matrix dynamics using discrete cells: fiber orientation and tissue regeneration. *J. Theor. Biol.*, 199(4):449–71, 1999.

LA Davidson, AM Ezin, and R Keller. Embryonic wound healing by apical contraction and ingression in xenopus laevis. *Cell Motil. Cytoskel.*, 53(3):163–76, 2002.

A Desmoulière, A Geinoz, F Gabbiani, and G Gabbiani. Transforming growth factor-beta 1 induces alpha-smooth muscle actin expression in granulation tissue myofibroblasts and in quiescent and growing cultured fibroblasts. *J. Cell Biol.*, 122(1): 103–11, 1993.

T Desta, J Li, T Chino, and DT Graves. Altered fibroblast proliferation and apoptosis in diabetic gingival wounds. *J. Dental Res.*, 89(6):609–14, 2010.

RP Dickinson and RJ Gelinas. Sensitivity analysis of ordinary differential equation systems: A direct method. *J. Comp. Phys.*, 21(2):123–43, 1976.

S Diridollou, F Patat, F Gens, L Vaillant, D Black, JM Lagarde, Y Gall, and M Berson. In vivo model of the mechanical properties of the human skin under suction. *Skin Res. Technol.*, 6(4):214–21, 2000.

HP Ehrlich. Wound closure: evidence of cooperation between fibroblasts and collagen matrix. *Eye*, 2(2):149–57, 1988.

HP Ehrlich and JBM Rajaratnam. Cell locomotion forces versus cell contraction forces for collagen lattice contraction: an in vitro model of wound contraction. *Tissue Cell*, 22(4):407–17, 1990.

AC Eringen. *Nonlinear Theory of Continuous Media*. McGraw-Hill, New York, 1962.

V Falanga. Wound healing and its impairment in the diabetic foot. *Lancet*, 366(9498): 1736–43, 2005.

JA Flegg, HM Byrne, and SDL McElwain. Mathematical model of hyperbaric oxygen therapy applied to chronic diabetic wounds. *B. Math. Biol.*, 72(7):1867–91, 2010.

C Flynn, A Taberner, and P Nielsen. Modeling the mechanical response of in vivo human skin under a rich set of deformations. *Ann. Biomed. Eng.*, 39(7):1935–46, 2011.

TR Fray, JE Molloy, MP Armitage, and JC Sparrow. Quantification of single human dermal fibroblast contraction. *Tissue Eng.*, 4(3):281–91, 1998.

YC Fung. Elasticity of soft tissues in simple elongation. *Am. J. Physiol.*, 213(6): 1532–44, 1967.

YC Fung. *Biomechanics: Motion, Flow, Stress, and Growth*. Springer, New York, 1990.

YC Fung. *Biomechanics: Material Properties of Living Tissues*. Springer, New York, 1993.

G Gabbiani. The myofibroblast in wound healing and fibrocontractive diseases. *J. Pathol.*, 200(4):500–3, 2003.

EA Gaffney, K Pugh, PK Maini, and F Arnold. Investigating a simple model of cutaneous wound healing angiogenesis. *J. Math. Biol.*, 45(4):337–74, 2002.

AN Gent. A new constitutive relation for rubber. *Rubber Chem. Technol.*, 69(1): 59–61, 1996.

K Ghosh, Z Pan, E Guan, S Ge, Y Liu, T Nakamura, X Ren, M Rafailovich, and RAF Clark. Cell adaptation to a physiologically relevant ECM mimic with different viscoelastic properties. *Biomaterials*, 28(4):671–9, 2007.

HP Giele, K Liddiard, K Currie, and FM Wood. Direct measurement of cutaneous pressures generated by pressure garments. *Burns*, 23(2):137–41, 1997.

JW Godwin and N Rosenthal. Scar-free wound healing and regeneration in amphibians: immunological influences on regenerative success. *Differentiation*, 87(1): 66–75, 2014.

A Goriely and D Moulton. Morphoelasticity: a theory of elastic growth. In *New Trends in the Physics and Mechanics of Biological Systems*, pages 153–75. Oxford University Press, 2011.

A Goriely and R Vandiver. On the mechanical stability of growing arteries. *IMA J. Appl. Math.*, 75(4):549–70, 2010.

A Goriely, M Destrade, and M Ben Amar. Instabilities in elastomers and in soft tissues. *Q. J. Mech. Appl. Math.*, 59(4):615–30, 2006.

A Goriely, DE Moulton, and R Vandiver. Elastic cavitation, tube hollowing, and differential growth in plants and biological tissues. *Europhys. Lett.*, 91(1):18001, 2010.

H Grillo, G Watts, and J Gross. Studies in wound healing: I. Contraction and the wound contents. *Ann. Surg.*, 148(2):145–60, 1958.

F Grinnell, M Zhu, MA Carlson, and JM Abrams. Release of mechanical tension triggers apoptosis of human fibroblasts in a model of regressing granulation tissue. *Exp. Cell Res.*, 248(2):608–19, 1999.

J Gross, W Farinelli, P Sadow, R Anderson, and R Bruns. On the mechanism of skin wound "contraction": a granulation tissue "knockout" with a normal phenotype. *P. Natl. A. Sci. USA*, 92(13):5982–6, 1995.

HC Han and YC Fung. Residual strains in porcine and canine trachea. *J. Biomech.*, 24(5):307–15, 1991.

RT Hart. A theoretical study of the influence of bone maturation rate on surface remodeling predictions: Idealized models. *J. Biomech.*, 23(3):241–57, 1990.

K Hehenberger, JD Heilborn, K Brismar, and A Hansson. Inhibited proliferation of fibroblasts derived from chronic diabetic wounds and normal dermal fibroblasts treated with high glucose is associated with increased formation of L-lactate. *Wound Repair Regen.*, 6(2):135–41, 1998.

B Hinz. Masters and servants of the force: the role of matrix adhesions in myofibroblast force perception and transmission. *Eur. J. Cell Biol.*, 85(3-4):175–81, 2006.

B Hinz. Formation and function of the myofibroblast during tissue repair. *J. Invest. Dermatol.*, 127(3):526–37, 2007.

B Hinz, D Mastrangelo, C Iselin, C Chaponnier, and G Gabbiani. Mechanical tension controls granulation tissue contractile activity and myofibroblast differentiation. *Am. J. Path.*, 159(3):526–37, 2001.

GA Holzapfel. Biomechanics of soft tissue. In *The handbook of materials behavior models*, pages 1049–63. Academic Press Boston, 2001.

GA Holzapfel, R Eberlein, P Wriggers, and HW Weizsäcker. A new axisymmetrical membrane element for anisotropic, finite strain analysis of arteries. *Commun. Numer. Meth En.*, 12(8):507–17, 1996.

CO Horgan and G Saccomandi. Constitutive modelling of rubber-like and biological materials with limiting chain extensibility. *Math. Mech. Solids*, 7(4):353–71, 2002.

C Huang, T Leavitt, LR Bayer, and DP Orgill. Effect of negative pressure wound therapy on wound healing. *Curr. Prob. Surg.*, 51(7):301–31, 2014.

JD Humphrey. Review Paper: Continuum biomechanics of soft biological tissues. *Proc. Roy. Soc. Lond. A Mat.*, 459(2029):3–46, 2003.

E Jacquet, G Josse, F Khatyr, and C Garcin. A new experimental method for measuring skin's natural tension. *Skin Res. Technol.*, 14(1):1–7, 2008.

WJ Jeffcoate, P Price, and KG Harding. Wound healing and treatments for people with diabetic foot ulcers. *Diabetes Metab. Res.*, 20(Suppl 1):S78–89, 2004.

D Kessler, S Dethlefsen, I Haase, M Plomann, F Hirche, T Krieg, and B Eckes. Fibroblasts in mechanically stressed collagen lattices assume a synthetic phenotype. *J. Biol. Chem.*, 276(39):36575–85, 2001.

DP Kiehart. Wound healing: The power of the purse string. *Curr. Biol.*, 9(16): R602–5, 1999.

CW Kischer. Alteration of hypertrophic scars induced by mechanical pressure. *Arch. Dermatol.*, 111(1):60, 1975.

JK Knowles. The finite anti-plane shear field near the tip of a crack for a class of incompressible elastic solids. *Int. J. Fracture*, 13(5):611–39, 1977.

MS Kolodney and RB Wysolmerski. Isometric contraction by fibroblasts and endothelial cells in tissue culture: a quantitative study. *J. Cell Biol.*, 117(1):73–82, 1992.

WS Krawczyk. A pattern of epidermal cell migration during wound healing. *J. Cell Biol.*, 49(2):247–63, 1971.

K Langer. On the anatomy and physiology of the skin: Ii. skin tension (with 1 figure). *Brit. J. Plast. Surg.*, 31(2):93–106, 1978.

BJ Larson, MT Longaker, and HP Lorenz. Scarless fetal wound healing: a basic science review. *Plast. Reconstr. Surg.*, 126(4):1172–80, 2010.

IE Lin and LA Taber. A model for stress-induced growth in the developing heart. *J. Biomech. Eng.*, 117(3):343–9, 1995.

SQ Liu and YC Fung. Zero-stress states of arteries. *J. Biomech. Eng.*, 110(1):82–4, 1988.

L Loeb. A comparative study of the mechanism of wound healing. *J. Med. Res.*, 41 (2):247–81, 1920.

EA Lumpkin and MJ Caterina. Mechanisms of sensory transduction in the skin. *Nature*, 445(7130):858–65, 2007.

C Marchese, J Rubin, D Ron, A Faggioni, MR Torrisi, A Messina, L Frati, and SA Aaronson. Human keratinocyte growth factor activity on proliferation and differentiation of human keratinocytes: differentiation response distinguishes KGF from EGF family. *J. Cell. Physiol.*, 144(2):326–32, 1990.

P Martin. Wound healing: aiming for perfect skin regeneration. *Science*, 276(5309): 75–81, 1997.

P Martin and J Lewis. Actin cables and epidermal movement in embryonic wound healing. *Nature*, 360(6400):179–83, 1992.

L Martínez-Santamaría, CJ Conti, S Llames, E García, L Retamosa, A Holguín, N Illera, B Duarte, L Camblor, JM Llaneza, JL Jorcano, F Larcher, Á Meana, MJ Escámez, and M Del Río. The regenerative potential of fibroblasts in a new diabetes-induced delayed humanised wound healing model. *Exp. Dermatol.*, 22(3): 195–201, 2013.

S McDougall, J Dallon, J Sherratt, and P Maini. Fibroblast migration and collagen deposition during dermal wound healing: mathematical modelling and clinical implications. *Philos. T. Roy. Soc. A*, 364(1843):1385–405, 2006.

MH McGrath and RH Simon. Wound geometry and the kinetics of wound contraction. *Plast. Reconstr. Surg.*, 72(1):66–72, 1983.

S Mendez-Eastman. Guidelines for using negative pressure wound therapy. *Adv. Skin Wound Care*, 14(6):314–23, 2001.

SN Menon, JA Flegg, SW McCue, RC Schugart, RA Dawson, and SDL McElwain. Modelling the interaction of keratinocytes and fibroblasts during normal and abnormal wound healing processes. *P. Biol. Sci.*, 279(1741):3329–38, 2012.

M Meyer and DA McGrouther. A study relating wound tension to scar morphology in the pre-sternal scar using langers technique. *Brit J. Plast. Surg.*, 44(4):291–4, 1991.

Q Mi, B Rivière, G Clermont, DL Steed, and Y Vodovotz. Agent-based model of inflammation and wound healing: insights into diabetic foot ulcer pathology and the role of transforming growth factor-β1. *Wound Repair Regen.*, 15(5):671–82, 2007.

CC Miller, G Godeau, C Lebreton-DeCoster, A Desmouliere, B Pellat, L Dubertret, and B Coulomb. Validation of a morphometric method for evaluating fibroblast numbers in normal and pathologic tissues. *Exp. Dermatol.*, 12(4):403–11, 2003.

Y Mitsui and EL Schneider. Relationship between cell replication and volume in senescent human diploid fibroblasts. *Mech. Ageing Dev.*, 5:45–56, 1976.

JL Monaco and WT Lawrence. Acute wound healing an overview. *Clin. Plast. Surg.*, 30(1):1–12, 2003.

M Mooney. A theory of large elastic deformation. *J. Appl. Phys.*, 11(9):582–92, 1940.

DE Moulton and A Goriely. Possible role of differential growth in airway wall remodeling in asthma. *J. Appl. Physiol.*, 110(4):1003–12, 2011.

H Murata, L Zhou, S Ochoa, A Hasan, E Badiavas, and V Falanga. Tgf-β_3 stimulates and regulates collagen synthesis through tgf-β_1-dependent and independent mechanisms. *J. Invest. Dermatol.*, 108(3):258–62, 1997.

KE Murphy, CL Hall, SW McCue, and SDL McElwain. A two-compartment mechanochemical model of the roles of transforming growth factor β and the tissue tension in dermal wound healing. *J. Theor. Biol.*, 272:145–59, 2011.

JD Murray, PK Maini, and RT Tranquillo. Mechanochemical models for generating biological pattern and form in development. *Phys. Rep.*, 171(2):59–84, 1988.

JV Nauman, PG Campbell, F Lanni, and JL Anderson. Diffusion of insulin-like growth factor-i and ribonuclease through fibrin gels. *Biophys. J.*, 92(12):4444–50, 2007.

B Nedelec, A Ghahary, PG Scott, and EE Tredget. Control of wound contraction. Basic and clinical features. *Hand Clin.*, 16(2):289–302, 2000.

JF North and F Gibson. Volume compressibility of human abdominal skin. *J. Biomech.*, 11(4):203–7, 1978.

RW Ogden. *Non-linear elastic deformations*. Courier Corporation, 1997.

L Olsen, JA Sherratt, and PK Maini. A mechanochemical model for adult dermal wound contraction: On the permanence of the contracted tissue displacement profile. *J. Theor. Biol.*, 177(2):113–28, 1995.

L Olsen, PK Maini, JA Sherratt, and J Dallon. Mathematical modelling of anisotropy in fibrous connective tissue. *Math. Biosci.*, 158(2):145–70, 1999.

JH Omens and YC Fung. Residual strain in rat left ventricle. *Circ. Res.*, 66(1):37–45, 1990.

HM Peacock, EAB Gilbert, and MK Vickaryous. Scar-free cutaneous wound healing in the leopard gecko, Eublepharis macularius. *J. Anat.*, doi: 10.1111/joa.12368, 2015.

GF Pierce, TA Mustoe, J Lingelbach, VR Masakowski, GL Griffin, RM Senior, and TF Deuel. Platelet-derived growth factor and transforming growth factor-beta enhance tissue repair activities by unique mechanisms. *J. Cell Biol.*, 109(1):429–40, 1989.

G Pietramaggiori. Tensile forces stimulate vascular remodeling and epidermal cell proliferation in living skin. *Ann. Surg.*, 246(5):896–902, 2007.

WH Press, WT Vetterling, SA Teukolsky, BP Flannery, and E Greenwell Yanik. Numerical recipes in fortran–the art of scientific computing. *SIAM Rev.*, 36(1): 149–50, 1994.

A Rachev, N Stergiopulos, and JJ Meister. A model for geometric and mechanical adaptation of arteries to sustained hypertension. *J. Biomech. Eng.*, 120(1):9–17, 1998.

RK Randolph and M Simon. Dermal fibroblasts actively metabolize retinoic acid but not retinol. *J. Invest. Dermatol.*, 111(3):478–84, 1998.

R Reihsner, M Melling, W Pfeiler, and EJ Menzel. Alterations of biochemical and two-dimensional biomechanical properties of human skin in diabetes mellitus as compared to effects of in vitro non-enzymatic glycation. *Clin. Biomech.*, 15(5): 379–86, 2000.

R Rezakhaniha, E Fonck, C Genoud, and N Stergiopulos. Role of elastin anisotropy in structural strain energy functions of arterial tissue. *Biomech. Model. Mechan.*, 10(4):599–611, 2011.

JM Rhett, GS Ghatnekar, JA Palatinus, M O'Quinn, MJ Yost, and RG Gourdie. Novel therapies for scar reduction and regenerative healing of skin wounds. *Trends Biotechnol.*, 26(4):173–180, 2008.

WM Ringsdorf and E Cheraskin. Vitamin C and human wound healing. *Oral Surg. Oral Med. O.*, 53(3):231–6, 1982.

RS Rivlin. Large elastic deformations of isotropic materials I. *Philos. T. Roy. Soc. A*, 240(822):459–90, 1948a.

RS Rivlin. Large elastic deformations of isotropic materials III. *Philos. T. Roy. Soc. A*, 240(823):509–25, 1948b.

AB Roberts, BK Mccune, and MB Sporn. Tgfβ: Regulation of extracellular matrix. *Kidney Int.*, 41(5):57–9, 1992.

EK Rodriguez, A Hoger, and AD McCulloch. Stress-dependent finite growth in soft elastic tissues. *J. Biomech.*, 27(4):455–67, 1994.

KU Sandvig, E Haaskjold, R Bjerknes, SB Refsum, and K Kravik. Cell kinetics of conjunctival and corneal epithelium during regeneration of different-sized corneal epithelial defects. *Acta Ophthalmol.*, 72(1):43–8, 2009.

RA Segal, RF Diegelmann, KR Ward, and A Reynolds. A differential equation model of collagen accumulation in a healing wound. *B. Math. Biol.*, 74(9):2165–82, 2012.

M Shah, DM Foreman, and MWJ Ferguson. Control of scarring in adult wounds by neutralising antibody to transforming growth factor β. *Lancet*, 339(8787):213–14, 1992.

LF Shampine and MW Reichelt. The Matlab ODE Suite. *SIAM J. Sci. Comput.*, 18 (1):1–22, 1997.

JE Shaw, RA Sicree, and PZ Zimmet. Global estimates of the prevalence of diabetes for 2010 and 2030. *Diabetes Res. Clin. Pr.*, 87(1):4–14, 2010.

JA Sherratt and JD Murray. Models of epidermal wound healing. *P. Biol. Sci.*, 241 (1300):29–36, 1990.

JA Sherratt and JD Murray. Epidermal wound healing: the clinical implications of a simple mathematical model. *Cell Transplant.*, 1(5):365–371, 1992.

Q Shi and RW King. Chromosome nondisjunction yields tetraploid rather than aneuploid cells in human cell lines. *Nature*, 437(7061):1038–42, 2005.

MR Singh, S Saraf, A Vyas, V Jain, and D Singh. Innovative approaches in wound healing: trajectory and advances. *Artif. Cell. Nanomedicine Biotech.*, 41(3):202–12, 2013.

R Skalak, G Dasgupta, M Moss, E Otten, P Dullemeijer, and H Vilmann. Analytical description of growth. *J. Theor. Biol.*, 94(3):555–77, 1982.

WS Slaughter. *The linearized theory of elasticity*. Birkhauser, Boston, 2003.

AJM Spencer. *Continuum Mechanics*. Longman, London, 1980.

WK Stadelmann, AG Digenis, and GR Tobin. Physiology and healing dynamics of chronic cutaneous wounds. *Am. J. Surg.*, 176(2):26S–38S, 1998.

T Sun, S Adra, R Smallwood, M Holcombe, and S MacNeil. Exploring hypotheses of the actions of tgf-β1 in epidermal wound healing using a 3d computational multiscale model of the human epidermis. *PloS one*, 4(12):e8515, 2009.

LA Taber. A model for aortic growth based on fluid shear and fiber stresses. *J. Biomech. Eng.*, 120(3):348–54, 1998.

LA Taber. Biomechanics of cardiovascular development. *Annu. Rev. Biomed. Eng.*, 3:1–25, 2001.

LA Taber. Towards a unified theory for morphomechanics. *Philos. T. R. Soc. A*, 367 (1902):3555–83, 2009.

LA Taber and DW Eggers. Theoretical study of stress-modulated growth in the aorta. *J. Theor. Biol.*, 180(4):343–57, 1996.

AB Tepole and E Kuhl. Systems-based approaches toward wound healing. *Pediatr. Res.*, 73(4-2):553–63, 2013.

JA Thackham, SDL McElwain, and RJ Long. The use of hyperbaric oxygen therapy to treat chronic wounds: A review. *Wound Repair Regen.*, 16(3):321–30, 2008.

P Tracqui, DE Woodward, GC Cruywagen, J Cook, and JD Murray. A mechanical model for fibroblast-driven wound healing. *J. Biol. Sys.*, 3(4):1075–84, 1995.

RT Tranquillo and JD Murray. Continuum model of fibroblast-driven wound contraction: Inflammation-mediation. *J. Theor. Biol.*, 158(2):135–72, 1992.

BD Uhal, C Ramos, I Joshi, A Bifero, A Pardo, and M Selman. Cell size, cell cycle, and alpha -smooth muscle actin expression by primary human lung fibroblasts. *Am. J. Physiol. Lung Cell Mol. Physiol.*, 275(5):998–1005, 1998.

N Unwin. Epidemiology of lower extremity amputation in centres in europe, north america and east asia. *Brit. J. Surg.*, 87(3):328–37, 2000.

ML Usui, JN Mansbridge, WG Carter, M Fujita, and JE Olerud. Keratinocyte migration, proliferation, and differentiation in chronic ulcers from patients with diabetes and normal wounds. *J. Histochem. Cytochem.*, 56(7):687–96, 2008.

RN Vaishnav and J Vossoughi. Residual stress and strain in aortic segments. *J. Biomech.*, 20(3):235–9, 1987.

FJ Vermolen and E Javierre. A finite-element model for healing of cutaneous wounds combining contraction, angiogenesis and closure. *J. Math. Biol.*, 65(5):967–96, 2012.

SM Wahl, H Wong, and N McCartney-Francis. Role of growth factors in inflammation and repair. *J. Cell. Bioch.*, 40(2):193–9, 1989.

LM Wakefield, TS Winokur, RS Hollands, K Christopherson, AD Levinson, and MB Sporn. Recombinant latent transforming growth factor beta 1 has a longer plasma half-life in rats than active transforming growth factor beta 1, and a different tissue distribution. *J. Clin. Invest.*, 86(6):1976–84, 1990.

DC Walker, G Hill, SM Wood, RH Smallwood, and J Southgate. Agent-based computational modeling of wounded epithelial cell monolayers. *IEEE T. Nanobiosci.*, 3(3):153–63, 2004.

PN Watton, Y Ventikos, and GA. Holzapfel. Modelling the mechanical response of elastin for arterial tissue. *J. Biomech.*, 42(9):1320–5, 2009.

GT Watts, HC Grillo, and J Gross. Studies in wound healing: II. The role of granulation tissue in contraction. *Ann. Surg.*, 148(2):153–60, 1958.

HV Waugh and JA Sherratt. Macrophage dynamics in diabetic wound dealing. *Bull. Math. Biol.*, 68(1):197–207, 2006.

HV Waugh and JA Sherratt. Modeling the effects of treating diabetic wounds with engineered skin substitutes. *Wound Repair Regen.*, 15(4):556–65, 2007.

HJ Wearing and JA Sherratt. Keratinocyte growth factor signalling: a mathematical model of dermal-epidermal interaction in epidermal wound healing. *Math. Biosci.*, 165(1):41–62, 2000.

S Werner, T Krieg, and H Smola. Keratinocyte-fibroblast interactions in wound healing. *J. Invest. Dermatol.*, 127(5):998–1008, 2007.

VW Wong, M Sorkin, JP Glotzbach, MT Longaker, and GC Gurtner. Surgical approaches to create murine models of human wound healing. *J. Biomed. Biotech.*, 969618:1–8, 2011.

LK Wrobel, TR Fray, JE Molloy, JJ Adams, MP Armitage, and JC Sparrow. Contractility of single human dermal myofibroblasts and fibroblasts. *Cell Motil. Cytoskelet.*, 52(2):82–90, 2002.

M Wu and M Ben Amar. Growth and remodelling for profound circular wounds in skin. *Biomech. Model. Mechan.*, 14(2):357–70, 2015.

F Xu, C Zhang, and DT Graves. Abnormal cell responses and role of TNF-α in impaired diabetic wound healing. *Biomed. Res. Int.*, 2013(1):1–9, 2013.

G Xu, PV Bayly, and LA Taber. Residual stress in the adult mouse brain. *Biomech. Model. Mechan.*, 8(4):253–62, 2009.

C Xue, A Friedman, and CK Sen. A mathematical model of ischemic cutaneous wounds. *P. Natl. Acad. Sci.*, 106(39):16782–7, 2009.

L Yang, CX Qiu, A Ludlow, MWJ Ferguson, and G Brunner. Active transforming growth factor-β in wound repair. *Am. J. Pathol.*, 154(1):105–11, 1999.

L Yang, TM Witten, and RM Pidaparti. A biomechanical model of wound contraction and scar formation. *J. Theor. Biol.*, 332:228–48, 2013.